NEW INSIGHTS INTO THE AGE AND PALAEOENVIRONMENTS OF THE UPPER CRETACEOUS FIQA FORMATION OF OMAN USING CALCAREOUS NANNOFOSSIL BIOSTRATIGRAPHY AND INORGANIC GEOCHEMISTRY

by

ZAINAB ABDULLAH ISSA AL RAWAHI

A thesis submitted to the University of Birmingham for the degree of DOCTOR OF PHILOSOPHY

School of Geography, Environment and Earth Sciences

College of Life and Environmental Sciences

University of Birmingham

November 2019

ABSTRACT

Planktonic microfossils recovered from the deep marine shales and marls of the Fiqa Formation, Oman, deposited through ~15 Ma, from the late Coniacian to earliest Maastrichtian provide a window into Late Cretaceous tropical, pelagic ecosystems. In this thesis I present new records based on well-preserved calcareous nannofossil assemblages and inorganic geochemistry to provide new information on the chronostratigraphic subdivision, palaeoenvironments, high-resolution correlation and sequence stratigraphy of the Fiqa Formation. This study is based on the examination of 341 cuttings and side core samples from 11 hydrocarbon exploration wells distributed across a palaeobathymetric gradient within the Upper Cretaceous Aruma Basin. Results include the first detailed taxonomic analysis of Late Cretaceous nannofossils from the Fiqa Formation including the identification of two new species; a new biozonation scheme for the Fiqa Formation that is correlated into the global UC biozonation scheme of Burnett et al. (1998); new biostratigraphic correlations across the basin and integration with regional sequence stratigraphy; and finally, integration of nannofossil assemblage data with detailed bulk rock carbon isotope and element composition analysis and the reconstruction of long-term palaeoenvironmental change and basin evolution, both in space across Oman and through time.

ACKNOWLEDGEMENT

Thank you for Petroleum Development Oman for sponsoring my studies and for the staff of PDO Stratigraphy Team for providing project data and technical support. Thank you for Dr Tom Dunkley Jones for supervising the project and providing continuous help throughout the duration of my PhD and for Earth Science Department staff and doctoral researchers for their support.

To My parents, siblings and in-laws, thank you for your long standing patience and support. Fahd, thank you for everything you have done for me through this journey.

TABLE OF CONTENTS

Appendices

LIST OF ILLUSTRATIONS

List of Figures

Chapter 3

Chapter 4

List of Plates

LIST OF TABLES

CHAPTER 1

INTRODUCTION

The Upper Cretaceous sequences of Oman have been subjected to various geological studies since the beginning of hydrocarbon exploration in the early 20th century. These sequences represent an important part of the Cretaceous hydrocarbon play in Oman and the Middle East, being regional seal units for the underlying hydrocarbon-productive sequences (Forbes et al., 2010). In this context, a sound understanding of the various geological and engineering aspects of these units is important to the hydrocarbon industry. A range of sedimentological, stratigraphical and geophysical research has been undertaken on outcrops and subsurface sections that span different parts of the Upper Cretaceous of Oman (e.g. Glennie et al., 1973; Glennie et al., 1974; Lippard et al., 1986; Robertson, 1987; Hughes-Clark, 1988; Alsharhan and Nairn, 1990; Boote et al., 1990; Ziegler, 2001; Forbes et al., 2010). This PhD study exclusively focuses on the, geologically-complex, Coniacian to Maastrichtian Fiqa Formation of the subsurface of Oman (Glennie et al., 1973; Glennie et al., 1974; Hughes-Clark, 1988; Forbes et al., 2010). The limited control on the age of the borehole sequences included in this study and the potential for diachroneity within the Fiqa Formation across Oman provided the motivation to apply new techniques to improve stratigraphic correlations of this formation in the subsurface. This study is part of ongoing exploration projects sponsored by Petroleum Development Oman (PDO), focusing on enhancing the understanding of the evolution of the Upper Cretaceous Aruma Basin, and on the application of nannofossil biostratigraphy and bulk sediment geochemical analyses to provide new information on the chronostratigraphic

subdivision, high-resolution correlation, sequence stratigraphy and palaeoenvironmental reconstruction of the Fiqa Formation.

1 Objectives

This research aims to utilise the rich and diverse calcareous nannoplankton assemblages of the subsurface Fiqa Formation, recovered from a number of hydrocarbon exploration wells distributed a cross the Upper Cretaceous Aruma Basin of Oman, along with the analysis of geochemical data to provide a new, higher resolution bio-chronostratigraphic subdivision for the Formation. Palaeoenvironmental interpretations of this data will also inform various geological aspects including sequence stratigraphy and tectonic evolution, as well as the development of enhanced spacial and temporal palaeoenvironmental maps using nannofossil biostratigraphy, assemblage analysis and geochemical analysis. The Fiqa Formation is considered in PDO as relatively understudied and requires further work in order to model the development of the basin during the Late Cretaceous. For example, the age of the transition from the exposed mid-Cretaceous carbonate platform to the onset of deeper marine deposition within the basal Fiqa Formation, as well as the age of the transition from these deeper marine facies to shallower marine deposition in the upper part of the formation are both poorly constrained (e.g. Hughes-Clark, 1988; Forbes et al., 2010). Moreover, the microfossil biofacies previously used to provide biostratigraphic constraints within the Fiqa Formation are potentially diachronous, the degree of which can only be constrained against independent stratigraphic controls, which I aim to provide through detailed nannofossil biostratigraphy which is more facies independent. Integration of detailed biostratigraphic and geochemical work with other geological information like sedimentology and seismic data, as well as the

comparison with other Upper Cretaceous successions in the Tethys ocean and elsewhere would help to assess the tectonic, sea level and climatic drivers of observed environmental changes within the Aruma Basin and their evolution through space and time. The main objectives of this study are:

1. Detailed nannofossil taxonomy, assemblage composition and its palaeoenvironmental and palaeoceanographic significance: to carry out a detailed taxonomic analysis of the Late Cretaceous Tethyan calcareous nannofossil species recovered from the Fiqa Formation. Also, to analyse the changes in the nannofossil assemblages through time, from a representative study well and compare it to global nannofossil assemblages. The taxonomic and assemblage composition analysis will form the basis for later biostratigraphic, tectonic and sequence stratigraphic applications. The assemblage change analysis will provide a basic background into the palaeoenvironmental and palaeoceanographic status of the basin during the time of Fiqa Formation deposition.

2. Biostratigraphy and sequence stratigraphy: to establish a new high resolution biostratigraphic scheme using calcareous nannofossil for the Upper Cretaceous subsurface sequences of Oman. This new biostratigraphy will be correlated to existing local microfossil and global nannofossil zonation schemes and used to refine them where possible. Moreover, nannofossil age dating will be used to assess the suspected diachroneity of microfossil biofacies and to constrain the age of the top and base of the Fiqa Formation, as well as the intra-formational transition from deeper to shallower facies across the basin. Finally, this new biostratigraphic scheme will be applied to generate a

new basin wide, well-to-well stratigraphic correlation, and will be integrated with the local and regional sequence stratigraphy of Oman and Arabia.

3. Integrated inorganic geochemistry, statistical analysis of bulk sediment element data and nannofossil assemblages and its palaeoenvironmental interpretation: bulk rock carbonate isotope analysis and bulk sediment elemental concentrations from X-ray fluorescence analysis (XRF), to assist with both nannofloral assessment of the Fiqa Formation palaeoenvironment and to understand broad scale stratigraphic correlation and depositional evolution across the basin, both in space across Oman and through time.

2 Study Area, Geological Settings and Hydrocarbon Potential of the Fiqa Formation of Oman

2.1 Study Area

This study is based on eleven hydrocarbon exploration wells from the North and South of Oman (Fig. 1). The study wells are distributed along a palaeobathymetric gradient across the basin, which also evolves through time during the Late Cretaceous interval. Two wells (W-1 and W-2) are located at the northern basin margin, close to an active thrust belt associated with Late Cretaceous ophiolite emplacement. Three wells (W-3, W-4 and W-5) are located at the thickest and deepest part of the basin in northern Oman. Two wells (W-6 and W-7) are located at a shallower part of the basin in central Oman and four wells (W-8, W-9, W-10 and W-11) are located at the shallowest part of the basin to the south of Oman. Figure 1 shows a brief comparison between the study wells. A lithological summary, gamma ray (GR) logs, the sampled intervals (nannofossil, microfossil and geochemical samples) and samples types

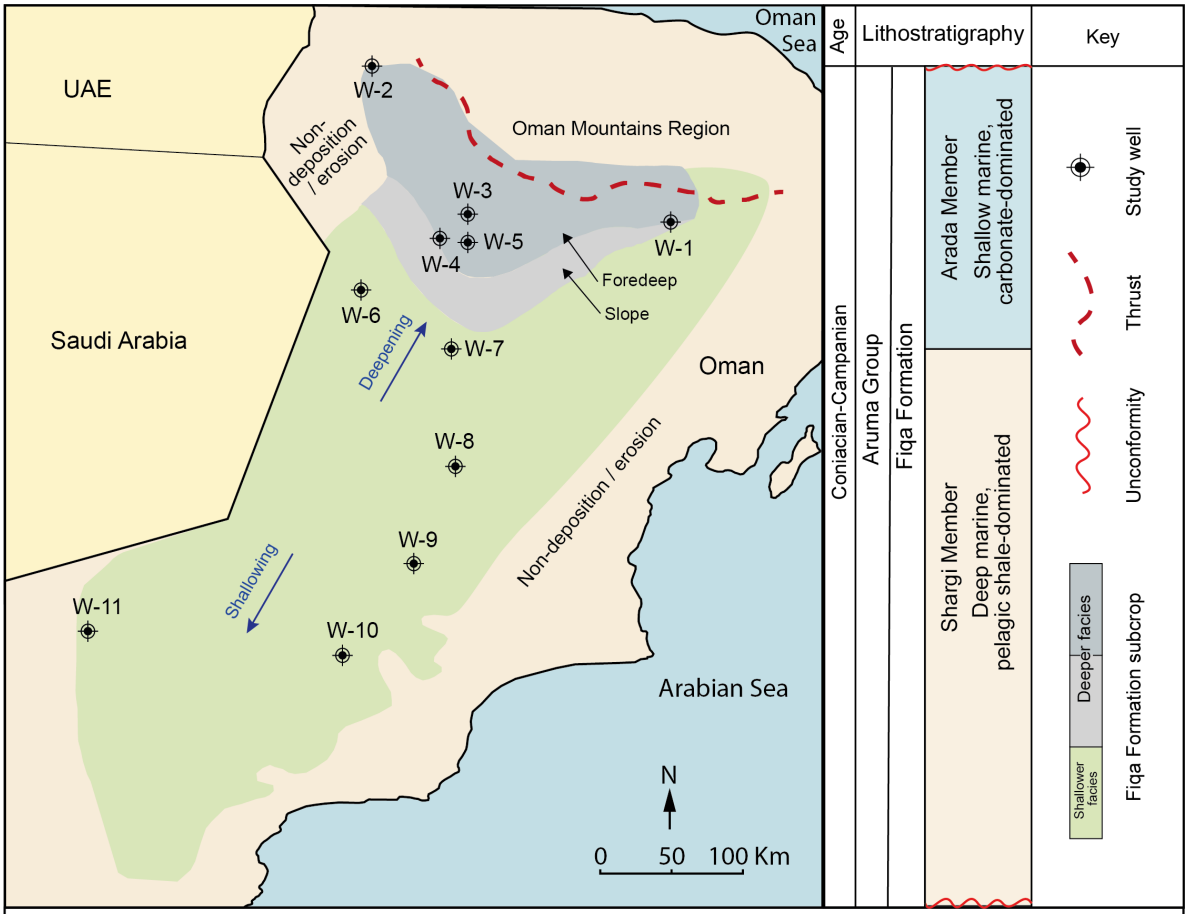

Deepening ← → Shallowing

NE — Foredeep basinal setting — Shallower basin — Shallow marine-transitional — SW

Study Wells	W-1	W-2	W-3	W-4	W-5	W-6	W-7	W-8	W-9	W-10	W-11
Samples number & type (CU: cutting; SC: sidewall core; CO: core)	11 CU, 8 SC, 1 CO	17 CU	10 CU	17 CU, 33 SC	35 CU, 9 CO	22 CU	30 CU	24 CU	13 CU	11 SC	8 CU
Top Fiqa Fm (meters below ground surface)	110.5	2106.8	3.35	18.3	555	597.1	411	582	436	603.5	685.7
Fiqa Fm Thickness (m)	850.1	1066.2	898.85	1330.1	1261	418.2	649	275	125	42	191.3
Lithostratigraphic units	Juweiza, Arada & Shargi Mbrs	Arada & Shargi Mbrs	Shargi Mbr	Arada & Shargi Mbrs	Arada & Shargi Mbrs	Arada & Shargi Mbrs	Arada & Shargi Mbrs	Arada & Shargi Mbrs	Arada & Shargi Mbrs	Arada & Shargi Mbrs	Arada & Shargi Mbrs
Lithological notes	More clastic input into the Fiqa Fm		Thicker Shargi Mbr, Fiqa Fm is dominated by deeper marine shale lithology			Thicker Arada Mbr, Fiqa Fm is dominated by shallow marine carbonates lithology					

Figure 1. Simplified lithostratigraphy of the Fiqa Formation of Oman (after Forbes et al., 2010) and a map of the Upper Cretaceous Fiqa Formation subcrop with projected slope and foredeep basin based on siesmic data (Modified after Giner et al., 1992). The study wells are shown in the map and compared in the underlying table. Abbreviations: Fm, Formation; Mbr, Member.

(cutting, sidewall core, core) for each well are illustrated in Figure 2. All microfossil samples were analysed by PDO and their sub-contracted micropalaeontological consultancies (Packer et al., 2000; Packer, 2001a; b) but are integrated and interpreted into the nannofossil and geochemical analyses of this study. See appendices A to C for detailed lists of samples included in this research.

2.2 Geology, Stratigraphy and Tectonic Settings

The stable sedimentation of the Permian to mid-Cretaceous carbonate shelf sequences in Oman ended abruptly at the end Cenomanian at ~ 93.5 Ma due to major regional tectonic events (Ali et al., 2013). The end Cenomanian to Turonian was a period of uplift and erosion in Oman, with a regional unconformity that separates the mid-Cretaceous Wasia group from the overlying Upper Cretaceous Aruma Group, known as the Wasia-Aruma break (Glennie et al., 1973). Emergence at this time was due to the collision of Arabia with a Tethyan subduction zone (Droste and Van Steenwinkel, 2004) that resulted in uplift related to structural flexing along the northeastern edge of the Arabian Platform in response to compressional deformation and loading ahead of an advancing thrust sheet, known as the Semail ophiolite obduction event (Glennie et al., 1973; Glennie et al., 1974; Cooper et al., 2014). During this event, a Cenomanian-aged Tethyan oceanic crust and upper mantle, and associated mid-Permian to Cenomanian marine rocks (Sumeini, Hawasina and Haybi complexes) were progressively thrusted over the northeastern margin of Oman (Glennie et al. 1973; Lippard et al., 1986; Ali et al., 2013). The oceanic crust, now obducted as the Semail ophiolite, is dated as Cenomanian (~96-95 Ma), with the start of emplacement soon after its formation (Rioux et al. 2012) and was completed by the early Maastrichtian at ~ 70 Ma

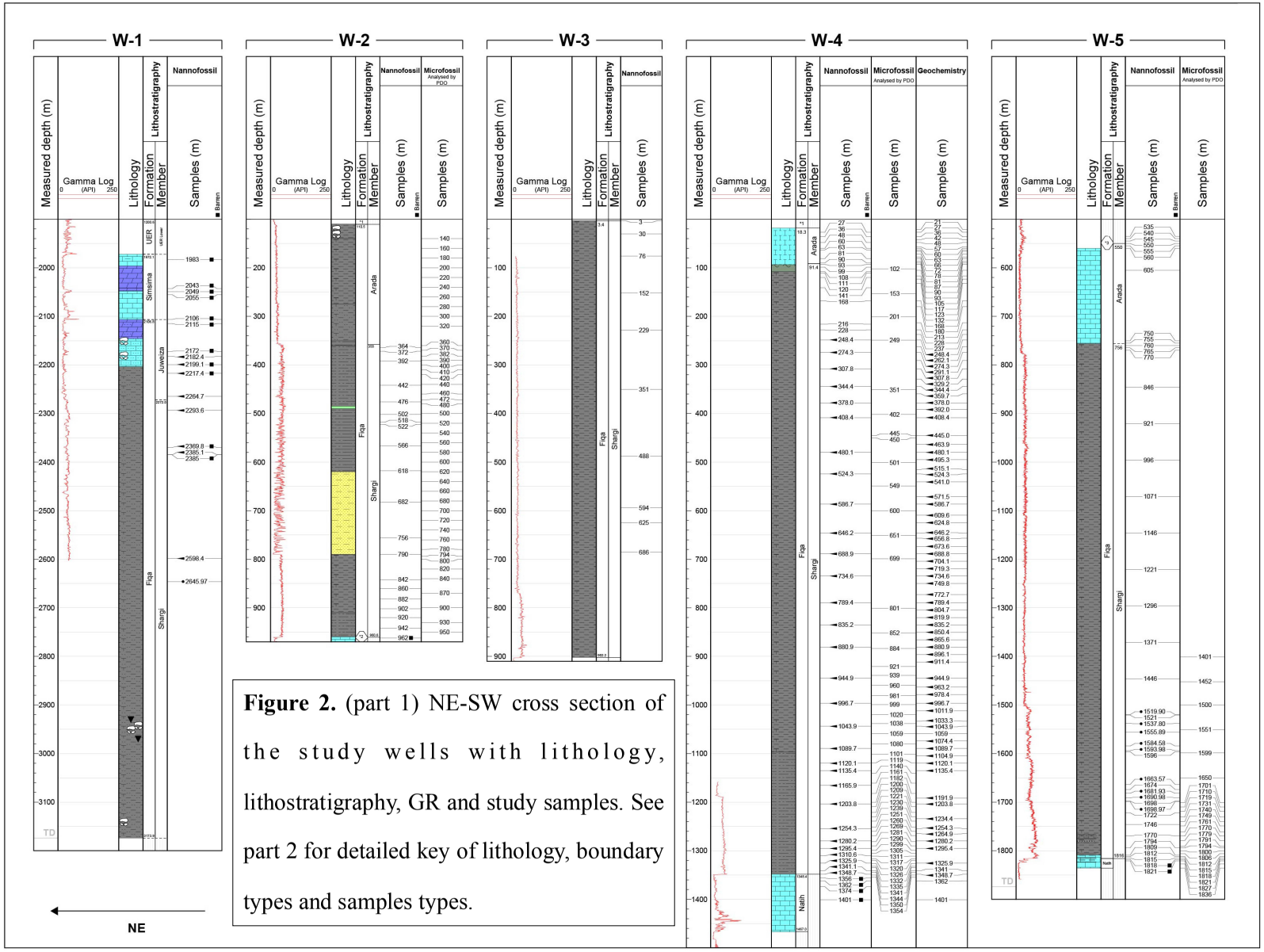

Figure 2. (part 1) NE-SW cross section of the study wells with lithology, lithostratigraphy, GR and study samples. See part 2 for detailed key of lithology, boundary types and samples types.

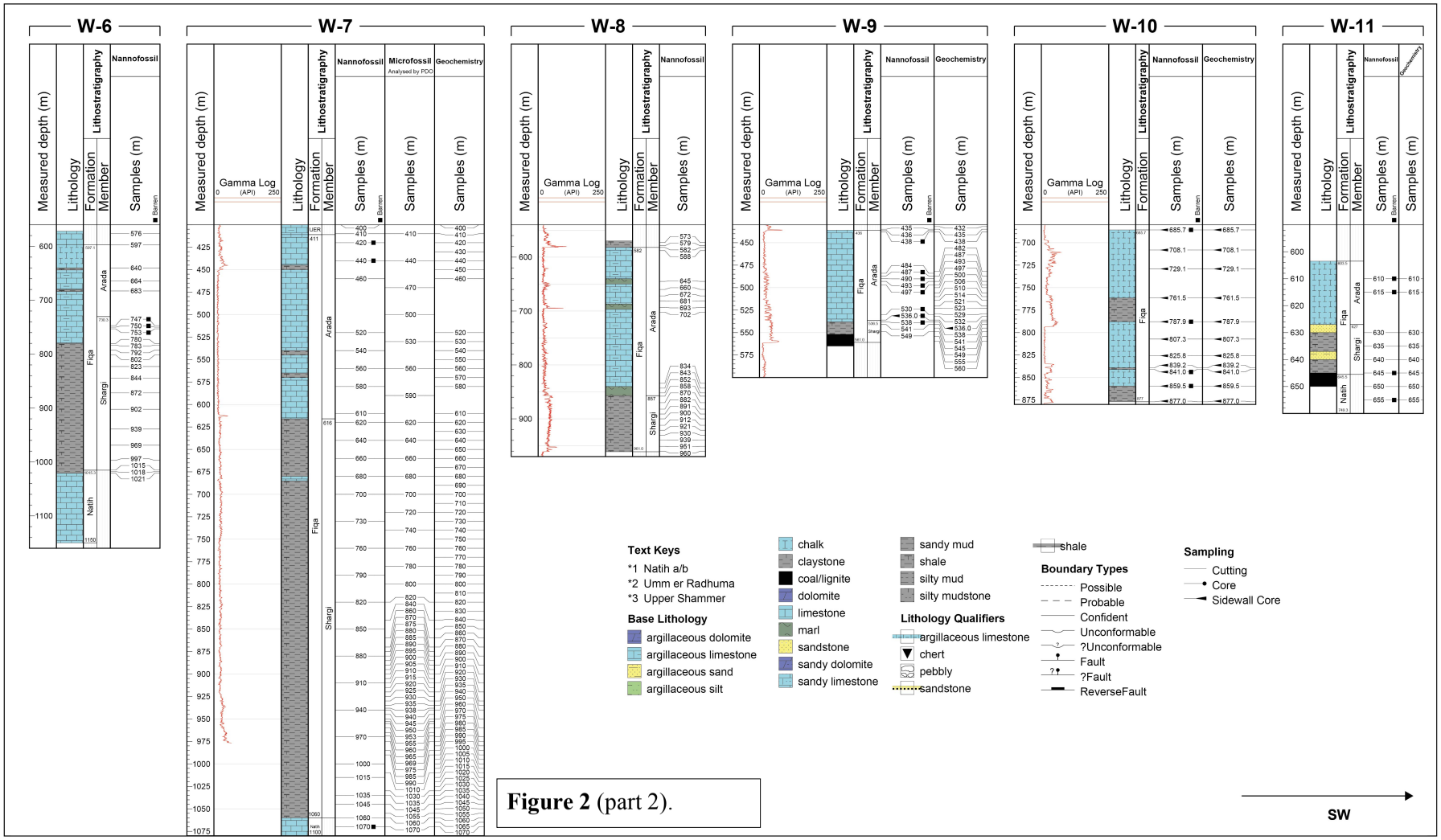

Figure 2 (part 2).

(Searle, 2007). After the initial collision, the regional uplift and the associated major depositional hiatus, a progressive loading and down-flexure of the continental lithosphere in front of the advancing thrust sheets caused regional subsidence, marine flooding and the development of deep marine basin, including a foredeep setting (Fig. 1) where the fine grained sediments of the Fiqa Formation were deposited (Glennie et al., 1973). As thrust migration continued, the basin, known as the Aruma Basin, deepened and extended to cover much of North and Central Oman (Romine and Stuart-Smith, 2003). Some of the accommodation space in the basin is potentially generated by reactivated basement faults (NW-trending Najd faults) and sub-surface movement of extensive, deeply buried Palaeozoic salt (Pollastro, 1999). In addition, the obduction of Late Jurassic-aged (~150 Ma) oceanic crust in eastern Oman at ~ 65 Ma, the Masirah ophiolite obduction event (Gaina et al., 2015), could also have contributed to the latest stages of the Aruma Basin development although its effect is still poorly known. As a result, very thick Upper Cretaceous sequences, up to 4.3 km, were deposited in the Aruma Basin (Glennie et al., 1973). The Fiqa Formation of Oman - dated as Coniacian to Campanian using microfossils (e.g. Sikkema, 1991; Droste, 2001; Osterloff et al., 2001; Packer et al., 2002) - is part of the Coniacian to upper Maastrichtian Aruma Group (Forbes et al., 2010). The Fiqa Formation includes a sequence of thick, deep marine shales deposited in a basinal setting (Shargi Member) followed by shallower water carbonate units (Arada Member). The shale of the Shargi Member is thickest in the north and thins to the south, and the carbonates of the Arada Member, on the other hand, thickens southward (Forbes et al., 2010). These two members are found across most of the subsurface of Oman. The Arada carbonates outcrop in the Huqf area, and the Shargi shales outcrop on the southern flanks of the Oman Mountains (Hughes-Clark, 1988). The deposition of the Fiqa

Formation was followed by a shallow marine sedimentation of the Simsima Formation during most of the Maastrichtian as the obduction event continued (Glennie et al., 1973).

2.3 Hydrocarbon Potential

Since the discovery of gas-bearing sand layers within the Fiqa Formation in northern Oman in the early 1980s, it has been considered as a new gas- and possibly oil- play with considerable stratigraphic and structural trapping potential (Horsfield, 1983). These include a potential stratigraphic trap within the Santonian sand-prone lithologies onlapping into deeper marine shale of the lower part of the Formation, which is occasionally mapped in seismic sections in the northern parts of the basin (Giner et al., 1992). Other possible stratigraphic trap units are the lowstand submarine turbidite fans within deeper parts of the north and east of the basin (Filbrandent et al., 2004), but this remains tentative due to intense calcite cementation in the turbiditic sand of North Oman (Nour El Din, 1992). Sand layers deposited in faulted areas or in rim synclines around rising salt domes during Santonian and Campanian tectonic movements are considered potential stratigraphic and structural traps, however, sand may not have reached to inverted and faulted areas around major fault systems (Filbrandent et al., 2004). Several internal PDO studies, undertaken in mid 1990s and early 2000s to assess the hydrocarbon potential of submarine fans seen in seismic data in the north and east of Oman, recommended additional work on the Fiqa Formation including the development of improved palaeoenvironmental and biostratigraphic age control. The current significance of the Fiqa Formation in the petroleum industry is being an important, regional seal unit for the underlying mid-Cretaceous reservoirs (Forbes et al., 2010). The Fiqa play is currently considered in PDO as understudied with more work required to unravel the basin fill

sequences, structures, reservoir presence and its quality, understanding the source area and the sediment entry points. A combination of seismic data, biostratigraphy and sedimentology could improve our understanding of the Late Cretaceous basin development in Oman.

3 An Overview of Late Cretaceous Climate and Palaeogeography

The Late Cretaceous was a period of global warming (Frakes et al., 1992), with major eustatic high sea level (e.g. Miller et al., 2005; Haq et al., 1987). Based on oceanic isotope temperature data from Cretaceous fossils and bulk rock analysis, the peak of warmth during the mid Cretaceous (Cenomanian - Turonian) was followed by a slight cooling through the late Turonian to Santonian, a slight warming in the Campanian and a further cooling in the Maastrichtian (Frakes et al., 1992; Jarvis et al., 2006; Keller, 2008; Cramer et al., 2011; Linnert et al., 2014b; O'Brien et al., 2017). It is clear that the Late Cretaceous climate was much warmer than average Phanerozoic time but was a time of cooling from the super greenhouse worlds of the Cenomanian-Turonian, toward the K-Pg boundary. Generally, the Coniacian to Campanian sea level stayed relatively high for long periods until it began to decline gradually during the Maastrichtian (Haq, 2014). Figure 3 shows temperature and ice volume (reflecting sea level) reconstructions of Cramer et al. (2011) since the Early Cretaceous, with the study interval highlighted. These curves has been generated using geochemical data obtained from benthic foraminifera ($\delta^{18}O$ and Mg/Ca).

During the Late Cretaceous, Oman was located at a tropical palaeolatitude (van Hinsbergen et al., 2015) at the Northeastern margin of Arabia, along the Southwestern margin of the Tethys Ocean (Fig. 4). Late Cretaceous palaeogeography was characterised by a reduction of the total

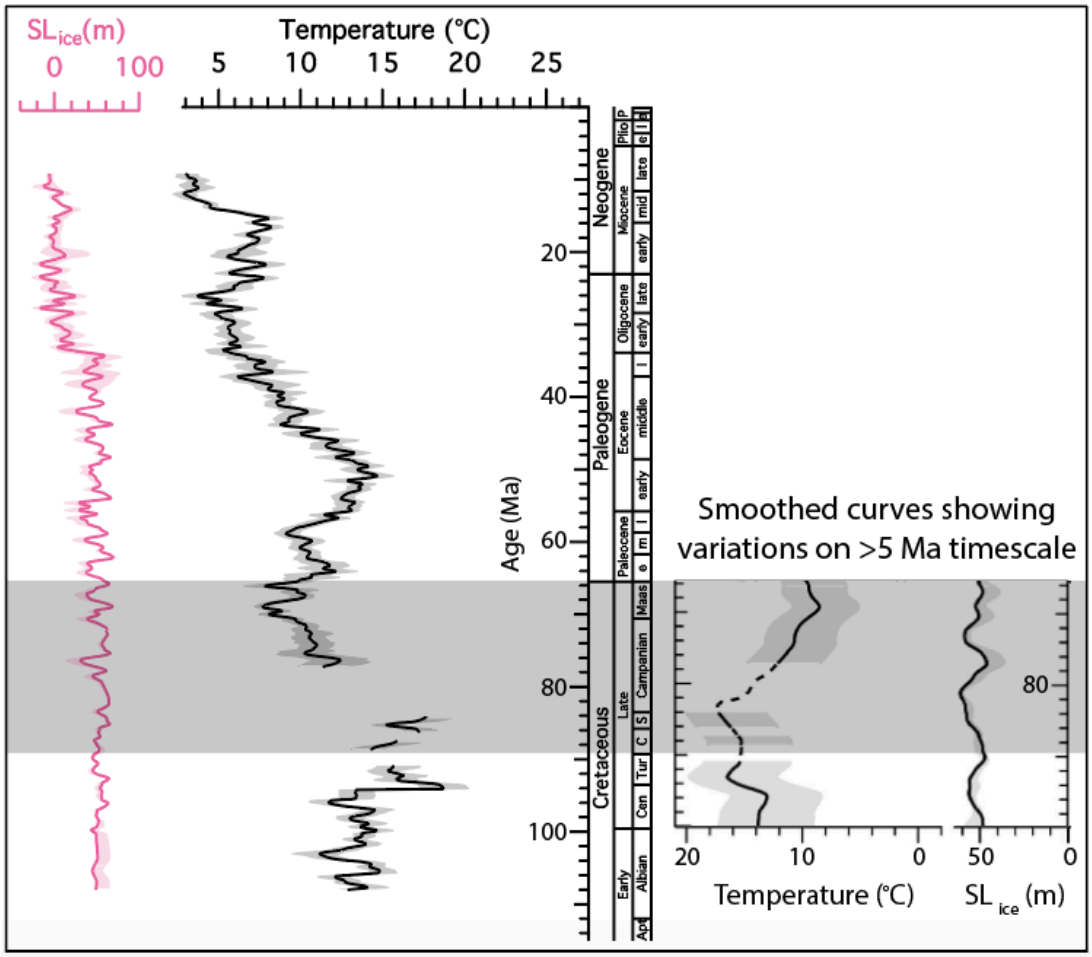

Figure 3. Temperature and sea level records of Cramer et al. (2011) with the Late Cretaceous interval highlighted.

land area due to submergence of large parts of the continents under shallow seas as a result of the global highstand (Torsvik and Cocks, 2016), and included Arabia as one of these partly submerged cratons through most of the Cretaceous (Fig. 4). The location of Arabia near the tropics during this time interval might suggest a relatively high nutrient influx into marginal basins due to increased tropical runoff and sediment delivery regime. Through this period, Arabia moved northward as far-field result of the opening of the South Atlantic after separation and divergence of Africa and South America (Ziegler, 2001).

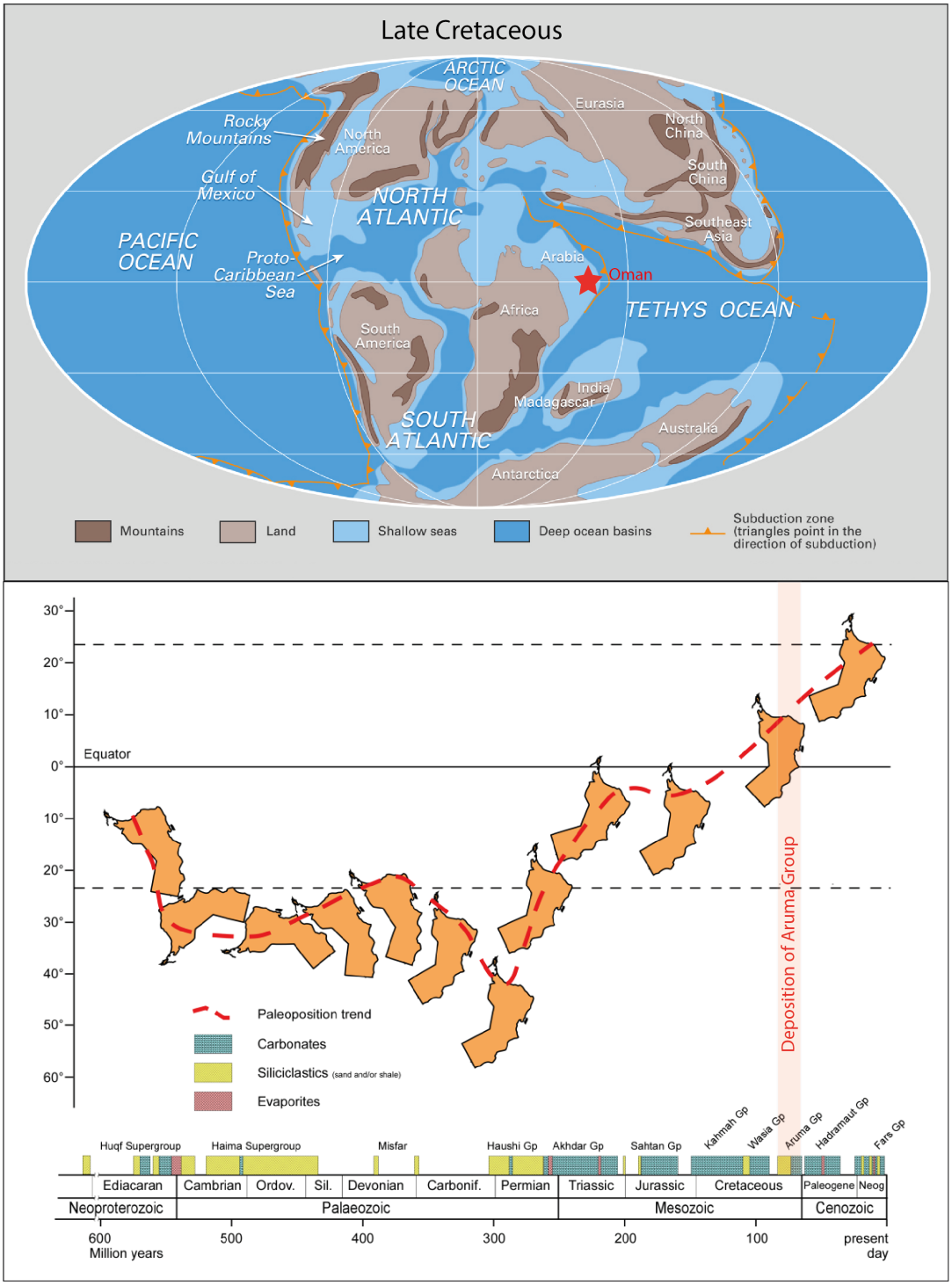

Figure 4. Location of Oman during the Late Cretaceous in a regional palaeogeographic map adapted from the Cretaceous maps of Encyclopaedia Britannica (https://www.britannica.com/science/Cretaceous-Period/media/142729/146755, last access: January 2019) and palaeolatitudinal positions of Oman throughout the geologic time (from Droste, 2012) with the palaeolatitude position of the study interval highlighted.

4 Calcareous Nannofossil Evolution, Biostratigraphy and Nannofossils Research in Oman

4.1 Late Cretaceous Nannofossil Evolution and Biostratigraphy

Calcareous nannoplankton are hemipelagic marine organisms distributed throughout the photic zone in a wide range of environments extending from the near-shore to the open oceans (Haq, 1998). Although not as specific in depth habitat as benthic microfaunas, calcareous nannofossils can be used to provide a quick general indication of palaeo-bathymetry, as the abundance and diversity of this group tends to increase basin-ward. Despite their distribution in wide range of marine environments, nannofossils are best preserved in fine-grained, low energy hemi-pelagic to pelagic deposits due to their tendency to wash out in higher energy environments, like for instance, turbidite or sand-dominated shelf systems which reduce the chance of their preservation in the rock record (e.g. Perch-Nielsen, 1989). Therefore, results are usually affected by the lithology studied. Diagenesis can also bias results by reducing the preservation of nannofossils as a whole, or through selective loss of fragile taxa (e.g. Roth, 1984). For instance, nannofossil dissolution can occur in organic-carbon-rich lithologies, as well as overgrowth and recrystallisation of nannofossils in carbonate-rich sediments as a result of burial diagenesis.

Global records of nannofossil diversity by Bown et al. (2004) show a diversity peak in the Late Cretaceous (Fig. 5). This peak started after the Turonian and continued toward the K-Pg boundary. Diversification through this interval has been linked to relative cooling within the warm Cretaceous climate and the associated sea level fall, increased nutrient cycling, greater provincialism and the evolution of endemic taxa (Bown et al., 2004; Keller, 2008). Figure 5

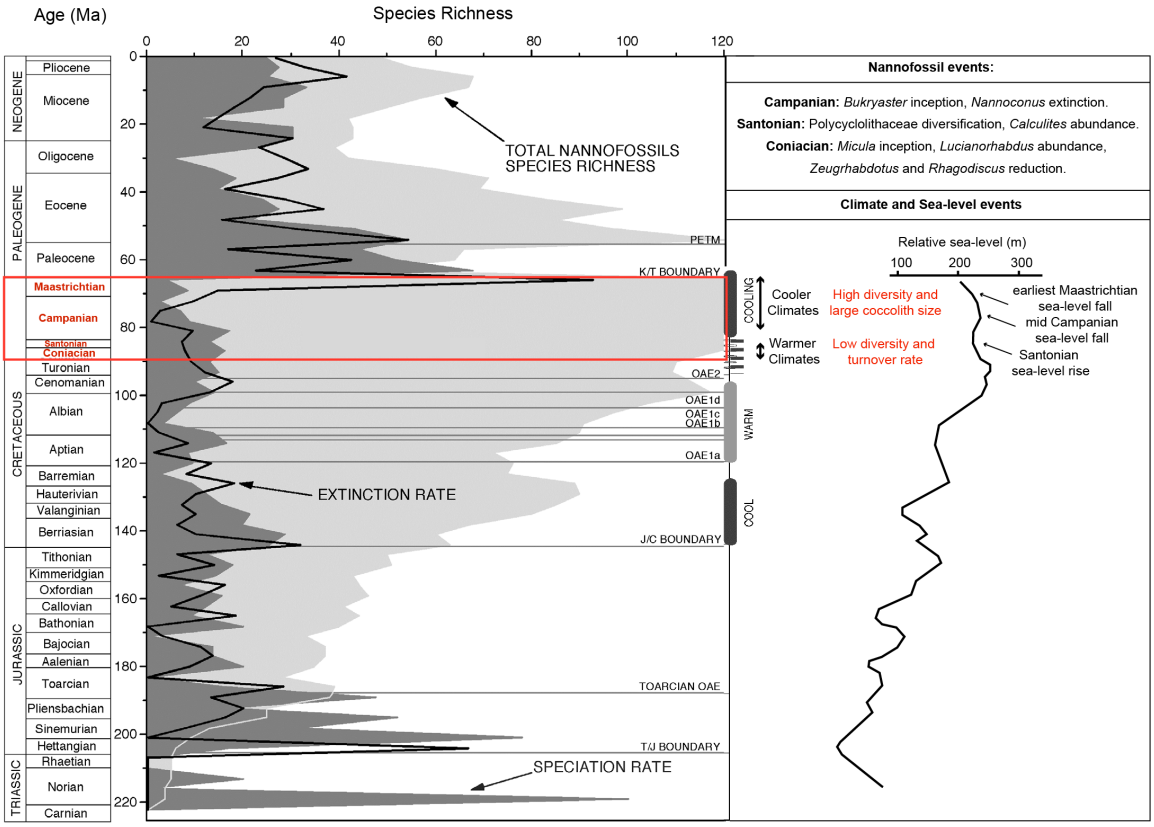

Figure 5. Nannofossil diversity (pale shading) with speciation rate (dark shading) and extinction rate (black line) correlated to climate and sea level events and main Late Cretaceous nannofossil events (from Burnett, 1998; Bown et al. 2004; Cramer et al., 2011).

summarises the main events in the nannofossil record from Burnett (1998) and Bown et al. (2004) with information from the climate and sea level records of Cramer et al. (2011). The main nannofossil groups that dominated the Cretaceous period are shown in Figure 6 with the interval of study highlighted.

Calcareous nannofossils have proven to be very useful for Jurassic to Pleistocene biostratigraphy. Given their very small size, generally < 30 µm (Bown and Young, 1998a), they allow investigation of small samples such as ditch cuttings and sidewall samples as well as non destructive sampling of core samples due to the small volume needed for analysis. Calcareous nannofossil analyses are thus one of the most useful tools for biostratigraphy

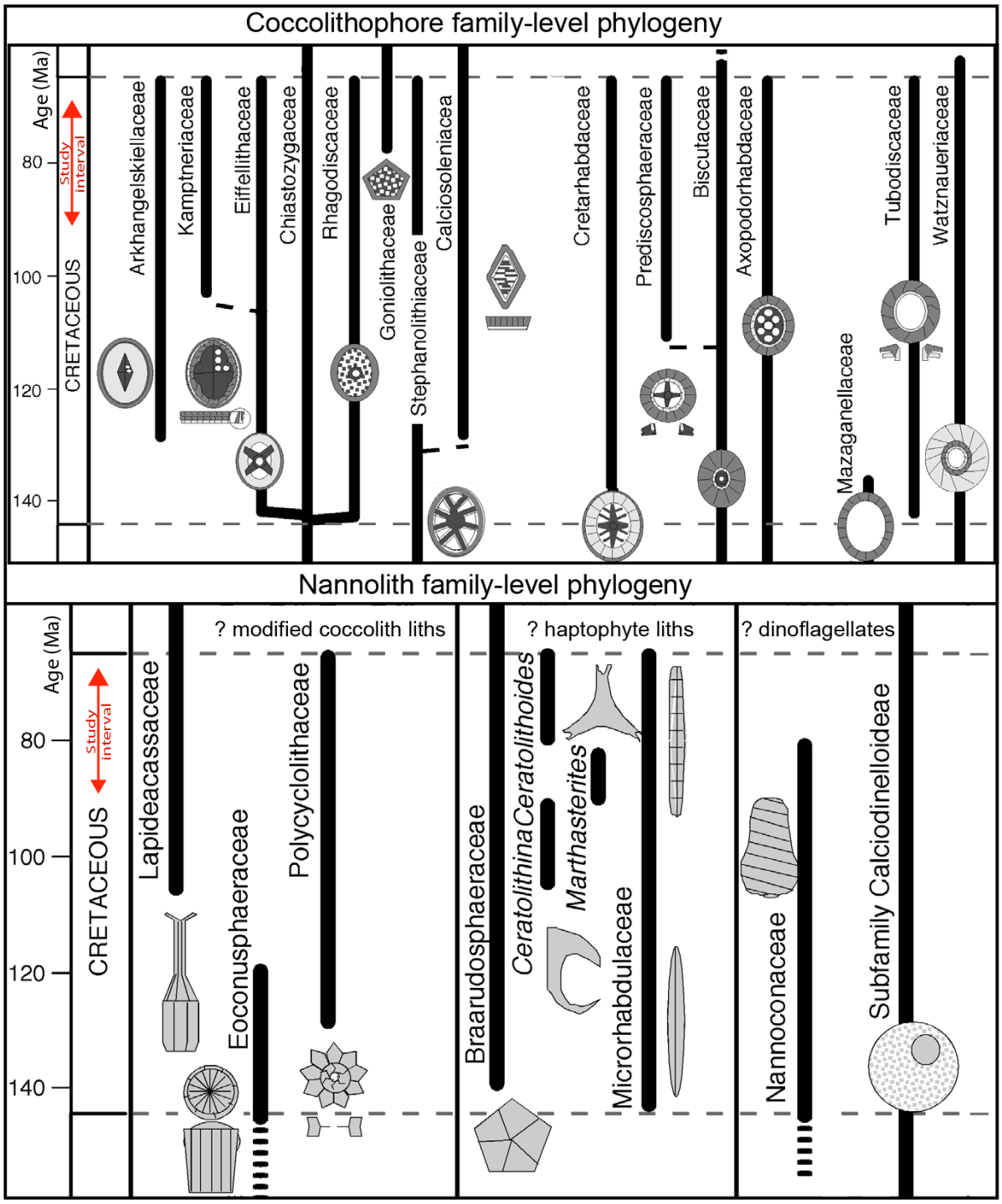

Figure 6. Coccolithophore and nannolith family-level phylogeny during the Cretaceous (from Bown et al., 2004).

available in the petroleum industry, where samples are usually expensive to collect and are available in limited quantities. Moreover, the relatively rapid rates of evolution within the calcareous phytoplankton and the presence of nannofossil-bearing sediments across nearly all

continents, allowed the development of detailed biostratigraphic age zonations for marine sediments (Gartner, 1977). The planktonic nature, and associated near cosmopolitan or at least wide-spread distribution of calcareous nannofossil taxa also provides a significant potential for worldwide correlation of marine sediments and allowed the development of global zonation schemes. For the Late Cretaceous, several zonation schemes have been developed including the CC zonation scheme by Sissingh (1977) that is modified further by Perch-Nielsen (1985) and the UC zonation scheme of Burnett (1998) which is followed in this study as being more comprehensive, including bioevents from different palaeolatitudes and biogeographic provinces across oceanic and shelf settings, including distinctive bioevents for the Tethyan Realm.

4.2 Nannofossils Research from the Jurassic to Neogene Subsurface Strata of Oman

Analyses of calcareous nannofossils from the Jurassic to Neogene sequences of Oman are very limited. Here, previous biostratigraphic work and its significance for age dating of subsurface formations and correlation of hydrocarbon wells is discussed, as well as the further potential application of nannofossil analyses as a fast and cost-effective biostratigraphic tool.

The Jurassic Sahtan Group (Fig. 7), a sequence of clastic deposits at the base and shallow marine carbonates at the top, is dated using microfaunal and palynological schemes as late Aalenian to early Tithonian (Forbes et al., 2010). Due to the dominance of shallow marine carbonate facies, the applicability of nannoplankton biostratigraphy is very limited. Woollam et al. (1999) analysed several samples from the Hanifa/Jubaila and Tuwaiq Mountain Formations of the Sahtan Group, which yielded poorly preserved, low diversity nannofossil assemblages, on the basis of which it was not possible to assign a biozone.

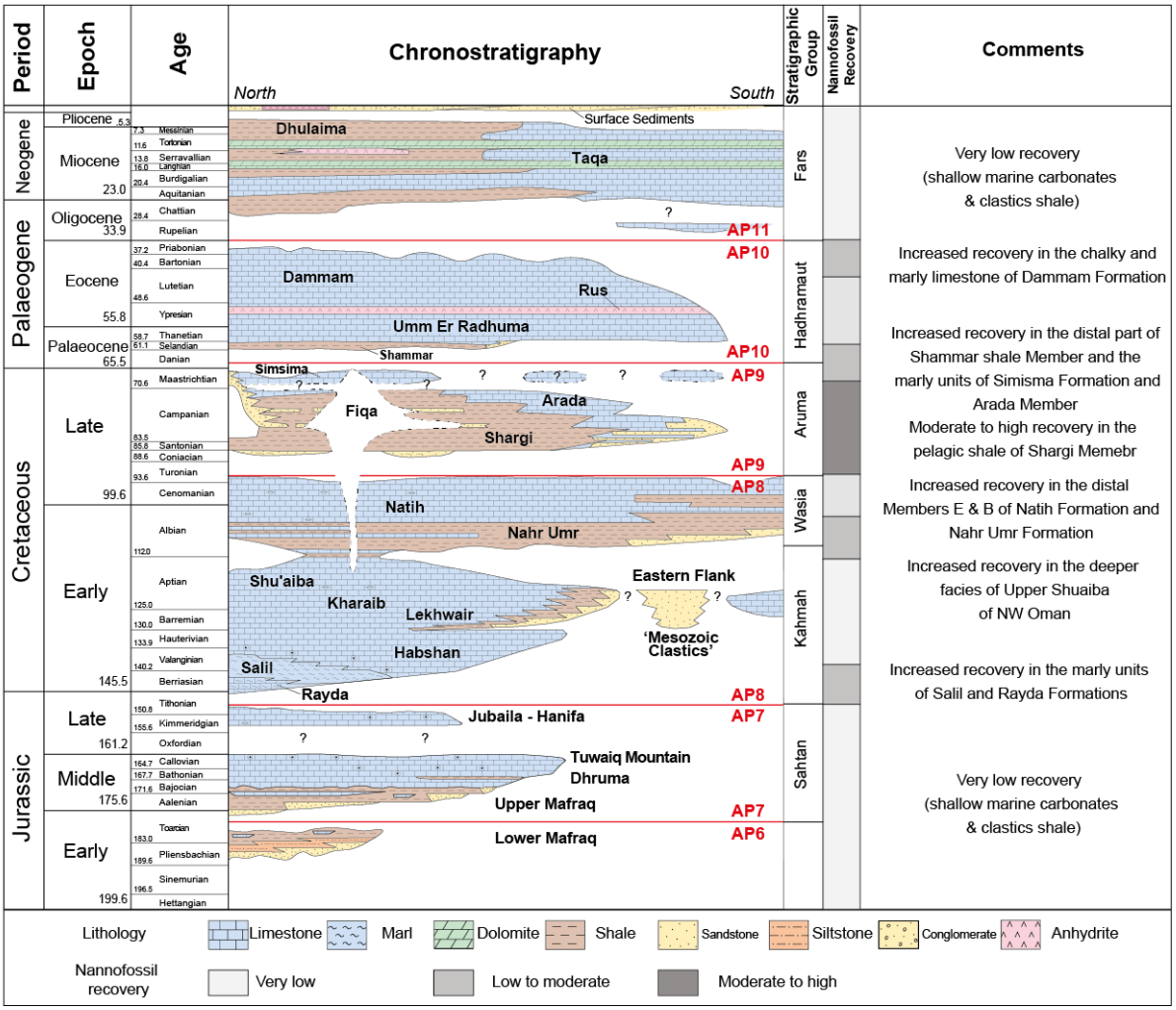

Figure 7. Summary of the chronostratigraphy (from Forbes et al., 2010) and nannofossil recovery in the Jurassic to Neogene subsurface geology of Oman. AP6 to AP11 are the tectono-stratigraphic megasequences of the Arabian Plate.

The thick carbonate sequences of the Upper Jurassic to Lower Cretaceous Kahmah group (Fig. 7) are dated based on microfossils as upper Tithonian to upper Aptian (Forbes et al., 2010). Nannofossil biostratigraphy provided useful age control for the sediments of the Aptian Upper Shuaiba Member in the Bab Basin of northwestern Oman, although these sediments are only known from sporadic core material in Oman (e.g. van Buchem et al., 2002; Gombos et al., 2008; Packer and Starkie, 2008). Calcareous nannofossils have also been

recovered from, and used for the stratigraphy of the lowermost Cretaceous Formations of Oman, especially the marly units of the Salil and Rayda Formations which show moderate to good recovery of nannofossils (e.g. Sikkema, 1991; Woollam et al., 1999; Packer and Starkie, 2005). The carbonate Kharaib, Lekhwair, and Habshan Formations are either barren of calcareous nannofossils or show very poor recovery, as are the shale units within these carbonates (Booth, 2015), which may be the result of diagenesis.

The Mid-Cretaceous Wasia Group (Fig. 7) has been dated using foraminifera as uppermost Aptian to middle Turonian with many uncertainties remaining (Forbes et al, 2010). Application of nanofossil biostratigraphy is limited to the shale units within the predominantly shallow marine carbonates of the Natih Formation; i.e. Natih B, Natih D and basal part of Natih E Members (Varol, 1996; Jacovides and Varol, 2000 and Packer, 2004). Nannofossil recovery within these shale units is highly variable which could be the result of local diagenetic effects. In the Nahr Umr Formation, nannoplankton may provide good facies independent markers; however the recovery appears to be highly variable and locally inconsistent as the lithology is highly affected by terrestrial input reducing the chance of nannofossil recovery (Packer et al., 2004). If improved, nannofossil dating could provide new constraints on the currently uncertain age dating of these Formations.

The Coniacian to Upper Maastrichtian Aruma Group (Fig. 7) has been dated based mainly on planktonic foraminifera (Forbes et al. 2010). The applicability of nannofossil biostratigraphy is high in the Fiqa Formaion of this study, especially in the deep marine shales of the Shargi Member but lower in the shallow marine carbonates of the Arada Member and the Simsima Formation.

The Paleocene-Eocene Hadhramaut Group (Fig. 7) is dated based on large benthic foraminifera as Selandian to Priabonian (Forbes et al., 2010). A nannofossil zonation has been achieved by Packer and Starkie (2008) in the chalky and marly limestone of Dammam Formation from one hydrocarbon well in South Oman. Application of nannofossil biostratigraphy is very limited in the evaporite and carbonate sequences of the Rus Formation and in the shallow marine carbonates of Umm Er Radhuma Formation, which are lithologies unfavourable to nannofossil preservation, but could be applied in the deeper marine shales of the Shammar Member of basal Umm Er Radhuma Formation.

The Oligocene to Miocene Fars Group (Fig. 7) is dated based on large benthic foraminifera as Chattian to Messinian (Forbes et al., 2010). The applicability of nannoplankton biostratigraphy in this group is very low due to the deposition in a shallow marine environment with high clastic input, that is sometimes restricted to reefal and lagoonal settings. Limited nannofossil analyses have been carried out and show very little to no recovery (Packer et. al., 2004; Packer and Starkie, 2008).

From the formations discussed above (see Fig. 7), it is clear that nannofossil recovery is highly affected by lithology (Fig. 8), which is directly related to the depositional setting of the formations (Fig. 9). The distribution and abundance of nannofossil in the subsurface stratigraphy of Oman changes between continental shelf, slope, and oceanic depositional settings. It tends to be very low toward the land and low toward the sea in back barrier to inner shelf deposits (e.g. the carbonates of Sahtan, Kahmah, Wasia, Hadhramaut and Fars Groups). It becomes moderate to rich in outer shelf deposits (e.g. Salil and Rayda Formations, upper Shuaiba Formation of northwest Oman, Natih E and B members, parts of Arada

Member and Simsima Formation, Shammar Member and Dammam Formation) and abundant to super abundant in intra basinal settings (e.g. Shargi Member) (Fig. 7). As discussed above, due to the lithological restrictions, nannofossil recovery depends on the palaeogeographic position of the well, i.e. distal wells yield better nannofossil recovery than proximal wells (e.g. Varol, 1996). Nannofossil recovery may still be sporadic in distal wells due to the effects of diagenesis. Therefore, nannofossil biostratigraphy can be applied with the best results to open marine, basinal deposits rather than to shelf

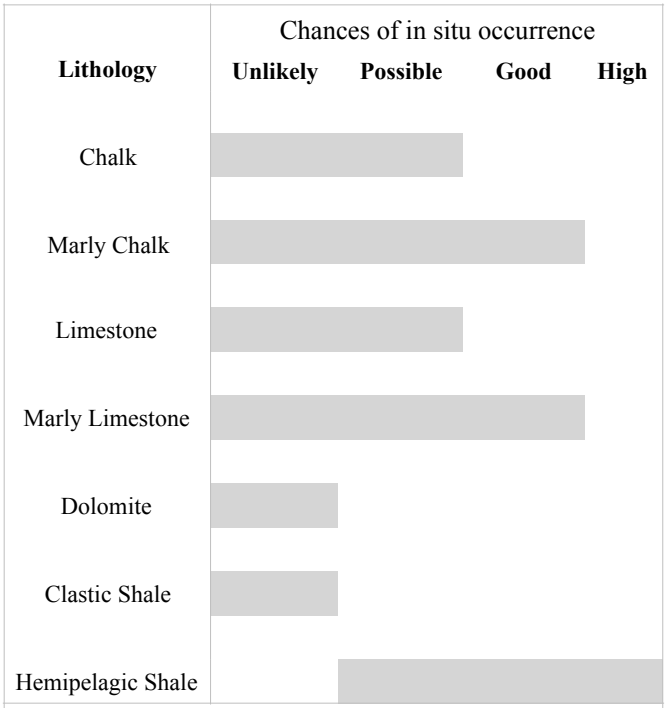

Figure 8. Chances of in situ occurrence of nannofossils in different lithological units as seen in the subsurface formations of Oman.

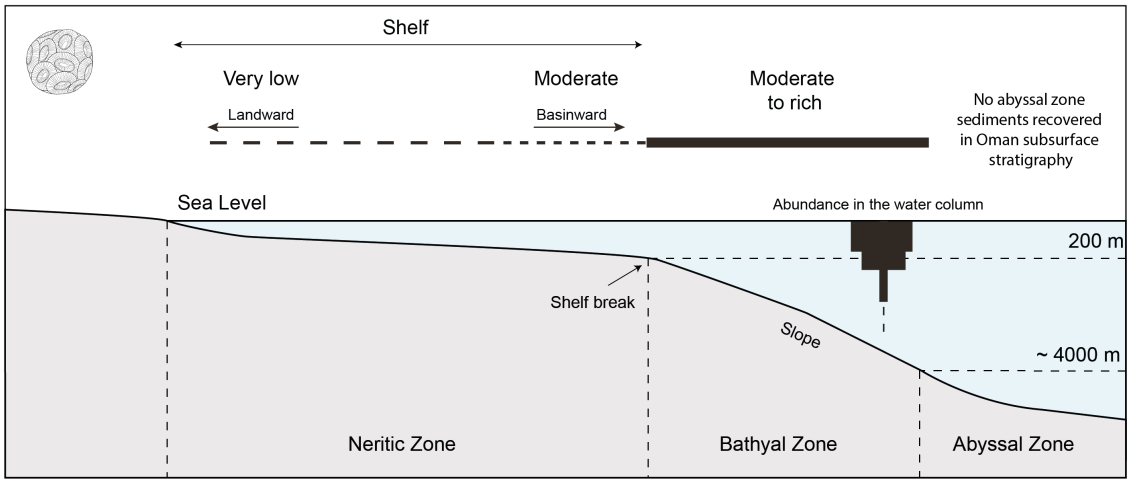

Figure 9. Palaeo-bathymetric distribution model of nannofossils as observed in the Cretaceous to Palaeocene rock units of Oman.

carbonates which characterise most of the stratigraphy of Oman. However, nannofossil biostratigraphy is highly applicable to some of the key subsurface hydrocarbon-related units, especially the Fiqa Formation which forms the main Cretaceous seal unit and hosts potential stratigraphic traps. Moreover, the study of nannofossils in Cenozoic units could provide promising results for improving the understanding of the Cenozoic hydrocarbon plays.

5 Research Methodology

This study includes the analysis of 341 cutting, sidewall core and core samples from 11 hydrocarbon exploration wells. These include 11 cuttings, 8 sidewall cores and 1 core from W-1, 17 cuttings from W-2, 10 cuttings from W-3, 17 cuttings and 33 sidewall cores from W-4, 35 cuttings and 9 cores from W-5, 22 cuttings from W-6, 30 cuttings from W-7, 24 cuttings from W-8, 13 cuttings from W-9, 11 sidewall cores from W-10 and 8 cuttings from W-11 (Figs. 1, 2). A total of 657 nannopalaeontological and geochemical analyses has been undertaken on these samples (see appendix A for different analysis performed on the samples).

The selection of the wells is based on the availability of samples in PDO samples stores as well as the availability of additional geological data such as completion logs, gamma ray logs, geological and microplalaeontological reports for the selected intervals of the Fiqa Formation. Given the availability of samples and geological data, the wells are then chosen to cover different palaeobathymetric positions of the basin (shallow to deep marine settings). The sampling strategy for each well is generally limited by the availability of samples but aim to stratigraphically cover both the carbonate-dominated Arada and the shale-dominated Shargi Members of the Fiqa Formation with a focus on the top and base of the formation, as well as

the transition from the Arada to Shargi Members where highest sampling resolution is obtained (sampling resolution ranging from 1 m to more than 50 m depending on samples availability; Fig. 2). The samples are predominantly grey to green hemipelagic shale with some silty/ sandy shale samples and carbonate dominated samples ranging from marly shale to chalk and limestone. The majority of available samples are washed cuttings, which are cutting samples that have been washed with water in order to remove any drilling mud residue to avoid erroneous results especially for the geochemical analysis of bulk rock sediments.

Generally, cutting samples are used with caution for micropalaeontological analyses in the petroleum industry due to high probability of caving (fall of cuttings from the borehole wall into deeper intervals during drilling) and therefore affect the accuracy of bioevent base occurrences that could be extended downhole to older intervals. Given that the majority of available samples are cuttings and in order to reduce the possible effects of caving in this study, only the dominant lithology in each bag of cutting samples is selected. Moreover, cuttings which are distinctively larger than the dominant size of cuttings, as well as cuttings with distinct elongate or concave shape has been avoided as they can be mechanically caved from upper intervals during drilling. Analysis of some core and sidewall core samples as well as knowing the location of casing points (casing and cementing of the overlying borehole wall so that no further cuttings are caved into deeper intervals below the casing point) also helped to control the potential effects of caving (location of casing points for each well is illustrated in the charts of digital appendix 1).

The samples are prepared as simple smear slides following the technique of Bown and Young (1998b). Small amount of sample is mounted over glass microscope slide, gently crushed, mixed with water and evenly spread with flat-sided toothpick creating stripped effect with

thicker and thinner areas to allow recognition of smaller and larger fractions of the taxa present in the assemblage. The samples are then examined under the light microscope at 1000× and 1250× magnifications. The cascading count technique of Styzen (1997) is used to count the nannofossil species present in the samples. This technique is selected and used in this study as being one of the most representative counting methods for providing an estimate of the overall nannofossil assemblage composition in a 100 fields of view (FOV), allowing the recognition of both large and small taxa, as well as abundant and rare taxa.. All taxa are counted in the first 10 FOV, and the number of species that reaches more than 10 occurrences are multiplied by x10 and are not counted further. The remaining taxa are counted in the next 40 FOV and the species that reach more than 10 occurrences are multiplied by x5 in the second 10 FOV, by x3.33 in the third 10 FOV, by x2.5 in the forth 10 FOV and by x2 in the fifth 10 FOV. Rarer taxa are continued to be counted in the remaining 50 FOV.

6 Thesis Overview

The thesis is based on three main chapters which are respectively, published, submitted for publication in peer-reviewed journal and in a publishable format. The first two chapters are co-authored with the main supervisor of the project - they were both written by me with guidance from my supervisor. Data collection, sample analyses and interpretation was solely undertaken by me, under the supervision of the second author. The thesis (Fig. 10) is outlined as follows:

Chapter 1 is an introduction; **Chapter 2** is a modified form of a published paper about nannofossil taxonomy and broad scale assemblage change; **Chapter 3** is a detailed biostratigraphic study using nannofossil assemblages, compared to previous biostratigraphic

zonations and its application to sequence stratigraphy; **Chapter 4** is a study of the palaeoenvironmental evolution of the basin based on nannofossil assemblage and bulk rock geochemical data; **Chapter 5** is a summary, conclusions and recommendations for future work.

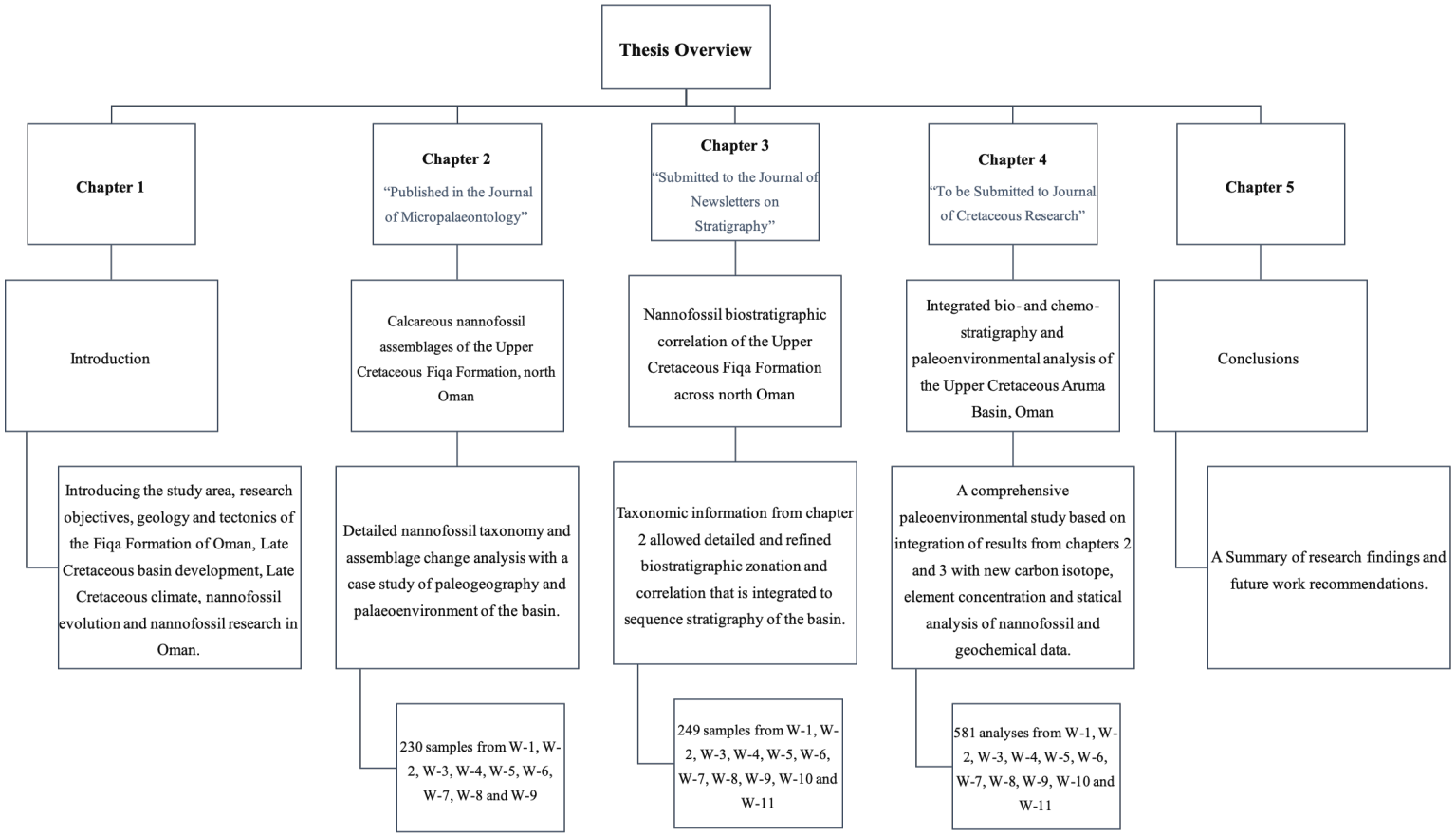

Figure 10. Summarised overview of the thesis.

CHAPTER 2

CALCAREOUS NANNOFOSSIL ASSEMBLAGES OF THE UPPER CRETACEOUS FIQA FORMATION, NORTH OMAN

(A version of this chapter is published in the Journal of Micropalaeontology. Co-author: Tom Dunkley Jones. Data collection, sample analyses, data interpretation and writing of the paper have been undertaken by Zainab Al Rawahi under the guidance and supervision of Tom Dunkley Jones. Detailed documentation of the nannofossil and microfossil assemblage composition for each well is available in the attached digital appendix 1)

Abstract. This study presents the first detailed calcareous nannofossil assemblage data from the Upper Cretaceous succession of the subsurface Aruma Basin, North Oman. The taxonomic description and documentation of assemblage composition are based on extensive quantitative analysis of ditch cuttings and side-wall samples from nine hydrocarbon exploration wells across North Oman. The samples studied from those wells cover the Coniacian to lowermost Maastrichtian deep marine shales and marls of the subsurface Fiqa Formation. These fine-grained siliciclastic deposits often yield moderately to well-preserved nannofossil assemblages, especially in the Campanian intervals. Consequently, diverse assemblages have been recorded from the Fiqa Formation, with a total cumulative diversity of 200 species, including two new species, *Staurolithites ormae* sp. nov. and *Chiastozygus fahudensis* sp. nov., which are illustrated and described. Extensive imaging of this diversity is provided here, as are stratigraphic distributions of the main components from a key reference well in north Oman, W-4. Poorly described groups such as *Staurolithites* are closely investigated and their utility for stratigraphic applications is highlighted. Relative abundances of nannofossil taxa

with strong palaeoenvironmental preferences have revealed new insights into the palaeo-productivity of the basin. High-fertility species like *Discorhabdus ignotus*, *Biscutum constans* and *Zeugrhabdotus erectus* show substantial variations in abundance throughout the Fiqa Formation, reflecting long-term shifts in the productivity conditions of the basin. This is supported by abundance patterns of *Watznaueria barnesiae* and *Micula staurophora* that show a broadly inverse correlation with the high-fertility species. The Fiqa Formation represents a key regional seal unit for the Cretaceous hydrocarbon reservoirs of Oman, as well as being a productive unit elsewhere in the Arabian Peninsula. Beyond the Aruma Basin of Oman, this study will provide a key reference point for future biostratigraphic or palaeoenvironmental analyses of the Late Cretaceous calcareous nannofossil assemblages across the Middle East and other southern Tethyan areas.

1 Introduction

The Fiqa Formation sensu Hughes Clark (1988) and Forbes et al. (2010) in the subsurface of northern Oman provides a unique window into truly hemipelagic, Late Cretaceous ecosystems of the Arabian Peninsula. Deposited through ~15 Ma, from the Coniacian to earliest Maastrichtian, it consists of very thick sequences of marls and shales, interpreted as representing deposition in a deep marine setting within a foreland basin developed in the north of Oman (Glennie et al., 1974). These sediments often yield well-preserved and abundant hemipelagic microfossils, including calcareous nannofossils, that have great potential for environmental, evolutionary and biostratigraphic studies. The Fiqa Formation and its equivalents across the Arabian Peninsula are key regional seals for Lower to middle Cretaceous hydrocarbon reservoirs. These units are also hydrocarbon productive in some localities. The rich nannofossil

recovery within the Fiqa Formation has the potential to resolve some of the subsurface stratigraphic complexities related to regional correlations within a thick and homogeneous yet assumed diachronous lithology by providing a higher-resolution correlation between different hydrocarbon wells. Past unpublished industry studies have touched on these applications, but generally have focused on stratigraphically or spatially limited well-to-well correlations (e.g. Lauer, 1973; Sissingh, 1974; Prins and Roersma, 1983; Varol, 1996, 1997). None of these unpublished reports describe the calcareous nannofossil assemblage composition, provide extensive images, or integrate their findings into a regional or global context such as the globally applied zonation schemes of Sissingh (1977), Perch-Nielsen (1985) and Burnett (1998). Although substantial micropalaeontological analyses associated with hydrocarbon exploration activity have also been undertaken in the region for more than 40 years, the vast majority of this work and data remains unpublished in industry reports.

The few available published studies of Late Cretaceous calcareous nannofossils in the Middle East are limited to biostratigraphic applications. This includes the biostratigraphic study of Coniacian–Maastrichtian chalky and marly sequences of Lebanon by Müller et al. (2010) in which they provided a brief description of the nannofossil markers used for biostratigraphic subdivision as part of a general revision of the Cretaceous and Cenozoic stratigraphy of the country. Other nannofossil biostratigraphic studies include the upper Campanian–Maastrichtian upper Mahara group of Yemen (Al-Wosabi and Alaug, 2013), the upper Santonian to Maastrichtian Abu Roash and Khoman formations in the northwestern desert of Egypt (Mandur, 2016), the Coniacian to Maastrichtian Themed and Sudr formations of Sinai, Egypt (Faris and Abu Shama, 2006; Farouk and Faris, 2012), and the upper Campanian to lower Maas-

trichtian Shiranish Formation of NE Iraq (Farouk et al., 2018a). In Iran, Late Cretaceous nannofossil biostratigraphy has been studied by several authors, but the most detailed studies were achieved by Razmjooei et al. (2014), Foroughi et al. (2017) and Razmjooei et al. (2018) for the Gurpi and Abtalkh Formations of South and North Iran, respectively, in which nannofossil biozonations were developed for the studied sections. All of these studies mostly focus on solving stratigraphic problems like age constraint and hiatus recognition, whereas very little information is published on assemblage composition, their changes through time or their potential palaeoenvironmental significance.

The Late Cretaceous epoch was one of the warmest periods of the Phanerozoic with a global sea level that was 100 ± 50 m higher than today (Miller et al., 2005). The sea level record of Cramer et al. (2011) indicates a relatively high sea level throughout the Coniacian to Maastrichtian with minor variations, like the increase in sea level during the Santonian and sea level drop during the mid-Campanian, Campanian–Maastrichtian boundary and toward the end Maastrichtian. Global compilations of benthic foraminiferal oxygen-isotope ($\delta^{18}O$) data by Friedrich et al. (2012) indicate conditions of peak warmth close to the Cenomanian–Turonian boundary, with warm, yet relatively cooler climates persisting into the Coniacian and Santonian. In the early Campanian, benthic foraminiferal $\delta^{18}O$ compositions shift to more positive values by over 1 ‰, indicating a significant (> 4 $^{\circ}C$) cooling of high-latitude oceans (Friedrich et al., 2012). The best available long-term records of ocean surface temperatures through this interval also indicate substantial cooling, of a similar magnitude, through the Campanian (Linnert et al., 2014b).

The Late Cretaceous is associated with an acme in calcareous nannofossil diversity. The detailed record of Cretaceous nannofossil diversification by Bown et al. (2004) shows a diversity peak after the Turonian that continued until the mid-Maastrichtian before it began to decline toward the K–Pg boundary. The highest diversity is recorded in the Campanian, a time that is also marked by large coccolith size, a characteristic feature that continued until the mid-Maastrichtian. Compared to the Campanian diversification, the Coniacian and Santonian are characterised by low diversity and a low turnover rate (Burnett, 1998). Bown et al. (2004) suggest that cooling within a greenhouse-mode climate system (e.g. Campanian–early Maastrichtian cooler climates) may have stimulated diversification via greater differentiation of the photic zone environment, biogeographic partitioning and increased numbers of endemic taxa at both low and high latitudes. Keller (2008) also related the increased diversity of microfossil and nannofossil groups during the Cretaceous cooling periods to increased weathering, runoff, upwelling and nutrient cycling, while more stable diversity is associated with high sea levels during the warmest Cretaceous intervals (e.g. Turonian-Santonian).

During the Late Cretaceous, deposition of the Fiqa Formation occurred on the northeastern margin of the African– Arabian plate at an equatorial palaeolatitude in the eastern Tethys. The detailed documentation of calcareous nannofossil assemblages at this location thus also fills a gap between the austral and western Tethys provinces. Given the quality of preservation and stratigraphic continuity of nannofossil assemblages from the Fiqa Formation, they will be important for future assessments of Late Cretaceous provincialism. The temporal coverage provided by the Fiqa Formation, from the Coniacian to earliest Maastrichtian, and the quality of preservation of truly tropical calcareous nannofossil assemblages, also has the potential to

constrain patterns of tropical diversity. Such data will help to address the question of whether the continued rise in global diversity is primarily driven by the diversification of mid- to high-latitude flora through the Late Cretaceous.

This paper aims to address a number of the questions outlined above by providing the first detailed study of calcareous nannofossil assemblages through the Late Cretaceous Fiqa Formation. The excellent preservation within the formation includes some rarely reported and poorly documented Late Cretaceous taxa. The quality of this preservation provides the basis for further application of these assemblages for biostratigraphic and palaeoenvironmental interpretations. It is the aim of this paper to provide a first overview of the taxonomy and broad patterns of calcareous nannofossil assemblage change through the Fiqa Formation. The paper will also provide a key reference point for other studies of Late Cretaceous nannofossil assemblages across the Middle East and other southern Tethyan areas.

2 Depositional Setting of the Fiqa Formation

In North Oman the carbonate platform that had developed on a passive continental margin during the Early Cretaceous was progressively flooded during Coniacian times, which resulted in the deposition of extensive deep marine shales and marls of the Fiqa Formation in a foreland basin setting (Glennie et al., 1974) referred to as the Aruma Basin. This basin formed as a result of crustal loading associated with over-thrusting and emplacement of oceanic crust known as the Sumail ophiolite and other associated sheets onto the eastern margin of the Arabian Peninsula (Bechennec et al., 1990). This occurred as a result of a major compressional tectonic phase associated with the closure of the Neotethys Ocean (Lippard et al., 1986). The basin was deeper proximal to the thrusted sheets in the north and west of Oman and shallowed

toward the southeast as seen from seismic and well data (Forbes et al., 2010). Using the palaeolatitude calculator method of van Hinsbergen et al. (2015), the basin was located at a tropical palaeolatitude during the time of deposition, which is consistent with regional palaeogeographic reconstructions (Fig. 1).

The subsurface Fiqa Formation is part of the Upper Cretaceous Aruma Group of Oman and is widespread throughout Oman, reaching a thickness of more than 1 km in the northwest (Boote et al., 1990). It is separated into lower shale-dominated facies of the Shargi Member and upper carbonate-dominated facies of the Arada Member (Forbes et al., 2010) (Fig. 2b). The formation is thicker and predominantly hemipelagic shale in the north, thinning and changing into shallower marine facies to the south and southeast of Oman (Forbes et al., 2010) (Fig. 2c). In the northern Oman mountains (known as the Al-Hajar Mountains), the time equivalent lithostratigraphic units to the subsurface Fiqa Formation are the local, nearshore facies mapped as the Muti Formation, Juweiza Formation and Qahlah Formation (Glennie et al., 1974). These formations were deposited at the northern margins of the basin in close proximity to the advancing thrust sheets (Robertson, 1987). The Juweiza and Qahlah formations are also referred to the subsurface clastic-dominated intervals proximal to the Oman mountains (Fig. 2c). The Fiqa Formation is chronostratigraphically correlated with the Gurpi Formation southeast of the Zagros Mountains of Iran, the Aruma Formation in Kuwait and Saudi Arabia, and the Aruma Formation and the Fiqa Formation of the United Arab Emirates (Ziegler, 2001) (Fig. 2a).

Some of the first published foraminiferal biostratigraphy work assigned an age of Santonian to Campanian to the Fiqa Formation (e.g. Glennie et al., 1974). The micropalaeontological

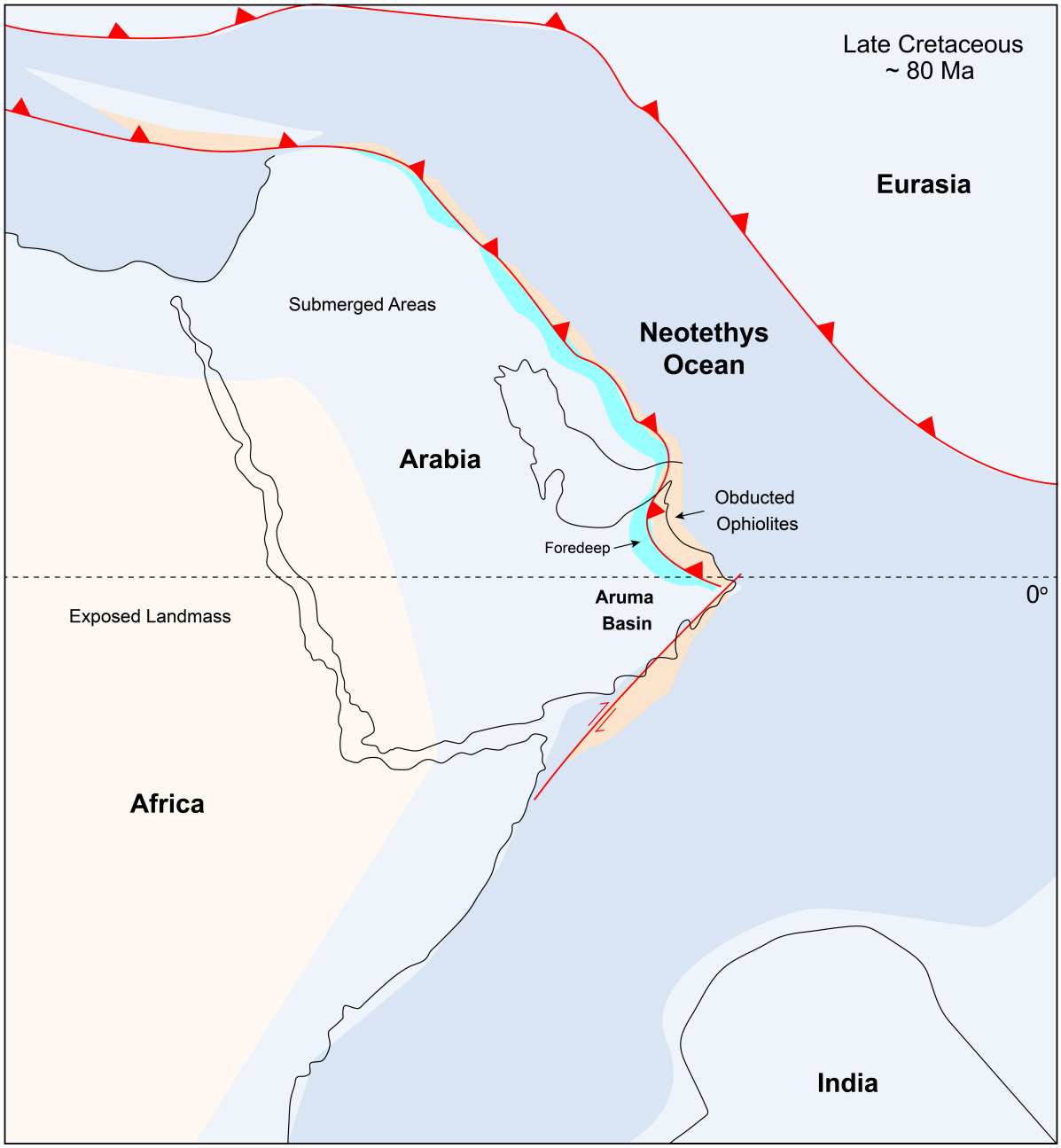

Figure 1. Palaeoceanographic and tectonic reconstruction of Arabia showing the location of the Aruma Basin. Modified from Barrier and Vrielynck (2008) with information from van Hinsbergen et al. (2015).

facies have since been extensively studied for exploration purposes, with the most recent age assignment of late Coniacian to late Campanian based on the local planktonic foraminiferal zonation schemes of Sikkema (1991), revised by Osterloff et al. (2001) and Packer (2002). Micropalaeontological analysis from northern Oman by Packer (2002) indicates a neritic envi-

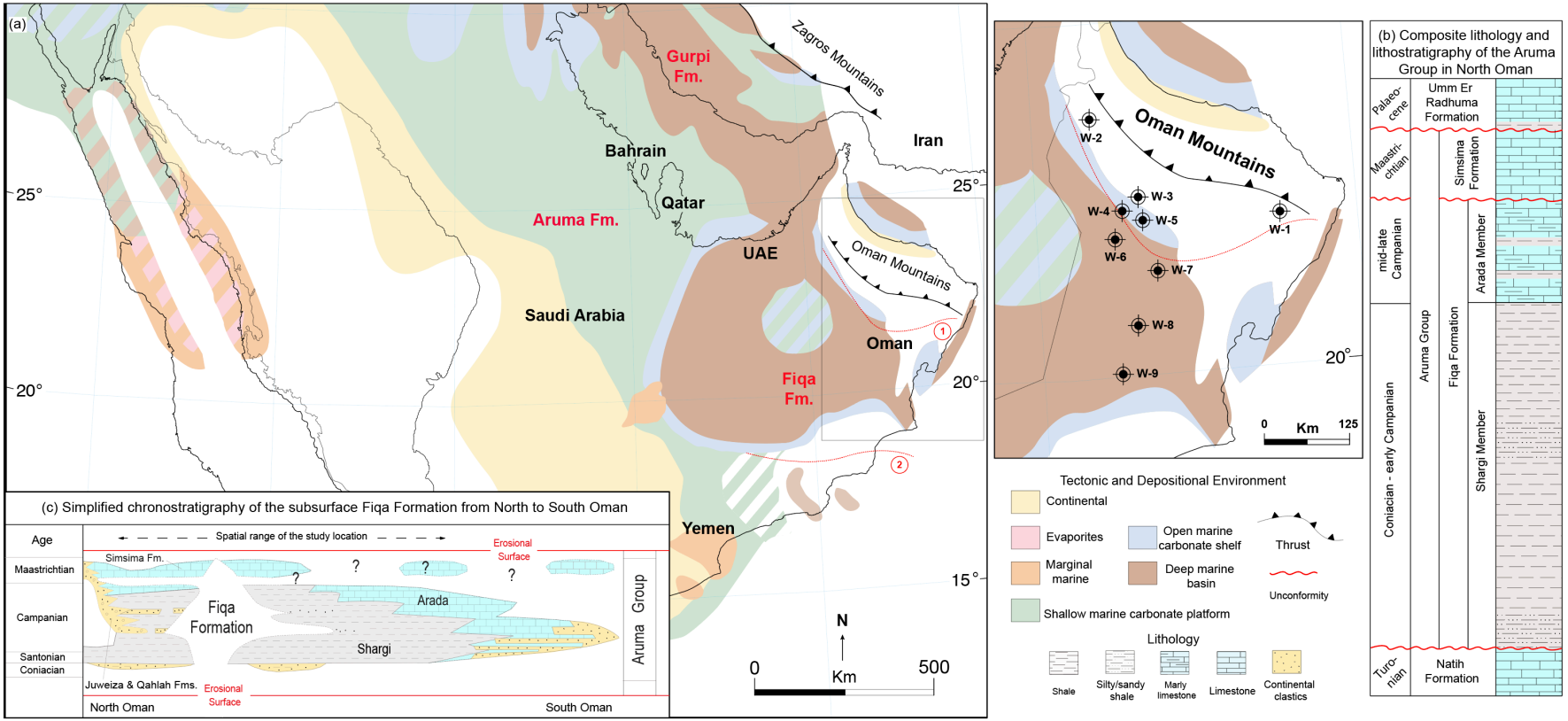

Figure 2. (a) Location of the study wells in a regional palaeofacies map of the Late Cretaceous (modified after Ziegler, 2001) showing the deposition of the Fiqa Formation and its equivalents (Gurpi and Aruma formations): (1) outline of the foredeep part of the basin in North Oman; (2) extent of the Aruma Basin in Oman. (b, c) Lithology, lithostratigraphy and chronostratigraphy of the Aruma Group in Oman (adapted from Forbes et al., 2010).

ronment developed during the deposition of the Fiqa Formation within the early stages of foreland basin development. It deepened into upper to middle bathyal settings with rapid rates of sediment deposition during most of the Santonian to middle Campanian. These deep marine conditions were interrupted by several episodes of shallowing of sea level. During most of the late Campanian to Maastrichtian, sea level continued to fall with a generally high- energy, shallow marine environment developing over most of North and interior Oman.

3 Material and Methods

The study is based on the quantitative analysis of 230 subsurface samples provided by the Petroleum Development Oman (PDO) from the Upper Cretaceous Fiqa Formation. Samples included ditch cuttings and side-wall cores from nine hydrocarbon exploration wells from North and Central Oman (Fig. 2a). Samples were prepared as simple smear slides following the standard technique of Bown and Young (1998b). The cascading count technique of Styzen (1997) is followed using 100 fields of view. Species observation and description are based on light microscopy in cross-polarised and phase-contrast light using a Zeiss Scope.A1 at 1250× magnification and GXM-XPLPOLTEC-2 at 1000× magnification. Digital images were captured with Q-imaging and GXCAM-U3-5 cameras using QImaging and ToupLite softwares. All of the samples have been used to identify and image taxa and to understand the general patterns of assemblage change; one reference section from North Oman, W-4, is used here to provide a more detailed description of the changing nannofossil assemblage composition observed through the Fiqa Formation and its potential palaeoenvironmental and palaeogeographic applications. The total number of samples analysed from W-4 is 50. An additional 91 samples from W-4 are analysed for element concentrations using X-ray fluorescence (XRF).

Samples are prepared as pressed pellets following the method of Takahashi (2015) and analysed using a Bruker S8 TIGER WDXRF elemental analysis system. Calcium weight percentage is presented in this study. Details on samples preparation, counting technique, sampling strategy and resolution and samples number and type for each well are available in Chapter 1 (see Chapter 1; Sect. 5 and Figs. 1-2).

4 Results

4.1 Stratigraphic Age

Based on calcareous nannofossil biostratigraphy (Al Rawahi and Dunkley-Jones, unpublished data) (see Chapter 3) the studied Fiqa successions span the late Coniacian to late Campanian nannofossil Zones UC11 to UC16 and possibly the earliest Maastrichtian UC17 nannofossil zone of the Burnett (1998) scheme for the Tethyan realm (UC^{TP}).

The recovered succession within W-4 is dated to lie within the late Coniacian to early Campanian Zones UC11 to UC14 (Fig. 4). The identification of UC14 is based on the presence of *Bukryaster hayi* and base *Broinsonia parca parca* at 111 m; that of UC12–13 is based on the observation of base *Broinsonia parca parca* to top *Lithastrinus septenarius* at 1280 m. UC11 is based on the top *Lithastrinus septenarius* and the presence of *Quadrum gartneri*.

4.2 Preservation

Due to the susceptibility of coccoliths to dissolution and overgrowth, the preservation of nannofossil in the study wells can be variable across lithologies and with different burial depths. Quantifying the quality of preservation through a succession is important as variations may

cause preservational bias on the resulting assemblage data (Thierstein, 1980; Roth, 1984). To describe the preservation, a general preservation scale has been applied here, which is outlined below.

– VG: very good – no evidence of dissolution and/or recrystallisation, no alteration of primary morphological characteristics, and specimens identifiable to the species level.

– G: good – little or no evidence of dissolution and/or recrystallisation; primary morphological characteristics unaltered or only slightly altered; specimens identifiable to the species level.

– M: moderate – specimens exhibit some etching and/or recrystallisation; primary morphological characteristics somewhat altered; however, most specimens identifiable to the species level.

– P: poor – specimens were severely etched or overgrown; primary morphological characteristics largely destroyed; fragmentation has occurred; specimens often could not be identified at the species and/or generic level.

Based on a visual inspection of etching and overgrowth the preservation is very good to good in the soft, grey shale layers of the Shargi Member and in the soft, grey marl layers of the Arada Member. The quality of preservation decreases to moderate as the amount of coarser clastic input increases up-hole in well sections, for example in the silty and sandy grey shale horizons of the Shargi Member. Intervals of highly compacted shale within the lower Shargi Member are sometimes present and have moderate to poorly preserved nannofossil assemblages with indications of dissolution and overgrowth. A further reduction of preservation is

recorded in the carbonate-rich, white chalk and argillaceous limestone layers of the Arada Member, where nannofossil recovery is very poor.

In the well-preserved nannofossil assemblages of the Campanian and upper Santonian intervals, the assemblages are characterised by the common presence of coccospheres (e.g. Plate 7, fig. 37; Plate 8, fig. 10; Plate 11, fig. 36) and consistent occurrence of holococcoliths such as *Bilapillus*, *Munarinus*, *Octolithus*, *Ottavianus*, *Russellia* and *Nicholasia* (Plates 8–9). The presence of such a diversity of holococcolith species is indicative of excellent preservation with minimal taphonomic or diagenetic dissolution (e.g. Roth and Bowdler, 1981; Roth, 1984). These intervals are also characterised by the abundance of small placolith species, such as *Biscutum constans* (Plate 7, figs. 25–27) and *Discorhabdus ignotus* (Plate 7, figs. 35–37), and murolith coccoliths like *Corollithion* species (Plate 7, figs. 11–14) and small *Zeugrhabdotus* species (Plate 2, figs. 26–42; Plate 3, figs. 1– 21). Moreover, fine central area structures such as cross-bars, plates and perforations are preserved in many species; this includes, for example, the case of *Broinsonia verecundia* (Plate 1, figs. 22–28) and *Helicolithus blairiae* (Plate 6, figs. 33–42), for which fine central area structures are observed that are not seen either in the holotype or paratype specimens. Well-preserved larger taxa are characterised by the presence of fine central area structures, as observed in the plate perforations of *Arkhangelskiella cymbiformis* (Plate 1, figs. 3–4). Generally, the quality of nannofossil preservation decreases slightly and assemblages are reduced in diversity and abundance down-hole toward the Coniacian intervals.

4.3 Species Richness

Across the study wells, highly diverse assemblages (> 70 species per sample) are present within the Campanian intervals. Species richness is only slightly lower in the lower Maastrichtian, with lower diversities of holococcoliths, *Stauorolithites* and *Broinsonia* and an absence of *Corollithion* and *Ahmuellerella*, and during the Santonian and lower Coniacian intervals with a peak of 40–55 species per sample in the shale and grey marl intervals. Such high diversity compares favourably with the global diversity estimates of Bown et al. (2004) for the Late Cretaceous. In W-4 (Fig. 3), the highest species richness is present in the outer shelf settings (as defined by the microfaunal associations, PDO data), rather than in shallower shelf

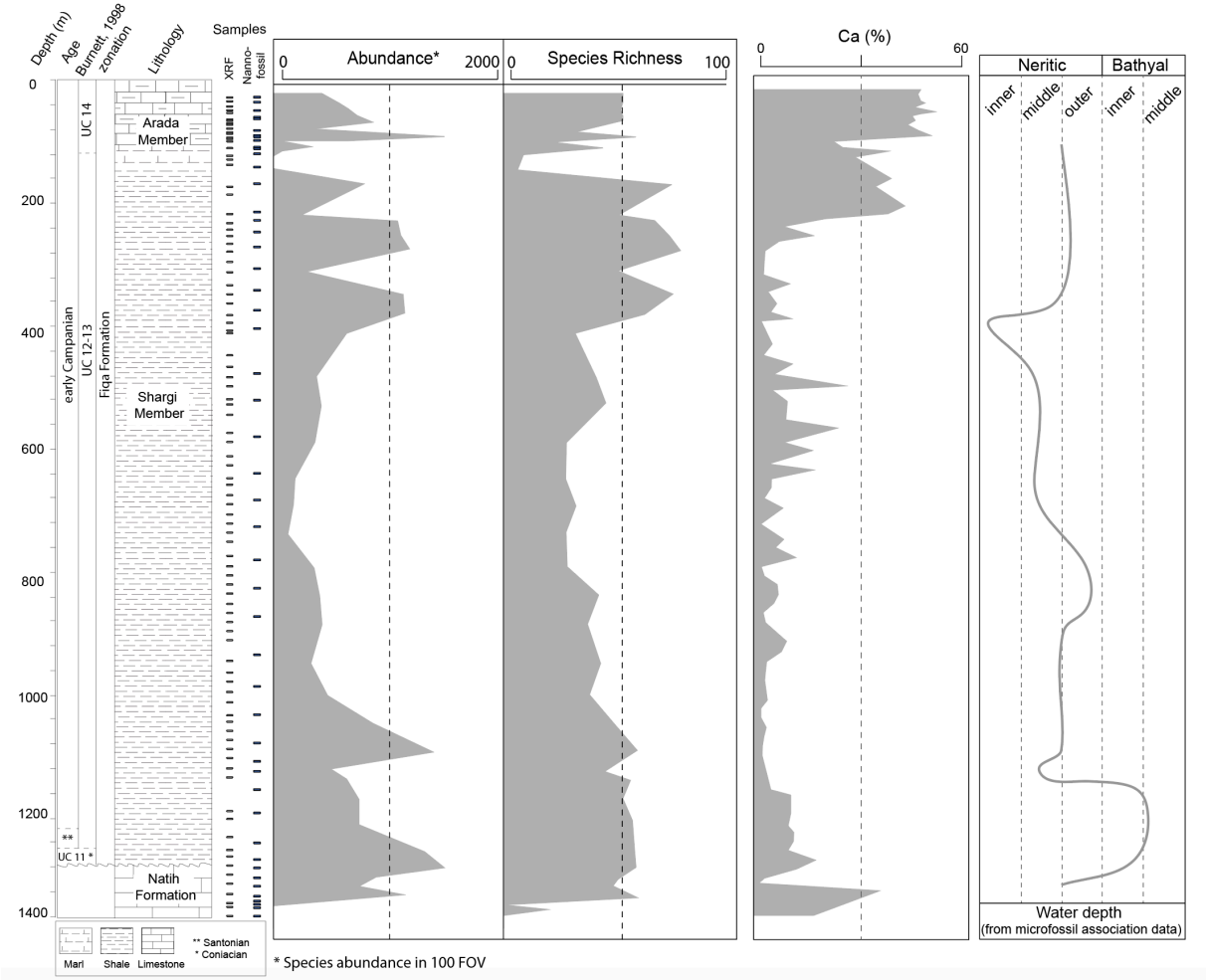

Figure 3. Nannofossil abundance and diversity in the Fiqa Formation compared to Ca wt % and palaeo-depth, W-4.

or deeper oceanic settings which are characterised by reduced abundances and species richness. These intervals are also correlated with increased calcium carbonate content (Ca > 10 wt %) (Fig. 3).

In general, the overall average diversity is around 40 species per sample, which changes only slightly depending on nannofossil preservation and the loss of smaller and solution-sensitive taxa. This might reflect a general stability in the depositional environment. Even though the species richness does not change dramatically, the assemblages are continuously fluctuating in composition, which is not reflected in the nearly homogeneous lithology of the formation. The main trends of the assemblage fluctuations are discussed below.

4.4 Assemblage Composition

4.4.1 General Assemblage Composition

Throughout the Fiqa Formation in the study wells, calcareous nannofossil assemblages are characterised by high abundances of the placolith coccoliths *Watznaueria barnesiae* and *Prediscosphaera cretacea* with an average abundance of 20%–25%, whilst peak abundances can range up to 60%–64%. *Prediscosphaera* species (Plate 8, figs. 2–6, 12) are dominated by *P. cretacea* and *P. grandis*, with less common taxa including *P. spinosa*, *P. bukryi* and *P. stoveri*. *Watznaueria barnesiae* (Plate 8, figs. 9–10) is dominant, with minor contributions from other species (Plate 8, figs. 11, 13–16, 18–19) including *W. bayacki*, *W. quadriradiata* and *W. ovata*, which occur more frequently in the upper parts of lower Campanian intervals. *Watznaueria fossacincta* and *W. biporta* are very rare and sporadic. Other frequently occurring species include the placolith coccoliths *Cribrosphaerella ehrenbergii* (Plate 7, figs. 20–22), *Biscutum*

constans (Plate 7, figs. 25– 27) and *Discorhabdus ignotus* (Plate 7, figs. 35–37) and the murolith coccoliths *Eiffellithus* (Plate 5, figs. 2–42; Plate 6, figs. 1–9), *Corollithion* (Plate 7, figs. 11–14), *Zeugrhabdotus* (Plate 2, figs. 26–42; Plate 3, figs. 1–21) and *Tranolithus* (Plate 2, figs. 14–25). Common nannoliths include *Micula staurophora* (Plate 11, figs. 14–20). *Cylindralithus biarcus*, *Manivitella pemmatoidea*, *Loxolithus armilla* and *Ahmuellerella octoradiata* are also common and show a consistent presence throughout the formation. The dominance of these taxa is typical for Late Cretaceous Tethyan assemblages (e.g. Wagreich, 1992; Lees, 2007). The assemblage patterns of the main genera from W-4 are represented in Figure 4. It is considered as an example well from north Oman with the most continuously sampled interval of the Fiqa Formation, covering the Coniacian to lower Campanian. The changing patterns of the main groups and their composition in W-4 are described below.

Cribrosphaerella ehrenbergii is common and consistently present with peaks in abundance of around 10% (Fig. 4). The rim can have irregular or elliptical outlines. However, these rim outlines are very rare and encountered only in the more abundant and well-preserved samples. *Corollithion* is another common genus that can contribute to more than a third of the total assemblage within the lower Campanian (Fig. 7). This genus is represented by common *C. signum*, less abundant *C. exiguum* and rare occurrences of *C. kennedyi*. *Zeugrhabdotus* species represent a consistent component of the assemblage throughout the section with an average abundance of 3% of the total assemblage (Fig. 4). The most common species include *Z. diplogrammus*, *Z. erectus*, *Z. bicrescenticus* and *Z. clarus*. Rare occurrences of *Z.* cf. *Z. xenotus*, *Z. trivectis*, *Z. sigmoides*, *Z. scutula*, *Z. praesigmoides*, *Z. noeliae*, *Z. howei*, *Z. embergeri* and *Z. acanthus* have been recorded sporadically in the formation. *Zeugrhabdotus*

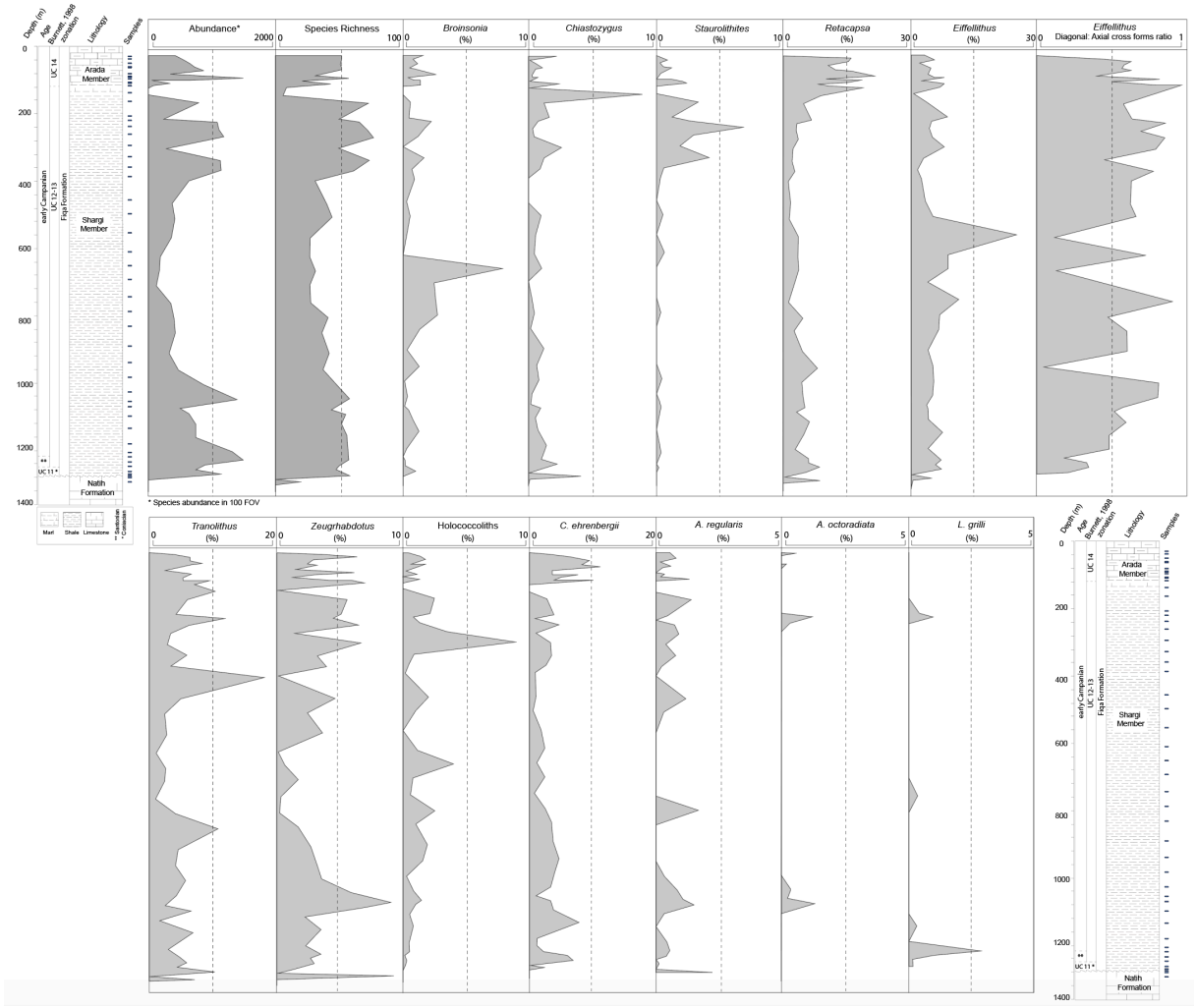

Figure 4. Abundance distribution patterns of the main components in the nannofossil assemblages, W-4.

biperforatus and *Z. noeliae*, which are important markers in the UC global zonation scheme of Burnett (1998), are very rare with inconsistent occurrences in this section. These low abundances make determining their biostratigraphically important first and last occurrences difficult. *Tranolithus* species (Fig. 4), represented mainly by *T. orionatus* (< 1% to 16%) and *T. minimus* (< 1% to 4%), are very important component of the assemblage throughout the Fiqa Formation, although *T. gabalus* is rare and sporadic. *Micula* species (Plate 11, figs. 14–29) are common and mainly represented by *M. staurophora*, which is highly abundant in several intervals and increases in abundance from < 1% to 14% of the total assemblage within the lower

Campanian (Fig. 7). *Retecapsa* species (Plate 7, figs. 39–42) are consistently present throughout the Fiqa Formation, with *R. angustiforata* being the most dominant, followed by *R. crenulata* and *R. surirella*, whilst *R. schizobrachiata* and *R. ficula* are rare. There is an important and continuous abundance peak in *Retacapsa*, which increases from 3% to 14%, toward the upper parts of lower Campanian intervals (Fig. 4). *Gartnerago*, mainly represented by *G. segmentatum* and *G. obliquum*, is another consistent component of the assemblages that fluctuates in abundance from 0.1% to 3%. *Gartnerago praeobliquum* is less common, although smaller and very rare morphotypes *G.* cf. *G. ponticula* and *G.* cf. *G. praeobliquum* are present. *Rhagodiscus* species of *R. angustus*, *R. splendens* and *R. reniformis* are present throughout the Fiqa Formation but make up only about 1% of the total assemblage. *Placozygus* (Plate 2, figs. 7–10) is observed with a generally low abundance but with consistent occurrences and is mainly represented by *P. spiralis*, with rare occurrences of *P. fibuliformis*. *Calciosolenia fossilis* (Plate 8, fig. 17) is very rare but found sporadically in many intervals. Holococcoliths (Fig. 4) are diverse and represented by common genera of *Calculites* (Plate 8, figs. 26–41), *Lucianorhabdus* (Plate 9, figs. 3–9) and *Owenia* (Plate 9, fig. 10), as well as rarer genera (Plate 9, figs. 11–41) of *Bilapillus*, *Munarinus*, *Octolithus*, *Ottavianus*, *Russellia*, *Duocameratus* and *Nicholasia*. Characteristic features of the upper Campanian to lower Maastrichtian intervals of the Fiqa Formation that are not encountered in W-4 but in W-7 and W-8 include the more frequent occurrence of *Helicolithus* (Plate 6, figs. 10–42) and *Uniplanarius* (Plate 11, figs. 4–10) species. *Helicolithus* species are diverse, consistently present and dominated by *H. compactus* and *H. trabeculatus*. The abundance of *Uniplanarius* species – *U. sissinghii*, *U. gothicus* and *U. trifidus* – is generally very low, but this gradually increases towards the uppermost Campanian and lower Maastrichtian intervals, reaching 2% of the total

assemblages in W-8. In W-4, *Uniplanarius* species are absent and *Helicolithus* species are represented by *H. leckiei* that is found sporadically throughout the formation and *H. blairiae* that is consistently present during most of the Santonian and Coniacian intervals. The top of *H. blairiae* within the Santonian could be of biostratigraphic significance in the area.

The overall assemblage composition and characteristics are similar to the Late Cretaceous Tanzanian assemblages studied by Lees (2007). This includes the identification of several of the new heterococcolith species described from the Tanzanian Drilling Project materials like *Eiffellithus lindiensis* (Plate 5, figs. 12–15), *Staurolithites halfanii*, *S. handleyi* (Plate 4, figs. 1–4), *S. ngurumahambaensis* (Plate 4, figs. 19– 22) and the holococcolith species *Bilapillus wadeae* (Plate 9, figs. 14–15), *Calculites cyclops* (Plate 8, figs. 34–41) and *Duocameratus leariae* (Plate 9, figs. 38–39). Assemblages are also similar to the Tanzanian assemblages in the frequent occurrence of holococcoliths and very small (< 3 μm) taxa. A full list of the taxa present in the analysed samples is available in the systematic palaeontology section.

4.4.2 Notes on the Taxonomy and Assemblage Composition of the Common Late Cretaceous Genera in the Fiqa Formation

Arkhangelskiella. Occurrences of the genus *Arkhangelskiella* are sporadic in most intervals, with generally low abundances. This group has been widely studied due to its high variability in coccolith size and its possible evolutionary (e.g. Varol, 1989; Thibault, 2010) and palaeoenvironmental (e.g. Linnert and Mutterlose, 2009a) significance. *Arkhangelskiella cymbiformis*, for instance, has been subdivided into several morphogroups based on coccolith size and rim width (e.g. Varol, 1989; Thibault, 2010). In this study, however, due to the relative rarity of this genus, the group is subdivided into three main species following the defini-

tion of Burnett (1997). *Arkhangelskiella cymbiformis* (Plate 1, figs. 3–4) includes all large species (> 8 μm) with relatively narrow rims (< 1 μm), whilst all smaller forms are included within *A. confusa* (Plate 1, figs. 1–2). All large forms with a thick rim (> 1.5 μm) are included into *A. maastrichtiensis* (Plate 1, figs. 5–6).

There is one exceptional interval during which this group becomes very common in the few uppermost Campanian to lower Maastrichtian samples from W-8, for which specimens show great variation in coccolith size and rim width (e.g. Plate 1, figs. 5–6). Hence, the morphometric subdivision of Varol (1989) and Thibault (2010) could be potentially applied only in these intervals. These samples are the only ones in which *Arkhangelskiella maastrichtiensis*, which has a very thick rim relative to *A. cymbiformis* and *A. confusa*, has been recorded. The observed specimens of *A. maastrichtiensis*, however, show great size variations and could be equivalent to the morphogroups *A. cymbiformis* var. N (small), *A. cymbiformis* var. W (medium) and *A. cymbiformis* var. SW (large) of Thibault (2010). Although these distinctions have potential for future morphometric application, this subdivision is not followed here as it is beyond the scope of this study and only few samples exhibited such variation.

Broinsonia. Species of the genus *Broinsonia* represent one of the most significant groups within the Fiqa Formation (Fig. 4), with several species that either evolved and/or go extinct within the studied succession. Four main species of *Broinsonia – B. signata*, *B. enormis*, *B. parca* and *B. verecundia* (Plate 1, figs. 7–28) – have been identified and we follow the taxonomy of Linnert et al. (2014a) and Wise (1983). In their biometric study, Linnert et al. (2014a) grouped all specimens with a cross-shaped central area structure into *B. signata* and all medium-sized specimens with a plate-like central structure into *B. enormis*. In the studied succes-

sion, *B. signata* is consistent throughout the upper Coniacian to lower Campanian intervals, before its abundance gradually decreases and it eventually disappears in the uppermost Campanian. *Broinsonia verecundia* has lower abundances but is consistently present throughout the Campanian. Therefore, the top of *B. signata* and top and base of *B. verecundia* could be of potential stratigraphic significance in the area if correlated with existing global zonation schemes of nannofossils, i.e. the UC scheme (Burnett, 1998) and CC scheme (Sissingh, 1977; modified by Perch-Nielsen, 1985). Subspecies of *B. parca* also exist and are separated based on the classification of Wise (1983) into *B. parca parca* (plate width is 1–2× of the margin width; Plate 1, figs. 7–8) and *B. parca constricta* (plate width is < 1× of the margin width; Plate 1, figs. 9–10). *Broinsonia parca expansa* (plate width is > 2× of the margin width) is absent in almost all samples. In this study, bases of the subspecies of *B. parca parca* and *B. parca constricta* have been recorded within the lower Campanian, which agrees with the UC global zonation scheme of Burnett (1998).

Eiffellithus. Species of *Eiffellithus* represent a consistent component of the assemblage throughout the Fiqa Formation contributing 2%–8% up to 20% of the total abundance (Fig. 4). An influx and diversification of *Eiffellithus* are recorded within the Campanian of the section, including *E. gorkae*, *E. turriseiffelii*, *E. parallelus*, *E. collis*, *E. angustus*, *E. perchnielseniae*, *E. phantasma*, *E. nudus* and *E. lindiensis* (Plate 5, figs. 2–42; Plate 6, figs. 1–9). The detailed subdivision of *Eiffellithus* species by Shamrock and Watkins (2009) is followed here in order to evaluate the potential significance of the genus for biozonation schemes. The species are assigned to two main groups based on the orientation of the cross-bars relative to the longitudinal axis of the coccolith: a group with axial crosses and a group with diagonal

crosses. In the Fiqa Formation, medium to small species of diagonal-cross forms like *E. gorkae*, *E. casulus*, *E. parallelus* and *E. collis* are more abundant than the larger species *E. turriseiffelii* and *E. keio*. *Eiffellithus parallelus*, *E. turriseiffelii* and *E. keio* have distinctive cross-bars and could be easily differentiated; however, the smaller forms of *E. gorkae*, *E. casulus* and *E. collis* are tricky to separate. *Eiffellithus collis* is the smallest (≤ 4 μm) with a distinctive elongate outline (Plate 6, figs. 4–9). *Eiffellithus casulus* has a very similar coccolith morphology to *E. turriseiffelii* but is smaller (≤ 8 μm) (Plate 5, figs. 39–42). It is differentiated from *E. gorkae* by the constricted cross of the latter compared to the longer and more pointed cross of *E. casulus*. Species with intermediate orientation of the central cross (20–44° orientation from the axial position, Shamrock and Watkins, 2009) like *E. phantasma* and *E. perch-nielseniae* are least abundant and are grouped into the diagonal-cross forms.

The main factor used to differentiate between the axial-cross species is the size. *Eiffellithus angustus* is the largest and most bifurcate species with a size of ≥ 14 μm (Plate 5, figs. 2–5). *Eiffellithus eximius* is less furcate with a size of ≥ 8 μm (Plate 5, figs. 6–9). *Eiffellithus nudus* lacks distal bifurcation and is ≤ 7 μm (Plate 5, figs. 10–11). It is also characterised by slightly oriented cross-bars within 20° of the longitudinal axis, a feature that distinguishes it from other small axial-cross forms like *E. lindiensis*. In this study, all recorded *E. lindiensis* show an axially aligned cross with a size of < 4 μm (Plate 5, figs. 12–15). Unlike other axial-cross forms, *E. lindiensis* is mostly present in the upper Campanian to lower Maastrichtian intervals.

Eiffellithus species with diagonal-cross forms are generally more common than the axial-cross forms in most intervals. The ratio between diagonal-cross and axial-cross forms is plotted in Figure 4. It shows the dominance of axial-cross forms during the Coniacian and Santonian, which is mainly contributed by *E. eximius* (10%–20% of the total assemblage), followed by the dominance of diagonal-cross forms throughout most of the lower Campanian.

Chiastozygus. Representatives of the genus *Chiastozygus* are typically low in abundance, generally < 3 % of the total assemblage, but are consistently present throughout the Fiqa Formation, with minor peaks in the Campanian (Fig. 4). The most common species are *C. synquadriperforatus* and *C. amphipons* with sporadic occurrences of other species such as *C. bifarius*, *C. trabalis* and *C. litterarius* (Plate 4, figs. 28–41). This genus is characterised by a simple rim and diagonal cross-bars, with species typically distinguished by the number of rim cycles (unicyclic vs. bicyclic) and the cross-bar appearance (complexity and interference). Differentiation of *Chiastozygus* species can be difficult in the light microscope; the main distinguishing features are illustrated in Figure 5. Species with unicyclic rims include *C. amphipons*, *C. bifarius* and *C. litterarius*. *Chiastozygus amphipons* has a relatively dark rim with very simple cross (Plate 4, figs. 28–29) similar to *C. bifarius*, but the latter is distinguished by a bright, birefringent cross (Plate 4, figs. 30–32). *Chiastozygus litterarius* can be distinguished from other unicyclic-rim species by the thick rim and a cross that is weakly birefringent (Plate 4, figs. 33–35). *Chiastozygus trabalis* could be easily identified by its bicyclic rim with a bright inner cycle and a complex cross (Plate 4, figs. 37–38). *Chiastozygus synquadriperforatus* is characterised by a smaller size than most of the other species and cross-bars with different sizes, with one bar being longer than the other (Plate 4, fig. 36). The new species, *Chias-*

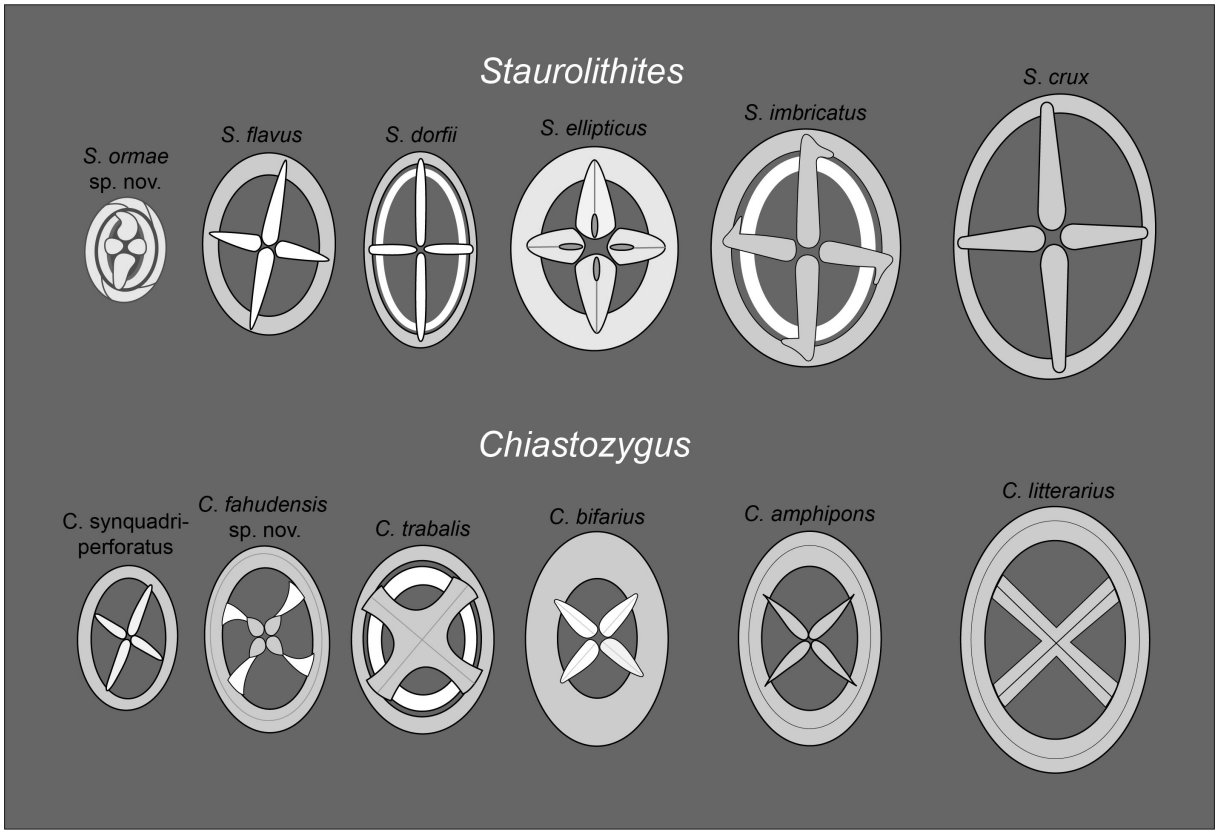

Figure 5. Characteristic features of the main species of *Staurolithites* and *Chiastozygus* under the light microscope compared to the new species *C. fahudensis* sp. nov. and *S. ormae* sp. nov.

tozygus fahudensis sp. nov., has a distinctive bright cross with a rosette-shaped central feature and indistinct rim (Plate 4, figs. 39–41). It occurs consistently throughout the section. A detailed description of the species is found within the systematic palaeontology section.

Staurolithites. *Staurolithites* species are found in Coniacian to Campanian samples but occur more frequently in the Campanian with an average abundance of 4 % (Fig. 4). Representatives of this genus are characterised by a simple central axial cross, with species distinguished by their rim morphology (unicyclic vs. bicyclic) and the appearance of the central cross-bars. According to Perch-Nielsen (1985), there are many more species described in the original description of the group by Grun and Zweili (1980) than can be distinguished in the light microscope. Due to their limited stratigraphical significance, there are few studies that further dis-

cuss this group with species descriptions mostly based on scanning electron microscope images. This make species of *Staurolithites* difficult to separate under light microscope. The main distinguishing features under the light microscope for the most dominant species are illustrated in Figure 5 and highlighted below.

Staurolithites crux is simply constructed with a unicyclic narrow rim and wide central area spanned by a simple cross (Plate 3, figs. 28–29). *Staurolithites dorfii* is narrowly elliptical, with a bicyclic rim. It has a distinctively bright cross and inner rim cycle (Plate 3, figs. 30–34). *Staurolithites ellipticus* is broadly elliptical with a thick cross that fills most of the central area (Plate 3, fig. 37). *Staurolithites flavus* is unicyclic and could be easily distinguished by its highly birefringent cross (Plate 3, figs. 35–36). *Staurolithites imbricatus* is characterised by its birefringent, bicyclic rim (Plate 3, figs. 38–40). The new species, *Staurolithites ormae* sp. nov., is characterised by its small size and bright, bicyclic rim. The central area is filled by a thick, birefringent cross that is slightly offset from the axial position (Plate 4, figs. 9–16). A detailed description of this species is found in the systematic palaeontology section.

5 Discussion

Through the Fiqa Formation, nannofossil assemblages show some distinct variations in species compositions. These variations are recorded in a lithology that is almost homogeneous. In this paper we focus on these nannofossil assemblage changes across the Fiqa Formation recovered from well W-4. In this section, the most distinct abundance changes are discussed and compared to previous studies of Late Cretaceous nannofossil environmental preferences and responses to environmental change. The new data presented here provide impor-

tant information on the palaeoenvironments of the Aruma Basin and help constrain the biogeographic distribution of key Cretaceous species.

5.1 Palaeobiogeographic Significance

Here we investigate the abundances, within the Fiqa Formation, of Late Cretaceous taxa with known strong latitudinal controls on their biogeographic distributions (Fig. 6). Species that dominate nannofossil assemblages of the Fiqa Formation (Sect. 4.4.1) are generally typical of tropical Late Cretaceous Tethyan assemblages (e.g. Wagreich, 1992; Lees, 2007). For instance, relative abundances of *W. barnesiae*, in some intervals reaching more than 30%, is similar to latest Campanian assemblages from Blake Nose (DSDP Site 390A; Linnert and Mutterlose, 2009b) and the Indian Ocean sites of Lees (2002). The other dominant group is made up of the cosmopolitan species of *Prediscosphaera* (Roth and Bowdler, 1981), which are present throughout the succession. The cosmopolitan species *Cretarhabdus* and *Retecapsa* (Roth and Bowdler, 1981), however, have generally low abundances, with *Retecapsa* becoming more frequent only within the lower Campanian (Fig. 4). *Discorhabdus ignotus* is found to be common in the austral to temperate palaeobiogeographic zones of Lees (2002) but is also common to abundant in this tropical site (Fig. 6b). In the North Atlantic, *D. ignotusis* is relatively common in assemblages from the low-latitude Blake Nose (e.g. DSDP Site 390A; Linnert and Mutterlose, 2009b), but less abundant in samples from the Goban Spur (DSDP Site 549; Linnert et al., 2011) and North Sea area (e.g. Linnert et al., 2016). The consistent occurrence of *Prolatipatella multicarinata* in this study further supports its status as a tropical taxon (Lees, 2002; 2007). The relative rarity of Campanian *Lucianorhabdus* and *Calculites obscurus* within the Fiqa Formation assemblages compared to most Late Cretaceous succes-

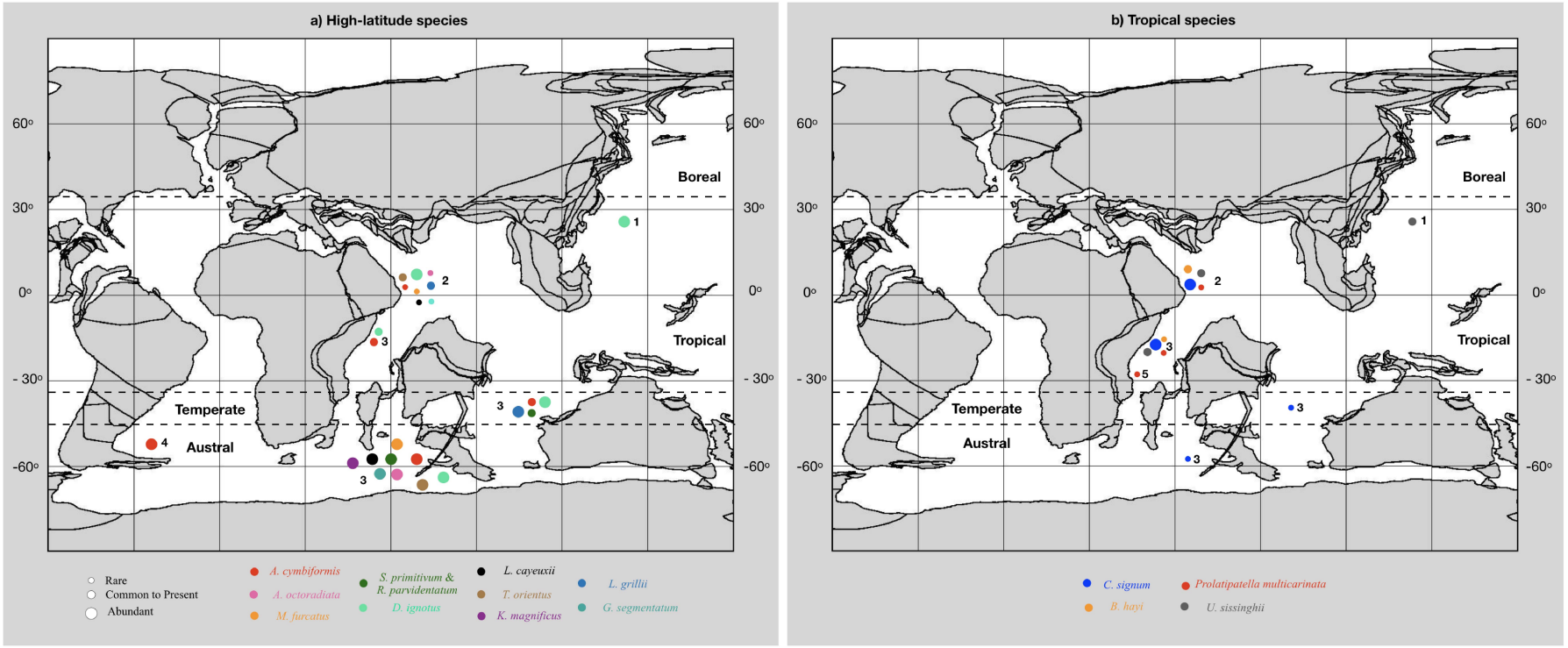

Figure 6. Distribution of selected (a) high-latitude and (b) tropical taxa compared to their status in the study area. Abundance data from (1) Lees and Bown (2005); (2) this study; (3) Lees (2002); (4) Therisin (1981); (5) Lees (2007). Palaeobiogeographic zones from Lees (2002) and Lees and Bown (2005). 75 Ma reconstruction map adapted from the PALEOMAP project (http://www.odsn.de/odsn/services/paleomap/ paleomap.html, last access: July 2018).

sions, especially from high-latitude provinces (e.g. Thierstein, 1976; Wind, 1979; Lees, 2002), is also consistent with the observation of Lees (2007) that these are not tropical taxa. The observations of this study support the rare to absent status of the common and previously described higher-latitude, cooler-water taxa (Fig. 6a). The cool-water *Repagulum parvidentatum* (e.g. Wise, 1983, 1988; Crux, 1991; Street and Bown, 2000; Lees, 2002) is, as expected, absent from the assemblages of this study. Other higher-latitude species that are either absent or rare in the Fiqa Formation include the rare *Ahmuellerella octoradiata* and *Gartnerago segmentatum* (Wind, 1979; Thierstein, 1981), the extremely rare *Kamptnerius magnificus*, *Reinhardtites anthophorus* and *Reinhardtites levis*, and the absent *Nephrolithus frequens* (Lees, 2002), *Seribiscutum primitivum* (e.g. Roth and Bowdler, 1981; Crux, 1991; Street and Bown, 2000; Lees, 2002) and *Crucibiscutum*. The typically high-latitude species *Arkhangelskiella cymbiformis* (e.g. Wind, 1979; Thierstein, 1981) is very rare in the study area. The same is true for *B. parca expansa*, which is rarely recorded from the tropical palaeobiogeographic zone (Lees, 2002) and is absent from almost all samples from the Fiqa Formation. *Marthasterites furcatus* is commonly found in the austral palaeobiogeographic zone of Lees (2002) and is present in both the temperate and tropical zones; in the Fiqa Formation, *M. furcatus* is extremely rare. *Ahmuellerella octoradiata*, which was used by Lees (2002) as an indicator of cooling of surface water masses in the Late Cretaceous low-latitude oceans, shows two main peaks through the Fiqa Formation (Fig. 4). These peaks are usually correlated with increased abundances of *Lithastrinus grillii* (Fig. 4), which is also considered a potential temperate, "cooler" shelf taxon by Lees (2002). *Helicolithus blairiae*, which showed a potentially limited palaeogeographic range to the Western Interior Seaway of North America (Kita et al., 2016),

is present in the Fiqa Formation. This observation provides a new insight into the geographical distribution of this rare Santonian species.

5.2 Palaeoenvironmental Significance

Variation in nannofossil abundances and assemblage composition often reflects changes in the palaeoenvironmental conditions of ocean surface waters like nutrient supply, detrital input and surface water salinity (Mutterlose et al., 2005). One of the strongest assemblage changes recorded in W-4 is an interval of very low *Watznaueria barnesiae* abundances within the lower Campanian. This event occurs within a wider succession that hosts well-preserved and abundant nannofossil assemblages. *Watznaueria barnesiae* is one of the most robust nannofossil species of the Mesozoic and is often one of the few morphologies remaining in assemblages that have been subject to substantial dissolution (e.g. Roth and Bowdler, 1981). The dominance of *W. barnesiae* in Mesozoic nannofossil assemblages across a range of preservation states and locations, however, shows the wide ecological tolerance and biogeographic distribution of this species. The extent of this ecological range is illustrated in a study of Late Jurassic coccolith-rich laminae, which are interpreted to represent annual or seasonal blooms (Lees et al., 2006). Laminae with near mono-specific assemblages of *W. barnesiae* clearly show an ecological tolerance of this species to unusual conditions in the restricted Wessex Basin that exclude other taxa. This evidence suggests the need for caution when interpreting the relative abundance of *W. banesiae* as a palaeoenvironmental proxy, as this may reflect the relative increase or decrease in the abundance of other species, rather than a direct response of *W. barnesiae* to environmental change (Lees et al., 2005). It is, however, hard to explain the intervals of low *W. barnesiae* abundance in this record by simple dilution by other taxa, as it

is actually dominant in intervals with the most diverse assemblages (see species richness, Fig. 4). Instead lower *W. barnesiae* abundances strongly correlate with more neritic conditions as independently determined from benthic microfossil assemblages (Fig. 7). The interval of low *Watznaueria barnesiae* is also characterised by elevated abundances of *Biscutum constans* and *Zeugrhabdotus erectus* with peaks of *Discorhabdus ignotus* and *Corollithion signum*. It succeeds an interval of elevated abundance of *Micula staurophora*. This interval is also correlated with a high abundance of *Prediscosphaera cretacea*, with a *W. barnesiae* to *P. cretacea* ratio falling from > 0.5 to < 0.2 (Fig. 7). As noted above, these intervals of low and extremely low *W. barnesiae* within the Fiqa Formation occur where microfossil association data (unpublished PDO microfossil data) indicate a shallower shelf environment (Fig. 7). This shallower setting is also supported by the consistent presence of "nearshore" and continental margin taxa such as *Broinsonia* spp. (Roth and Bowdler, 1981), *Nannoconus* spp. and *Braarudosphaera* spp. (Roth and Bowdler, 1981; Wyton and Bown, 2007). This link between low *Watznaueria* abundance and the development of neritic conditions is compelling, with *Watznaueria* abundance always high in intervals of increased water depth in the formation, which agrees with Atlantic shelf-to-ocean transects from the mid-Cretaceous (Roth and Bowdler, 1981). However, intervals of relatively reduced water depths are not always marked by lower abundances of *W. barnesiae*. For example, the *W. barnesiae* to *P. cretacea* ratio still fluctuates within the shallow water intervals and can reach 0.5 and rarely up to 0.8. In the Indian Ocean, *W. barnesiae* has been previously found to be abundant in both shelf and open-ocean locations in Lees (2002). Together this indicates that the dominant control on the *W. barnesiae* to *P. cretacea* ratio is not water depth per se, but rather other environmental factors, such as temperature (e.g. Bukry, 1973; Thierstein, 1981; Roth and Bowdler, 1981; Thierstein, 1981; Shafik,

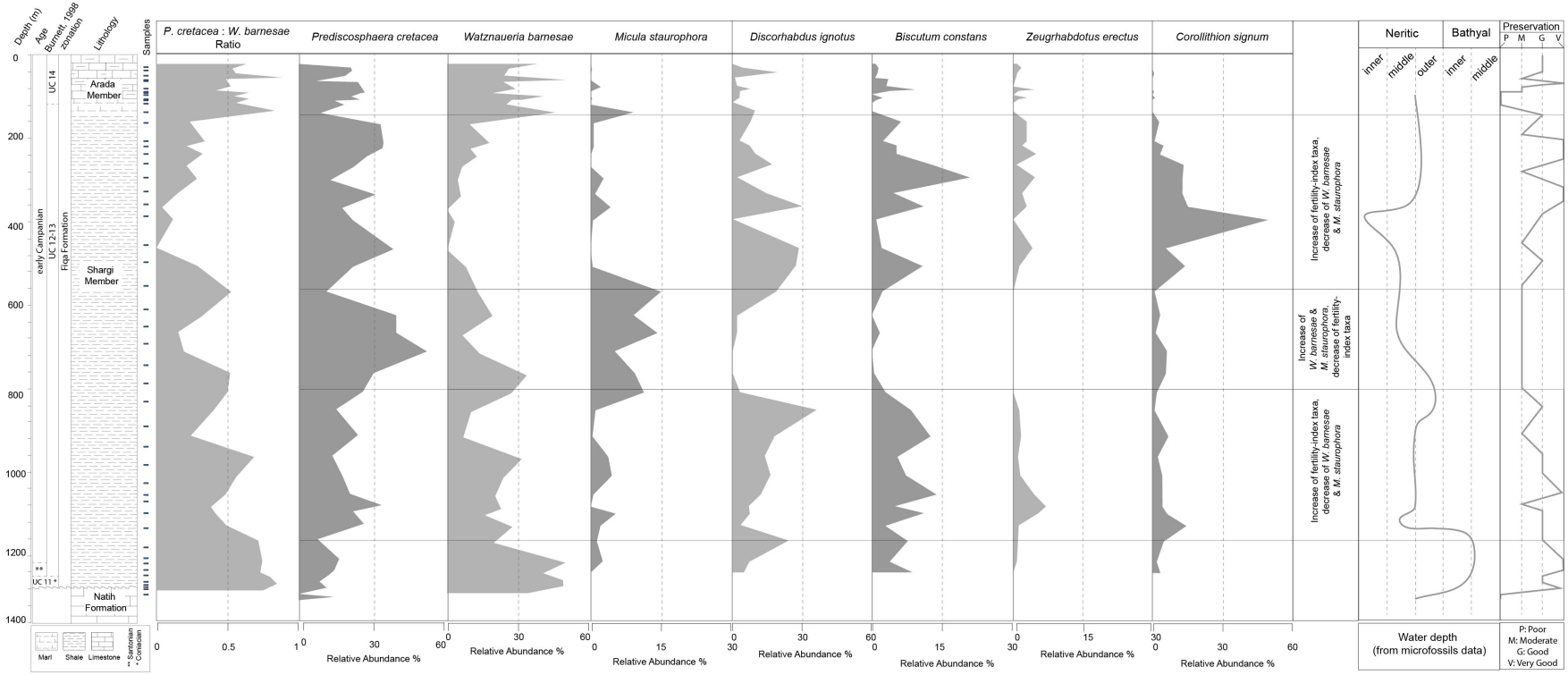

Figure 7. Changing abundance patterns of proxy marker taxa in the W-4, integrated with Ca% and palaeoenvironment.

1990; Watkins et al., 1996; Lees, 2002) and nutrient status (e.g. Erba et al., 1992; Williams and Bralower, 1995; Fisher and Hay, 1999), which are often coupled to relative water depth but can vary independently. Even though the influence of temperature on abundances of *W. barnesiae* has been debated in several studies as mentioned previously, the Aruma Basin is a tropical location close to the Equator where temperature fluctuations are likely to be small, even through a generally cooling Late Cretaceous climate (see Sect. 1). This is supported by the presence of characteristic tropical nannofossil assemblages throughout the formation and the lack of high-latitude taxa as discussed in Section 5.1. In contrast, factors associated with the well-documented tectonically active status of the basin (see Sect. 2) and the sea level change as shown from the study data are more compelling (Fig. 7). *Watznaueria barnesiae* has been linked to oligotrophic surface water conditions by Roth and Bowdler (1981) based on its low abundances in mid-Cretaceous palaeo-upwelling locations, with many subsequent studies showing similar trends (e.g. Erba et al., 1992; Williams and Bralower, 1995; Fisher and Hay, 1999). This link is further supported by the inverse correlation of *W. barnesiae* with high fertility indices that has been widely recorded in different locations (e.g. Roth, 1981; Roth and Bowdler, 1981; Erba, 1992, 2004; Erba et al., 1992; Williams and Bralower, 1995; Fisher and Hay, 1999; Street and Bown, 2000).

The most widely used taxa with high surface water fertility are *Biscutum constans* and *Zeugrhabdotus erectus*, an association that was first noted by Roth (1981). The higher nutrient preference of these taxa is supported by their co-occurrence with other indicators of high fertility and their peaks in intervals of high surface water productivity during the mid-Cretaceous (e.g. Erba, 1992; Mutterlose et al., 2005). Lees et al. (2005) argued that discrepancies in the

distribution of these species, and a potential lack of taxonomic refinement, could lead to erroneous palaeoenvironmental interpretations. It is also suggested that *B. constans* is only abundant in high latitudes during the Late Cretaceous when *Z. erectus* remains generally rare in such locations (Thierstein, 1981; Lees, 2002). This is true for the study area as the relative abundance of these species is generally low (< 8% for *Z. erectus*; <20 % for *B. constans*), but with elevated abundances of both taxa during the low W. *barnesiae* intervals (Fig. 7). Peaks of *B. constans* (10%–20%) are usually more prominent and more frequent than those in *Z. erectus* (4%– 6%). This might reflect episodes of more mesotrophic than eutrophic environments based on the findings of Erba (1992) that noted an increased abundance of *B. constans* at lower levels of fertility relative to *Z. erectus*. Peaks of *Prediscosphaera* have also been associated with increased surface water productivity and mesotrophic conditions by several authors (Eleson and Bralower, 2005; Hardas and Mutterlose, 2007). *Discorhabdus ignotus* is another high-fertility-related taxon (Erba, 1992; Herrle, 2002; Herrle et al., 2003) that also has major abundance peaks during the intervals of low *Watznaueria barnesiae* abundance (Fig. 7). *Discorhabdus ignotus* peaks (10%–30%) start just before any drop in the abundance of *Watznaueria barnesiae* and prior to peaks of *B. constans* and *Z. erectus*. High variation in the abundance of *D. ignotus* might reflect relatively unstable trophic conditions in the basin. There are intervals during which this species rapidly fluctuates in abundance from 2%–3% to > 15%. Moreover, a prominent abundance increase in *Corollithion* spp. – mainly represented by *C. signum* – coincides with the decrease in *Watznaueria barnesiae* abundance (Fig. 7). The onset of a peak in *Corollithion* is usually accompanied or followed by a minor increase in *Biscutum constans*. Peaks of *Corollithion* spp. are also associated with peaks of *Discorhabdus ignotus*. Due to its marked abundance increase from < 5% to > 40%, which is correlated with

elevated abundance of other fertility-index taxa, *Corollithion* spp. might also represent a potential fertility-related indicator. It is also worth noting a relative abundance increase in the nannolith species *Micula staurophora* (up to 15%) prior to peaks of *C. signum*, which further supports the potential of this species as a proxy marker (see Lees et al., 2005). Therefore, the trends of low *W. barnesiae* and the associated increased abundances of *Biscutum constans*, *Zeugrhabdotus erectus*, *Discorhabdus ignotus*, *Corollithion signum* and *Prediscosphaera cretacea* might indicate episodes of increased nutrient supply to the basin corresponding to intervals of shallower shelf settings, which might in turn indicate episodes of increased detrital input into the basin. Overall, this study of the long-term calcareous nannofossil assemblage compositions within a basin subject to dynamic tectonics and relative sea level change provides a useful "natural experiment" to test the sensitivity of nannofossil taxa to external environmental drivers. Given the persistent tropical palaeo-location of the study site, within a long-term greenhouse climate state, we propose that most of these observed changes represent responses to surface water nutrient status and/or salinity and turbidity tolerances as shoreline proximity changes through time.

6 Conclusions

The calcareous nannofossil assemblages from the Upper Cretaceous Aruma Basin are well-preserved, abundant and diverse, allowing for a detailed and improved taxonomic description of some poorly documented and/or described Cretaceous species and the identification of two new species. *Staurolithites*, *Chiastozygus* and *Eiffellithus*, a significant component of the formation, are described in detail and their problematic taxonomy is discussed. A detailed description of other main groups encountered in the studied section and the community change

through time provided valuable information for palaeoenvironment and biostratigraphy. The assemblages also provided valuable environmental proxy data. Changes in the abundance of *Biscutum constans*, *Zeugrhabdotus erectus*, *Discorhabdus ignotus* and *Corollithion signum* in relation to *Watznaueria barnesiae* suggested episodes of elevated productivity during the neritic-dominated basin of the Campanian. With limited detailed work published on nannofossil taxonomy and biostratigraphy from the Upper Cretaceous sequences in the Middle East, this study presents new data that can be integrated with future work to improve our understanding of the assemblage changes in this part of the Cretaceous oceans and to apply and improve the global zonation schemes for this location and time interval. The major assemblage changes and the inception and extinction of nannofossil events can help to improve the biostratigraphic dating and the understanding of the palaeogeographic setting, sea level change and the basin subsidence history when correlated with existing geological data on the basin.

7 Systematic Palaeontology

Two new heterococcolith species, *Staurolithites ormae* sp. nov. and *Chiastozygus fahudensis* sp. nov., are discussed here. The species description follows the guidelines of Young et al. (1997) and the higher taxonomic classification is based on Bown and Young (1997). This section is followed by a species list for all taxa recorded in this study. Illustrations of the species are presented in Plates 1–11.

Staurolithites ormae sp. nov. Plate 4, figs. 9–16.

Derivation of name

The name derivation is after the Al Arma Mountains (pronounced as “Al Ormah”), where the type section of the Aruma Group–Formation was first described; “Ormah” is also the true Arabic pronunciation of Aruma.

Diagnosis

This is a small species (3.5–4.5 μm) of *Staurolithites* with bright bicyclic rim. The central area is filled by a thick, birefringent cross that is slightly offset from the axial position. The cross and the bicyclic rim show very high birefringence under the cross-polarised light microscope.

Differentiation

This new species is distinguished from other *Staurolithites* species by its small size, high bire-fringence and complex construction of the cross-bars that fills most of the central area.

Holotype

Plate 4, fig. 9 (fig. 10 same specimen).

Holotype dimensions

L=4.5μm,W =3.9μm.

Paratype

Plate 4, fig. 11 (fig. 12 same specimen).

Type locality

W-6, NW Oman.

Type level

UC12-13^{TP}, upper Santonian to lower Campanian.

Occurrence

W-4, W-6, W-7, late Santonian to late Campanian

Chiastozygus fahudensis sp. nov. Plate 4, figs. 39–41.

Derivation of name

The name derivation is after the Fahud oil field (W-4), from which the species was first identified.

Diagnosis

This is a medium-sized (5–7μm) species of *Chiastozygus* with a simple unicyclic, indistinct rim and characteristic bright cross with a rosette-shaped central feature.

Differentiation

This new species is distinguished from other *Chiastozygus* species by its distinctive bright cross and the rosette-shaped central feature.

Holotype

Plate 4, fig. 39 (fig. 40 same specimen).

Holotype dimensions

L=6μm,W =4.6μm.

Paratype

Plate 4, fig. 41.

Type locality

W-3, N Oman.

Type level

UC14 ^{TP}, lower Campanian.

Occurrence

W-3, W-4, W-6, W-7, W-8; late Coniacian to late Campanian.

Species List

Ahmuellerella octoradiata (Górka, 1957) Reinhardt & Górka, 1967

Ahmuellerella regularis (Górka, 1957) Reinhardt & Górka, 1967

Amphizygus brooksii Bukry, 1969

Amphizygus minimus Bukry, 1969

Arkhangelskiella confusa Burnett, 1997

Arkhangelskiella cymbiformis Vekshina, 1959

Bilapillus wadeae Lees, 2007

Biscutum constans (Górka, 1957) Black in Black and Barnes, 1959

Biscutum coronum Wind & Wise in Wise & Wind, 1977

Biscutum hattneri Wise, 1983

Biscutum magnum Wind & Wise in Wise & Wind, 1977

Biscutum melaniae (Górka, 1957) Reinhardt, 1969

Biscutum notaculum Wind & Wise in Wise & Wind, 1977

Braarudosphaera africana Stradner, 1961

Braarudosphaera batilliformis Troelsen & Quadros, 1971

Braarudosphaera bigelowii (Gran & Braarud, 1935) Deflandre, 1947

Braarudosphaera primula Black, 1973

Braarudosphaera turbinea Stradner, 1963

Broinsonia enormis (Shumenko, 1968) Manivit, 1971

Broinsonia parca (Stradner, 1963) Bukry, 1969

Broinsonia parca constricta Hattner et al., 1980

Broinsonia parca expansa Wise & Watkins in Wise, 1983

Broinsonia parca parca (Stradner, 1963) Bukry, 1969

Broinsonia signata (Noël, 1969) Noël, 1970

Broinsonia verecundia Wind & Wise in Wise & Wind, 1977

Bukryaster hayi (Bukry, 1969) Prins & Sissingh in Sissingh, 1977

Bukrylithus ambiguus Black, 1971

Calciosolenia fossilis (Deflandre in Deflandre & Fert, 1954) Bown in Kennedy et al., 2000

Calculites cyclops Lees, 2007

Calculites obscurus (Deflandre, 1959) Prins & Sissingh in Sissingh, 1977

Calculites ovalis (Stradner, 1963) Prins & Sissingh in Sissingh, 1977

Calculites percernis Jeremiah, 1996

Ceratolithoides aculeus (Stradner, 1961) Prins & Sissingh in Sissingh, 1977

Ceratolithoides sesquipedalis Burnett, 1997

Ceratolithoides verbeekii Perch-Nielsen, 1979

Chiastozygus amphipons (Bramlette & Martini, 1964) Gartner, 1968

Chiastozygus bifarius Bukry, 1969

Chiastozygus garrisonii Bukry, 1969

Chiastozygus litterarius (Górka, 1957) Manivit, 1971

Chiastozygus platyrhethus Hill, 1976

Chiastozygus fahudensis sp. nov. Al Rawahi

Chiastozygus synquadriperforatus Bukry, 1969

Chiastozygus trabalis (Górka, 1957) Burnett, 1997

Coccolithus pelagicus (Wallich 1877) Schiller, 1930

Corollithion exiguum Stradner, 1961

Corollithion kennedyi Crux, 1981

Corollithion madagaskarensis Perch-Nielsen, 1973

Corollithion signum Stradner, 1963

Cretarhabdus conicus Bramlette & Martini, 1964

Cribrosphaerella ehrenbergii (Arkhangelsky, 1912) Deflandre in Piveteau, 1952 *Crucibiscutum salebrosum* (Black, 1971) Jakubowski, 1986

Cruciellipsis cuvillieri (Manivit, 1966) Thierstein, 1971

Cylindralithus biarcus Bukry, 1969

Cylindralithus sculptus Bukry, 1969

Cylindralithus serratus Bramlette & Martini, 1964

Discorhabdus ignotus (Górka, 1957) Perch-Nielsen, 1968

Duocameratus leariae Lees, 2007

Eiffellithus angustus Bukry (1969)

Eiffellithus casulus Shamrock in Shamrock & Watkins (2009)

Eiffellithus collis Hoffmann (1970)

Eiffellithus eximius (Stover, 1966) Perch-Nielsen, 1968

Eiffellithus gorkae Reinhardt, 1965

Eiffellithus keio Shamrock & Watkins (2009)

Eiffellithus lindiensis Lees, 2007

Eiffellithus nudus Shamrock & Watkins (2009)

Eiffellithus parallelus Perch-Nielsen, 1973

Eiffellithus perch-nielseniae Shamrock & Watkins (2009)

Eiffellithus phantasma Shamrock & Watkins (2009)

Eiffellithus striatus (Black, 1971) Applegate & Bergen, 1988

Eiffellithus turriseiffelii (Deflandre in Deflandre & Fert, 1954) Reinhardt, 1965

Eprolithus floralis (Stradner, 1962) Stover, 1966

Eprolithus moratus (Stover, 1966) Burnett 1998

Eprolithus rarus Varol, 1992

Gartnerago cf. *G. praeobliquum* Lees, 2007

Gartnerago obliquum (Stradner, 1963) Noël, 1970

Gartnerago praeobliquum Jakubowski, 1986

Gartnerago segmentatum (Stover, 1966) Thierstein, 1974

Gorkaea obliqueclausus (Varol, 1991) Varol & Girgis, 1994

Gorkaea pseudanthophorus (Bramlette & Martini, 1964) Varol & Girgis, 1994

Grantarhabdus meddii Black, 1971

Helicolithus blairiae Kita, Watkins & Bergen 2016

Helicolithus compactus (Bukry, 1969) Varol & Girgis, 1994

Helicolithus leckiei Bown, 2005

Helicolithus trabeculatus (Górka, 1957) Verbeek, 1977

Hexalithus gardetiae Bukry, 1969

Hexalithus noeliae Loeblich & Tappan, 1966

Kamptnerius magnificus Deflandre, 1959

Lithastrinus grillii Stradner, 1962

Lithastrinus quadricuspis Farhan, 1987

Lithastrinus septenarius Forchheimer, 1972

Lithraphidites carniolensis Deflandre, 1963

Loxolithus armilla (Black in Black & Barnes, 1959) Noël, 1965

Loxolithus bicyclus Kanungo, 2005

Lucianorhabdus cayeuxii Deflandre, 1959

Lucianorhabdus maleformis Reinhardt, 1966

Manivitella pemmatoidea (Deflandre in Manivit, 1965) Thierstein, 1971

Marthasterites furcatus (Deflandre in Deflandre & Fert, 1954) Deflandre, 1959 *Microrhabdulus belgicus* Hay & Towe, 1963

Microrhabdulus decoratus Deflandre, 1959

Microrhabdulus undosus Perch-Nielsen, 1973

cf. *Micula adumbrata* Burnett, 1997

Micula clypeata Lees & Bown, 2005

Micula premolisilvae Lees & Bown, 2005

Micula cf. *M. prinsii* Perch-Nielsen, 1979

Micula staurophora (Gardet, 1955) Stradner, 1963

Munarinus keadyi Risatti, 1973

Munarinus lesliae Risatti, 1973

Nannoconus spp.

Nicholasia baileyi Lees, 2007

Octolithus multiplus (Perch-Nielsen, 1973) Romein, 1979

Ottavianus giannus Risatti, 1973

Ottavianus terrazetus Risatti, 1973

Owenia hillii Crux, 1991

Placozygus banneri Lees, 2007

Placozygus fibuliformis (Reinhardt, 1964) Hoffmann, 1970

Placozygus spiralis (Bramlette & Martini, 1964) Hoffmann, 1970

Prediscosphaera bukryi Perch-Nielsen, 1973

Prediscosphaera columnata (Stover, 1966) Perch-Nielsen, 1984

Prediscosphaera cretacea (Arkhangelsky, 1912) Gartner, 1968

Prediscosphaera grandis Perch-Nielsen, 1979

Prediscosphaera majungae Perch-Nielsen, 1973

Prediscosphaera microrhabdulina Perch-Nielsen, 1973

Prediscosphaera ponticula (Bukry, 1969) Perch-Nielsen, 1984

Prediscosphaera spinosa (Bramlette & Martini, 1964) Gartner, 1968

Prediscosphaera stoveri (Perch-Nielsen, 1968) Shafik & Stradner, 1971

Prolatipatella multicarinata Gartner, 1968

Quadrum gartneri Prins & Perch-Nielsen in Manivit et al., 1977

Reinhardtites anthophorus (Deflandre, 1959) Perch-Nielsen, 1968

Reinhardtites levis Prins & Sissingh in Sissingh, 1977

Retacapsa angustiforata Black, 1971

Retacapsa crenulata (Bramlette & Martini, 1964) Grün in Grün and Allemann, 1975

Retacapsa ficula (Stover, 1966) Burnett, 1997

Retacapsa octofenestrata (Bralower in Bralower et al., 1989) Bown in Bown & Cooper, 1998

Retacapsa schizobrachiata (Gartner, 1968) Grün in Grün and Allemann, 1975

Retacapsa surirella (Deflandre & Fert, 1954) Grün in Grün and Allemann, 1975

Rhagodiscus angustus (Stradner, 1963) Reinhardt, 1971

Rhagodiscus indistinctus Burnett, 1997

Rhagodiscus pancostii Lees, 2007

Rhagodiscus pseudoangustus Crux, 1987

Rhagodiscus reniformis Perch-Nielsen, 1973

Rhagodiscus splendans (Deflandre, 1953) Verbeek, 1977

Russellia bukryi Risatti, 1973

Russellia laswellii Risatti, 1973

Staurolithites cf. *S. ngurumahambaensis* Lees, 2007

Staurolithites crux (Deflandre & Fert, 1954) Caratini, 1963

Staurolithites dorfii (Bukry, 1969) Burnett, 1997

Staurolithites ellipticus (Gartner, 1968) Lambert, 1987

Staurolithites flavus Burnett, 1997

Staurolithites handleyi Lees, 2007

Staurolithites imbricatus (Gartner, 1968) Burnett, 1997

Staurolithites mielnicensis (Górka, 1957) Perch-Nielsen, 1968 sensu Crux in Lord, 1982 *Staurolithites ourmae* sp. nov. Al Rawahi

Staurolithites zoensis Burnett, 1997

Tegumentum stradneri Roth & Thierstein, 1972

Tetrapodorhabdus decorus (Deflandre in Deflandre & Fert, 1954) Wind & Wise 1983 *Thoracosphaera saxea* Stradner (1961)

Tranolithus gabalus Stover, 1966

Tranolithus minimus (Bukry, 1969) Perch-Nielsen, 1984

Tranolithus orionatus (Reinhardt, 1966a) Reinhardt, 1966b

Tranolithus stemmerikii Thibault & Sheldon, in Thibault 2010

Uniplanarius gothicus (Deflandre, 1959) Hattner & Wise, in Wind & Wise 1983

Uniplanarius sissinghii (Perch-Nielsen, 1986) Farhan 1987

Uniplanarius trifidus (Stradner in Stradner & Papp, 1961) Hattner & Wise, in Wind & Wise 1983

Watznaueria barnesae (Black in Black & Barnes, 1959) Perch-Nielsen, 1968

Watznaueria bayackii Worsley, 1971

Watznaueria fossacincta (Black, 1971) Bown in Bown & Cooper, 1989

Watznaueria ovata Bukry, 1969

Watznaueria quadriradiata Bukry, 1969

Zeugrhabdotus acanthus Reinhardt, 1965

Zeugrhabdotus bicrescenticus (Stover, 1966) Burnett in Gale et al., 1996

Zeugrhabdotus biperforatus (Gartner, 1968) Burnett, 1997

Zeugrhabdotus blowii Lees, 2007

Zeugrhabdotus cf. *Z. xenotus* (Stover, 1966) Burnett in Gale et al., 1996

Zeugrhabdotus clarus Bown, 2005

Zeugrhabdotus diplogrammus (Deflandre in Deflandre & Fert, 1954) Burnett in Gale et al., 1996

Zeugrhabdotus embergeri (Noël, 1959) Perch-Nielsen, 1984

Zeugrhabdotus erectus (Deflandre in Deflandre & Fert, 1954) Reinhardt, 1965

Zeugrhabdotus cf. *Z. fissus* Grün & Zweili, 1980

Zeugrhabdotus cf. *Z. scutula* (Bergen, 1994) Rutledge & Bown, 1996

Zeugrhabdotus howei Bown in Kennedy et al., 2000

Zeugrhabdotus noeliae Rood et al., 1971

Zeugrhabdotus praesigmoides Burnett, 1997

Zeugrhabdotus sigmoides (Bramlette & Martini, 1964) Bown & Young, 1997

Zeugrhabdotus trivectis Bergen, 1994

Plate 1

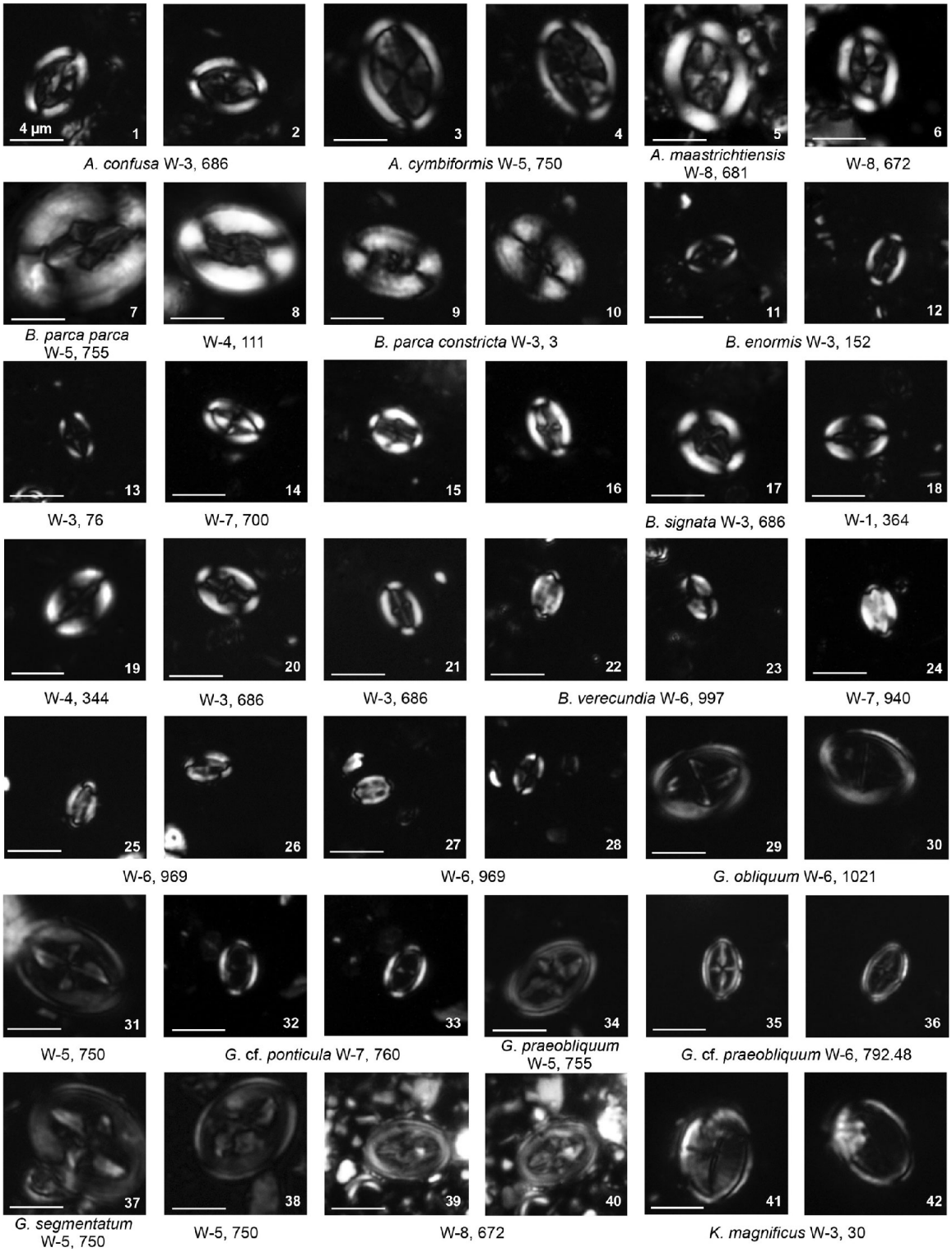

Arkhangelskiales Arkhangelskiellaceae: *Arkhangelskiella, Broinsonia*; *Kamptneriaceae*: *Gartnerago*, *Kamptnerius*.

Plate 2

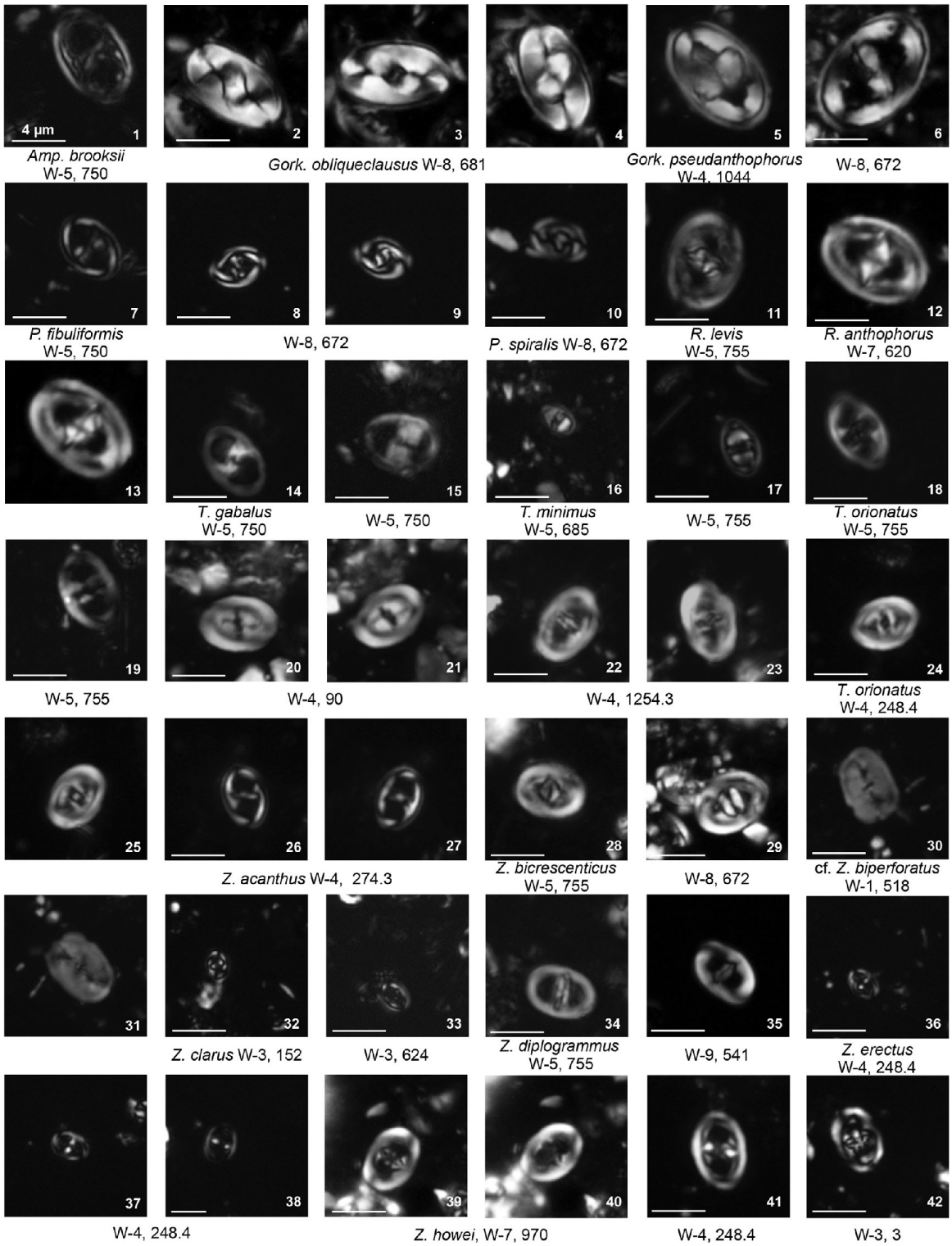

Eiffellithales Chiastozygaceae: *Amphizygus*, *Gorkaea*, *Placozygus*, *Reinhardtites*, *Tranolithus, Zeugrhabdotus.*

Plate 3

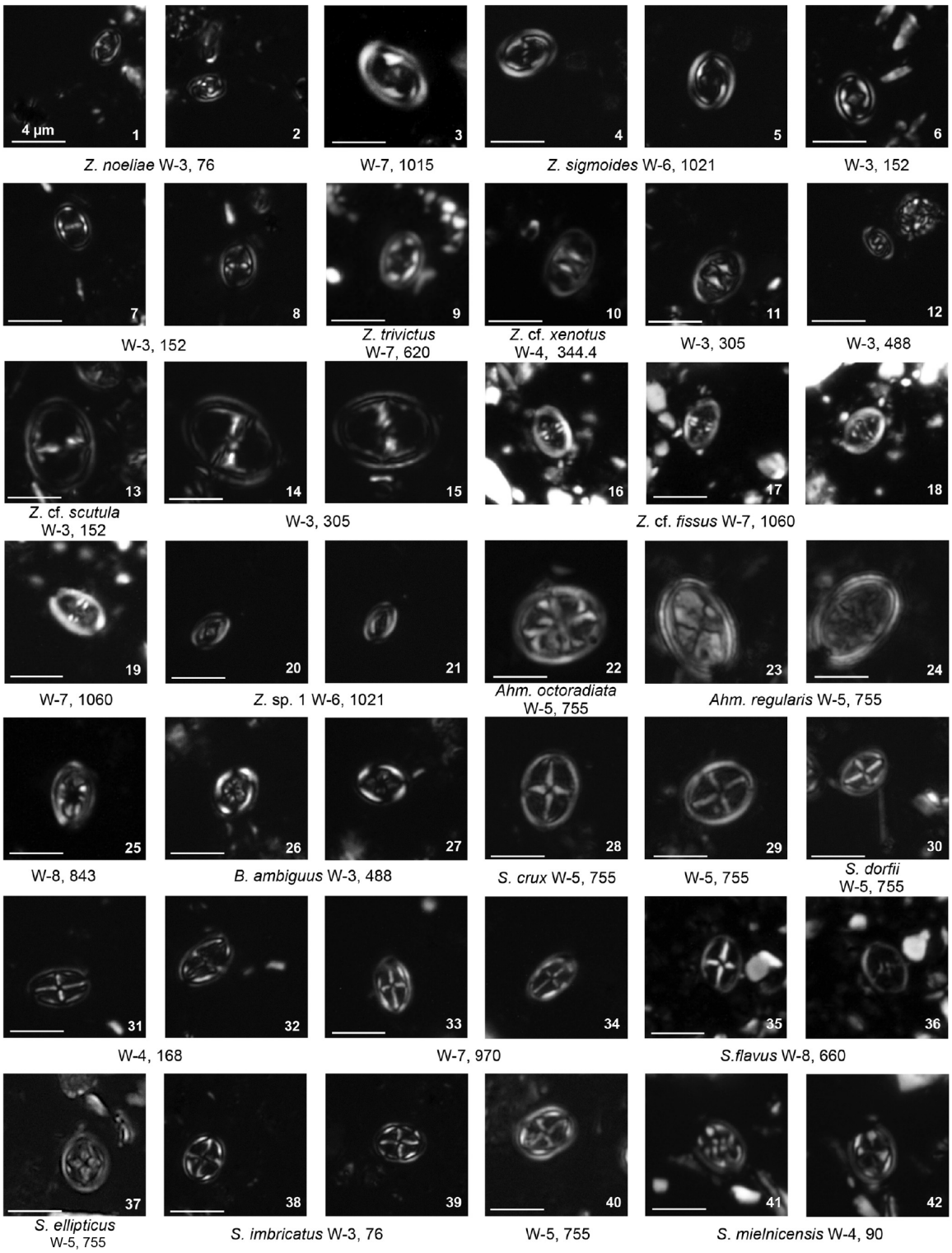

Eiffellithales Chiastozygaceae: *Zeugrhabdotus, Ahmuellerella, Bukrylithus, Staurolithites*.

Plate 4

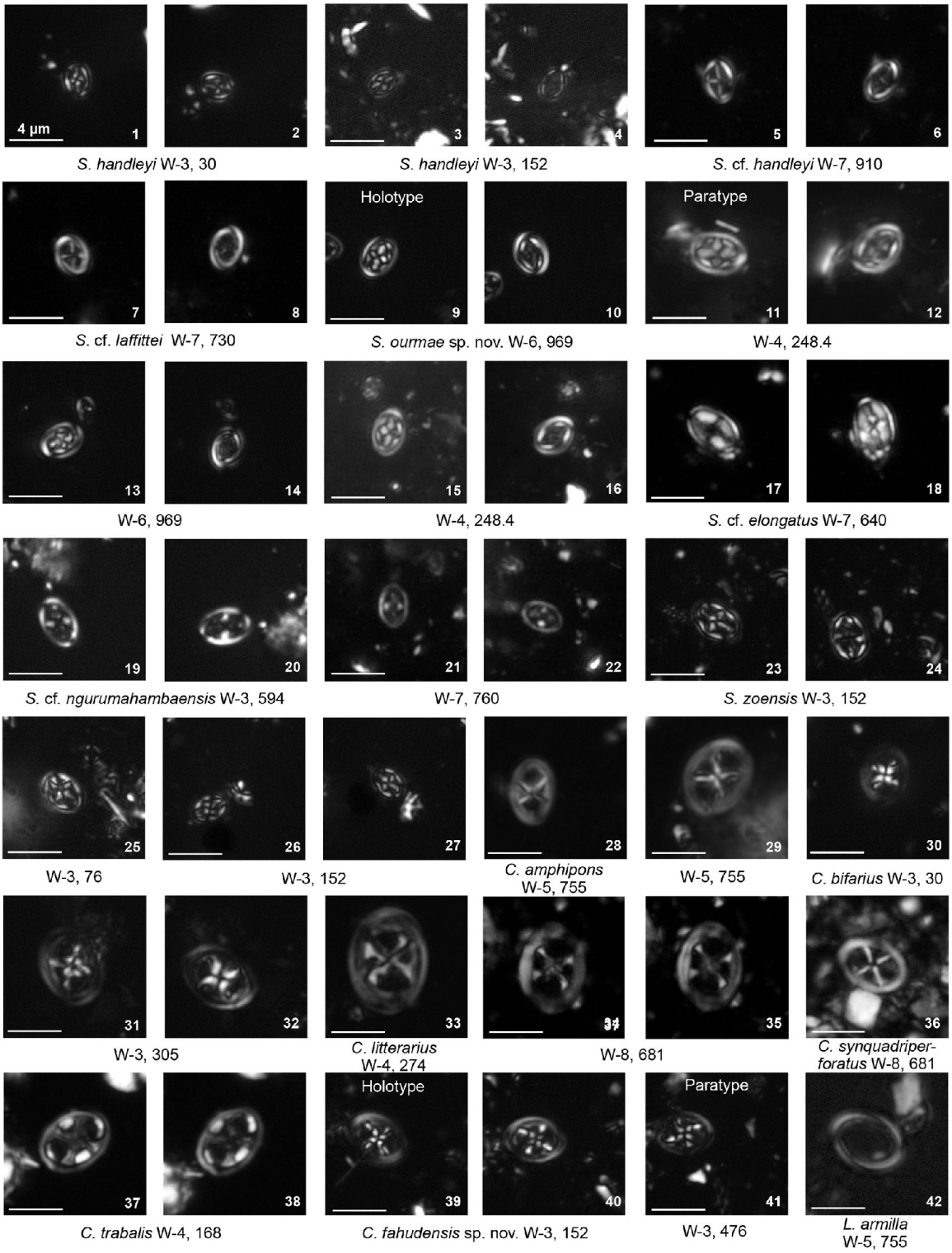

Eiffellithales Chiastozygaceae: *Staurolithites, Chiastozygus, Loxolithus*.

Plate 5

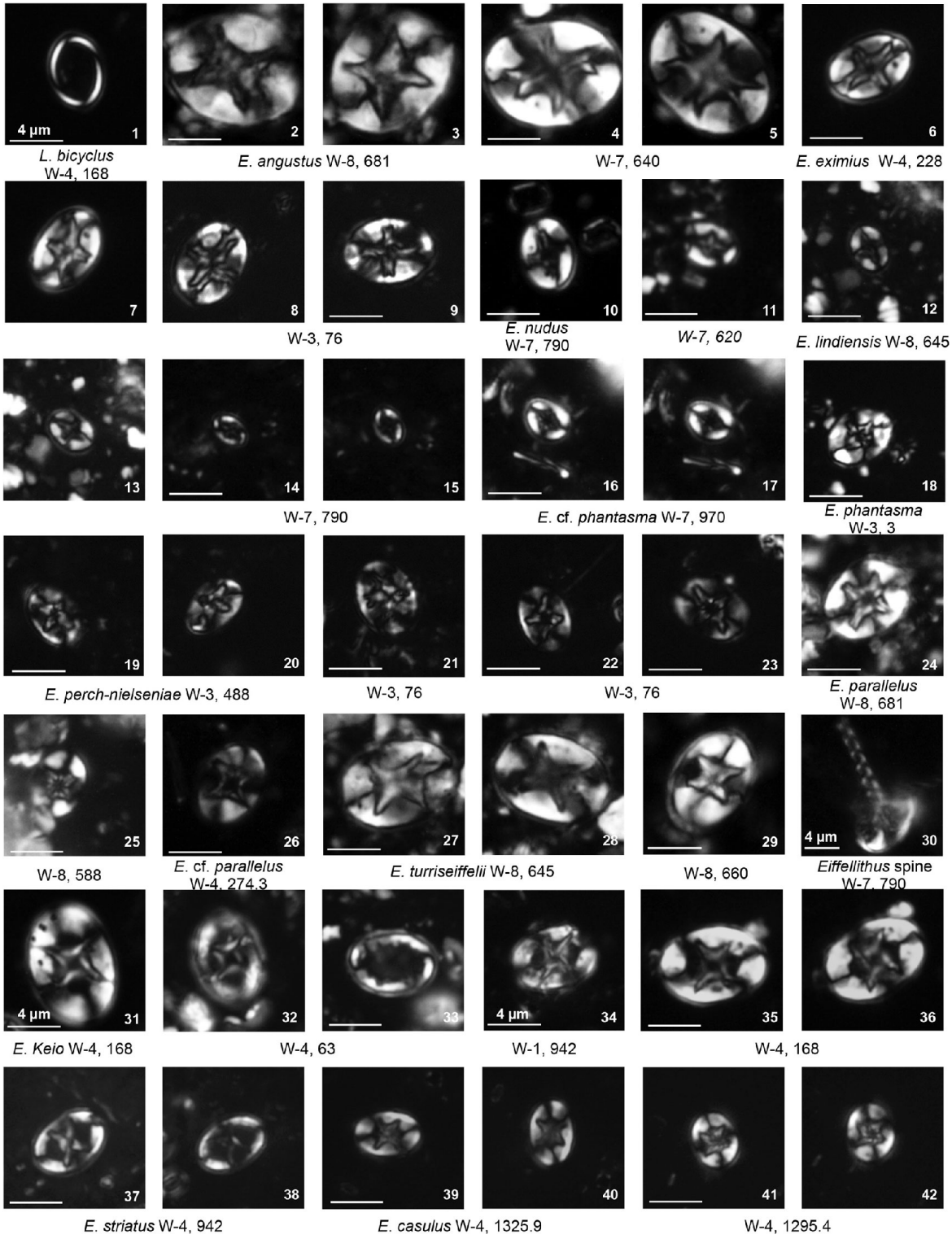

Eiffellithales Chiastozygaceae: *Loxolithus;* Eiffellithaceae: *Eiffellithus*.

Plate 6

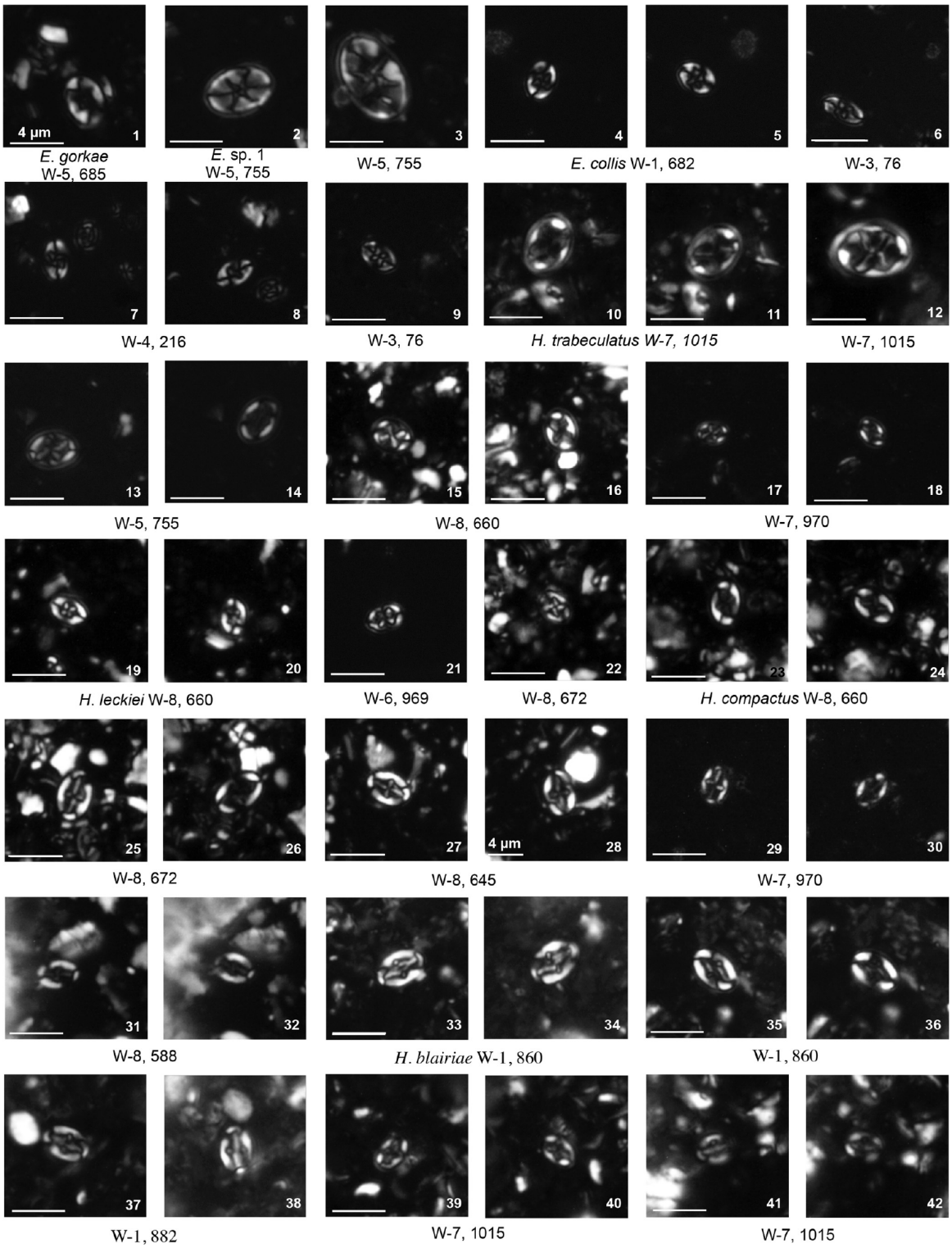

Eiffellithales Eiffellithaceae: *Eiffellithus*, *Helicolithus*.

Plate 7

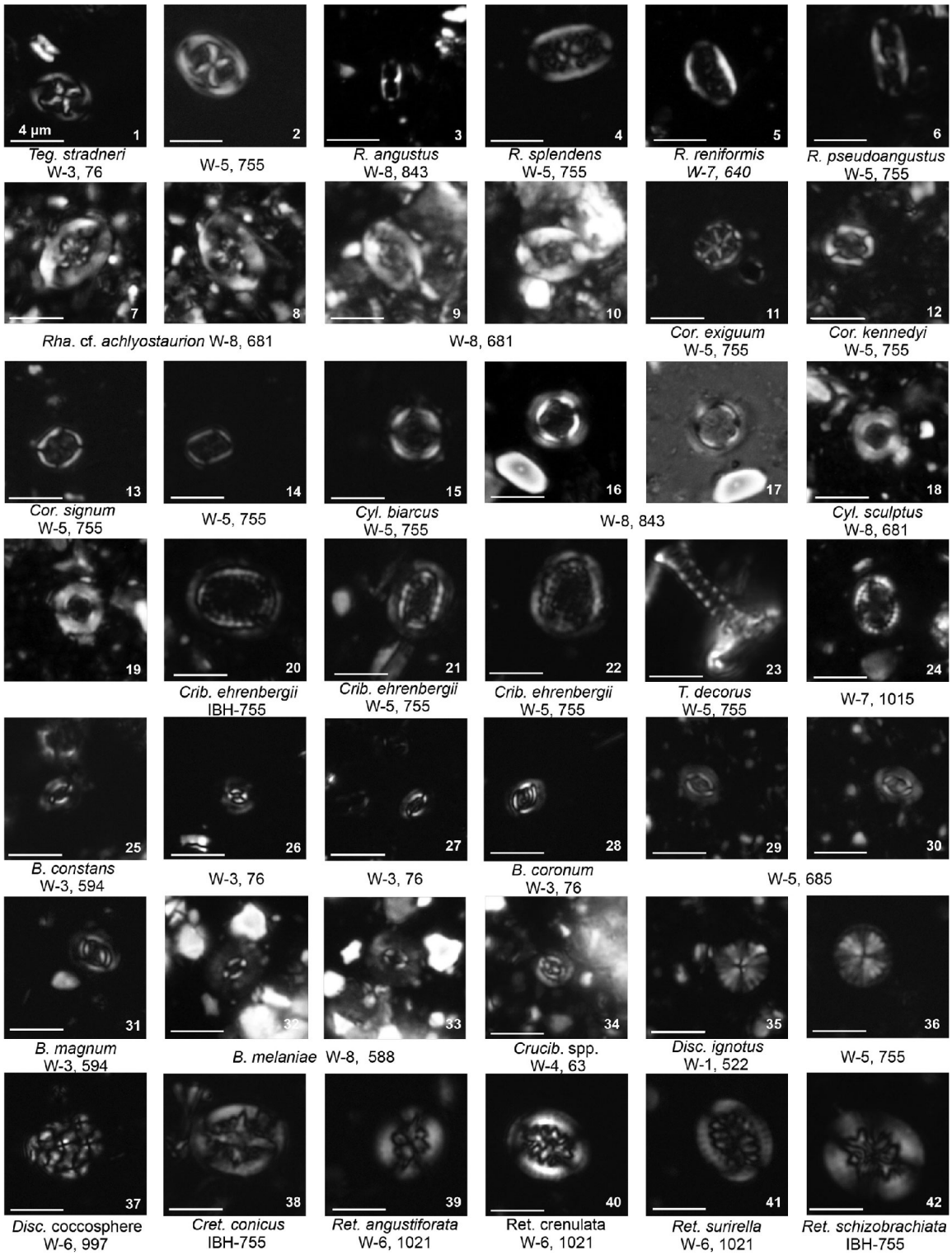

Eiffellithales Eiffellithaceae: *Tegumentum*; Rhagodiscaceae: *Rhagodiscus*. **Stephanolithiales** Stephanolithiaceae: *Corollithion, Cylindralithus*. **Podorhabdales** Axopodorhabdaceae: *Cribrosphaerella, Tetrapodorhabdus*; Biscutaceae: *Biscutum, Discorhabdus*; Cretarhabdaceae: *Cretarhabdus, Retecapsa*.

Plate 8

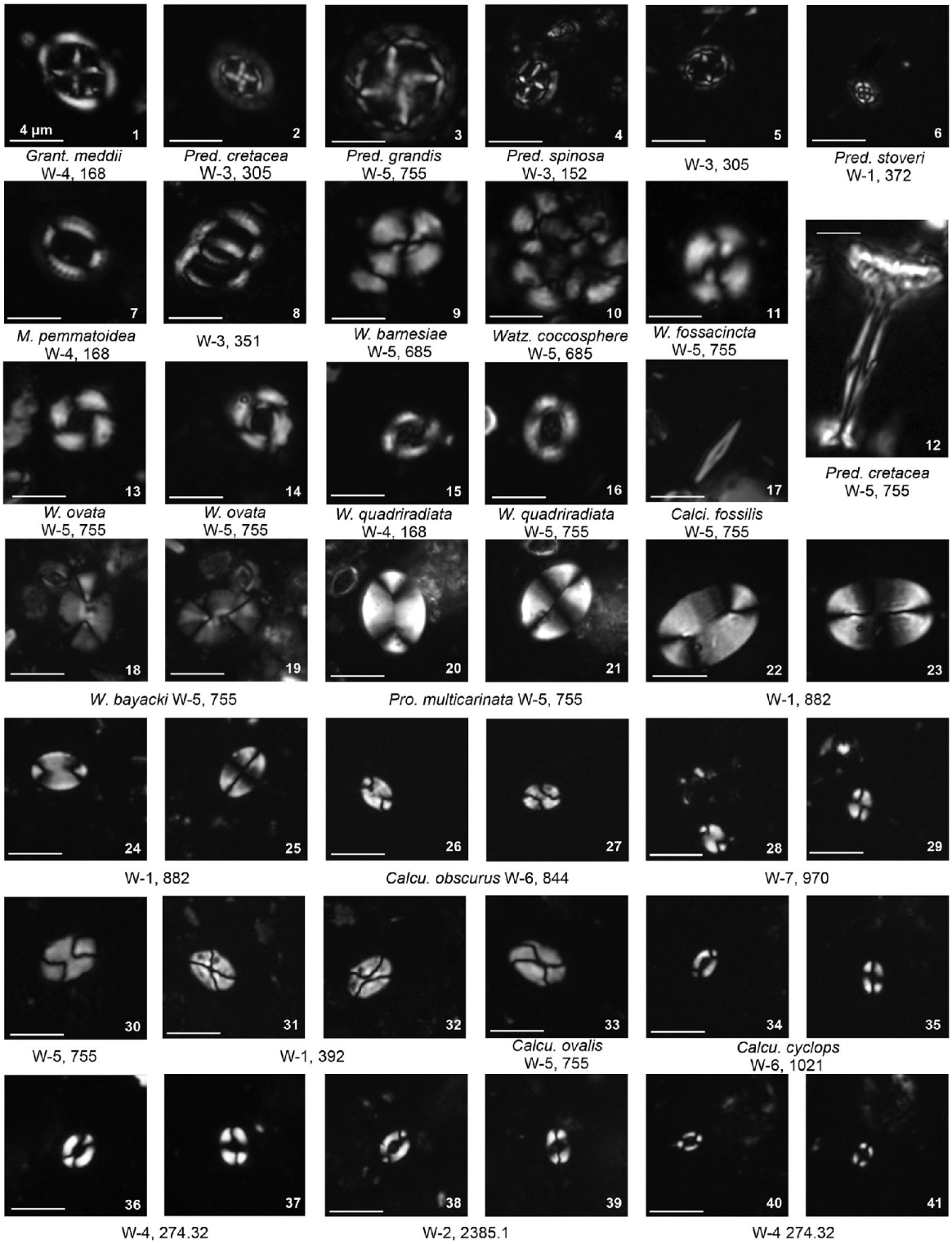

Podorhabdales Cretarhabdaceae: *Grantarhabdus*; Prediscosphaeraceae: *Prediscosphaera*; Tubodiscaceae: Manivitella; **Watznaueriales** Watznaueriaceae: *Watznaueria*; **Syracosphaerales** Calciosoleniaceae: *Calciosolenia*; **heterococcoliths inc sedis** placoliths inc sedis: *Prolatipatella*; **holococcoliths** common genera: *Calculites*.

Plate 9

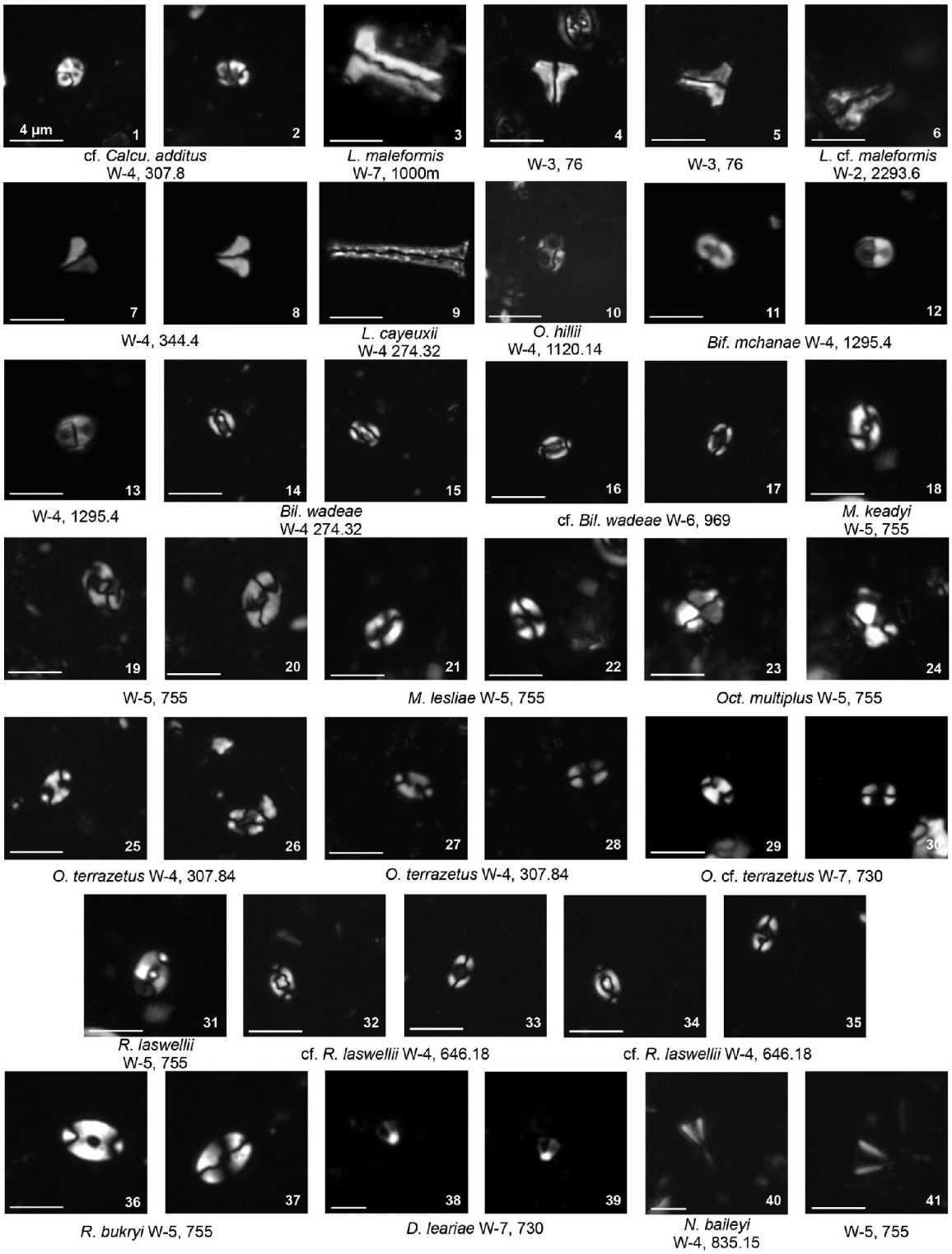

Holococcoliths common genera: *Calculites, Lucianorhabdus, Owenia*. Rarer genera: *Bifidalithus, Bilapillus, Munarinus, Octolithus, Ottavianus, Russellia, Duocameratus, Nicholasia*.

Plate 10

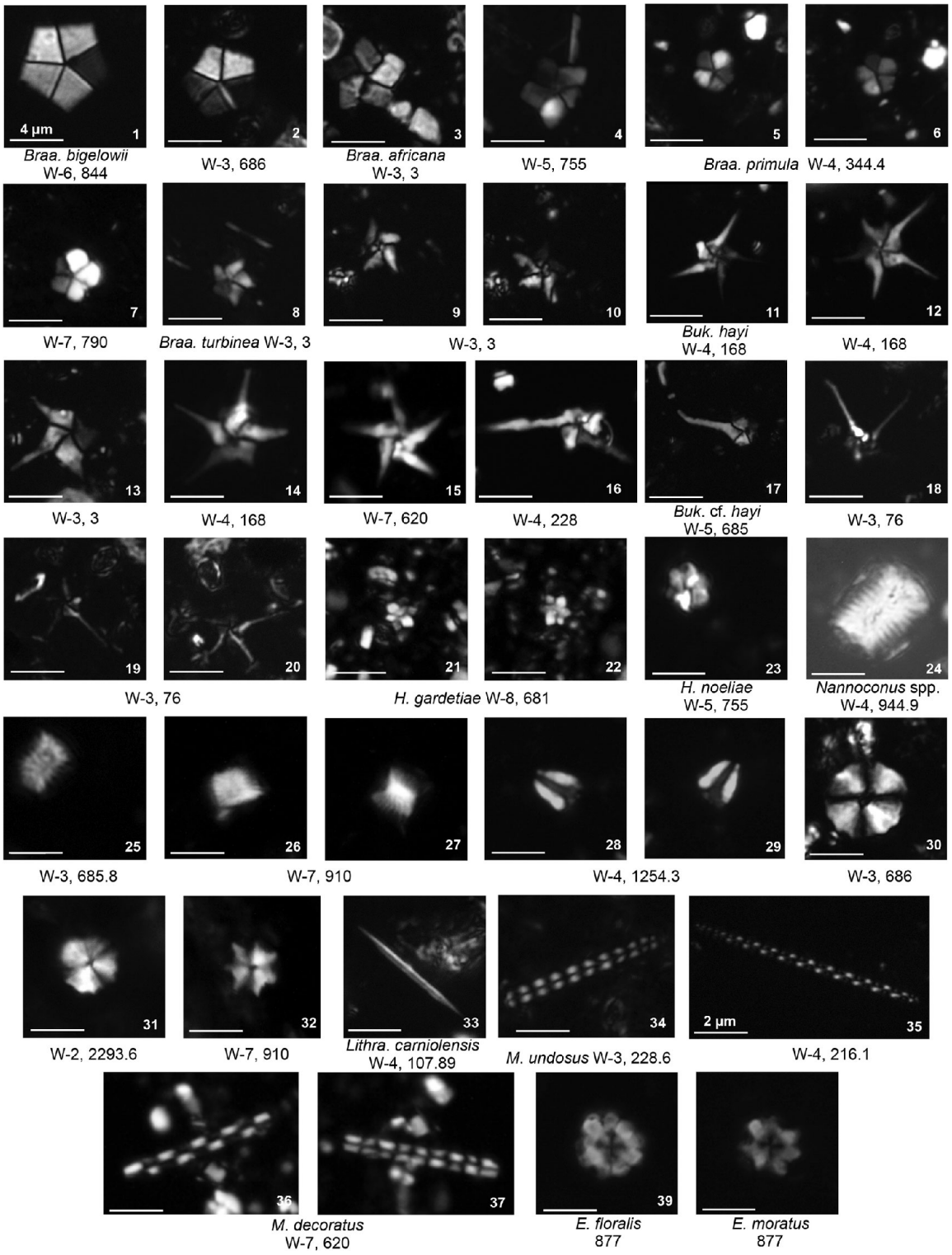

Nannoliths Braarudosphaerales Braarudosphaeraceae: *Braarudosphaera*, *Bukryaster*, *Hexalithus*; Nannoconaceae: *Nannoconus*. **Nannoliths inc sedis** Microrhabdulaceae: *Lithraphidites*, *Microrhabdulus*; Polycyclolithaceae: *Eprolithus*.

Plate 11

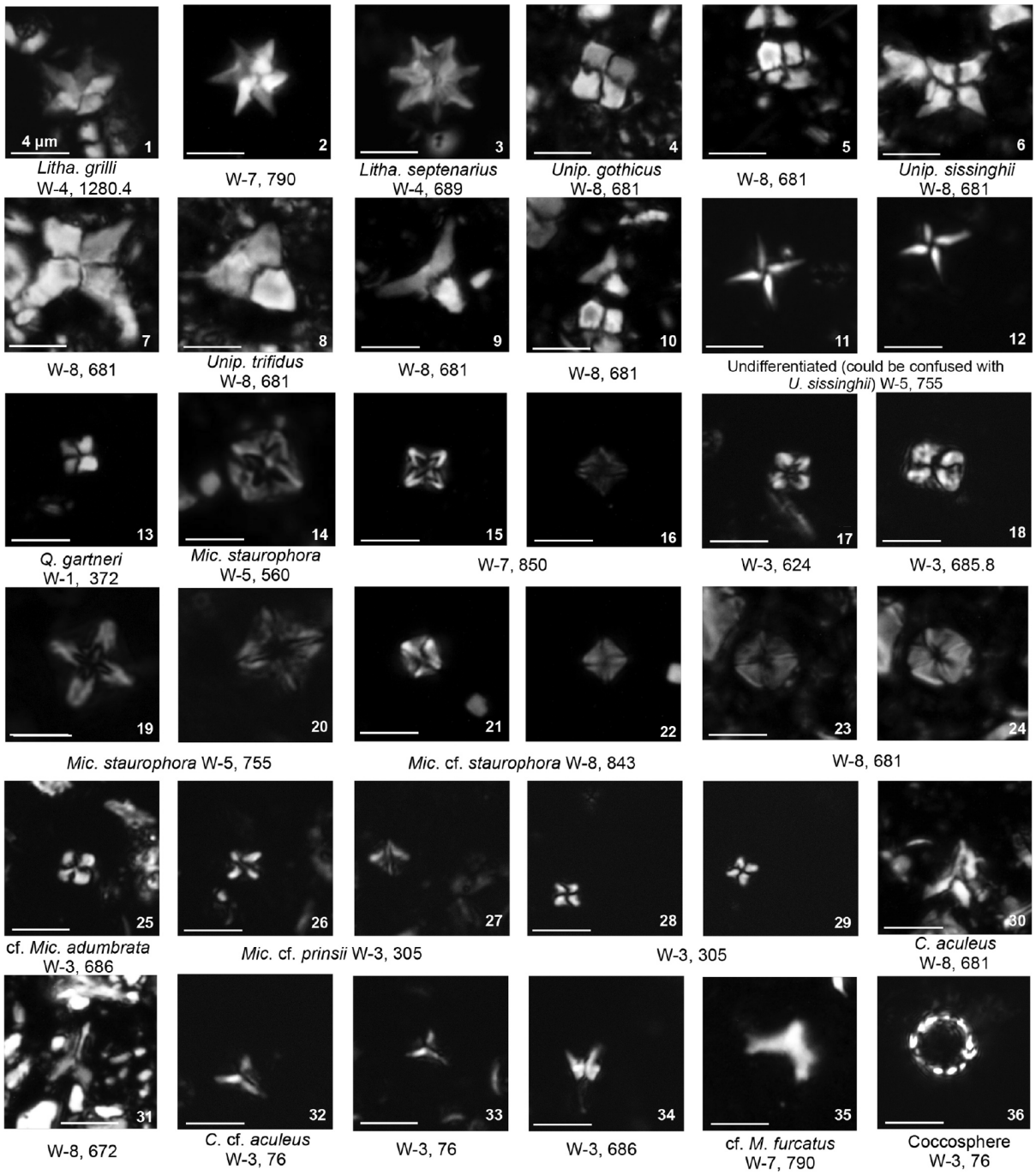

Nannoliths inc sedis Polycyclolithaceae: *Lithastrinus*, *Uniplanarius*, *Quadrum*, *Micula*. **Nannoliths inc sedis – other**: *Ceratolithoides*, *Marthasterites*.

CHAPTER 3

NANNOFOSSIL BIOSTRATIGRAPHIC CORRELATION OF THE UPPER CRETACEOUS FIQA FORMATION ACROSS NORTH OMAN

(A version of this chapter is submitted to the Journal of Newsletters on Stratigraphy. Co-author: Tom Dunkley Jones. Data collection, sample analyses, data interpretation and writing of the paper have been undertaken by Zainab Al Rawahi under the guidance and supervision of Tom Dunkley Jones. Detailed documentation of the nannofossil and microfossil assemblage composition for each well is available in the attached digital appendix 1. Marker species range charts are attached in digital appendix 2)

Abstract. Here we provide a new biostratigraphic framework for the Upper Cretaceous Fiqa Formation of Oman based on the extensive examination of calcareous nannofossil assemblages within 249 samples from 11 hydrocarbon exploration wells. Nannofossil assemblages are typically well preserved and complement existing microfaunal data. The UC biozonation scheme of Burnett et al. (1998) for the Tethyan Province is useful in the lower Maastrichtian and upper Campanian intervals, but less so in the mid-Campanian to upper Coniacian where many of the global marker taxa are either absent or present with rare, sporadic occurrences. A total of 5 local, consistent supplementary biohorizons are recognised through UC11 to UC17 (upper Coniacian-lower Maastrichtian), including 3 biohorizons within the poorly constrained lower Campanian to Santonian UC12-13 zones. These include the top *Helicolithus blairiae* bioevent as a potential marker for the transition from early Campanian to late Santonian. Detailed correlation of nannofossil biohorizons and lithostratigraphy across the study area also proved the diachronous nature of the transition from the carbonates of the Arada Member to

the shales of the Shargi Member, which changes from the lower to upper Campanian between the north and south of the study area. Calcareous nannofossil biostratigraphy also reveals diachroneity at the top and base of the Fiqa Formation; at its base upper Coniacian sediments are only preserved in the north of the basin, whilst at its top lower Maastrichtian sediments are only recorded in the south of the basin. Our new biostratigraphy is compared against previous stratigraphic studies of the Aruma Basin and correlated to major sequence stratigraphic events of the Arabian Plate, as well as the tectonic evolution of the basin. This new zonation provides a practical biostratigraphic scheme, with improved resolution, suitable for future geological and exploration studies in the region.

1 Introduction

The fine-grained shales of the Upper Cretaceous Fiqa Formation, Oman, were deposited in the tectonically active Aruma basin, contemporaneous to the emplacement of the Late Cretaceous ophiolite in what is now part of North Oman Mountains (Glennie et al., 1974). These active tectonic processes resulted in a complicated subsurface geology, with unconformities bounding both the top and base of the Fiqa Formation. These unconformities are thought to be diachronous but are poorly constrained by chronostratigraphy (e.g. Forbes et al., 2010). Within the Fiqa Formation the timing of a progressive transition from deeper to shallower water marine facies across the basin is also poorly known (e.g. Glennie et al., 1973; Hughes-Clark, 1988; Forbes et al., 2010). These changes in facies are represented in stratigraphic subdivisions of the Fiqa Formation, but correlations from well-to-well remain tentative because lithological variations and down-hole log characters of the predominantly homogeneous shales are subtle (Forbes et al., 2010). These fine-grained shales of the Fiqa Formation are, however, re-

gionally important as a major seal unit for most of the underlying mid-Cretaceous hydrocarbon reservoirs in Oman. Constraining thickness and age relationships of the Fiqa Formation across the Aruma Basin is thus important for hydrocarbon exploration activities. Improved estimates of depositional ages and diachroneity across the basin will also inform models of basin development related to ophiolite emplacement.

Work to develop a Fiqa Formation biostratigraphy has been ongoing for the past 50 years, mostly in unpublished industry reports of the Petroleum Development Oman (PDO). The best of these micropalaeontological studies included analyses of foraminifera, dinoflagellate, spore and pollen assemblages to provide paleoenvironmental and chronostratigraphic constraints within the Formation (e.g. Clarke and Hoogkamer, 1967; Carr et al., 1998; Packer, 2001a; Mohiuddin, 2002 and Packer, 2002). The zonation schemes of these studies are summarised in Figure 1. The first palynological zonation for the Formation, established by Clarke and Hoogkamer (1967), had one zone of Coniacian to Campanian age, but was replaced by a three-fold zonation spanning ?Turonian to late Campanian age (Mohiuddin, 2002). Disagreement between these schemes and their low resolution (Fig. 1), emphasised the need for calcareous nannofossil and microfossil biostratigraphy, which are more easily applicable to the marine successions of the Upper Cretaceous Fiqa Formation.

The first PDO studies based on calcareous microfossil assemblages (Clarke and Hoogkamer, 1967) assigned the Fiqa Formation to the late Santonian to earliest Campanian based on the *Globotruncana carinata* Microzone (Fig. 1). Further work on planktonic foraminiferal assemblages (Glennie et al., 1974), also identified a Santonian to Campanian depositional age based on outcrop samples. This was followed by a Coniacian to early Campanian zonation scheme

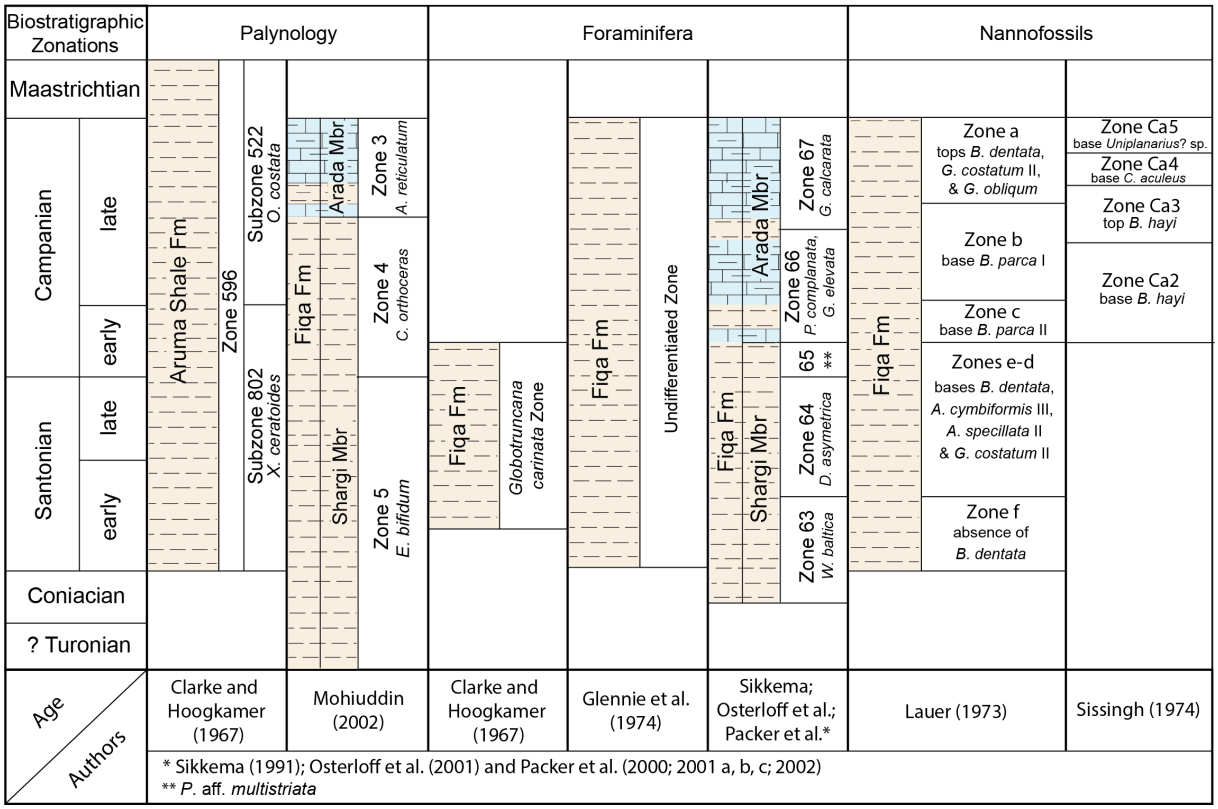

Figure 1. Summary of the previously established local zonation schemes for the Fiqa Formation of Oman.

developed by Sikkema (1991) that was later compiled by Droste (2001) and modified by Osterloff et al. (2001) with more sections and samples studied, mainly from the subsurface. More comprehensive studies were undertaken for a series of exploration projects (Packer et al. 2000; 2001 a, b, c; 2002) with new comments and improvements to the initial zonation scheme of Osterloff et al. (2001). These new schemes provided a higher resolution zonation, mainly based on planktonic foraminifera (Fig. 1), especially in the basal part of the lower, Shargi Member of the Fiqa Formation which was the focus of the exploration projects. The upper, Arada Member of the Fiqa Formation remained less comprehensively studied, with the chronostratigraphic transition between the two members remaining unresolved (Forbes et al., 2010). A disadvantage of these microfossil zonations, however, is the facies-dependent occur-

rence of many species, with for example, changes in water depth causing diachroneity in base or top biohorizons. For example, within the lower Campanian intervals (e.g. microfossil Zone F65) of the Fiqa Formation the presence or absence of water depth-sensitive biofacies are predominantly driven by relative sea level change (Packer, 2001a).

Nannofossil biostratigraphy, on the other hand, is more facies-independent, allowing more precise temporal correlation between different palaeoenvironment and widely separated areas (e.g. Raffi et al. 2006). Despite the fact that nannofossils are abundant within the Fiqa Formation and have been investigated in several unpublished PDO studies (e.g. Lauer, 1973; Sissingh, 1974), there is no detailed nannofossil biozonation scheme for the Fiqa Formation or correlation to the global schemes. The pioneering work of Lauer (1973) on the Fiqa Formation nannofossils, produced a six-fold zonation (Fig. 1) using only the rapid evolutionary trends within the Arkangelskiellaceae family, including *Arkhangelskiella*, *Broinsonia* and *Gartnerago*. The Arkangelskiellaceae are, however, relatively rare in the section and are highly sensitive to dissolution, which can make identification difficult, and the zonation scheme was not well integrated into a global chronostratigraphy. This was followed by a more comprehensive study of selected Late Cretaceous nannoplankton bioevents across the world (Tunisia, Turkey, France, The Netherlands, Denmark and U.S) including 3 hydrocarbon wells from Oman (Sissingh, 1974). Six Campanian zones were tentatively proposed (Fig. 1), but with difficulties in adequately establishing the range of a number of key markers (Sissingh, 1974). New calcareous nannofossil biostratigraphic data from the Fiqa Formation are thus important for regional correlation and studies of basin evolution, as well as to provide a reference section for further development of robust global biozonation schemes.

Nannofossil biostratigraphy has been successfully used to constrain the age of various Upper Cretaceous sequences along the Southwestern margin of the Tethys Ocean. These include the Coniacian-Maastrichtian marl and chalk sequences of Lebanon (Müller et al., 2010), the Coniacian to Maastrichtian Themed and Sudr Formations of Egypt (Faris and Abu Shama, 2006; Farouk and Faris, 2012), the upper Campanian to Maastrichtian upper Mahara group of Yemen (Al-Wosabi and Alaug, 2013) and the Campanian Abtalkh Formation of Iran (Foroughi et al., 2017). High-resolution nannofossil biostratigraphy has also been correlated to carbon isotope stratigraphy across stage boundaries, including the Santonian/Campanian transition in the Kef and Aboid Formations of Tunisia (Farouk et al., 2018b); the Campanian/ Maastrichtian transition in Shiranish Formation of Iraq (Farouk et al., 2018a) and the stage boundaries of the Upper Cretaceous Gurpi Formation of Iran (Razmjooei et al., 2014; Razmjooei et al., 2018). Here, we present new calcareous nannofossil biostratigraphic data from the Fiqa Formation and seek to integrate it into these wider regional stratigraphic studies.

This paper builds on the results of the first detailed study of the nannofossil assemblages in the area by Al Rawahi and Dunkley Jones (2019a) (see Chapter 2) by providing detailed new biostratigraphic data from 11 wells that recover the Fiqa Formation across Oman. This new data will be integrated with the previous industry reports on microfossil assemblages and stratigraphy by Sikkema (1991), Osterloff et. al. (2001), Packer et al. (2000) Packer (2001a; b; c) and Packer (2002). The study aims to provide a new biostratigraphic framework and correlate it to the standard global zonation schemes. This new framework can then be used to constrain the age of the Fiqa Formation's top, base and the regional transition between the car-

bonate and shale facies of the Formation. To achieve this, biostratigraphic data will be integrated with lithologic interpretations of wire line logs and core/cuttings descriptions. The nannofossil biostratigraphy also aims to improve the sequence stratigraphy for the Fiqa Formation, with an ultimate aim of an improved understanding of the basin history and its complex interrelationship with regional Late Cretaceous tectonic events, including the ophiolite emplacement.

2 Geological and Tectonic Settings

The Upper Cretaceous Fiqa Formation *sensu* Standring (1967) in Sugden and Standring (1975); Hughes-Clark (1988) and Forbes et al. (2010) of the subsurface North Oman is part of an extensive succession of variable units of marine shales, marls and limestones deposited over most of Oman and parts of the Middle East during the Late Cretaceous. The Fiqa Formation is part of the Aruma Group (Owen and Nasr, 1958), and in Oman is subdivided into two members; the Shargi Member dominated by deep marine shales, and the overlying shallower marine carbonate dominated Arada Member (Hughes-Clark, 1988; Forbes et al., 2010) (Fig. 2a). The Formation is bounded by the "Wasia-Aruma break" unconformity (Glennie et al., 1973) at its base, where is overlies the mid-Cretaceous shelf carbonate facies of the Natih Formation. At its top, the Fiqa Formation is unconformably overlain either by the Maastrichtian marginal marine beach and carbonate shelf facies of the Qahlah and Simsima Formations, Paleogene marine sediments or recent deposits (Glennie et al. 1974; Hughes-Clark, 1988; Nolan et al., 1990; Skelton et al., 1990; Forbes et al., 2010).

Close to the Oman Mountains in the north of the country, the Fiqa Formation is a very thick (> 1km) unit (Fig. 2b) comprised of mixed hemipelagic shale and carbonates, but thins toward

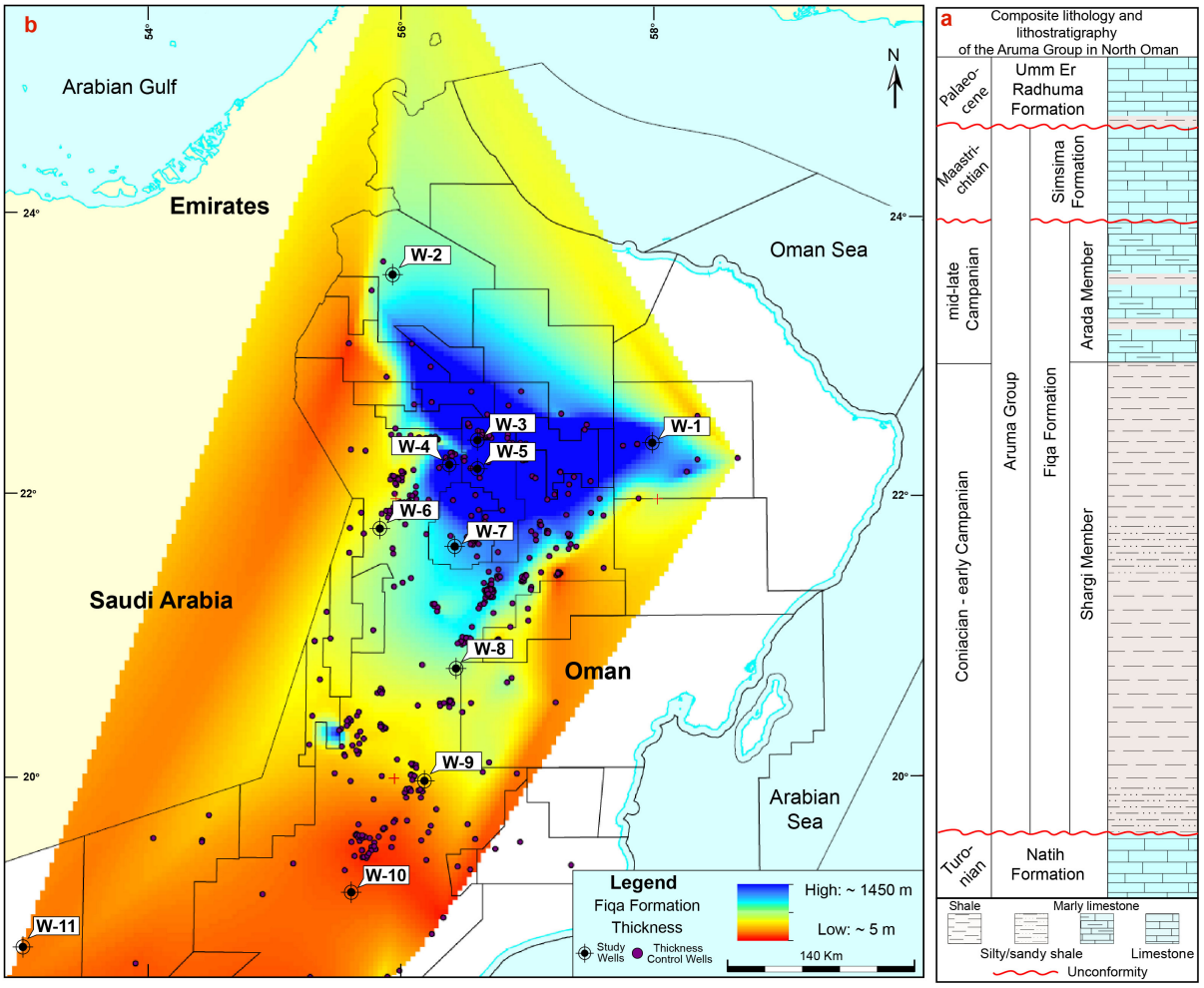

Figure 2. Composite lithology and lithostratigraphy of the Aruma group in Oman (a) (from Al Rawahi and Dunkley Jones, 2019a; see Chapter 2), and Fiqa Formation thickness map for the study area (b) with the location of the study wells.

the southeast as it gradually transitions into shallower marine facies (Forbes et al., 2010). Further to the east, the formation thickens again as it passes over the Huqf High area of East Oman and changes into a turbiditic succession within the down-faulted blocks bounding the Arabian Sea passive margin (Hughes-Clark, 1988). Planktonic foraminiferal dating assigns a late Coniacian to late Campanian age to the Fiqa Formation (Sikkema, 1991; Osterloff et al., 2001; Packer et al., 2000; Packer, 2001 a, b, c; 2002), whilst micropalaeontological facies analysis from several wells in northern Oman indicating an inner to middle neritic deposition-

al environment during the Coniacian-Santonian, deepening into outer neritic to upper bathyal during the Santonian-early Campanian, then shallowing again into middle to outer neritic settings toward the late Campanian upper part of the formation (Packer, 2002).

Tectonically, the Fiqa Formation was deposited in a rapidly subsiding deep marine foreland basin (Fig. 3a) developed over a passive carbonate shelf, that covered most of Oman (Glennie et al., 1973). The Aruma Basin was located at a tropical paleo-latitude during the Late Cretaceous (Fig. 3b) and formed during a major compressional tectonic events associated with the closure of the Tethys Ocean (e.g. Lippard et al., 1986; Searle, 1988; Warburton et al., 1990; Searle and Cox, 1999). Collision between the southward migrating Tethyan subduction zone and the northward migrating Arabian margin (Warburton et al., 1990), caused over thrusting of Tethyan oceanic crust and upper mantle, known as the Semail ophiolite, onto the Northeastern margin of Arabia (e.g. Glennie et al., 1973; Coleman, 1981; Lippard et al., 1986; Searle, 1988; Searle and Cox, 1999). Radiometric dating indicates that ophiolite emplacement of Cenomanian-aged crust started on the order of ~0.25–0.5 Ma after crust formation (Warren et al., 2005; Rioux et al., 2012). The process of emplacement continued through to the Maastrichtian, ca. 70 Ma (Searle, 2007) and resulted in a crustal loading and depression of the pre-existing carbonate platform margin and formation of a deep basin between the over-thrusted blocks and an emergent fore-bulge to the west of Oman (Warburton et al., 1990). Basin-wide burial history curves from exploration well data show extremely rapid subsidence in the mountain front during the Late Cretaceous which only declines after thrusting ends and the foreland basin fills (Warburton et al., 1990). The generation of this accommodation space within the Aruma basin is likely enhanced by the reactivation of basement faults and subsur-

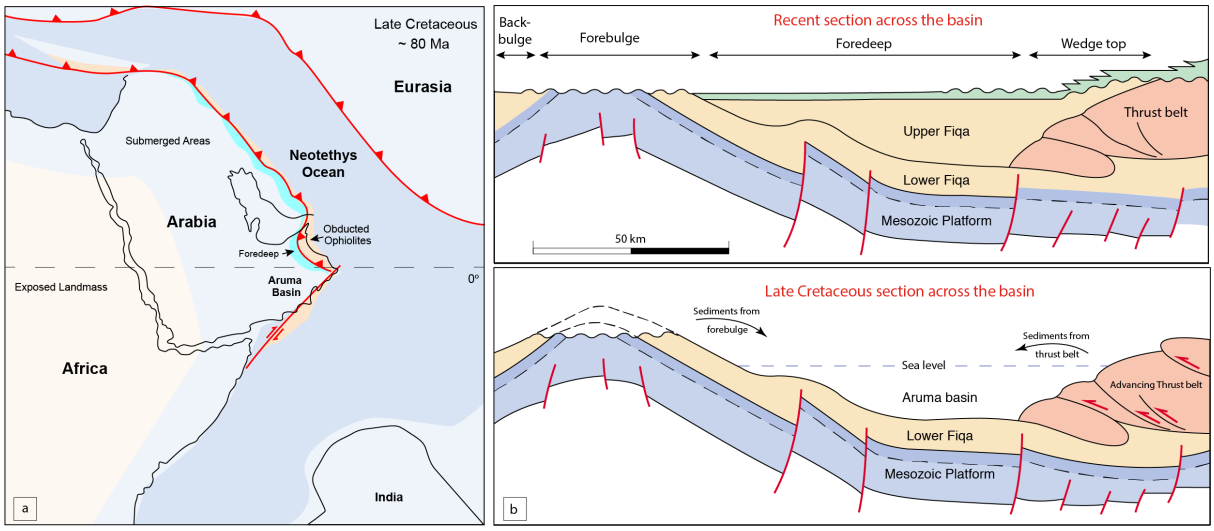

Figure 3. The location of the rapidly subsiding deep marine Aruma foreland basin at a tropical paleo-latitude during the Late Cretaceous (a) (from Al Rawahi and Dunkley Jones, 2019a; see Chapter 2), and its tectonics (b) with Late Cretaceous and recent sections across the basin (after Terken, 1999).

face salt movement (Pollastro, 1999). Seismic and well data suggest that the foreland basin started to form in the west of Central Oman during Coniacian-Santonian times and extended westward by the beginning of the Campanian (Scott, 1990).

The dynamics of this tectonically active basin resulted in temporal and regional variations in paleoenvironment and paleo-water depths at the time of Fiqa Formation deposition. Distinct lithological units, exposed at the surface, have been described as time equivalents to the subsurface Fiqa Formation or parts of it (Fig. 4). For example, the near-shore facies of the Muti (Glennie *et al*., 1974; Robertson, 1987) and Juweiza (Glennie *et al*., 1974) Formations of the North Oman Mountains represent tectonically-controlled conglomerate and carbonate debris facies at the basin margins (Robertson, 1987). These are laterally equivalent to the subsurface lower and upper parts of the Fiqa Formation respectively (Forbes et al., 2010). The Shargi Member of the Fiqa Formation in North Oman has been subdivided into an upper mixed clay-

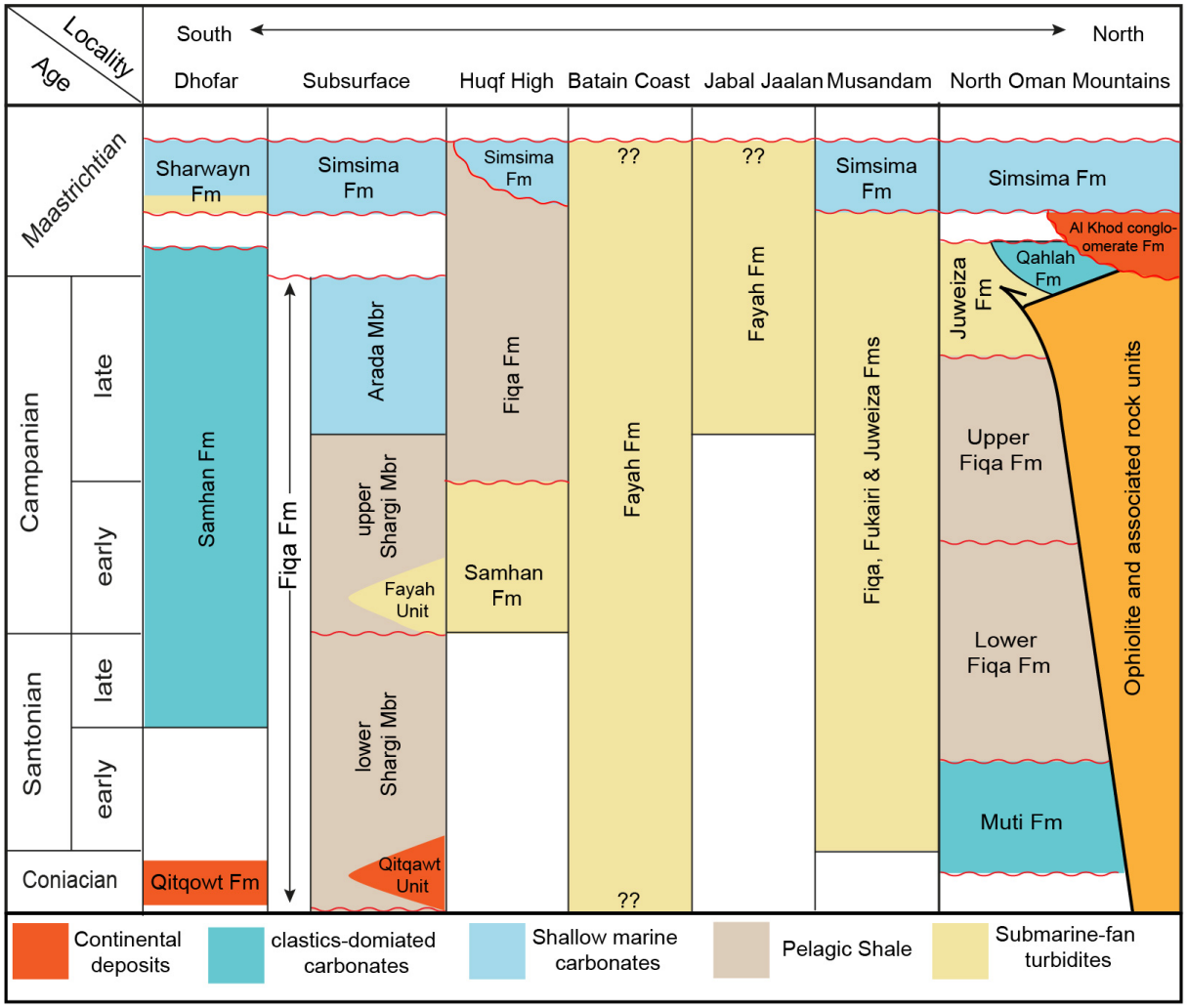

Figure 4. Correlation between different terms used for the Aruma Group and Fiqa Formation in surface and subsurface sections of Oman. From Hersi et al., 2016; Scott, 1991; Robertson, 1987; Glennie, 1974; Forbes et al., 2010; Packer et al., 2010; Searle, 2007; Searle and Ali, 2009 and Immenhauser et al., 1998. Abbreviations: Fm, Formation; Mbr, Member.

stone and turbiditic sandstone unit and a wide-spread lower claystone unit on the basis of wireline log characteristics and foraminifera biostratigraphy (Osterloff et al., 2001; Packer et al., 2000, Packer, 2002). The clastics of the Qitqawt Formation, which outcrop in the Huqf area (? Turonian-Santonian) of east Oman (Platel et al., 1995) and Dhofar region (Coniacian) of South Oman (Melinte et al., 2014) are thought to be equivalent to the Coniacian lowermost part of the lower Shargi Member, which also has more clastic content (Osterloff et al. 2001;

Packer, 2002). Both the Fayah Formation sandstone on the Batain Coast of northeast Oman (Shackleton et al., 1990) and the basal part of the marginal marine Campanian sandstone of the Samhan Formation in South and Central Oman (Schumann 1995; Philip and Platel, 1995; Hoffmann et al., 2016), are thought to be shallow water equivalents to the turbidite unit at the basal part of upper Shargi of North Oman (Osterloff et al., 2001; Packer, 2002; Filbrandt et al., 2004). In the wider Middle East, the Fiqa Formation of Oman passes into the shallower marine facies of the Fiqa and Aruma Formations eastward into the UAE, Saudi Arabia, Kuwait and Iraq (Ziegler, 2001). The most southerly extent of the Formation is represented by shoreline clastic and continental deposits from Yemen to Jordan (Powers et al., 1966 and Powers, 1968 in Alsharhan and Nairn, 1990). Toward the northeast, the formation is time equivalent to the pelagic shale and carbonates of the Gurpi Formation of Iran, which was deposited in a similar foreland basin setting (Ziegler, 2001). Given the complexity of these interrelationships, establishing chronostratigraphic correlations between sedimentary facies, both local and far-field, is critical for basin-fill and tectonic models as well as sequence stratigraphy. The aim of this study is to provide a basis for such chronostratigraphic correlations through the detailed calcareous nannofossil biostratigraphy of 11 hydrocarbon exploration wells across Oman.

3 Material and Methods

Calcareous nannofossil biostratigraphic and assemblage data were collected using standard polarising light microscopy and the cascading counting technique of Styzen (1997), with a total of 100 FOV (fields of view) counted for each sample. Slides were viewed using a Zeiss AxioScope A1 at 1250x magnification and GXM-XPLPOLTEC-2 at 1000x magnification. A

total of 249 samples were analyzed, including both cuttings and side wall core samples, from 11 hydrocarbon exploration wells (Fig. 2). Details on samples preparation, counting technique, sampling strategy and resolution and samples number and type for each well are available in Chapter 1 (see Chapter 1; Sect. 5 and Figs. 1-2). Biostratigraphic analyses were interpreted within the framework of the global Upper Cretaceous UC biozonation of Burnett (1998), and all bioevent ages are tied to the Geological Time Scale of Gradstein et al. (2012). Microfossil data discussed and illustrated in this study are based on the analysis of Packer et al. (2000) and Packer (2001a, b). The studied sections are distributed across the basin, from the deepest shale-dominated part (W-1 to W-7) to the shallowest carbonate-dominated part of the basin (W-8 to W-11) (Fig. 2). Samples from the Fiqa Formation of W-9 to W-11 lack calcareous nannofossils and are excluded from the biostratigraphic interpretations of this study. Sample material and slides will be deposited in PDO Sample Stores (XGL4 CoreShed Unit). The terms top (last occurrence, extinction) and base (first occurrence, inception) are used, and the biostratigraphic results are presented from younger to older units (downhole).

4 Results

Calcareous nannofossils are generally highly abundant within the Fiqa Formation. The preservation of nannofossils varies from very good to very poor depending on the sample lithology, with worse preservation in the carbonate dominated layers of the Arada Member and the silty horizons of the Shargi Member. Average species diversity is around 40 species per sample with maximum diversity of 70 species per sample in the most diverse early Campanian intervals. Nannofossil assemblage composition data through the Fiqa Formation of a type section, W-4, are provided in Al-Rawahi and Dunkley Jones (2019a) (see Chapter 2).

The marker species identified in the Fiqa Formation are listed in Tables 2 and 3, along with some foraminiferal bioevents identified within the Formation. The nannofossil bioevents are used to apply the UC^{TP} global zonation scheme for the Tethyan Province (see Burnett, 1998; pp.147-156, figs. 6.4 and 6.5). The studied sections span the UC17 to UC11 zones (upper Coniacian to lower Maastrichtian), including three stage boundaries: the Maastrichtian/Campanian, Campanian/Santonian and Santonian/Coniacian. The UC^{TP} zonation scheme is easily applicable to the upper Campanian and lower Maastrichtian successions, but is harder to apply to the upper Coniacian to mid-Campanian intervals due to the inconsistent occurrence or absence of many marker taxa in the studied samples. Therefore, four new local biohorizons are suggested to improve biostratigraphic resolution within the undifferentiated UC12-13 Zone. The status of the main UC^{TP} nannofossil marker events in the Fiqa Formation are highlighted in Table 1, while Figure 5 summarises the new nannoplankton biostratigraphic scheme constructed for the Fiqa Formation compared to the UC^{TP} global zonation scheme. Correlations between the study wells using the refined biostratigraphic scheme are shown in Figure 6. Nannofossil bioevents are tied to the Geological Time Scale 2012 (see Gradstein et al., 2012; pp. 1120-1121; appendix 3) their ages are shown in Table 2 and quoted in brackets in the folowing text. Below we discuss the key nannofossil biohorizons highlighted in Figure 5, within four major intervals spanning the upper Coniacian to lower Maastrichtian.

4.1 Upper Campanian to Lower Maastrichtian

In this study, following the zonation of Burnett et al. (1998), we identify the lower Maastrichtian succession based on top occurrences of *Tranolithus orionatus* and *Uniplanarius trifidus*. Top *T. orionatus* (71.01 Ma) is a useful marker for the lower Maastrichtian and defines the

base of UC18 zone, but was only encountered in one well, W-8 at a depth of 616.5±28.5 m. The failure to identify this biohorizon in other wells indicates either an absence of

Table 1. Tethyan bioevents of Burnett (1998) UCTP Scheme and their status in the study area. Bioevents status in the Fiqa Formation: 1. Consistently recorded bioevent in two or more wells; 2. Bioevent is recorded in one or two wells but with lower accuracy due to rare occurrence of the species; 3. Bioevent species is very rare and sporadic. 4. Bioevent species is not recorded in any sample.

Tethyan bioevents of Burnett, 1998 UCTP Scheme			**Bioevents status in the Fiqa Formation (this study)**					
Zone	**Sub-zone**	**Bioevent**	**1**	**2**	**3**	**4**	**Occurance**	**Local events**
UC 17		**Top *Tranolithus orionatus***		x			W-8	top *Eiffellithus angustus*; top *Eiffellithus lindiensis*
		Top *Acuturris scotus*				x		
		Top *Uniplanarius gothicus*		x			W-7; W-8	
		Top *Uniplanarius trifidus*		x			W-7; W-8	
		Base *Cribrosphaerella daniae*				x		
		Base *Nephrolithus frequens*				x		
UC 16		**Top *Broinsonia parca constricta***		x			W-8	
UC 15	e	**Top *Eiffellithus eximius***	x				W-7; W-8	
		Base *Nephrolithus corystus*				x		
		Top *Cylindralithus nieliae*				x		
		Top *Reinhardtites anthophorus*			x			
		Top curved spine				x		
		Top *Biscutum coronum*			x			
		Top *Seribiscutum primitivum*				x		
		Base *Eiffellithus parallelus*		x			W-7	
	d	Top *Lithastrinus grilli*		x			W-7; W-8	
		Base *Uniplanarius trifidus*		x			W-8	
	c	Base *Ceratolithoides arcuatus*				x		
		Base *Uniplanarius sissinghii*		x			W-7; W-8	
	b	Base *Hexalithus gardetiae*			x			
		Top *Zeugrhabdotus biperforatus*			x			
		Top *Retecapsa schizobrachiata*			x			
		Base *Lithastrinus quadricuspis*			x			
		Base *Ceratolithoides aculeus*		x			W-8	

Tethyan bioevents of Burnett, 1998 UC^{TP} Scheme			Bioevents status in the Fiqa Formation (this study)					
Zone	**Sub-zone**	**Bioevent**	**1**	**2**	**3**	**4**	**Occurance**	**Local events**
	a	**Base *Misceomarginatus pleni-porus***				x		
UC 14	d	Base *Staurolithites mielnicensis*		x				
		Top *Bukryaster hayi*	x				W-2; W-3; W-4; W-5; W-7	
		Base *Reinhardtites levis*			x			
		Base *Ceratolithoides verbeekii*				x		
	c	Base *Bukryaster hayi*	x				W-2; W-3; W-5	
	b	Base *Broinsonia parca constricta*	x				W-3; W-4; W-5; W-7	
	a	**Base *Broinsonia parca parca***	x				W-3; W-4; W-7	
UC 13		No marker species within UC13. This zone is defined as the interval from base *B. parca parca* to base *A. cymbiformis*.						Top *Nannoconus* spp.; base *Broinsonia verecundia*; Top *Helicolithus blairiae*
UC 12		**Base *Arkhangelskiella cymbiformis***		x			W-4; W-5	
		Base *Biscutum magnum*		x			W-1; W-7	
		Base *Biscutum dissimilis*				x		
		Top *Zeugrhabdotus noeliae*		x			W-5	
UC 11	c	**Top *Lithastrinus septenarius***	x				W-1; W-4; W-5	
		Base *Lucianorhabdus cayeuxii*			x			
	b	Top *Quadrum gartneri*		x			W-1; W-5	
	a	**Base Lithastrinus grilli**		x			W-4	

material this young due to erosion or non-deposition (e.g. W-3; W-4; W-5) or the poor recovery of calcareous nannofossils within shallow marine, crystalline, bioclastic limestones in the upper part of the Fiqa Formation in wells W-2 and W-7. The Campanian/Maastrichtian stage boundary (72.05 Ma) is located between nannofossil biohorizons top *U. trifidus* (lowermost Maastrichtian, 71.31Ma) and top *Broinsonia parca constricta* (uppermost Campanian; 72.02 Ma; base Zone UC17) at the GSSP type section of Tercis les Bains in Southwest France (Odin, 2001; Gardin et al., 2001b). Other Tethyan sections, such as in the Italian Apennines, show a similar ordering of these two biohorizons (Gardin et al., 2001a), although, in this

study, they are only recorded in W-8, and at the same stratigraphic level of 676.5±4.5 m. Top occurrences of *Eiffellithus angustus* and *Eiffellithus lindiensis* are recorded in W-8 within Zone UC17 at 616.5±28.5 m. These biohorizons are worth noting, as they may have wider

Table 2. Main bioevents recorded in the Fiqa Formation. B: base bioevent; T: top bioevent; N: nannofossil; F: foraminifera; (*) stratigraphic order of the bioevent in the Fiqa Formation is not consistent with the given GTS age.

	Bioevent	**Age (Ma) GTS 2012**	**(Sub) zone base**
T	*Tranolithus orionatus*	71.01	UC18
T	Uniplanarius spp.		
T	*Eiffellithus angustus*, *E. lindiensis*		
T	*Broinsonia parca Constricta*	72.02	UC17
T	*Eiffellithus eximius*	75.93	UC16
T	*Textularia* sp. 2		F66
T	*Lithastrinus grillii**	79.73	
B	*Uniplanarius sissinghii*	77.61	UC15c-e
T	*Bukryaster hayi*		
B	*Broinsonia parca Constricta*	81.38	UC15b-UC14b
B	*Broinsonia parca parca*	81.43	UC14a
B	*Bukryaster hayi**	81.25	
B	*Nannoconus* spp.		
B	*Globotruncana ventricosa**	79.9	
B	*Broinsonia verecundia*		
T	*Helicolithus blairiae*		
B	*Arkhangelskiella cymbiformis*	83.2	UC13
T	*Dicarinella asymetrica*	83.64	F65
B	*Globotruncanita elevata*	83.64	
T	*Dicarinella concavata*	83.64	
T	*Marginotruncana sinuosa*		
T	*Lithastrinus septenarius*	85.56	UC13-12

	Bioevent	Age (Ma) GTS 2012	(Sub) zone base
T	*Whiteinella baltica* (consistent)*	83.08	F64
T	*Quadrum gartneri*	86.44	
B	*Marthasterites furcatus*		
B	*Lithastrinus grillii*	86.5	UC11

stratigraphic value across the Southern Tethys area. The top occurrence of *E. angustus*, for example, is also reported to occur prior to top *Eiffellithus eximius* in the Gurpi Formation of Iran (Razmjooi et al., 2014). Al Rawahi and Dunkley Jones (2019a) (see Chapter 2) highlighted the potential biostratigraphic importance of *Eiffellithus* in the Fiqa Formation and discussed the main distinguishing features between the species of this group which are sometimes tricky to separate under the light microscope. The uppermost Campanian to lower Maastrichtian nannofossil assemblages of Zone UC17 are characterised by more frequent occurrences of *Placozygus* spp., *Helicolithus* spp. and highly abundant *Arkhangelskiella* spp. compared to the underlying older successions of Campanian to Coniacian age. Species of *Chiastozygus*, *Staurolithites* as well as diagonal-cross forms of *Eiffellithus* (taxonomic notes on these groups and their abundance patterns within the Fiqa Formation are given in Al Rawahi and Dunkley Jones, 2019a; see Chapter 2) like *E. parallelus*, *E. turriseiffelii* and *E. gorkae* are relatively more frequent in this interval compared to the underlying units as seen in W-8.

The biohorizon top *E. eximius* is also a good marker within the uppermost Campanian, representing the base of nannofossil Zone UC16, and is recorded in W-8 at 697.5±4.5 m and W-7 at 570±10 m. Nannofossil assemblage composition within UC16 is similar to the overlying intervals with the addition of frequently present species of *Uniplanarius*, including *U. gothicus*,

U. sissinghii and *U. trifidus*. The top *Lithastrinus grilli* (79.73 Ma) is the lowermost distinct biohorizon recorded in the upper Campanian of these sections, at 595±15 m in W-7 and 864±6 m in W-8.

Table 3. Calcareous nannofossil and selected foraminiferal bioevents recorded in the study wells. B: base event; T: top event; N: nannofossil; F: foraminifera. (*) stratigraphic order of the bioevent in the Fiqa Formation is not consistent with the given GTS 2012 age. W-6 is excluded as it lacks age diagnostic taxa, while W-9; W-10 and W-11 are mostly barren of nannofossils.

	Bioevent		Age (Ma) GTS 2012	(Sub) zone base	Sample Depth (m)			
					Top	Bot-tom	Mid-point	±
	Well: W-1							
B	*Broinsonia parca parca*	N	81.43	UC14a	372	392	382	10
T	*Textularia* sp. 2	F		F66	410	420	415	5
B	*Globotruncana ventricosa**	N	79.9		660	680	670	10
B	*Broinsonia verecundia*	N			842	860	851	9
T	*Helicolithus blairiae*	N			842	860	851	9
T	*Dicarinella asymetrica*	N	83.64	F65	840	870	855	15
T	*Lithastrinus septenarius*	N	85.56	UC12-13	860	882	871	11
T	*Quadrum gartneri*	N	86.44		882	902	892	10
	Well: W-2							
T	*Bukryaster hayi*	N			2264.66	2293.62	2279.1	14.5
B	*Broinsonia parca constricta*	N	81.38	UC15b-UC14b	2385.06	2598.42	2491.7	106.7
B	*Broinsonia parca parca*	N	81.43	UC14a	2598.42	2645.97	2622.2	23.8
B	*Bukryaster hayi**	N	81.25		2598.42	2645.97	2622.2	23.8
	Well: W-3							
T	*Bukryaster hayi*	N			3	3	3.0	0.0
B	*Broinsonia parca constricta*	N	81.38	UC15b-UC14b	228.6	350.52	289.6	61.0
B	*Bukryaster hayi**	N	81.25		350.52	487.68	419.1	68.6

	Bioevent		Age (Ma) GTS 2012	(Sub) zone base	Sample Depth (m)			
					Top	Bot-tom	Mid-point	±
B	*Broinsonia parca parca*	N	81.43	UC14a	624.84	685.8	655.3	30.5
	Well: W-4							
T	*Bukryaster hayi*	N			27	27	27.0	0.0
B	*Broinsonia parca constricta*	N	81.38	UC15b-UC14b	92.96	99.06	96.0	3.1
B	*Broinsonia parca parca*	N	81.43	UC14a	110.94	120.1	115.5	4.6
B	*Bukryaster hayi**	N	81.25		227.99	248.4	238.2	10.2
T	*Nannoconus* spp.	N			248.4	274.32	261.4	13.0
B	*Arkhangelskiella cymbiformis*	N	83.2	UC13	1135.38	1165.86	1150.6	15.2
B	*Broinsonia verecundia*	N			1203.8	1254.25	1229.0	25.2
T	*Helicolithus blairiae*	N			1203.8	1254.25	1229.0	25.2
T	*Dicarinella asymetrica*	F	83.64		1260.04	1269.19	1264.6	4.6
T	*Lithastrinus septenarius*	N	85.56	UC12-13	1254.25	1280.16	1267.2	13.0
T	*Dicarinella concavata**	F	83.64		1310.95	1317.04	1314.0	3.0
T	*Marginotruncana sinuosa*	F			1310.95	1317.04	1314.0	3.0
B	*Lithastrinus grillii*	N	86.5	UC11	1325.88	1341.12	1333.5	7.6
	Well: W-5							
T	*Bukryaster hayi*	N			555	560	557.5	2.5
B	*Broinsonia parca constricta*	N	81.38	UC15b-UC14b	770	846	808.0	38.0
B	*Bukryaster hayi**	N	81.25		921	996	958.5	37.5
B	*Broinsonia parca parca*	N	81.43	UC14a	1071	1146	1108.5	37.5
B	*Broinsonia verecundia*	N			1537.8	1555.89	1546.8	9.0
T	*Helicolithus blairiae*	N			1555.89	1584.58	1570.2	14.3
B	*Arkhangelskiella cymbiformis*	N	83.2	UC13	1698.97	1722	1710.5	11.5
T	*Dicarinella asymetrica*	F	83.64	F65	1731	1740	1735.5	4.5
T	*Lithastrinus septenarius*	N	85.56	UC12-13	1746	1770	1758.0	12.0
T	*Quadrum gartneri*	N	86.44		1770	1794	1782.0	12.0

	Bioevent		Age (Ma) GTS 2012	(Sub) zone base	Sample Depth (m)			
					Top	Bot-tom	Mid-point	±
B	*Marthasterites furcatus*	N			1770	1794	1782.0	12.0
T	*Whiteinella baltica* (consistent)	F		F64	1800	1806	1803.0	3.0
	Well: W-7							
T	*Textularia* sp. 2	F		F66	500	530	515	15
T	*Eiffellithus eximius*	N	75.93	UC16	560	580	570	10
T	*Lithastrinus grilli**	N	79.73		580	610	595	15
B	*Uniplanarius sissinghii*	N	77.61	UC15c-e	640	660	650	10
B	*Broinsonia parca parca*	N	81.43	UC14a	680	700	690	10
B	*Bukryaster hayi*	N	81.25		700	730	715	15
T	*Nannoconus* spp.	N			700	730	715	15
T	*Dicarinella asymetrica*	F	83.64	F65	930	935	932.5	2.5
T	*Helicolithus blairiae*	N			940	970	955	15
T	*Dicarinella concavata*	F	83.64		985	990	987.5	2.5
B	*Broinsonia verecundia*	N			1000	1015	1007.5	7.5
	Well: W-8							
T	*Tranolithus orionatus*	N	71.01	UC18	588	645	616.5	28.5
T	*Eiffellithus angustus*	N			588	645	616.5	28.5
T	*Eiffellithus lindiensis*	N			588	645	616.5	28.5
T	*Broinsonia parca constricta*	N	72.02	UC17	672	681	676.5	4.5
T	*Uniplanarius* spp.	N			672	681	676.5	4.5
T	*Eiffellithus eximius*	N	75.93	UC16	693	702	697.5	4.5
T	*Lithastrinus grillii**	N	79.73		858	870	864	6
B	*Uniplanarius sissinghii*	N	77.61	UC15c-e	882	891	886.5	4.5
B	*Ceratolithoides aculeus*	N	79	UC15b	930	939	934.5	4.5

4.2 Lower Campanian

Various early Campanian nannofossil events of the UC^{TP} scheme are missing in the studied sections (Table 1) which might reflect the paleobiogeographic differentiation of nannofossil assemblages during this time interval (Lees, 2002). Following the UC^{TP} scheme, the lower/ upper Campanian boundary lies between the base *U. trifidus* (76.82 Ma), which defines the base of Subzone U15d, and the base *Ceratolithoides arcuatus* within UC15c (Fig. 5). The base *U. trifidus* was not found in a consistent stratigraphic position between the studied successions, whilst *C. arcuatus* was not recorded in any sample from any well (Table 1). Into the lower Campanian, the base of *U. sissinghii* (77.61 Ma) defines the base of Subzone UC15c (Fig. 5), which in the Fiqa Formation, can only be resolved as a combined subzone UC15c-e. This biohorizon is recorded in W-7 at 650±10 m and W-8 at 886.5±4.5 m. In older intervals other calcareous fragments or inorganic crystallites could be misidentified as *U. sissinghii*, resulting in an erroneous range extension. Key distinguishing features of *U. sissinghii* are its four prominent, thick ray-like segments with more yellowish interference (Al Rawahi and Dunkley-Jones, 2019a; plate 11, figs. 6-7) (see Chapter 2) whereas the calcareous fragments have much thinner, bright ray-like segments with white interference (Al Rawahi and Dunkley-Jones, 2019a; plate 11, figs. 11-12) (see Chapter 2).

The absence of the marker taxa *Misceomarginatus pleniporus* and *Ceratolithoides verbeekii*, as well as the rare occurrence of *Ceratolithoides aculeus* and *Reinhardtites levis* (Table 1), and the limited number of sampled sections within this interval required the use of the combination Subzone UC15b-UC14b, with base defined by biohorizon base *B. parca constricta,* recorded in W-2 at 2491.7±106.7 m, W-3 at 289.6±61 m, W-4 at 96±3.1 m and W-5 at 808±38 m. The base *C. aculeus* occurs within the undifferentiated Subzone UC15b-UC14b, but it is

only recorded in W-8 at 934.5±4.5 m. Top *Bukryaster hayi* biohorizon, which is used in the UC^{TP} within the lower Campanian Subzone UC14d, is useful in these sections, and is reported in W-2 at 2279.14±14.5 m and W-5 at 557.5±2.5 m. In the UC^{TP} scheme base *B. hayi* defines base Subzone UC14c. Within the Fiqa Formation, however, base *B. hayi* is recorded below the base *Broinsonia parca parca* biohorizon, i.e. towards the top of UC13 or basal part of UC14, in W-4 and W-7 at depths of 238.2±10.2 m and 715±15 m respectively, whilst within W-3 and W-5 it is found above base *B. parca parca* biohorizon at 958.5±37.5 m and 419.1±68.6 m respectively (see Fig. 9). Similar observation of unreliability of base *B. hayi* is suggested for a Tethyan section from Tunisia studied by Farouk et al. (2018b). The base of Subzone UC14a is defined by biohorizon base *B. parca parca* which is recorded in W-1 at 382±10 m, W-2 at 2622.2±23.8 m, W-3 at 655.3±3.5 m, W-4 at 115.5±4.6 m, W-5 at 1108.5±37.5 m and W-7 at 690±10 m.

The nannofossil assemblages in UC15c-e, UC15b-UC14b and UC14a are characterised by the disappearance of all *Uniplanarius* spp. and a reduction of *Arkhangelskiella* spp., *Placozygus* spp. and *Helicolithus* spp. The assemblages are also characterised by increased abundance of *Chiastozygus* spp. and *Retecapsa* spp. relative to the underlying successions. *Broinsonia signata*, a consistent component of the Fiqa Formation nannofossil assemblages (Al Rawahi and Dunkley Jones, 2019a; see Chapter 2) has its first recorded appearance within UC15c-e in W-8 and within UC14-UC15b in W-7.

4.3 Upper Santonian to Lower Campanian

The late Santonian to early Campanian interval is challenging to subdivide with nannofossil bioevents, as distinctive tops or bases are rare within this relatively short interval of time. In

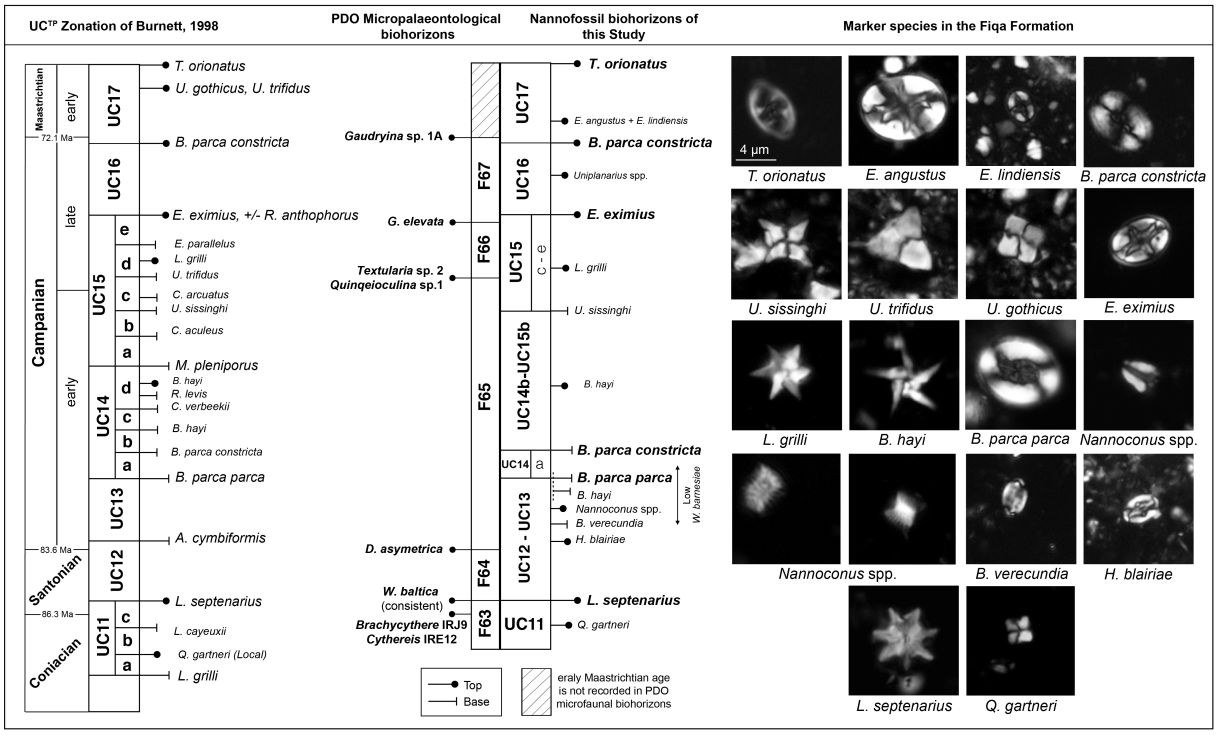

Figure 5. New nannofossil zonation scheme developed for the Fiqa Formation compared to the UC^{TP} scheme of Burnett (1998) and correlated to the local micropalaeontological scheme. Marker species plate from Al Rawahi and Dunkley Jones (2019a) (see Chapter 2).

the Fiqa Formation, this interval is placed within a combined nannofossil Zone UC12- UC13, from biohorizon base *B. parca parca* (lower Campanian; Burnett, 1998) to biohorizon top *Lithastrinus septenarius* (lower Santonian; Burnett, 1998). These zones are combined due to the unreliability of biohorizon base *Arkhangelskiella cymbiformis* (discussed below); that marks the base of UC13 in the UC^{TP} scheme. Alternative local biohorizons in the lowermost Campanian, which are recognised consistently across the study area, include the top *Nanno-conus* spp. which is recorded in W-4 at 261.4±13 m and W-7 at 715±15 m. This is followed downhole by the base *Broinsonia verecundia*, which has a base within lower Campanian (Burnett, 1998) and it is recorded in W-1 at 851±9 m, W-4 at 1229±25.2 m and W-5 at 1546.8±9 m. The lower Campanian planktonic foraminifera biohorizon base *Globotruncana*

ventricosa (Hardenbol et al., 1998) is recorded in W-1 at 670±10 m, providing support for a lower Campanian age.

The Campanian/Santonian boundary, which is placed towards the top of UC12 in the UC^{TP} scheme is not well constrained by nannoplankton events within the Tethyan realm, and might correspond to the start of global transgression that affected prevailing oceanic regime (Burnett, 1998). The Campanian/Santonian boundary (83.64 Ma) is placed between the base *A. cymbiformis* (base of UC13; 83.20 Ma) and base *Calculites obscurus* (84.08 Ma) (Ogg and Hinnov, 2012). Within the Fiqa Formation, the rarity of *A. cymbiformis*, makes its base difficult to pick, although it does become more frequent in the upper Campanian and lower Maastrichtian. Similar problems with the reliability of the base *A. cymbiformis* are suggested for other Tethyan sections from Tunisia (Farouk et al. 2018a) and Iran (Razmjooei et al. 2018). This pattern has been also reported by others, with *A. cymbiformis* believed to appear very rarely and sporadically within the latest Santonian and then disappearing until the later Campanian (J Lees 2018, personal communication, 18 July), whilst others report the base of this species earlier within the Santonian (e.g. Kita et al., 2017). In the Fiqa Formation, *A. cymbiformis* is rarely recorded in the lower Campanian, making identification of the base of UC13 problematic. The biohorizon base *C. obscurus* has been used to indicate either Santonian (base CC17 zone of Sissingh, 1977; Perch-Nielsen, 1985) or Coniacian (Burnett, 1998) age, and is known to be more consistently present in neritic environments than deeper water environments (Burnett, 1998; Wolfgring et al., 2018). Within the Fiqa Formation it is also difficult to place due to inconsistent occurrences in the studied sections.

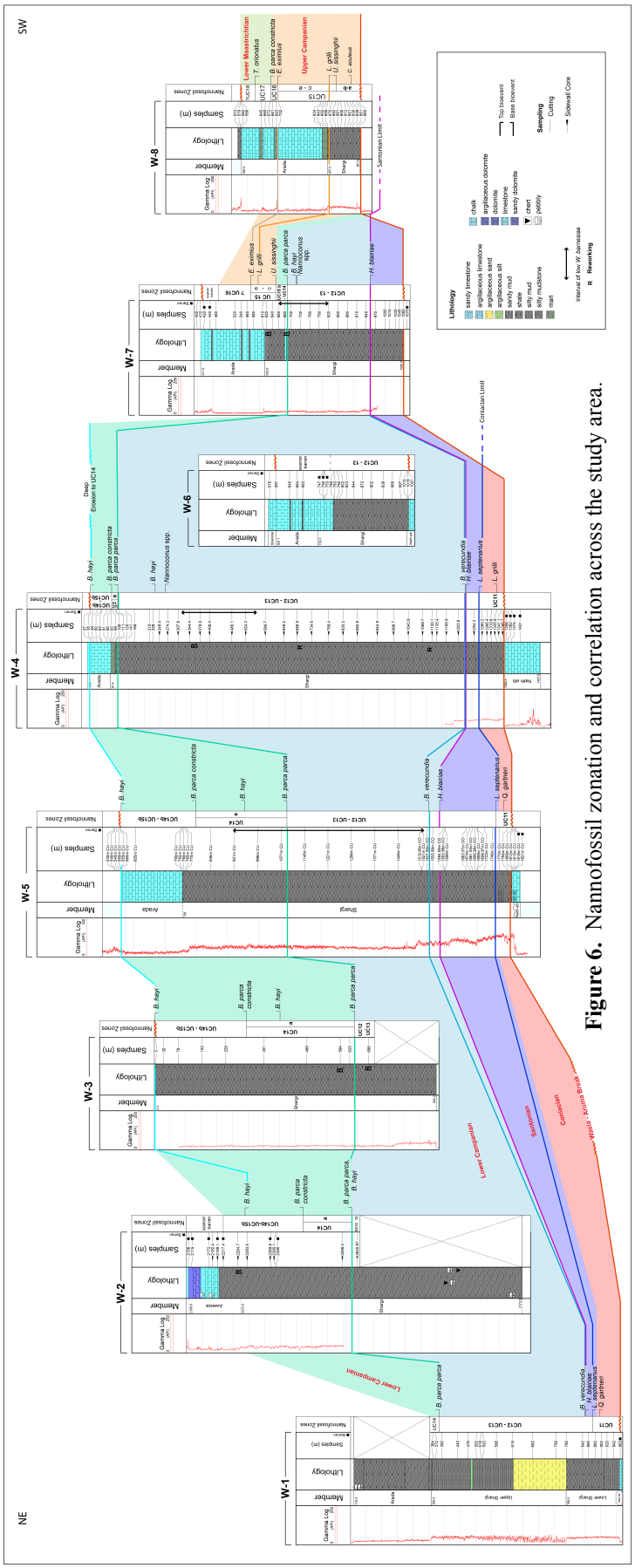

Figure 6. Nannofossil zonation and correlation across the study area.

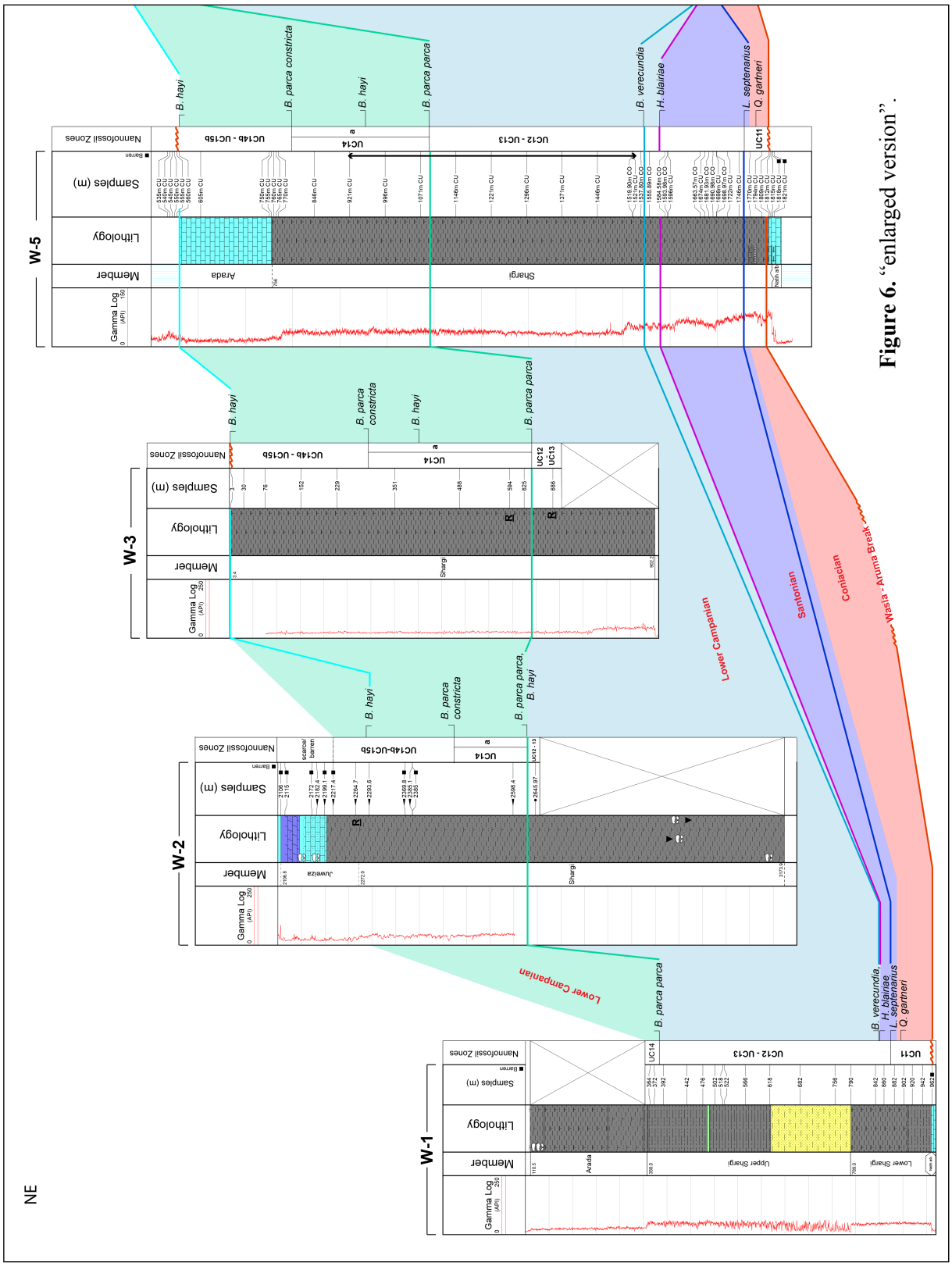

Figure 6. "enlarged version".

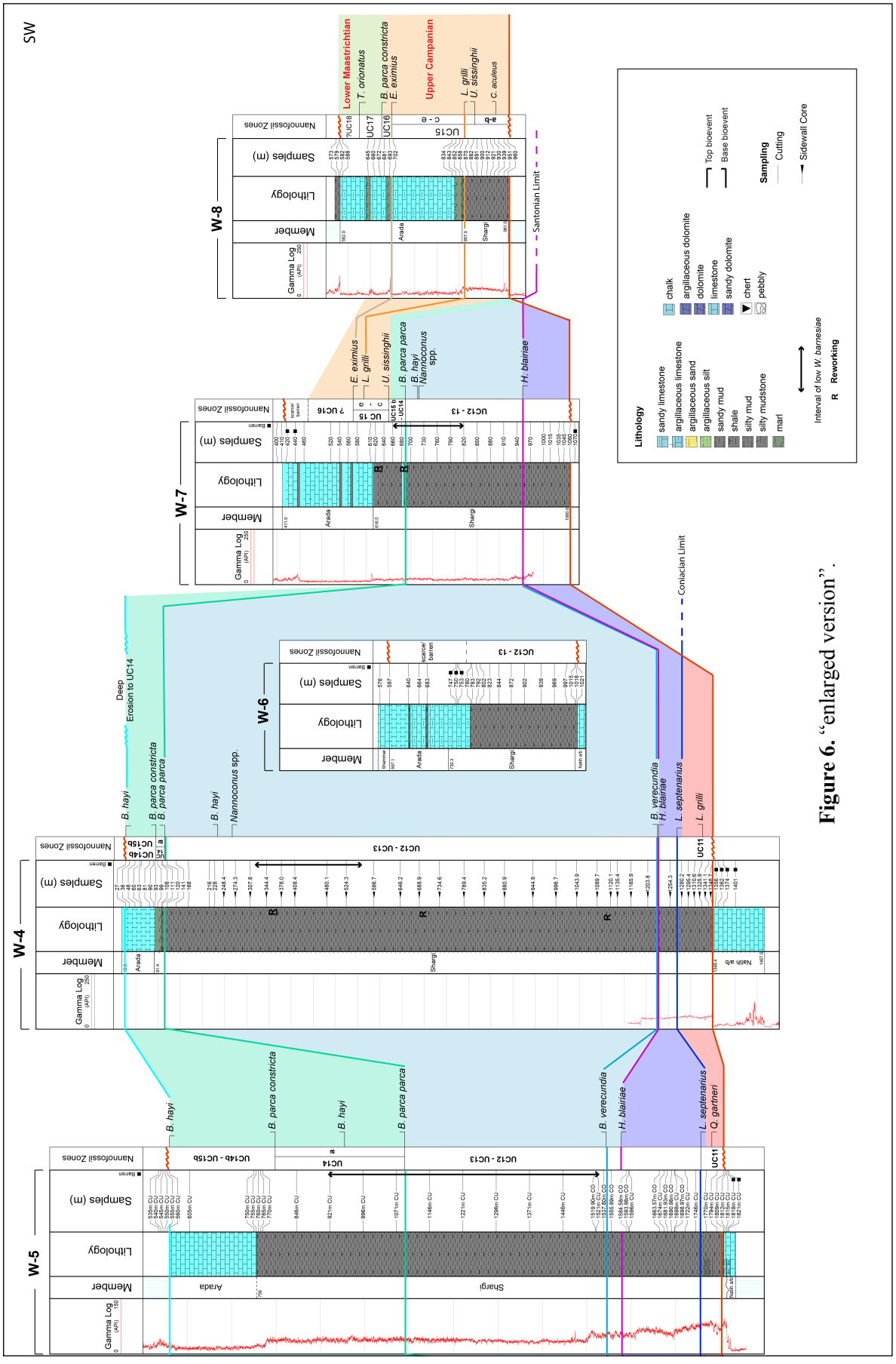

Figure 6. "enlarged version".

The base *Biscutum dissimilis* and *Biscutum magnum* biohorizons, within the uppermost part of Zone UC12, are used to identify the uppermost Santonian in Tethyan sections (Burnett, 1998), but in the Fiqa Formation *B. dissimilis* is absent and *B. magnum*, which is recorded in some samples, is not reliable due to the inconsistency of its base occurrence. In the Northern Alps of Austria - a proposed Northwest Tethyan reference section for the Santonian/Campanian boundary - Wolfgring et al. (2018) used top of the Santonian planktonic foraminifer *Dicarinella asymetrica* (83.64 Ma) and base *B. parca parca* (81.43 Ma) to place the boundary at a prominent palaeomagnetic reversal. The top of *D. asymetrica* is a well-established marker event for the topmost Santonian (e.g. Hardenbol et al., 1998; Ogg and Hinnov, 2012; Wolfgring et al., 2018) and has been well-constrained in the Fiqa Formation (Packer et al. 2000). In three wells (W-1, W-4 and W-7) the top *D. asymetrica* is close to biohorizon top *Helicolithus blairiae* (Table 3). Moreover, the occurrence of the upper Santonian planktonic foraminiferal taxa *Marginotruncana sinuosa* (top occurrence within *D. asymetrica* zone; Hardenbol et al., 1998) below the biohorizon tops *H. blairiae* and *D. asymetrica* in W-4 at 1314±3 m (Table 3), also support a Santonian age. On this basis, we propose that the top *H. blairiae* biohorizon is an alternative to the sporadic and inconsistent base of *A. cymbiformis*, for the vicinity of the Santonian/Campanian boundary in the Fiqa Formation. Top *H. blairiae* is recorded in W-1 at 851±9 m, W-4 at 1229±25.2 m, W-5 at 1570.2±14.3 m and W-7 at 955±15 m. Kita et al. (2016) suggests that *H. blairiae* may serve as an alternate marker for the Santonian or earliest Campanian as it is reliably recorded below base *B. parca parca* in the US Western Interior. In the Fiqa Formation, the biohorizon top *Zeugrhabdotus noeliae* was rarely and variably placed within this zone.

UC12-13 in the Fiqa Formation is very thick (Fig. 6) and characterised by more homogeneous assemblage composition compared to the overlying intervals. However, a distinct change in the assemblage composition represented by an interval of very low *Watznaueria barnesiae* abundance is recorded within the the lower Campanian that started from the upper part of UC12-13 in W-4, W-5 and W-7 (Fig. 6). Such reduction in the abundance of this common species in the Fiqa Formation and its palaeoenvironmental significance is discussed in detail by Al Rawahi and Dunkley Jones (2019a) (see Chapter 2).

4.4 Upper Coniacian to Lower Santonian

Burnett (1998) locates the Coniacian/Santonian boundary within Subzone UC11c, with the top of UC11c defined by the biohorizon top *Lithastrinus septenarius* (lower Santonian) and base of UC11c identified by the biohorizon base *Lucianorhabdus cayeuxii* (upper Coniacian). These biohorizons have been recognised across the Coniacian-Santonian boundary in several Tethyan locations including the Olazagutia section of northern Spain (Melinte and Lamolda, 2002) and the Romanian Carpathians section (Melinte and Lamolda, 2007), as well as in the Western Interior Seaway at Ten Mile Creek, Texas and the Boreal section at Seaford Head, England (Howe et al., 2007). Within the Olazagutia section, Melinte and Lamolda (2002) record the following sequence of nannofossil and planktonic foraminifera biohorizons, from older to younger, around the Coniacian/Santonian boundary: base *L. grillii* (upper Coniacian), base *Lucianorhabdus cayeuxii* (upper Coniacian), base *Calculites obscurus* (upper most Coniacian), base planktonic foraminifera *D. asymetrica* (lowermost Santonian), base planktonic foraminifera *Sigalia carpatica* (lower Santonian) and top *L. septenarius* (lower Santonian). In the Fiqa Formation, top *L. septenarius* biohorizon is recorded in W-1 at 871±11 m, W-4 at

1267.2±13 m and W-5 at 1758±12 m and is regarded as a robust marker for the lowermost Santonian, just above the Coniacian-Santonian boundary (Melinte and Lamolda, 2002; 2007).

The biohorizon base *L. cayeuxii*, which defines the base of UC11c is however, not a reliable marker within the Fiqa Formation due to its scarce occurrence in all wells, which may in turn relate to a preference of this species for shelf settings (Burnett, 1998). The Santonian-Coniacian boundary is thus hard to place, but the biohorizon top *Quadrum gartneri* (base of UC11b), which is placed at 892±10 m in W-1 and 1782±12 m in W-5, clearly indicates a Coniacian age (Burnett, 1998). The base of *Marthasterites furcatus*, recorded at 1782±12 m in W-5, is used to indicate Coniacian age by several authors (e.g. Gartner, 1968; Roth, 1973; Perch-Nielsen, 1979), which agrees well with the occurrence of the Coniacian planktonic foraminifera *Dicarinella concavata* in the interval 1770 to 1809 m in W-5. The base of *M. furcatus*, another shelf taxa according to Burnett (1998), is not observed in any other well. In W-4, *Q. gartneri* is not recorded in any sample but base *L. grillii* (base UC11a) is placed at 1333.5±7.6 m. In many settings the base *L. grillii* is located immediately below the top *Q. gartneri* (Burnett, 1998) within the middle (Wagreich, 1992) to upper (Varol, 1992) Coniacian, whilst at the Coniacian-Santonian GSSP section it is placed in the upper Coniacian, 15m below the boundary (Melinte and Lamolda, 2002). The lowest occurrence of the planktonic foraminifera *D. asymetrica* has been used as an indicator of the lower Santonian (e.g. Hardenbol et al., 1998), but is present in the Fiqa Formation within Coniacian intervals, for example in W-4 at 1317.04 m, in agreement with other observations of this species below the Coniacian-Santonian boundary (Howe et al., 2007).

The nannofossil assemblage of the Santonian and Coniacian are generally similar to Campanian assemblages, although with a noticeably higher abundance of *E. eximius*.

5 Discussion

The consistent nannoplankton biohorizons identified within this study provide important stratigraphic correlations across the studied borehole successions, and provide reference points for future stratigraphic studies of the Fiqa Formation of Oman. The nannofossil biostratigraphy presented here also integrates well with other established microfossil zonation schemes for the Fiqa Formation, especially those based on foraminifera (Sikkema 1991; Osterloff et. al. 2001; Packer et al., 2000; Packer, 2001 a; b; c; Packer, 2002) (Figs. 5 and 7). The Fiqa Formation is assigned a late Coniacian to late Campanian depositional age based on microfossil data (F63 to F67 biozones; Osterloff et. al. 2001; Packer et al., 2000; Packer, 2001a; b; c; Packer, 2002), whilst nannofossil biostratigraphy indicates a late Coniacian to early Maastrichtian age (UC11 to UC17 biozones). Nannofossil biostratigraphy also provides improved constraints around key stratigraphic divisions, such as the base *U. sissinghi* to locate the transition from the lower to upper Campanian, when the microfossil faunal Zone F66 covers both the early and late Campanian (Packer, 2001a) (Fig. 5). The Campanian/Maastrichtian transition, which has never been resolved in the Fiqa Formation using microfossil biostratigraphy, is also recognised based on the distinctive change in the nannofossil assemblage and the occurrence of biohorizon top *B. parca constricta*.

The correlations now provided by nannofossil biostratigraphy show that the Santonian microfossil Zone F64 and the early Campanian Zone F65 are both diachronous across the study area, with the top of both zones occurring in younger strata towards shallower facies in W-7

compared to deeper facies in W-1 (Fig. 7). Fundamental to understanding correlations between nannofossil and microfossil biostratigraphy of the Fiqa Formation, is a clear understanding of the basis of the microfossil zonation scheme. The microfossil zonation employed is a regional scheme that has been developed for the purposes of correlation across the Aruma Basin (Osterloff et. al. 2001). This scheme is an integration of both planktonic and benthic foraminiferal data, along with other microfossil groups including radiolaria and ostracods, and is based on both total microfossil assemblage change as well as the limited use of base or top of key foraminiferal marker taxa. As a result, this microfossil stratigraphy is subject to variations in the microfossil assemblages, especially the benthic faunas, that could be strongly dependent on changes in the depositional environments and paleo-water depth rather than reflecting true stratigraphic ranges (Packer, 2001a). For instance, microfossil-based paleodepth reconstructions for the lower Campanian successions indicate a middle to upper bathyal setting for W-1 and an inner to outer neritic setting for W-7 (Fig. 7) (Packer et al., 2000; Packer, 2001a). Foraminiferal assemblages in this interval are rich and diverse in W-1, dominated by agglutinating foraminifera and deep water planktonic taxa (Fig. 7). The assemblages in W-7, on the other hand, are characterised by shallow water taxa, including the presence of microgastropods and miliolids in some intervals, with significant depth-dependent compositional variations (Fig. 7). These paleo-depth differences are key for the placement of the top of microfossil zone F65, which is based on the top occurrence of the agglutinating benthic foraminifera, *Textularia* sp.2 (Fig. 5). In the more distal well, W-1, the top *Textularia* sp.2 occurs within UC13-12; 33 m below biohorizon base *B. parca parca*. In the more proximal well, W-7, the top *Textularia* sp.2 does not occur until the facies has deepened substantially, from an inner to outer neritic environment, within nannofossil zone UC16; 55m above biohorizon

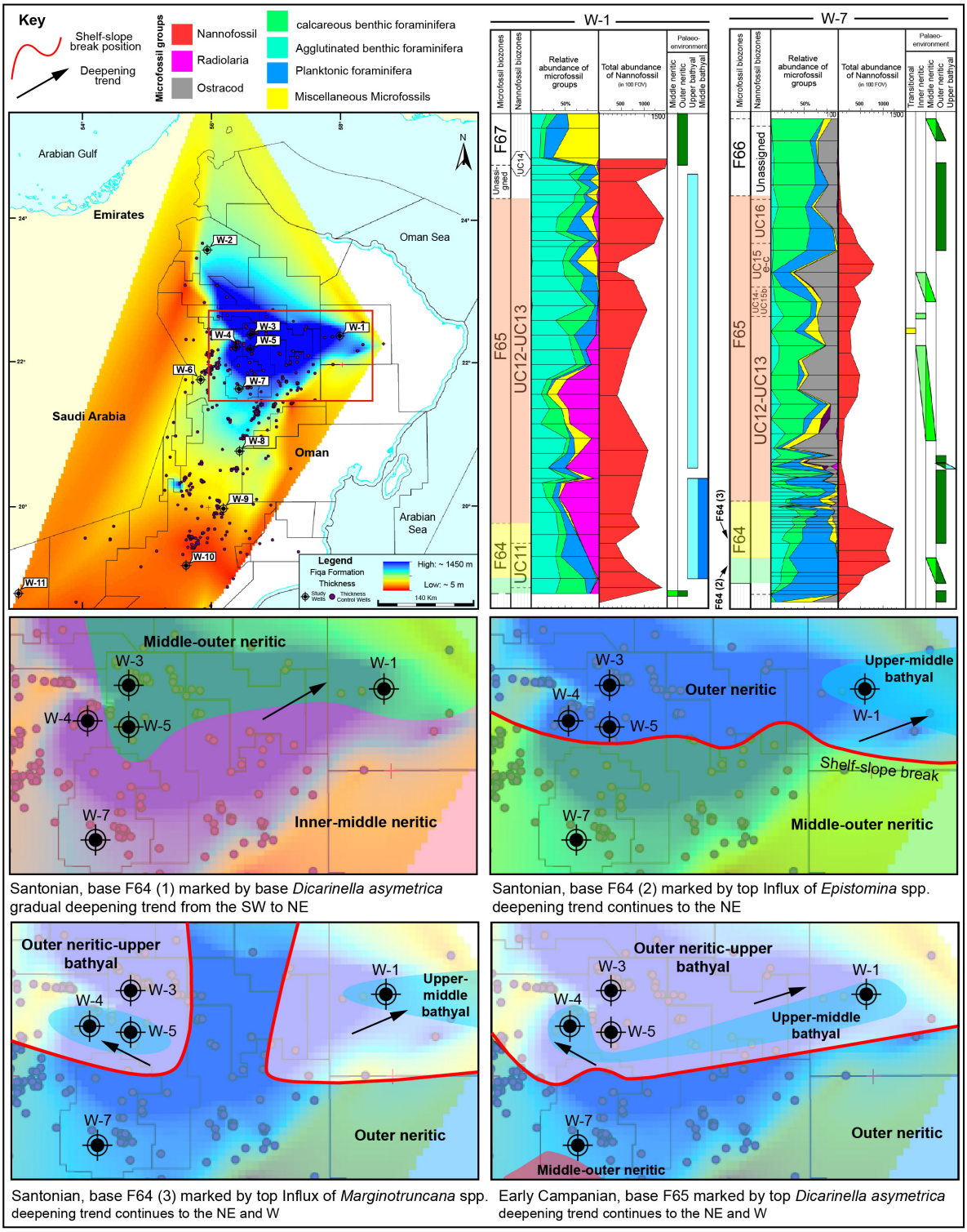

Figure 7. Palaeo-depositional setting of the Fiqa Formation from the Santonian to early Campanian (modified from Filbrandnt et al., 2004), and comparison of the diachronous F64 and F65 biozones with distinctive microfosssil vs nannofossil assemblages in W-1 and W-7.

top *E. eximius*. This integration of microfossil and nannofossil biostratigraphy confirms the suggestion of Packer (2001a) that events within the early Campanian F65 zone could be diachronous. Understanding this diachroneity is important for robust stratigraphic correlation between sites with different palaeodepths across the basin.

The Fiqa Formation nannofossil biohorizons identified here, are also useful in setting the Aruma Basin sequence stratigraphy into the wider context of the regional (Arabian sequence stratigraphy; Sharland et al., 2001) and local (North Oman sequence stratigraphy; Filbrandnt et al., 2004 and Packer, 2010) maximum flooding surfaces (MFSs) and sequence stratigraphic boundaries (SSBs). Together they provide a better understanding of the basin-fill, tectonic and paleoenvironmental history of the Aruma Basin. This includes new constraints on the age and diachroneity of the regional unconformities bounding the Fiqa Formation. The nannofossil assemblages are compared here to the available sequence stratigraphic interpretations of Packer et al. (2000) and Packer (2001a; b) for W-1, W-4, W-5 and W-7. The discussed sequence stratigraphic events of Filbrandnt et al. (2004) and Packer (2010) are SSB1, SSB2, SSB3, SSB4, MFS4 and MFS5. Sequence stratigraphic events of Sharland et al. (2001) are K160 MFS and K170 MFS.

The Mid-Cretaceous uplift and regression unconformity (Sharland et al., 2001), recognised across Arabia, and known as the Wasia-Aruma Break in Oman (Glennie et al., 1973), is the basal Fiqa Formation unconformity, separating it from the underlying Natih Formation. This erosional surface is indicated as SSB1 in Figure 8, which is the result of uplift, exposure and erosion related to structural flexing of the continent as a result of loading ahead of the advancing over-thrusted ophiolite into the northeastern part of Oman (Glennie et al., 1973; Droste

and Van Steenwinkel, 2004; Cooper et al., 2014). The Naith to Fiqa Formation transition is marked by a switch from the low gamma ray (GR), white/grey chalky limestone of the underlying Natih Formation, that are largely barren of nannofossils, into the nannofossil-rich, high GR, grey/green shale of the Shargi Member (Fig. 6). The onset of deposition following this sequence boundary is diachronous across the study area, by ~ 7 Ma, with the base of the Fiqa Formation being older in the north (Coniacian, UC11 in W-1, W-4 and W-5) and younger to the south (Santonian, UC13-12 in W-7; early-late Campanian, UC15 in W-8) (Fig. 6). This reflects the progressive deepening associated with the foreland basin formation that started in the north (Glennie et al., 1974) following SSB1. The earliest stages of the Fiqa Formation deposition in northern Oman are recorded as an influx of benthic and shallow water planktonic foraminifera in the lowermost part of the Sahrgi Member in a lowstand system tract (LST) (Filbrandnt et al., 2004). This LST is recorded in W-1 and is characterised by an upward decrease in nannofossil abundance (Fig. 8). Nannofossil assemblages are generally low following SSB1, as seen in W-4, W-5 and W-7, compared to the overlying sequences (Fig. 8). The onset of deposition following SSB1 is characterised by a relatively slow depositional rate during the Coniacian and Santonian in W-1, W-4 and W-5, and in the late Campanian in W-8 (Fig. 9). In W-7, a relatively faster depositional rate is recorded during the Santonian (Fig. 9).

In W-4 and W-5, SSB1 is followed by the regional K160 MFS of Sharland et al. (2001) that has been associated in Oman with high GR in the lower part of the Fiqa Formation near the base of the Shargi Member, and was given a Santonian age based on the *M. furcatus* nannofossil zone of Boote et al. (1990). The use of top *M. furcatus* to define the Santonian biozone of Boote et al. (1990) is not precise as it is widely recorded within Campanian sediments (e.g.

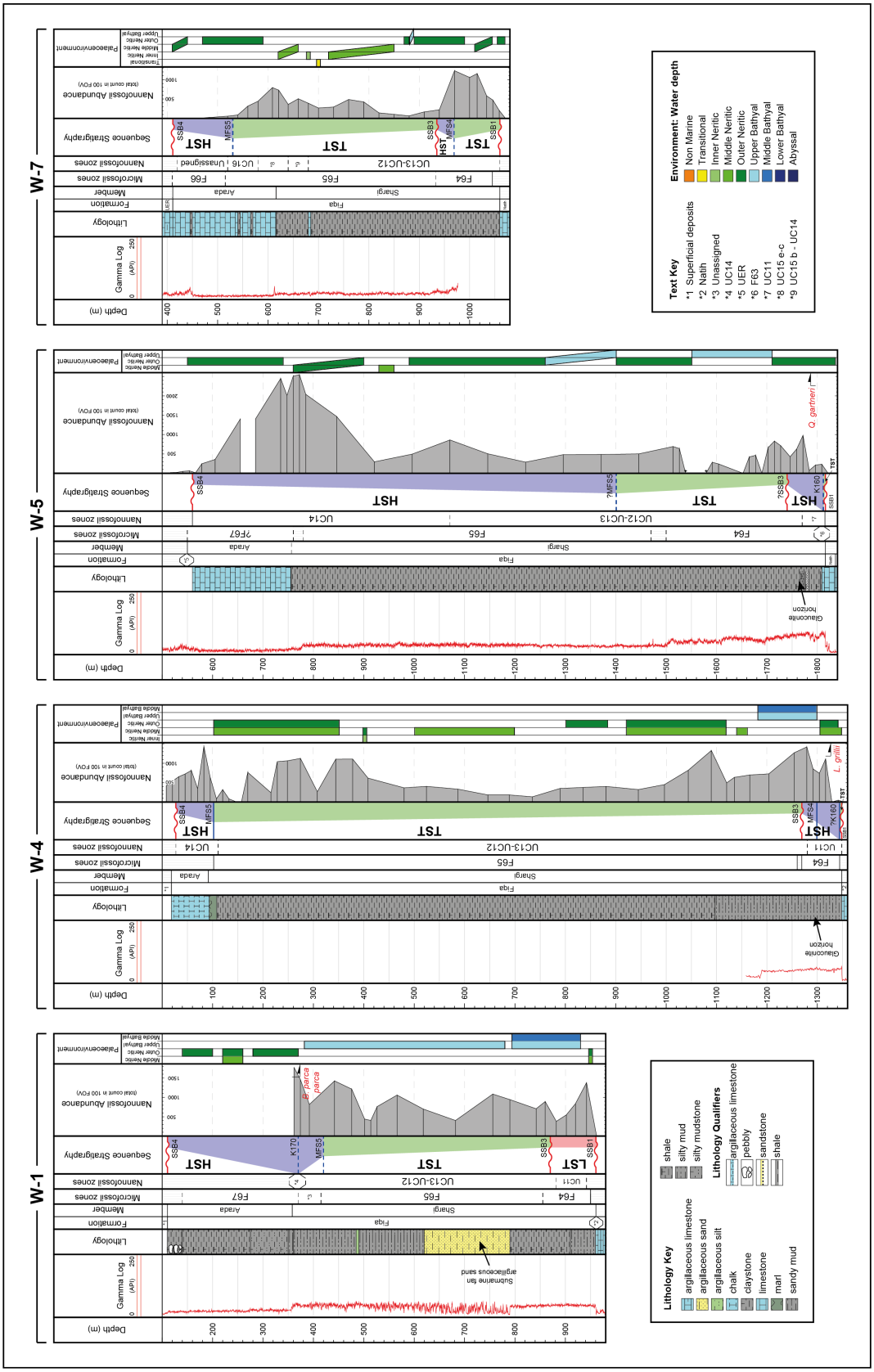

Figure 8. Sequence stratigraphic Correlation of selected wells compared to the palaeoenvironment and changes in nannofossil abundances. Palaeoenvironment and sequence stratigraphic interpretations from Packer et al. (2000) and Packer (2001a, b).

Sissingh, 1977; Perch-Nielsen, 1985) and not restricted to the Santonian, in addition, this species is rare and generally inconsistent within the study area. K160 MFS, on the other hand, occurs within Coniacian intervals in W-4 and W-5, 18 m below base *L. grilli* in W-4 and 18 m below top *Q. gartneri* in W-5, within the lowermost part of the Fiqa Formation near base UC11 (Fig. 8). This MFS, however, is not reflected in the nannofossil assemblages which are generally of low abundance around this level (Fig. 8). Nannofossil assemblages increase following K160 MFS in W-4 and W-7 (Fig. 8) and reach a peak around MFS4, a local maximum flooding surface recorded in North Oman by Packer (2010) based on influx of planktonic microfossils. Around 11 m following MFS4 in W-4, a consistent increase in GR is recorded and is suggested to correspond to the glauconite marker bed of Forbes et al. (2010) which is a silty/sandy level rich in chamosite ooids and glauconite, indicating low rates of deposition toward the base of the Fiqa Formation (Osterloff et al. 2001; Forbes et al., 2010) (see Fig. 9). In W-4 and W-5, this horizon is picked based on lithological and GR change within UC11, 15 m above biohorizon base *L. grilli* in W-4 and 14 m above biohorizon top *Q. gartneri* in W-5 (Fig. 8). Based on extensive stratigraphic review, Osterloff et al. (2001) believed that the glauconite marker bed is a regional horizon present throughout North Oman and provides a good stratigraphic event for optimising casing points, during drilling, within the lithologically-unstable shales of the basal Fiqa Formation, before reaching the underlying Natih Formation reservoir units.

Based on seismic data and changes in the microfossil assemblages, Filbrandnt et al. (2004) and Packer (2010) proposed a local SB – SSB2 – in North Oman following the glauconite horizon within the Santonian part of F64 biozone, in the lower part of Shargi Member. SSB2

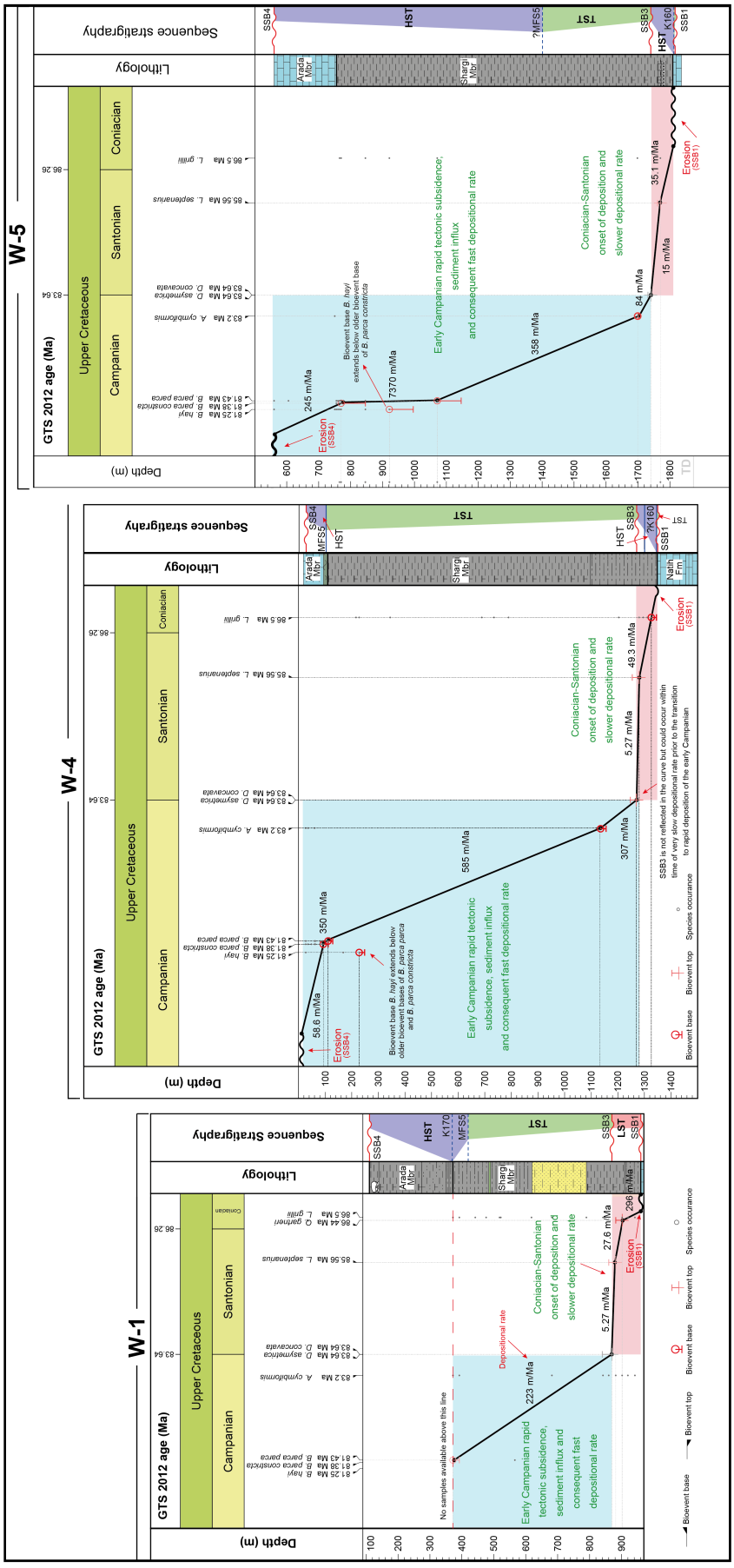

Figure 9. (part 1) Age-depth curves for the Fiqa Formation in the study area.

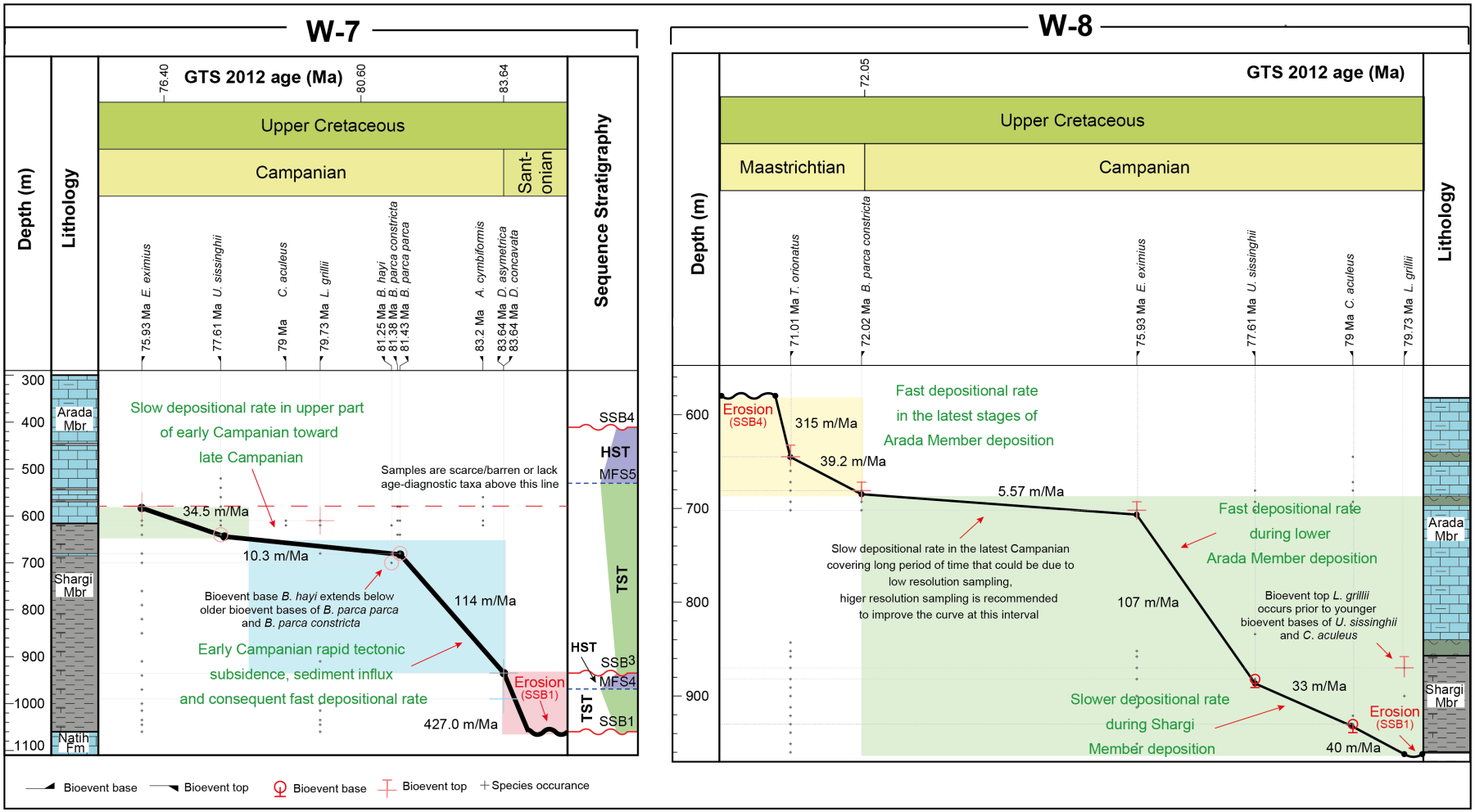

Figure 9. (part 2).

is a regression event with erosional channels incising into the underlying shale in the northernmost part of the basin (Filbrandnt et al., 2004) and is not recorded in the study area. The deposition of the lowest part of Shargi Member is followed by rapid deepening of relative sea level and the development of transgressive system tract (TST) and high stand system tract (HST) within the lower Shargi Member, characterised by claystones rich in radiolaria and deep-water planktonic foraminifera (Filbrandnt et al., 2004). Nannofossil abundances also increase in these sequences in W-4 and W-7 (Fig. 8). Relative shallowing of sea level is suggested at SSB3, the transition between the claystone-dominated lower (Santonian-early Campanian microfossil Zone F64) and the sandier, turbiditic upper (early Campanian Zone F65) parts of the Shargi Member (Filbrandnt et al., 2004) (Figs. 8, 9). In North Oman, SSB3 is associated with the collapse of a northward migrating delta slope, in response to progressive loading from the over-thrusted ophiolite (Filbrandnt et al., 2004), and resulted in the development of a lowstand fan recorded as a sand dominated interval in W-1 with a decrease in nannofossil abundance (Fig. 8). Although SSB3 is clearly followed by a reduction in nannofossil abundance in all wells (Fig. 8), it is not reflected in the constructed age-depth plots (Fig. 9) which could be the result of sub-sampling or the lack of age-diagnostic marker taxa within this time interval. A further increase in relative sea level is followed and resulted in the deposition of the thick hemipelagic shales of the upper part of the Shargi Member (early Campanian F65 biozone) (Fig. 10) rich in planktonic species (Packer et al., 2000; Packer, 2001a; b) including nannofossils (Fig. 8). This is reflected in the very fast rate of deposition starting at the onset of early Campanian deposition (Fig. 9). Throughout the deposition of F65, sea level remained relatively stable, reflecting a balance between sediment supply and a steady rise in relative sea level (Filbrandnt et al., 2004).

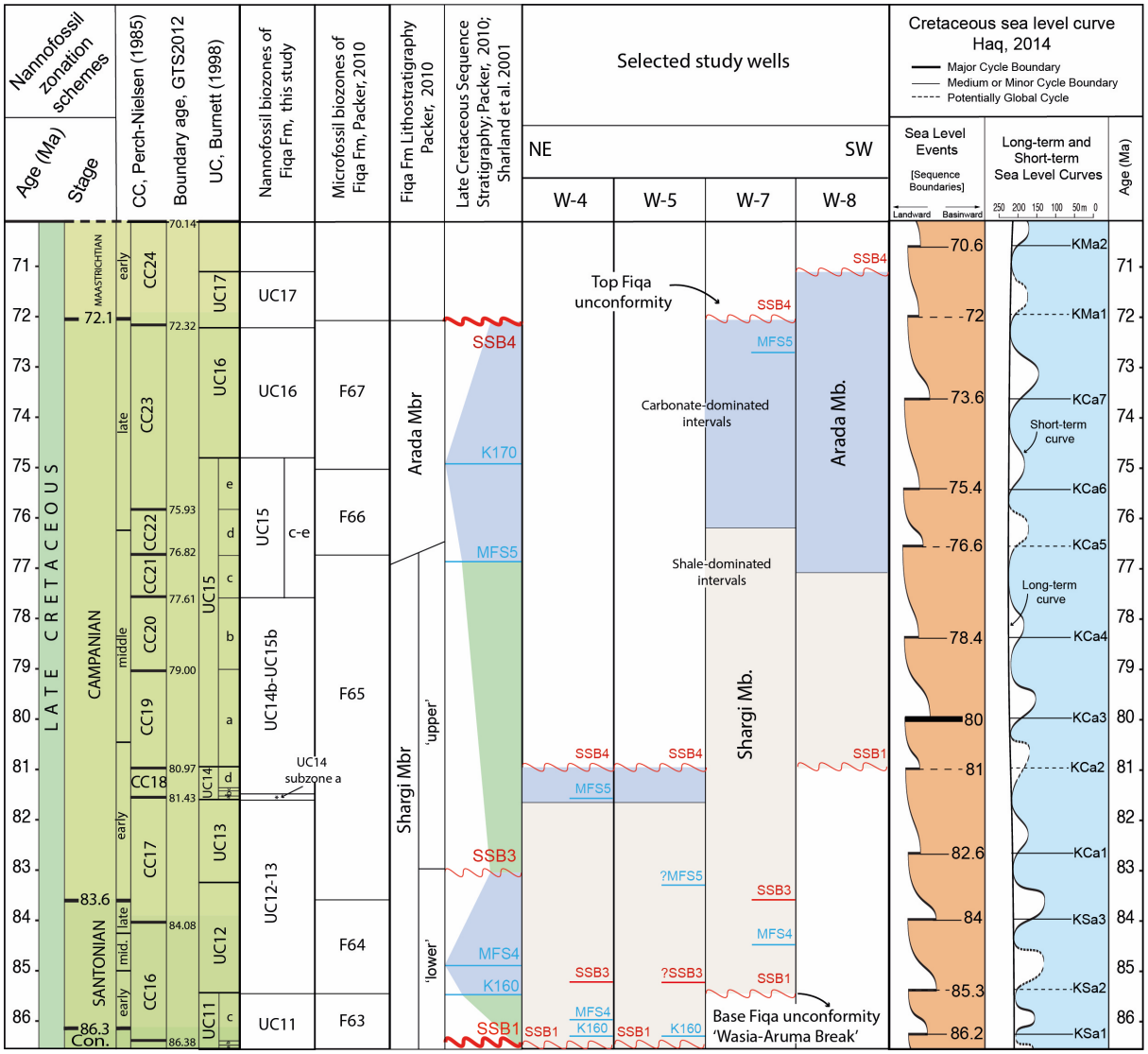

Figure 10. Summary of the biostratigraphy and sequence stratigraphy of the Fiqa Formation in the study area.

A shallowing of relative sea level followed and resulted in the deposition of the shallow marine carbonates of the Arada Member (Glennie et al., 1973). The Shargi/Arada transition is laterally variable across the basin (Hughes Clarke, 1988), including repeated vertical interlaying of the two characteristic lithologies in some areas which is also recorded in the study wells (Fig. 6). The rate of deposition is also variable at the transition across the study area (Fig. 9). Although suspected to be diachronous across the basin, this lithostratigraphic boundary is used in regional stratigraphic correlations in industry projects. The diachroneity of this

transition is now confirmed by nannofossil biostratigraphy, with an early Campanian (UC14) transition in the northern wells (W-4 and W-5), but a late Campanian (UC15c-e) transition at the southernmost localities (W-7 and W-8) (Figs. 6, 9).

During the early Campanian, there is a clear shallowing trend from deeper settings in the north and northeast, dominated by deep water planktonics, to shelf location in the southwest, with shallow water larger benthic foraminifera and ostracods (Packer et al., 2000). This regional pattern, is however, reversed with the onset of deposition of the shallow-water carbonates of the Arada Member, which occurs first in the north of the basin, in the early Campanian. At this time, palaeodepths in the south of the basin are slightly deepening. Together this pattern is consistent with regional tectonics associated with the emplacement of the Semail ophiolite, with rapid uplift associated with orogenic thrust tectonics in the north, and basin loading and subsidence to the south (e.g. Glennie et al., 1974; Searle and Cox, 1999; Ali and Watts, 2009). This is reflected in the southern well, W-8, where the Arada Member is characterised by fast depositional rate during most of late Campanian and Maastrichtian (Fig. 9).

Two MFS are recorded within the Arada Member, the first of which, MFS5, is based on an influx of planktonic microfossils in North Oman (Packer, 2010). Nannofossil abundance increases following MFS5 in W-1 and W-4, but remains extremely low in W-7 (Fig. 8). The second MFS is K170 (Sharland et al., 2001), which is placed at the base of the Fiqa Formation of the Haushi-Huqf area (Platel et al., 1995) and within the upper Fiqa marls of Central Oman Mountains foredeep (Boote et al, 1990). This event is dated as middle Campanian based on the *Globotruncana ventricosa* Foraminifera Biozone (middle Campanian-earliest late Campanian) of Platel et al. (1995). Packer (2010) placed this event at top late Campanian F66 bio-

zone based on top *Globotruncana elevata* (Fig. 10), however, in W-1, this event is correlated to the early Campanian UC14 nannofossil biozone and occurs 2 m above biohorizon base *B. parca parca*. K170 MFS is recorded only in W-1 and it is associated with maximum abundance and diversity of nannofossils around this level (Fig. 8).

At the top of the Fiqa Formation, the regional Mesozoic-Cenozoic unconformity (Sharland et al., 2001) is related to the end of ophiolite obduction and widespread regression. The age of this unconformity (SSB4) varies across the region, as recorded in the preserved successions at the top of the Fiqa Formation (Figs. 8, 9). This diachroneity reflects either temporal offsets in the end of basin subsidence - with the continued creation of accommodation space - or later differential erosion across the study area. Within the northern wells (W-3, W-4 and W-5), the top of the Fiqa Formation consists of lower Campanian sediments (UC14) (Fig. 6), which are directly overlain by Palaeocene sediments (UER Formation) in W-5 and by superficial sediments in W-3 and W-4 (Fig. 8). Toward the south, younger sediments are preserved at the top of the Fiqa Formation with uppermost Campanian sediments (UC16) preserved in W-7 and lower Maastrichtian sediments (UC17 and ?UC18) preserved in W-8 (Fig. 6), both are overlain by Palaeocene sediments (UER Formation) (Fig. 8). Across the region, this Mesozoic-Cenozoic unconformity is characterised by a transition from the marly, nannofossil-bearing carbonates of the Arada Member into the overlying shales of the basal UER Formation (Shammar Member), with sparse Palaeocene nannofossil assemblages dominated by *Coccolithus pelagicus*, as seen in W-5, W-6, W-7, W-8 and W-9. In W-8, W-9, and somewhat in W-5, this unconformity is marked by a GR spike in the basal shales of the UER Formation (Fig. 6). The deeper Campanian-Maastrichtian erosion or non-deposition in the northern wells is con-

sistent with the Late Cretaceous orogeny, with the north of Oman being proximal to the thrusted ophiolite and associated regional uplift, partial emergence and erosion during the early Maastrichtian (e.g. Nolan et al. 1990).

6 Conclusions

New calcareous nannofossil biostratigraphic dating for the Upper Cretaceous Fiqa Formation of Oman allowed the establishment of a late Coniacian to early Maastrichtian zonation scheme, integrated with the local foraminifera zonation scheme and sequence stratigraphy of Arabia. Nannofossil biozonation provided a finer resolution dating for the Formation, allowing better age control on different palaeobathymetric settings and enabled the subdivision of the formation into 7 zones with the recognition of different stage boundaries. The Campanian/ Maastrichtian transition in the Fiqa Formation is recorded for the first time based on the following nannofossil events from younger to older: top *T. orionatus* (early Maastrichtian); top *Uniplanarius* spp.; top *E. angustus* and *E. lindiensis* and top *B. parca constricta* (late Campanian). The Campanian/Santonian transition is characterised by the following bioevents from younger to older: base *B. parca parca* (lower Campanian); top *Nannoconus* spp.; base *Broinsonia verecundia;* top *Helicolithus blairiae;* top *Dicarinella asymetrica* (Santonian planktonic foraminifera); *Marginotruncana sinuosa* (Santonian planktonic foraminifera). The base *B. verecundia* and top *H. blairiae* are proposed as good alternative events to base *A. cymbiformis* for the identification of transition from the early Campanian into the Santonian in the Fiqa Formation due to their consistent occurrence around this level in the study area. The Coniacian/Santonian transition in the formation is characterised by the following bioevents from younger to older: top *Lithastrinus septenarius* (lower Santonian); top *Quadrum gartneri* (up-

per Coniacian); base *Marthasterites furcatus* (upper Coniacian); top *Dicarinella concavata* (Coniacian planktonic foraminifera); base *Lithastrinus grillii* (Middle? to Upper Coniacian). Nannofossil biostratigraphy allowed the recognition of diachroneity within the Fiqa Formation including the transition from the Arada to Shargi Members, which is early Campanian in the northern wells, and late Campanian to the south indicating an earlier onset of shallow marine deposition to the north. The base of the formation is also diachronous with upper Coniacian sediments in the north of the basin, ~7 Ma older than basal sediments in the south, consistent with the progressive deepening and foreland basin formation that started in northeastern part of Oman, proximal to the ophiolite obduction. The top of the formation is also diachronous, indicating differential erosion/non-deposition, with the youngest lower Maastrichtian sediments preserved only in the south of the basin. Correlating nannofossil biostratigraphy and assemblage changes to the local and regional sequence stratigraphy gave new insights into the tectonic controls on the paleoenvironment of the basin through time. Sequence stratigraphic events are reflected in the nannofossil assemblage changes including higher abundances recorded in the transgressive and highstand sequence tracts and maximum abundance and diversity recorded around the maximum flooding surfaces, while abundances are usually reduced following sequence stratigraphic boundaries during local tectonics and regression events.

CHAPTER 4

INTEGRATED BIO- AND CHEMO- STRATIGRAPHY AND PALEOENVIRONMENTAL ANALYSIS OF THE UPPER CRETACEOUS ARUMA BASIN, OMAN

Abstract. This study presents the first integrated bulk carbonate carbon isotope ($\delta^{13}C$) stratigraphy, bulk rock elemental data (X- ray fluorescence analyses) and nannofossil assemblage data through the upper Coniacian to upper Campanian Fiqa Formation, deposited within the Aruma Basin of Oman. The geochemical analyses, undertaken on 204 bulk rock samples from 5 hydrocarbon exploration wells are integrated with the analysis of nannofossil assemblages from 172 samples across a total of 8 exploration wells that span proximal and distal environmental settings, as well as additional micropalaeontological data (radiolaria, foraminifera) where available. The first biostratigraphically constrained $\delta^{13}C$ curve is constructed for the Fiqa Formation with comparisons to both global and regional $\delta^{13}C$ stratigraphies. Generally, $\delta^{13}C$ values of the Fiqa Formation are consistent with global $\delta^{13}C$ records but diverge in the early Campanian, where a regional negative $\delta^{13}C$ excursion event is associated with local tectonics, an increased sediment and nutrient flux and some degree of basin restriction that is clearly reflected in both bulk sediment elemental compositions as well as nannofossil and microfossil assemblages. Above this early Campanian excursion, and with increasing sea level and basin-ocean connections, $\delta^{13}C$ values are consistent with the global ocean. Distinctive variations in nannofossil assemblages are recorded, both through time and across the basin. The most marked assemblage change is an interval of low *Watznaueria barnesiae* relative abundance associated with increased abundances of high fertility taxa including *Corollithion signum*, *Biscutum constans*, *Discorhabdus ignotus* and *Zeugrhabdotus erectus*. This interval is associated with regression and increased sediment influx, inferred from existing sequence stratigraphic data, sediment composition and $\delta^{13}C$ records, which are the most likely drivers of this interval of elevated surface ocean nutrient conditions. Together these data provided a valuable new

stratigraphic, environmental and depositional framework for the Upper Cretaceous succession of the Aruma Basin within the mostly homogeneous shales and marls of the Fiqa Formation.

1 Introduction

The Upper Cretaceous, deep marine Fiqa Formation of Oman was deposited in a tectonically active, tropical basin, within a greenhouse climate state (Al Rawahi and Dunkley Jones, 2019a; see Chapter 2). The Fiqa Formation plays an important role in the petroleum industry in Oman, as a regional seal unit and an under-studied potential hydrocarbon play that needs new geological data to improve its stratigraphy and depositional models (e.g. Horsfield, 1983; Giner et al., 1992; Filbrandt et al., 2004; PDO XEM report, 2015). This is particularly important for the fine-grained lithologies within the Fiqa Formation, which in sediment character are largely homogeneous but do show facies variability in their microfossil content (e.g. Packer, 2001a; Al Rawahi and Dunkley Jones, 2019a; see Chapter 2; Al Rawahi and Dunkley Jones, 2019b in review; see Chapter 3).

Geochemical analyses, mostly undertaken on bulk sediments, are widely used for improving stratigraphic control and basin-wide correlations (e.g. Thöle et al., 2019). These chemo-stratigraphies are particularly useful when integrated with biostratigraphic and other geological data to provide a more comprehensive view on depositional environments, lateral facies changes and diachroneity at a basin scale (e.g. Vahrenkamp, 2010; Wohlwend et al. 2016; Wolfgring et al., 2018; Razmjooei et al., 2018). The recognition of global-scale carbon cycle perturbations preserved in down core carbon isotope ($\delta^{13}C$) records can provide the basis for far-field correlations between ocean basins (e.g. Wendler, 2013). Within Upper Cretaceous sequences, for example, several isotope excursion events in Cenomanian to Campanian $\delta^{13}C$ records from the English Chalk can be correlated to sections across Europe including in France, Germany, Italy and Spain (Jarvis et al. 2006). These $\delta^{13}C$ isotope excursion events are developing into a standard scheme for the Late

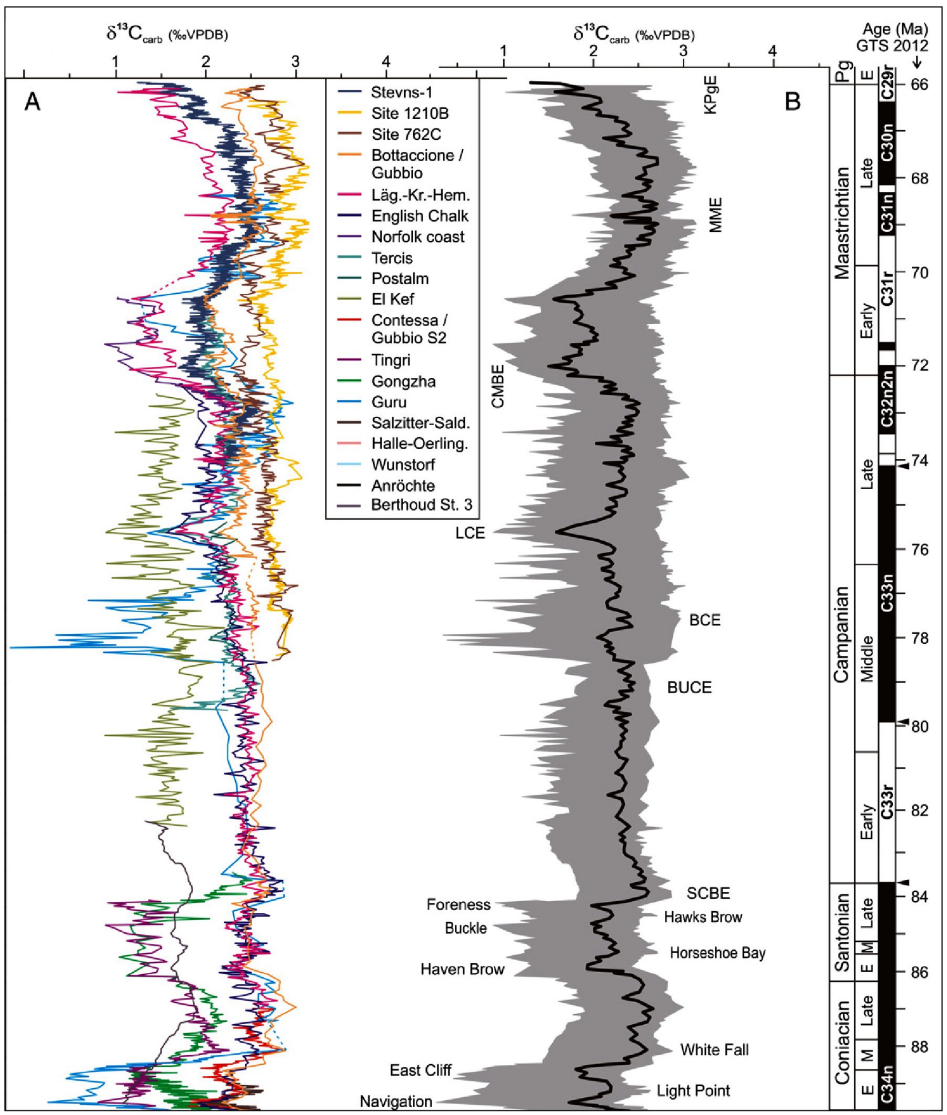

Figure 1. Global compilation of Late Cretaceous $\delta^{13}C$ curves (left) and global average $\delta^{13}C$ stack with the main excursion events (right), compiled by Wendler (2013).

Cretaceous (Wendler, 2013) (Fig. 1), useful for correlating between sections in disparate locations (e.g. Voigt et al., 2012; Razmjooei et al., 2018; Joo and Sageman, 2014). The most common Late Cretaceous $\delta^{13}C$ events which are recognised in various localities, and probably represent global-scale perturbations to the carbon cycle, include the positive excursions of the Santonian-Campanian boundary event (SCBE) and the mid-Campanian event (MCE), the negative excursions of the late Campanian event (LCE) and the Campanian-Maastrichtian boundary event (CMBE) and the positive excursion of the mid-Maastrichtian event (MME). These events have been recognised

across Boreal, Tethyan, Indian and South Atlantic sections (e.g. Jarvis et al. 2006; Voigt et al., 2010; Thibault et al., 2012; Wendler 2013) (Fig. 1).

Within the Cretaceous of Oman, stable isotope stratigraphies have been established for both the Aptian of the Shu'aiba Formation (Vahrenkamp, 2010) and the upper Albian to mid-Turonian Natih Formation (Wohlwend et al., 2016), including a detailed $\delta^{13}C$ record of Ocean Anoxic Event 2 (OAE2) and the Cenomanian-Turonian boundary. These isotope records have not yet been extended into the Upper Cretaceous Fiqa Formation, which is an aim of this study, although data are available from time-equivalent strata in the Middle East (e.g. Razmjooei et al., 2014; Razmjooei et al., 2018; Farouk et al., 2018a; b).

Long-term changes in the bulk elemental composition of sedimentary rocks, as often determined by X-ray fluorescence spectrometry (XRF), are also stratigraphically useful as they reflect sediment provenance, contributions from biogenic minerals (calcium carbonate and silica) and redox state during deposition especially when combined with isotope and microfossil data (Calvert and Pedersen, 2007). Within petroleum exploration, XRF analyses can provide stratigraphic information on borehole cuttings and side-wall core samples that generally lack sedimentary features (Rollinson, 1993; Ratcliffe et al., 2007). Sediment elemental data can also provide palaeoenvironmental information - especially a quantification of the balance between biogenic and siliciclastic components - to strengthen micropalaeontological interpretations (Calvert and Pedersen, 2007). The Petroleum Development Oman (PDO) have some unpublished elemental analyses of the Fiqa Formation, including two chemostratigraphic studies that examined the provenance of Upper Cretaceous sediments (Higgins and Howarth 1997a; b). These studies show a long-term shift in sediment source from the east and south Oman - Huqf area - to an increased ophiolite-derived, northerly-sourced, component in the upper part of the Fiqa Formation (Fig. 2).

The stable isotope and elemental geochemistry of Upper Cretaceous sediments in Oman is currently poorly known, but has potential to improve our understanding of basin-wide subsurface correlations. This study presents new $\delta^{13}C$ data from multiple subsurface sections of the Fiqa Formation to test the utility of carbon isotope stratigraphy within the Aruma Basin and establish a biostratigraphically-constrained $\delta^{13}C$ reference curve for the Upper Cretaceous of Oman. Further, we integrate these new analyses with bulk sediment elemental data and calcareous nannofossil assemblage data to determine variations in palaeoenvironments both through time and across the basin.

2 Geology and Subsurface Stratigraphy of the Study Area

The Fiqa Formation is part of the Upper Cretaceous Aruma Group of Oman, with a subsurface stratigraphy composed predominantly of deep-marine, homogenous hemipelagic shales (Shargi Member) overlain by, and sometimes interbedded with, shallower marine carbonates (Arada Member), the occurrences of which are highly variable across the subsurface (Owen and Nasr, 1958; Hughes-Clark, 1988; Forbes et al., 2010). The Fiqa Formation, most recently constrained as spanning the upper Coniacian to lower Maastrichtian (Al Rawahi and Dunkley Jones, 2019a; see Chapter 2; Al Rawahi and Dunkley Jones, 2019b in review; see Chapter 3), was deposited in a foreland basin - known as the Aruma basin - that developed during overthrusting of ophiolitic rocks and associated deep marine units onto the northeastern part of Oman (e.g. Glennie et al., 1974; Lippard et al., 1986; Searle, 1988; Searle and Cox, 1999). The Aruma basin is relatively small, extending along a distance around 540 km, from the south of the Oman Mountains to near the Dhofar Mountains (covering an area around 184,000 km^2 in Oman onshore only) but appears to have had strong palaeobathymetric gradients at various points through the Late Cretaceous. In the north of Oman, microfaunal assemblages indicate a change from neritic conditions in the Coniacian and earliest Santonian into bathyal conditions with rapid deposition during the late

Santonian to mid Campanian, but with subsequent shallowing in the late Campanian and into the Maastrichtian (Packer, 2001a; Packer, 2002; Al Rawahi and Dunkley Jones, 2019a; see Chapter 2; Al Rawahi and Dunkley Jones, 2019b in review; see Chapter 3).

During the earliest stages of ophiolite over-thrusting, the Arabian continental margin was dominated by rapid erosion of the uplifted basement fault blocks (Robertson, 1987) and of the fore-bulge that developed ahead of the advancing thrust belt (Warburton et al., 1990). This period of uplift and erosion is widely recorded throughout Oman as a regional Turonian-lower Coniacian hiatus known as the Wasia-Aruma break (Glennie et al., 1974). Severe erosional truncation is widely documented along the Lekhwair Arch, in western Oman, which was rapidly uplifted during the overthrusting event (Boote et al., 1990). From the late Coniacian and following the Wasia-Aruma break, sediments are believed to be sourced into the Aruma Basin from the uplifted eastern Oman margin in the Huqf and Batain Coast areas (Warburton et al., 1990; Higgins and Howarth 1997a; b; Filbrandt et al., 2004). As the over-thrusted blocks continued to rise toward the late Campanian, it likely became the dominant source of detrital sediments into the basin (Higgins and Howarth, 1997a; b). Toward the end of the Campanian, the basin became filled and a rise in sea level caused clastic supply from the drowned hinterland to cease, allowing shallow carbonate deposition to re-establish for most of the Maastrichtian and Paleocene (Warburton et al., 1990).

In the study area, the Fiqa Formation transitions from being shale-dominated in the north of the basin to carbonate-dominated in the south (Fig. 2). Eleven subsurface successions of the Fiqa Formation, recovered in exploration wells from across the Aruma Basin, have been included in this study (Fig. 2), with samples examined for calcareous nannofossil content from all wells. Five of these borehole successions were also analysed for geochemical data which are W-4, W-7, W-9, W-10 and W-11. The most northernly wells, W-1, W-2, W-3, W-4 and W-5 are located at the

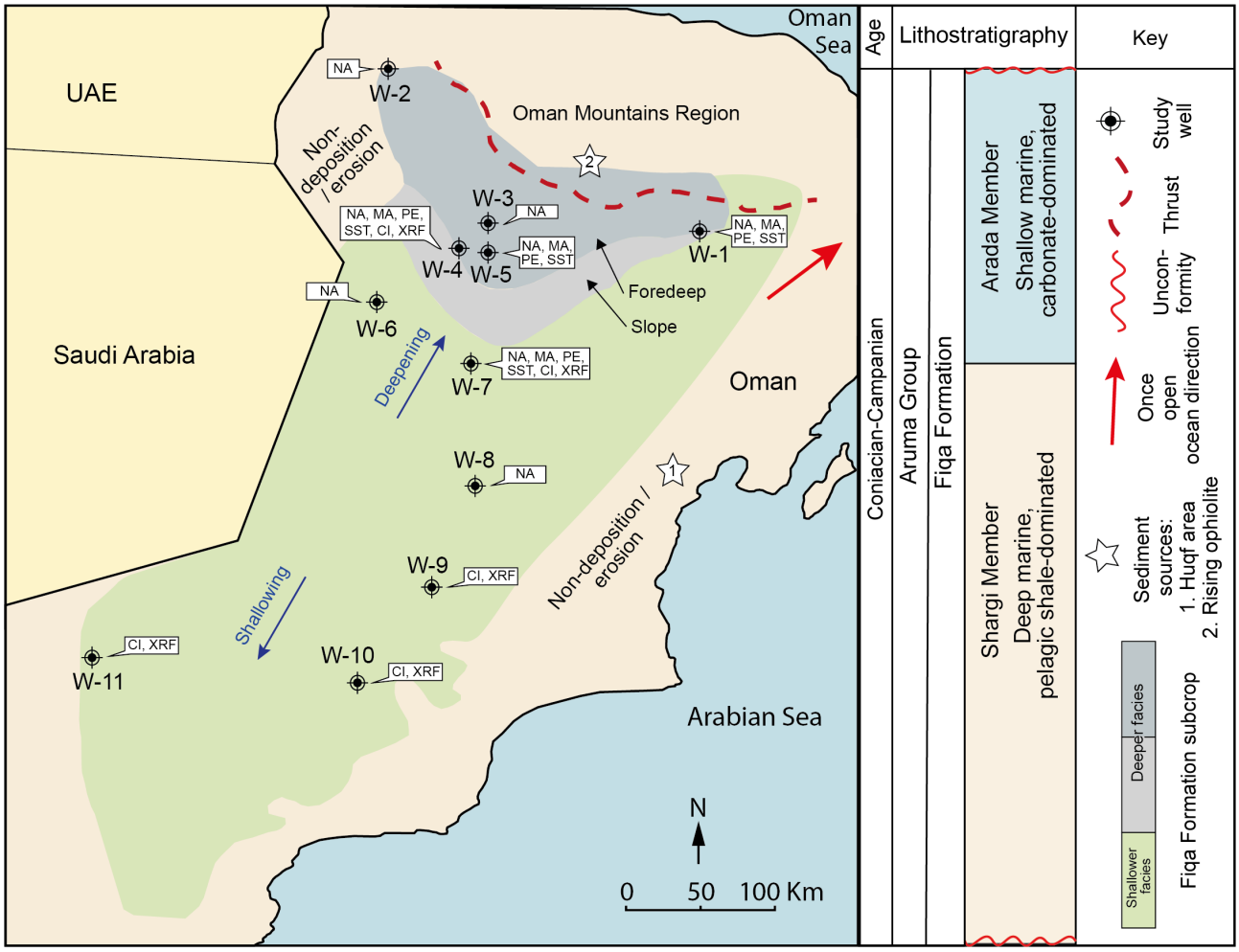

Figure 2. Subsurface lithostratigraphy of the Fiqa Formation (after Forbes et al., 2010) and the location of study wells in a subcrop map of the Fiqa Formation with projected slope and foredeep basin based on seismic data (modified after Giner et al., 1992). Available data included in this study is shown for each well as following: NA, nannofossil assemblage data; MA, microfossil assemblage data; PE, palaeoenvironment (water depth) from microfossil associations; SST; sequence stratigraphy from micropalaeontological interpretations; CI, carbon isotope; XRF; element data. Microfossil data included in this study is based on the analysis of Packer et al., (2000) and Packer (2001a, b). Projected direction of open ocean and sediment sources are from Filbrandt et al. (2004).

thickest and deepest part of the basin, closest to the active over-thrusted belt, where the Fiqa Formation is characterised by thick shale-dominated sequences. In W-4, for instance, a 1.3 km thick succession of deep marine shales of the Shargi Member are recovered, overlain by 73 m of Arada Member carbonates that are deeply eroded at the top (Al Rawahi and Dunkley Jones, 2019b in review; see Chapter 3). Moving southward to shallower parts of the basin, the Fiqa Formation thins,

and the proportion of Arada Member carbonates increases gradually. For instance, the carbonate to shale thickness ratios increase from 1:2 (205:444 m) in W-7, to 2:1 (275:104 m) in W-8, which is located in a shallower part of the basin, to the carbonate-dominated W-9 (4:1, 100.5:24.5 m) and W-10 (1:1, 24:18.5 m), which are located at the most proximal and shallowest part of the basin. In W-11, again in the proximal basin, the Fiqa Formation is 191.3 m thick, consisting of undifferentiated carbonate-dominated lithologies, occasionally interbedded with shale layers.

3 Material and Methods

A total of 204 samples were selected from five wells across the basin (Fig. 2) for bulk rock isotope (Sect. 3.1) and XRF (Sect. 3.2) analyses: 91 samples from W-4; 72 samples from W-7; 22 samples from W-9; 11 samples from W-10; and 8 samples from W-11 (see Chapter 1; Fig. 2 for sampling resolution and samples type for each well). The sampling strategy aimed to generate records from across the lithological (shale to carbonate) and palaeoenvironmental (shallow marine to bathyal) gradients suggested for the Aruma Basin. Analyses were also constrained by the availability of samples and contextual geological data, including lithological descriptions and gamma ray logs. Results of XRF analyses were also subjected to standard Principal Component Analyses (PCA) (Sect. 3.3).

The majority of the 204 samples analysed for geochemistry, as well as an additional 137 samples from the remaining 6 study wells, were also subjected to detailed analysis of calcareous nannofossils - the biostratigraphic results of which are contained in Al Rawahi and Dunkley Jones (2019b in review) (see Chapter 3), and assemblage data from W-4 only are included in Al Rawahi and Dunkley Jones (2019a) (see Chapter 2). Here, we integrate and interpret the available nannofossil assemblage data within a basin-wide palaeoenvironmental context. These results are integrated with existing microfossil assemblage data as generated by PDO and their sub-contracted

micropalaeontological consultancies (Packer et al., 2000; Packer, 2001a; b). Calcareous nannofossil assemblages from a total of 173 samples with good nannofossil preservation - 19 samples from W-1, 6 from W-2, 10 from W-3, 45 from W-4, 31 from W-5, 17 from W-6, 23 from W-7 and 22 from W-8 - were also subjected to PCA analysis (Sect. 3.3).

3.1 Bulk Rock Isotopes

Bulk rock analyses for carbon and oxygen isotopes ($\delta^{13}C$, $\delta^{18}O$) were carried out using a Continuous-Flow Isotope-Ratio Mass Spectrometry (CF-IRMS) at the University of Birmingham GEological Mass-Spectrometry laboratories (GEMS). Samples were oven dried at 50°C for 24 hours and then ground into fine powder using an agate pestle and mortar. These bulk sediment samples were then split for stable isotopic and XRF analyses (Sect. 3.2). Sub-samples for stable isotope analyses were weighed into 4 ml glass vials and sealed by a lid with a pierceable septum. Sample weights are varied in order that calcium carbonate content was maintained at near constant levels between analyses and ranged from ~250 μg for the carbonate rich samples to ~1000 μg for carbonate-poor lithologies. Vials were then heated to 50˚C, with the headspace replaced by pure helium using the Isoprime Multiflow preparation system. 200 μl of phosphoric acid was manually injected into each sample and left for a minimum of one hour, with the headspace gas then sampled and injected into the continuous-flow mass spectrometer. A duplicate was measured from each sample and a mean value was calculated for ^{13}C and ^{18}O composition. Results were calibrated using the International Atomic Energy Agency (IAEA) standards NBS 18 and NBS 19 and are given in per mille relative to the VPDB standard. An external precision better than 0.1 ‰ was achieved for both ^{13}C and ^{18}O. See appendix D for detailed results of the analysed samples.

3.2 X-Ray Fluorescence

Sample preparation for XRF analysis is after Takahashi (2015). About 0.5 g of rock powder from the dried and ground bulk sediments (Sect. 3.1) was weighed and blended with 0.1 g of wax powder (SpectroBlend 44μm powder) using an agate pestle and mortar. This mix was then formed into pellets using a manual press before analysis for elements concentration with a Bruker S8 TIGER WDXRF Elemental Analysis System at the University of Birmingham Centre for Chemical and Materials Analysis. See appendix E for detailed results of the analysed samples.

3.3 Statistical Analysis of XRF Data and Nannofossil Assemblages

To determine if consistent spatial and/or stratigraphic trends were present across many variables, PCA was performed on elemental concentration and nannofossil relative abundance data. These analyses were carried out using the PAST3 software (http://folk.uio.no/ohammer/past/, downloaded September 2016). Before applying the PCA, rare elements and species were excluded and all zero values were replaced by very small non-zero values. All abundance data was then resumed to 100%, and Additive Log Ratio (ALR) transformed using normalisation to *Cribrosphaerella ehrenbergii* for calcareous nannofossil assemblage data and aluminium for bulk elemental concentrations. This follows the approach of Weltje & Tjallingii (2008) and references therein. See appendix F for detailed results of the analysed samples.

4 Results

4.1 Stable Isotope Analysis

Cross-plots of $\delta^{18}O$ and $\delta^{13}C$ data are shown in Figure 3, divided by well and lithostratigraphic unit. It is clear that there is a higher variability in $\delta^{18}O$ than $\delta^{13}C$, and within this, $\delta^{18}O$ is more variable in the low-carbonate shales of the Shargi Member than the carbonates of the Arada Member. On the basis of the clear lithological control on $\delta^{18}O$ data and its variability, we infer that $\delta^{18}O$ analyses are

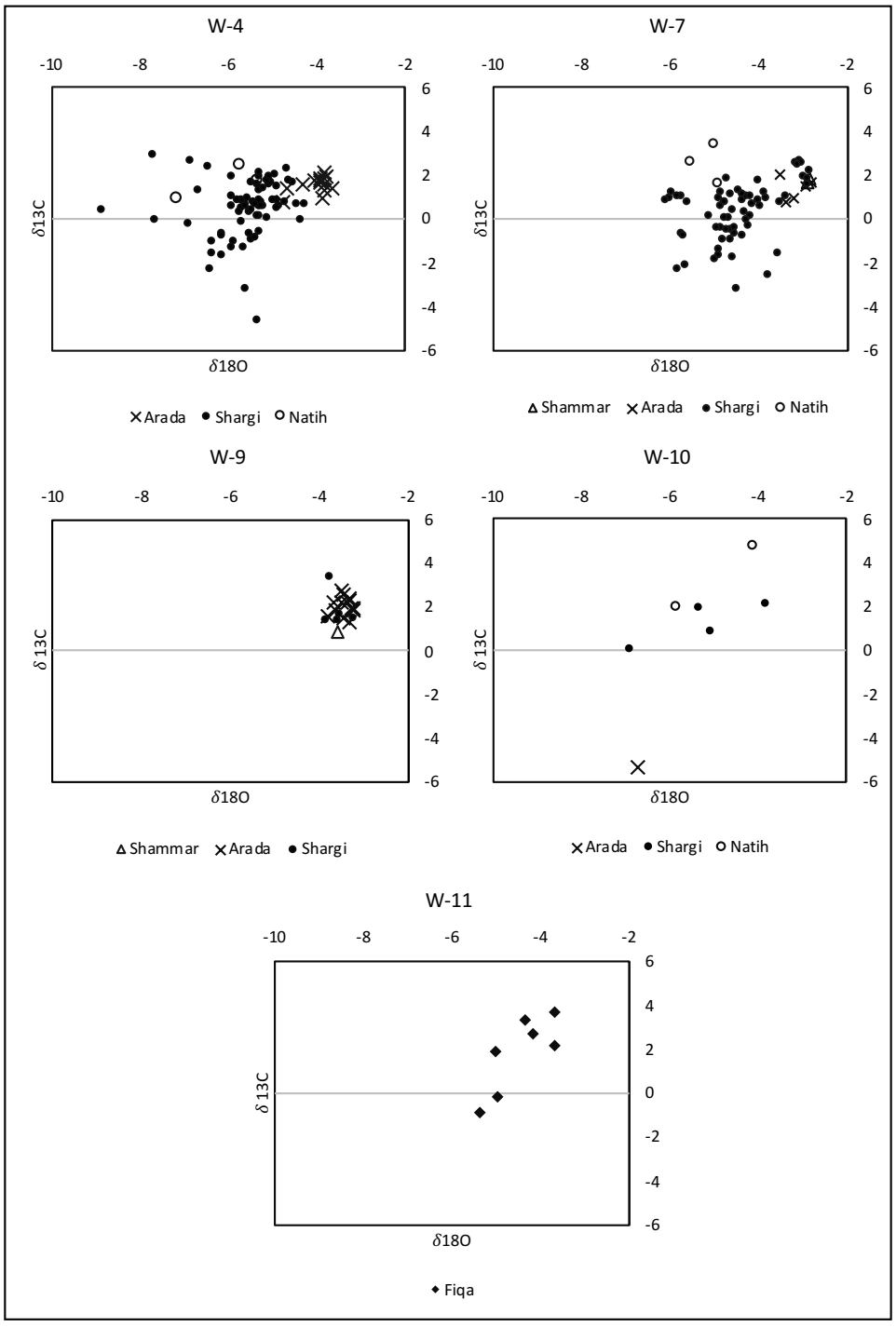

Figure 3. Carbon-oxygen cross plots for W-4, W-7, W-9, W-10 and W-11.

likely influenced by diagenetic carbonates, especially in the Shargi Member samples and are not considered further.

$\delta^{13}C$ data from the Fiqa Formation in the more expanded northern wells, W-4 and W-7, varies from 3‰ to -4‰ (Fig. 3). In the Coniacian (W-4 only) and Santonian part of the Formation, $\delta^{13}C$ values

vary between 0‰ and 1‰, which is followed by a negative excursion, with values down to -4‰, in the lowermost Campanian (see Fig. 12). Above this, $\delta^{13}C$ returns to positive values up to 2‰ for most of the lower Campanian and lower part of the upper Campanian, which is only preserved in W-7, but then decreases again to values with an average of 1.3‰ for the rest of the upper Campanian (see Fig. 12). In the southern wells, the $\delta^{13}C$ values are more stable for W-9, generally

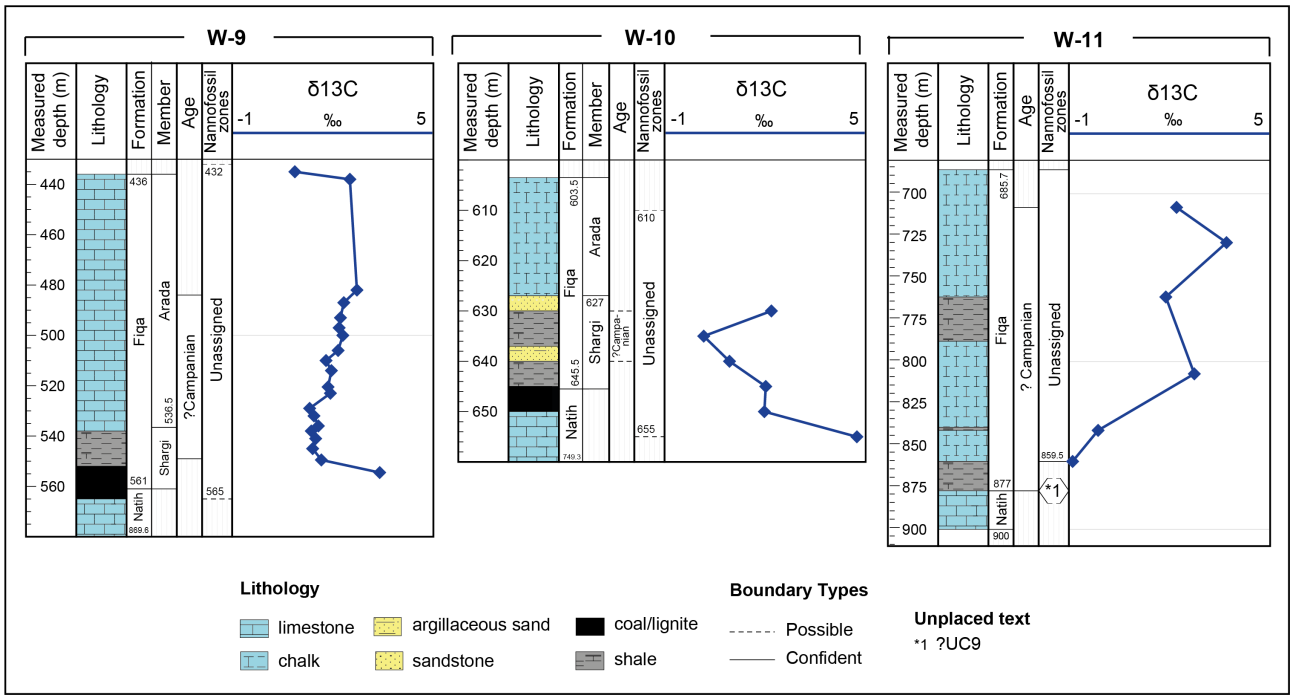

Figure 4. Carbon isotope curves for the southern wells.

around 2-3‰ (Fig. 4). Limited number of samples are available for W-10 and W-11 with values ranging from -1 to 5‰ (Fig. 4).

4.2 Bulk Rock Elemental Composition

Around 30 major and minor elements were detected in bulk rock XRF analyses, with key element ratios and absolute concentrations discussed below, including Ca/Si, Si/Fe, Si/Al, Fe/S, Si, Al, Ti, Fe and K, and plotted against depth (Figs. 5, 6, 7). The data is normalised through the use of element ratios in order to reduce the effects of diagenesis and other variables that affect the reflected compositions for each sample (Rollinson, 1993). Distinctive trends in these ratios can be used as indicators of particular geological processes (Calvert and Pedersen, 2007; Rothwell and

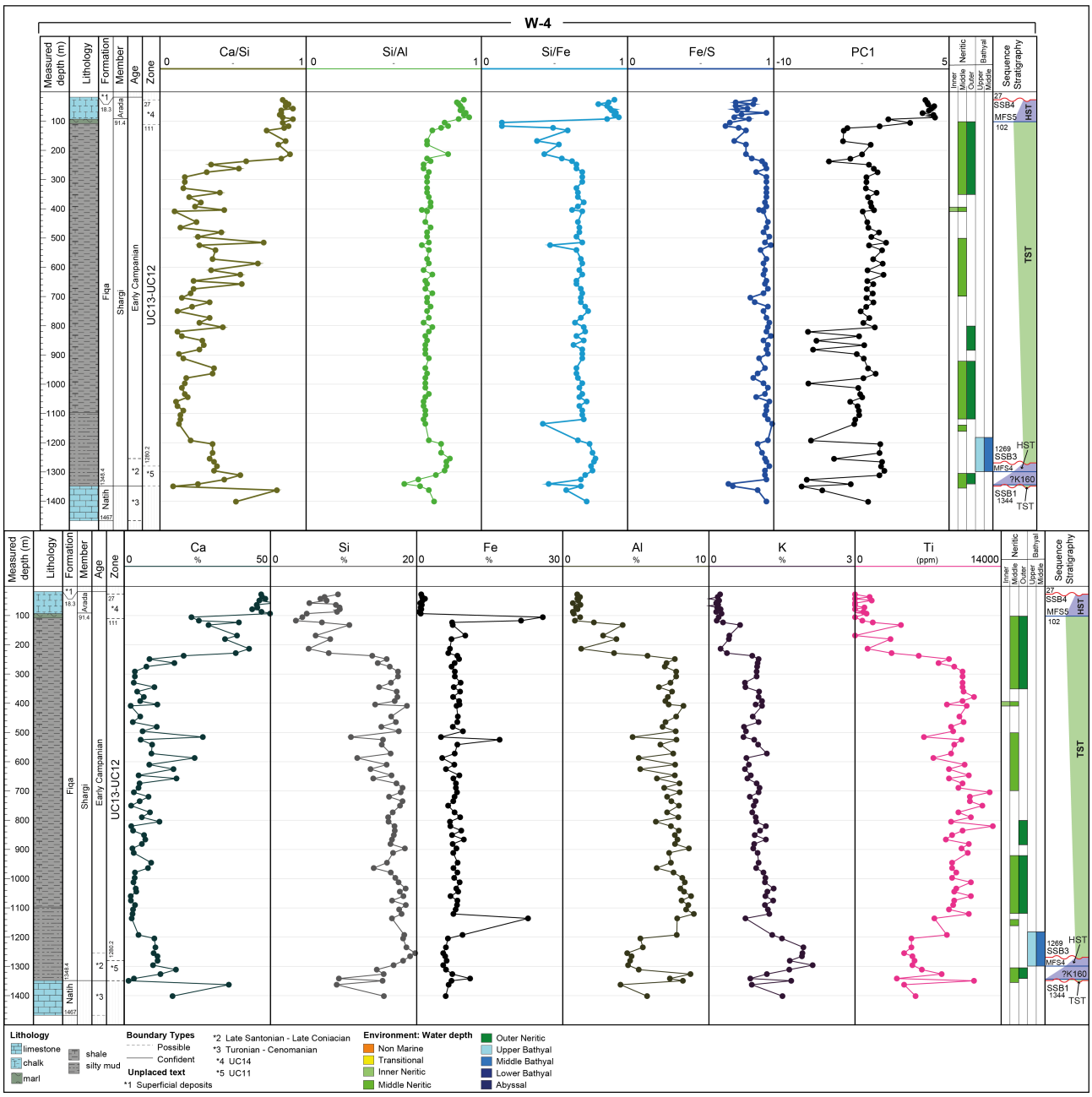

Figure 5. Elements concentration and ratios of W-4.

Croudace, 2015 and references therein). The Ca/Si ratio traces the relative abundance of calcium carbonate versus siliciclastic input, in this case reflecting the balance between deeper water shales and shallow marine carbonates. Moving from the carbonates of the Natih Formation to the shales of lower Fiqa Formation, the Ca/Si values decrease dramatically as seen in W-4, W-7, W-9 and W-10 (Figs 5, 6, 7). The Ca/Si follow exceptionally similar trend in both W-4 and W-7 (Figs. 5, 6), with higher values in the lowermost part of the Shargi member, before becoming more variable through the rest of this member and then increasing dramatically toward the Arada Member. In the southern

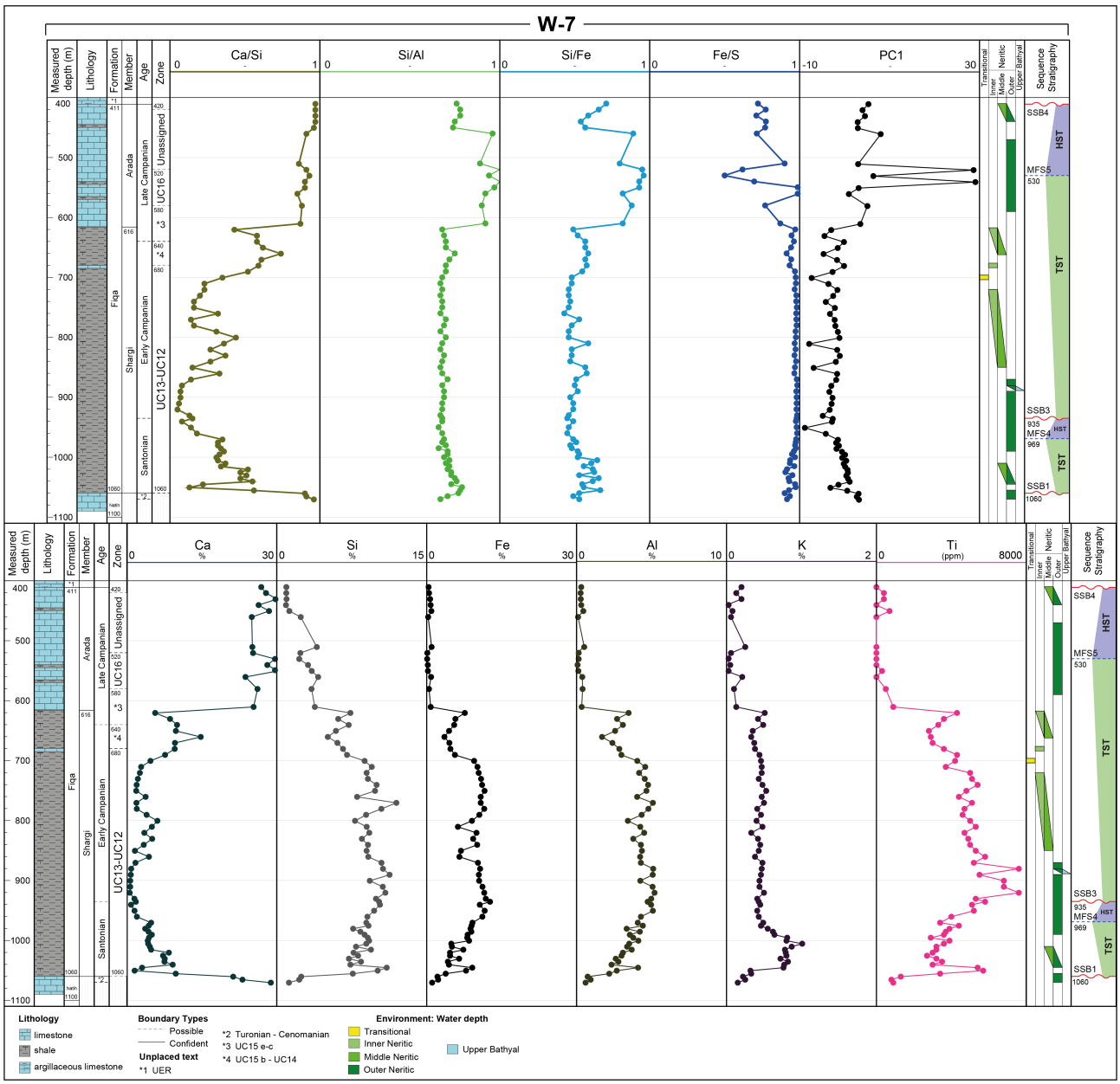

Figure 6. Elements concentration and ratios of W-7.

wells which are dominated by carbonates, W-9 and W-10, the ratio is generally higher but follow similar trend as the northern wells with lower values in the Shargi Member and higher values in the Arada Member (Fig. 7). W-11 shows highly variable ratio which might reflect the interbedded shale and carbonate units (Fig. 7). Laterally, the Ca/Si ratio decreases from the south to the north. Peaks of Ca/Si are seen in the carbonate rich horizons in the south (Fig. 7). The ratios of Si/Al and Si/Fe are used as weathering proxies and to reflect grain size and sediments maturity. Si/Al is assumed to represent quartz-rich (coarse fraction) to clay-rich (fine fraction) sediments in fine grained siliciclastic rocks (Calvert and Pedersen, 2007). The Si/Al ratio is generally high and very constant

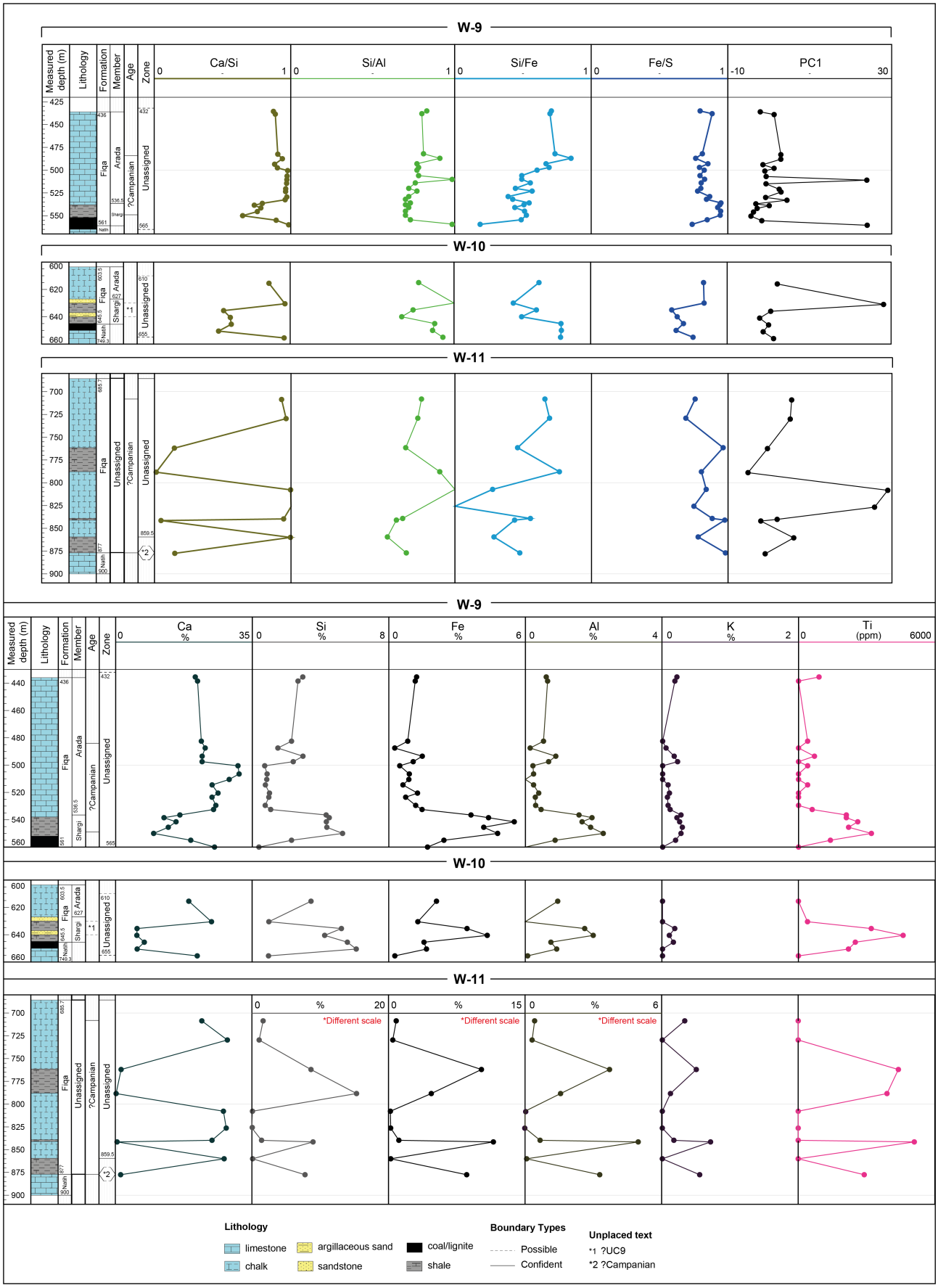

Figure 7. Elements concentration and ratios of the southern wells.

in W-4 with higher values at the lowermost part of the Shargi Member and a gradual increase toward the Arada Member (Fig. 5). In W-7, the Si/Al is more constant in the Shargi Member, but with a marked increase in the Arada Member (Fig. 6). Si/Fe has a very similar trend to Si/Al in both W-4 and W-7 but with more significant increase into the Arada Member in W-7 (Figs. 5, 6). In W-9 and W-10, both Si/Al and Si/Fe are generally high with gradual increase into the Arada Member (Fig. 7). The Si/Al and Si/Fe ratios are more fluctuating in W-11 (Fig. 7). Lower values of the Fe/S ratio can be used as an indicator of reducing conditions and presence of pyrite rich horizons (Calvert and Pedersen, 2007), but is generally high in all wells with minor reduction toward the uppermost Shargi and throughout the Arada Member which might reflect a reduction in Fe associated with increased carbonates rather than an increase in the amount of sulphur (pyrite). Element concentrations of Si, Al, Ti, Fe, K are used here as indicator of terrestrial input and all show similar trends in all wells except for W-11 where there is more variability. These elements tend to show higher concentrations throughout the Shargi Member, with minor fluctuations, but then sharply decrease toward the Arada Member.

4.3 Principal Component Analysis

4.3.1 Statical Analysis of XRF Data

Principal component analysis is undertaken for the elemental data available for W-4, W-7, W-9, W-10 and W-11. This analysis is a method of data reduction allowing the projection of a multivariate dataset down to a few dimensions in a way that preserves as much variance as possible and facilitates data visualisation (Hammer and Harper, 2006). The selected, most common elements, are listed in Table 1. The majority of the variance is represented in principal component factor 1, PC1 (~46%) and principal component factor 2, PC2 (~19%), with the remaining principal components (Table 2) not considered further. PC1 and PC2 loadings for each element - which

Table 1. List of elements included in the PC analysis.

Aluminum (Al)
Calcium (Ca)
Iron (Fe)
Potassium (K)
Magnesium (Mg)
Sulfur (S)
Silicon (Si)
Strontium (Sr)
Titanium (Ti)
Chlorine (Cl)
Sodium (Na)

Table 2. PCA results.

PC	Eigenvalue	% variance
1	34.88	45.82
2	14.78	19.42
3	10.83	14.23
4	8.13	10.68
5	3.81	5.00
6	1.86	2.44
7	0.77	1.01
8	0.56	0.74
9	0.31	0.41
10	0.18	0.24

Table 3. PC1 and PC2 loadings.

Variables	PC 1	PC 2
Ca	0.462	-0.278
Cl	0.489	0.349
Fe	0.243	-0.072
K	0.092	0.071
Mg	0.348	-0.144
Na	0.211	0.791
S	0.313	-0.164
Si	0.231	-0.039
Sr	0.403	-0.209
Ti	-0.012	0.269

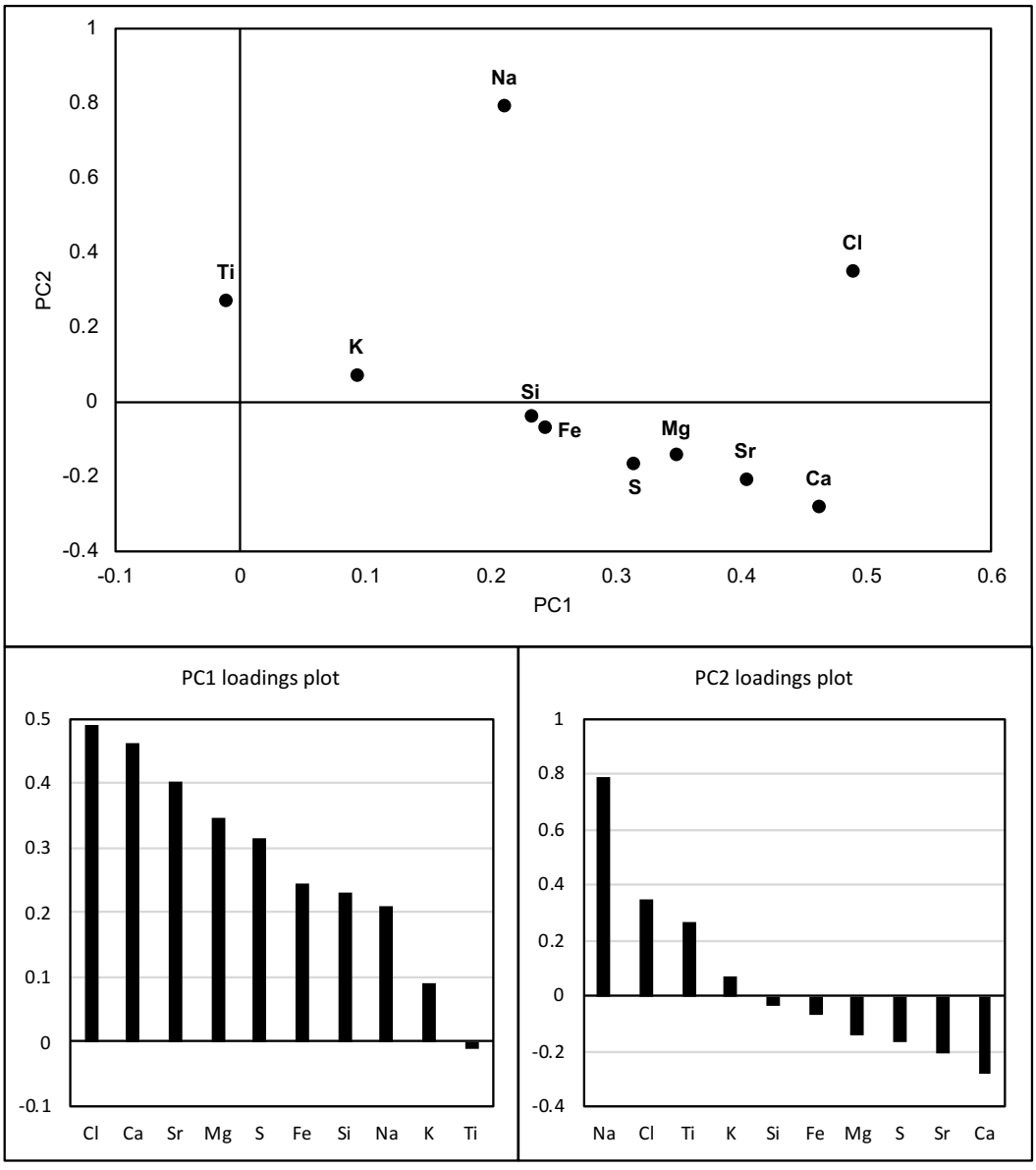

Figure 8. PC1 vs PC2 plot of element data for all wells with loading plots.

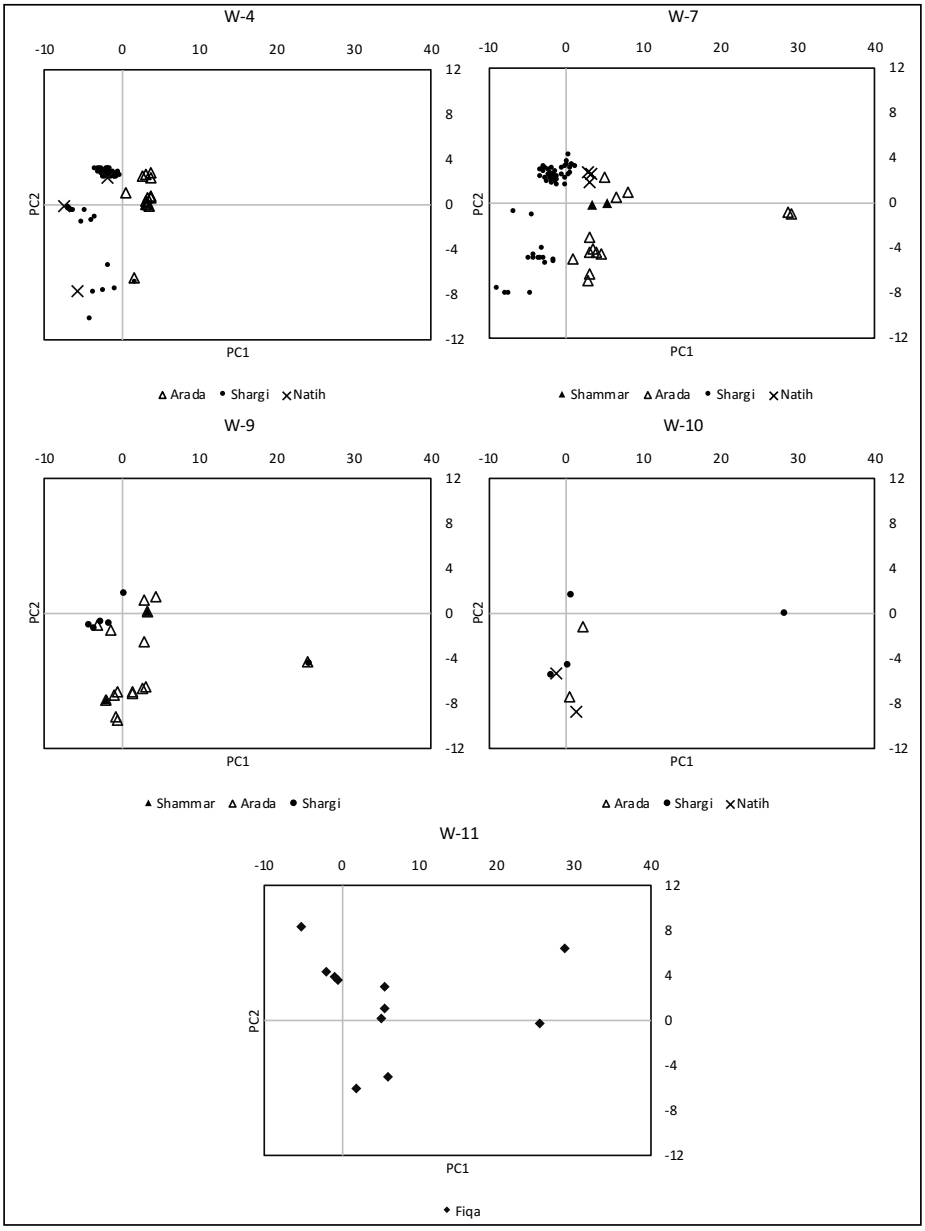

Figure 9. PC1 vs PC2 plots of element data.

represent how much each variable (element) contributes to each principal component - are listed in Table 3 and plotted in Figures 8 and 9. The most significant loadings on PC1 are on Cl and Ca (~0.5 loading value), with high positive loadings also shown by Sr (0.40), Mg (0.35) and S (0.31). Fe, Si and Na show similar loading values of ~ 0.2, while K has much lower loading value (0.092). Only Ti shows a negative loading on PC1 of -0.02. PC2 is characterised by high positive loading values on Na (~0.79), whilst Cl and Ti both have positive loading values of ~0.3. At the other extreme, PC2 has highest negative loadings on Ca, Sr, S and Mg. PC1 seems to follow lithological variations

within the Formation, the shale lithology of Shargi Member is characterised by more negative PC1 values while the carbonate lithology of the Arada Member show more positive PC1 values (Fig. 9). PC2 seems to be picking up compositional variations within the lithologies as both the Arada and Shargi samples are distributed a long broad positive and negative values of PC2 (Fig. 9).

4.3.2 Statistical Analysis of Nannofossil Assemblages

Calcareous nannofossil assemblages data from wells across the basin show assemblage changes both through time and across the basin. To understand these changes, and provide an accessible summary analysis of assemblage data from several hundred samples across 11 well successions, a standard multivariate PCA is undertaken. PCA is applied to selected samples from eight wells - W-1, W-2, W-3, W-4, W-5, W-6, W-7 and W-8 - which have good nannofossil recovery and preservation, while W-9, W-10 and W-11 are excluded as they yield scarce or are barren of nannofossils (Al Rawahi and Dunkley Jones, 2019a; see Chapter 2; Al Rawahi and Dunkley Jones, 2019b in review; see Chapter 3). The selected wells are distributed across the basin and across palaeo-bathymetric gradients. To improve the power of this analysis, only the most common nannofossil taxa are included in the analysis, either at species or generic level, or are grouped by morphotype (holococcoliths) (Table 4). Most of the variance (~47%) within the assemblage data is represented by PC1, and this will be the main focus of discussion. The rest of the principal components are listed in Table 5. PC1 and PC2 loadings - which represent how much each variable (nannofossil taxon) contributes to each principal component - are listed in Table 6 and plotted in Figures 10 and 11. All variables included in the analysis show positive loadings on PC1, with the most significant loadings on *Corollithion signum* (0.32), *Discorhabdus ignotus* (0.30), *Zeugrhabdotus erectus* (0.26), *Lithraphidites carniolensis* (0.26) and *Micula staurophora* (0.25). The least significant value related to PC1 is represented by *Watznaueria barnesae* (0.08). Wells in the deeper northern basin show more tightly clustered PC1 and PC2 scores (W-1, W-3, W-4 and

W-5), whilst wells in the shallower southern parts of the basin show significantly more scatter to both extremes of the PC1 axis - especially W-6, W-7 and W-8 - and in W-7 appears to follow the lithological differentiation between the Arada carbonates and Shargi shales, which supports a paleobathymetric influence on PC1.

Table 4. List of species and genera included in the PC analysis.

Ahmuellerella regularis
Biscutum constans
Broinsonia
Calculites obscurus
Chiastozygus
Corollithion signum
Cribrosphaerella ehrenbergii
Discorhabdus ignotus
Eiffellithus except *E. eximius*
Eiffellithus eximius
Holococcoliths
Lithraphidites carniolensis
Micula staurophora
Prediscosphaera cretacea
Prediscosphaera except *P. cretacea*
Retacapsa
Staurolithites
Tranolithus minimus
Tranolithus orionatus
Watznaueria barnesae
Zeugrhabdotus erectus
Zeugrhabdotus except *Z. erectus*

Table 5. PCA results.

PC	Eigenvalue	% variance
1	183.15	47.04
2	25.09	6.45
3	20.10	5.16
4	18.97	4.87
5	18.07	4.64
6	16.19	4.16
7	13.88	3.56
8	12.44	3.19
9	11.84	3.04
10	10.51	2.70
11	9.96	2.56
12	8.75	2.25
13	7.26	1.87
14	6.77	1.74
15	5.85	1.50
16	5.26	1.35
17	4.07	1.04
18	3.63	0.93
19	2.82	0.72
20	2.56	0.66
21	2.14	0.55

Table 6. PC1 and PC2 loadings.

Variables	**PC 1**	**PC 2**
Ahmuellerella regularis	0.228	-0.401
Biscutum constans	0.235	-0.060
Broinsonia	0.207	0.210
Calculites obscurus	0.241	0.148
Chiastozygus	0.200	0.176
Corollithion signum	0.316	0.288
Discorhabdus ignotus	0.296	0.046
Eiffellithus	0.166	0.124
Eiffellithus eximius	0.184	0.302
Holococcoliths	0.239	0.045
Lithraphidites carniolensis	0.259	-0.326
Micula staurophora	0.249	0.242
Prediscosphaera cretacea	0.179	0.121
Prediscosphaera	0.164	-0.117
Retacapsa	0.121	0.112
Staurolithites	0.235	-0.264
Tranolithus minimus	0.222	-0.340
Tranolithus orionatus	0.194	0.215
Watznaueria barnesae	0.084	0.013
Zeugrhabdotus erectus	0.259	-0.311
Zeugrhabdotus	0.163	-0.101

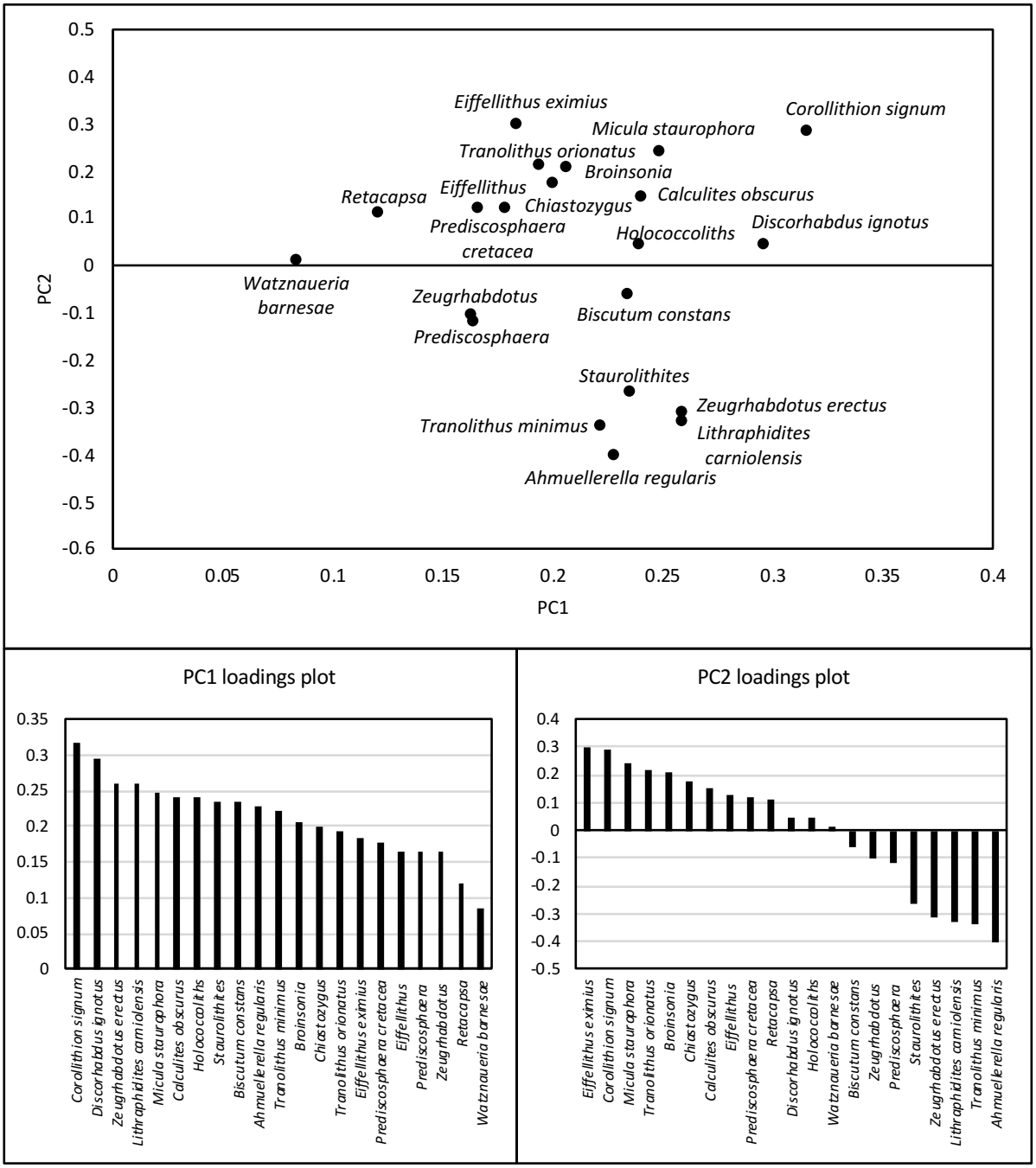

Figure 10. PC1 vs PC2 plot of nannofossil assemblages for all wells with loading plots.

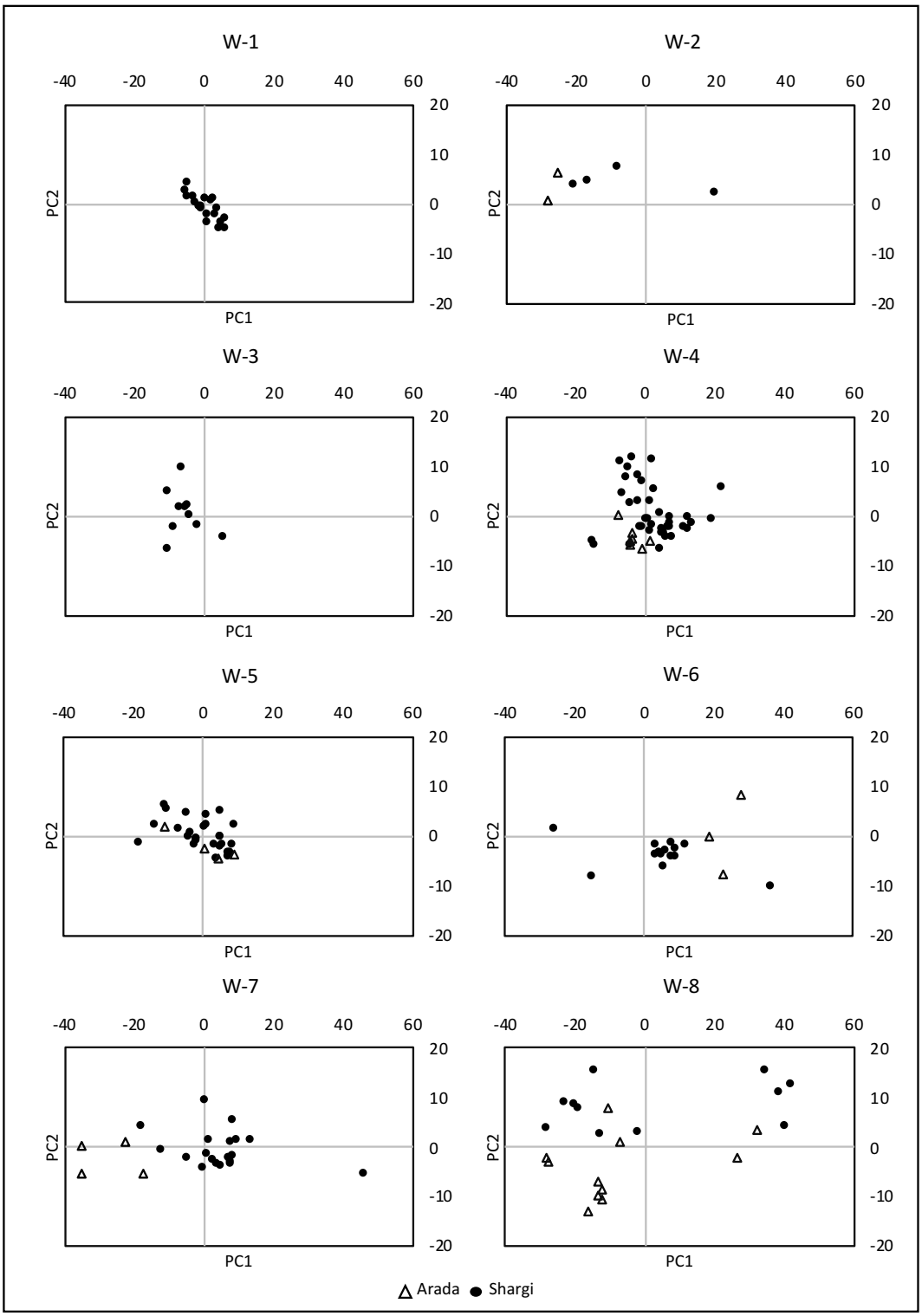

Figure 11. PC1 vs PC2 plots of nannofossil assemblages.

5 Discussion

5.1 Carbon isotope stratigraphy

The few samples analysed from the top of the Natih Formation in W-4, W-7 and W-10, have relatively high $\delta^{13}C$ values (~2.5‰) (Figs. 4, 12), comparable to the outcrop and subsurface samples of Wohlwend et al. (2016) who correlate these values with the globally recognised mid-Turonian positive $\delta^{13}C$ Tu10 Event of Voigt et al. (2007). The regional unconformity between the Natih and Fiqa Formation represents a depositional gap of ~ 2-3 Ma (Forbes et al., 2010), with the oldest, upper Coniacian, basal Fiqa sediments recorded in W-4 (Al Rawahi and Dunkley Jones, 2019b in review; see Chapter 3). Bulk carbonate $\delta^{13}C$ values within these upper Coniacian to lower Santonian sediments are relatively stable, around ~ 0.65‰, with a gradual shift toward lighter values up section (Fig. 12). This is similar to the trends in the $\delta^{13}C$ reference curves of the Tethyan Shahneshin section of Iran (Razmjooei et al., 2018), the Boreal English Chalk (Jarvis et al., 2006) and the Western Interior basin (Joo and Sageman, 2014).

Both wells W-4 and W-7 contain the Santonian-Campanian transition, identified by the top of planktonic foraminifera *Dicarinella asymetrica* (Santonian), the top of nannofossil *Helicolithus blairiae* (?Santonian) and base of nannofossil *Broinsonia verecundia* (earliest Campanian) (Al Rawahi and Dunkley Jones, 2019b in review; see Chapter 3). Although the Campanian-Santonian transition is globally associated with a positive $\delta^{13}C$ excursion of ~1.5-2.5‰ values, known as the SCBE (Fig. 1) (e.g. Jarvis et al., 2006; Joo and Sageman, 2014; Thibault et al., 2016; Farouk et al., 2018a,b; Razmjooei et al. 2018, Wolfgring et al., 2018), in the Fiqa Formation, $\delta^{13}C$ values remain similar to those of the Santonian and Coniacian around ~0.6‰. This is followed by a major negative excursion with high negative values down to -4‰, starting within lower part of the lower Campanian in W-4 and upper part of the upper Santonian in W-7 (Fig. 12). This distinctive event

starts around 1204 m in W-4 and 990 m in W-7, which is in close proximity to top nannofossil event *Helicolithus blairiae* at depths 1254.3 m and 970 m respectively (Fig. 12). This negative $\delta^{13}C$ excursion event is not recognised in $\delta^{13}C$ curves from other basins (Fig. 1) (Wendler, 2013), but its presence at the same biostratigraphic level in both W-4 and W-7, which are separated by ~ 100 km, implies a basin-wide perturbation to local carbon cycling. In both wells, this event occurs during a period of shallowing relative sea level - from upper-middle bathyal to middle-outer neritic in W-4 and from outer to inner-middle neritic settings in W-7 - and the development of a sequence stratigraphic boundary (SSB3 of Al Rawahi and Dunkley Jones, 2019b in review; see Chapter 3) followed by reduced nannofossil abundance in W-4 and W-7 (Fig. 12). A distinctive influx of radiolaria is associated with this interval in both wells, but is more pronounced in the deeper W-4 where it spans much of the negative $\delta^{13}C$ excursion (Fig. 12). Within bulk sediment XRF data, increased concentrations of Ti, Fe and Al in both wells (Figs. 5, 6), also indicate an increased input of terrestrial sediments at the onset of this negative shift. In a regional context, an integrated geological, seismic and biostratigraphic study (Filbrandt et al. 2004), found evidence for a major and sudden influx of sediment from the rising eastern Huqf source area (see Fig. 2 for location of Huqf area) starting in the early Campanian. This change is thought to have been driven by the blockage of sediment pathways toward the Tethys Ocean (see Fig. 2 for sediment route to open ocean) by tectonics associated with the obduction of ophiolitic rocks to the east of Oman (Masirah Ophiolite) (Filbrandt et al. 2004). W-7 is located in a more proximal setting - and it is closer to the Huqf source area (Fig. 2) - compared to the basinal setting of W-4 during upper Santonian and lower Campanian intervals (see Fig. 7 in Al Rawahi and Dunkley Jones, 2019b in review; Chapter 3), which might explain the earlier occurrence of the negative $\delta^{13}C$ excursion event in W-7.

The diversion of sediment into the Aruma Basin resulted in high sediment accumulation rates and rapid filling of the northern parts of the basin. The new identification of a regional negative $\delta^{13}C$

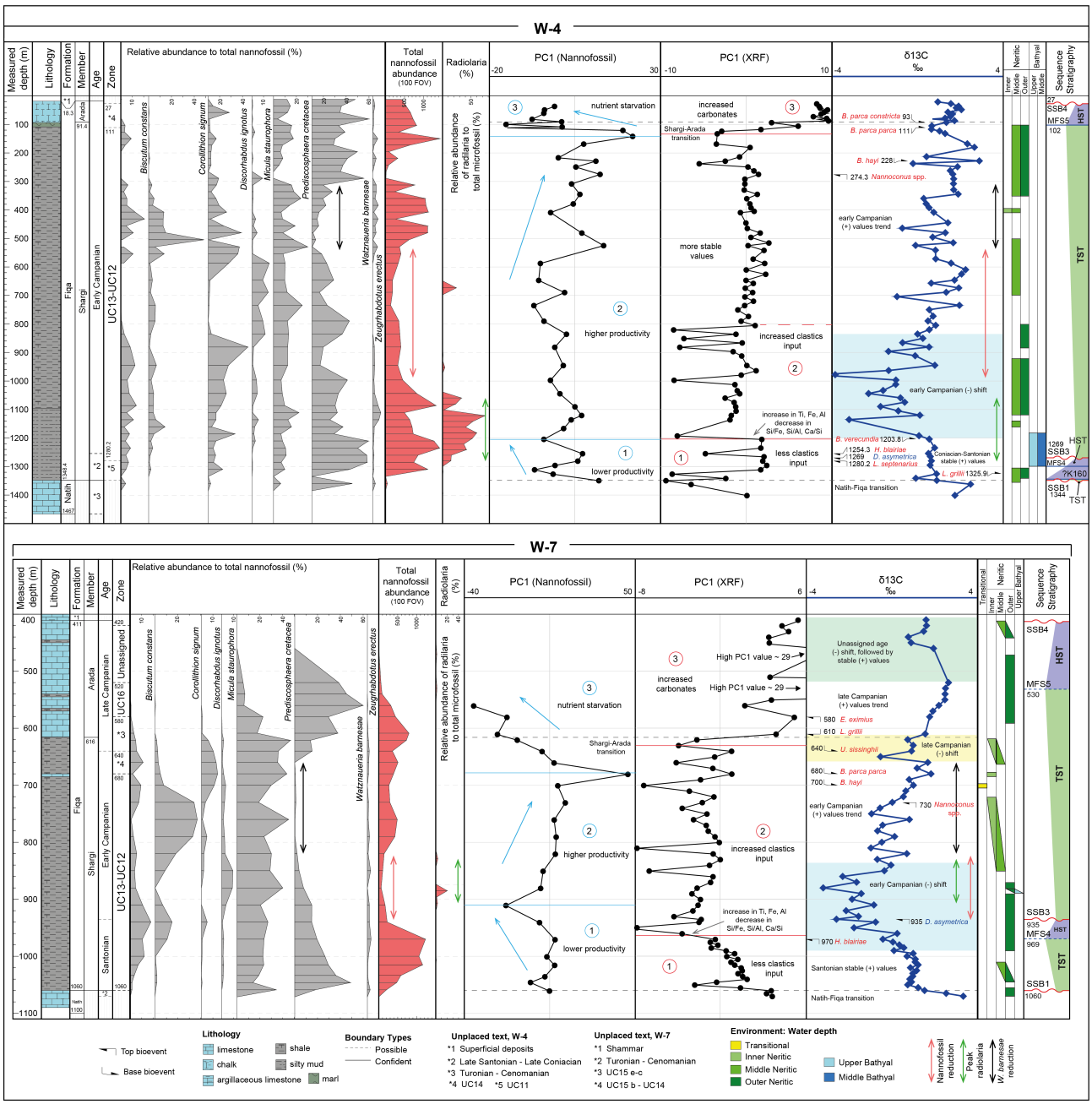

Figure 12. Summary of nannofossil assemblage changes and associated changes in $\delta^{13}C$ curve and element data in W-4 and W-7.

excursion within the Aruma Basin at this time, coupled with direct evidence for changes in sediment composition (Ti, Al, Fe) and plankton communities (radiolaria influx), indicates some degree of basin restriction - $\delta^{13}C$ divergence from global patterns - and increased sediment and nutrient flux.

The negative excursion event is followed by a general long term increase in $\delta^{13}C$ values through the remainder of the early Campanian as seen in W-4 and W-7 (Fig. 12) that is similar to the global $\delta^{13}C$ tends (Fig. 1) (Wendler, 2013). This increasing trend of $\delta^{13}C$ values, with a return towards values

consistent with the global ocean, is consistent with increasing sea level and basin-ocean connections, within a transgressive sequence tract (TST), toward maximum flooding surface (MFS5), and subsequent highstand sequence tract (HST) (Al Rawahi and Dunkley Jones, 2019b in review; see Chapter 3) (Fig. 12).

A second distinctive negative shift is recognised in W-7 at the base of late Campanian with $\delta^{13}C$ values ranging from 1 to -0.53‰ within the interval of 650 to 620 m (Fig. 12). This event is similar to the globally recognised late Campanian event ("LCE"; Fig. 1) which is characterised by a distinct negative excursion with a magnitude of 0.5–1‰, and is considered useful for global correlation, especially in the southern Tethys area (Wendler, 2013). This negative excursion event is followed by a long term increase into maximum recorded values of $\delta^{13}C$ throughout the late Campanian within a HST prior to the regional unconformity at the top of the Fiqa Formation (SSB4 of Al Rawahi and Dunkley Jones, 2019b in review; see Chapter 3) (Fig. 12).

5.2 Reconstructing Spatial and Temporal Palaeoenvironmental Change in the Aruma Basin

Nannofossil assemblages within the Fiqa Formation show distinctive variations through time, which have been associated with sea level and changing productivity (Al Rawahi and Dunkley Jones, 2019a; b in review) (see Chapters 2 and 3). One of the strongest assemblage changes within the Fiqa Formation is an interval of very low *Watznaueria barnesiae* abundances within the lower Campanian of W-4 (Al Rawahi and Dunkley Jones, 2019a) (see Chapter 2). Sediments through this interval contain well-preserved and abundant nannofossil assemblages including elevated abundances of high fertility-related taxa of *Biscutum constans* and *Zeugrhabdotus erectus* with peaks of *Discorhabdus ignotus* and *Corollithion signum* and a high abundance of *Prediscosphaera cretacea*. These variations have been linked to regressive episodes with increased nutrient supply (Al Rawahi and Dunkley Jones, 2019a; see Chapter 2). Here, these observations are extended

beyond a single well, to multiple spatially distributed locations, and are integrated with other environmental proxy data, including carbon isotope and bulk sediment compositions, in order to better understand the palaeoenvironmental evolution of the Aruma Basin.

5.2.1 Temporal Palaeoenvironment Change

The good stratigraphic coverage through W-4 and W-7 allows for an integrated assessment of trends in nannofossil assemblages, sediment compositions and carbon isotope through time. Changes in the nannofossil assemblage are highly related to changes in bulk sediment composition of the Fiqa Formation. Sediment composition is best represented by $PC1_X$ (PC1 of XRF data) which largely reflects the relative dominance of carbonate (higher $PC1_X$ values; Ca, Sr, Mg elements) versus siliciclastic (lower $PC1_X$ values; Si, Al, Na, K, Ti elements) lithologies (Fig. 8). For example, in W-4 and W-7, $PC1_X$ is positive within the Arada carbonates and more negative in the Shargi shales (Fig. 9). On the other hand, highest $PC1_N$ (PC1 of nannofossil assemblage data) loadings are related to high fertility taxa including *Corollithion signum*, *Discorhabdus ignotus* and *Zeugrhabdotus erectus,* whilst *Watznaueria barnesiae* has the lowest $PC1_N$ loading (see Al Rawahi and Dunkley Jones (2019a) (Chapter 2) and references therein for detailed discussion of environmental affinities of these species). Throughout W-4 and W-7, $PC1_N$ follows an opposite trend to $PC1_X$, i.e. intervals of increased clastic input (decreased PC1x) correlate to nannofossil indices of higher nutrient status (increased $PC1_N$). Based on these PC analyses, three main intervals can be identified in W-4 and W-7 and are shown on Figure 12.

Interval 1: the lower Fiqa Formation (Coniacian-Santonian and lowermost part of the early Campanian), deposited within a TST and HST at the base of the wells, is characterised by relatively lower clastic input (higher $PC1_X$) and lower nutrient status (lower $PC1_N$). The glauconite marker bed which indicates low rates of deposition toward the base of the Fiqa Formation (Al Rawahi and Dunkley Jones, 2019b in review; see Chapter 3) occurs within this interval in W-4. However, in the

lowermost part of Interval 1, there is relatively higher amount of terrestrial input reflected in $PC1_X$ curve - small peaks in Ti, Fe, Al, Si and K curves (Figs. 5, 6) - following the Wasia-Aruma break erosional surface (SSB1 of Al Rawahi and Dunkley Jones, 2019b in review; see Chapter 3) (Fig. 12).

Interval 2: this interval (early Campanian) is the thickest, deposited within a transgressive sequence tract following shallowing of sea level and the development of a local erosional surface (SSB3 of Al Rawahi and Dunkley Jones, 2019b in review; see Chapter 3) at the transition between the claystone-dominated lower parts of the Shargi Member to the sandier shales of the upper parts of this member (Al Rawahi and Dunkley Jones, 2019b in review; see Chapter 3). Interval 2 has elevated clastic input (negative shift in $PC1_X$) and higher nutrient status (increased $PC1_N$) throughout (Fig. 12). In W-4, this interval is characterised by a lower, more variable $PC1_X$ values and an upper, more stable $PC1_X$ values (Fig. 12) which might reflect the suggested shift to a balance between sediment supply and a steady sea level rise during the deposition of the thick shale units of the upper part of Shargi Member (Filbrandnt et al., 2004; Al Rawahi and Dunkley Jones, 2019b in review; see Chapter 3). The early Campanian negative $\delta^{13}C$ excursion event which has been related to a period of increased sediment influx into the basin, as shown in element concentration curves, nannofossil and microfossil assemblages (Sect. 5.1) is recorded at the lower part of this interval (Fig. 12). This negative excursion event marks the start of a change in the nannofossil assemblages with an increase in *Micula staurophora* recorded in both wells followed by a gradual reduction in *Watznaueria barnesiae* consistent with a transition to higher productivity taxa. All of the species noted above also show variations in relative abundance during the early Campanian negative $\delta^{13}C$ excursion event. This interval of reduction in *Watznaueria barnesiae* relative abundance coupled with an increase in *Corollithion signum* with or without an increase in *Biscutum constans*, *Discorhabdus ignotus* and *Zeugrhabdotus erectus* associated with a positive shift in $PC1_N$ curve is

also recorded in lower Campanian intervals within W-5 (dominated by outer neritic settings), W-6, W-7 (dominated by middle-outer neritic settings) and lower to upper Campanian intervals in W-8 (Figs. 13, 14). In W-4, microfossil association data from within this interval indicate a shallower shelf environment, which is consistent with the presence of nearshore and continental margin nannofossil taxa (e.g. *Broinsonia* spp., *Nannoconus* spp. and *Braarudosphaera* spp.) (Al Rawahi and Dunkley Jones, 2019a; see Chapter 2). Together these variations have been linked to regressive episodes with increased nutrient supply, which is now supported by the PCA, carbon isotope and elemental concentration data.

Interval 3: toward the top of the Fiqa Formation (lower-upper Campanian), a gradual increase into the most carbonate-rich / clastic-poor intervals (highest positive values of $PC1_X$), associated with lower nutrient status nannofossil assemblages (negative shift in $PC1_N$). The abundance of nannofossils starts to drop within these shallower marine facies (Fig. 12).

5.2.2 Spatial Variability in Palaeoenvironments

A comparison of $PC1_N$ vs $PC2_N$ values between wells across the basin (Fig. 11) also reveal a spatial variability in nannofossil assemblages. In wells W-1 and W-3, which are located in the deepest part of the basin (Fig. 1), $PC1_N$ stays tightly clustered with a limited range of $PC1_N$ values (Fig. 11). The *Watznaueria barnesiae* reduction interval is not recorded in these wells (Fig. 13), which are dominated by bathyal settings and where nannofossil abundances are generally high, and assemblages appear to be less affected by sea level or nutrient dynamics of the basin compared to wells towards the margins of the basin. The intervals recovered and studied from W-1 and W-3 are, however, shorter than other study wells (Fig. 13), which may contribute to some of the clustering of $PC1_N$ values. In contrast, W-2, W-4, W-5, W-6, W-7 and W-8 have a greater range in $PC1_N$ with high positive and negative values (Fig. 11). Well W-2 is located on the northern margin of the basin (Fig. 2) with significant input of coarse-grained clastic material (lithology log, Fig. 13), a limited

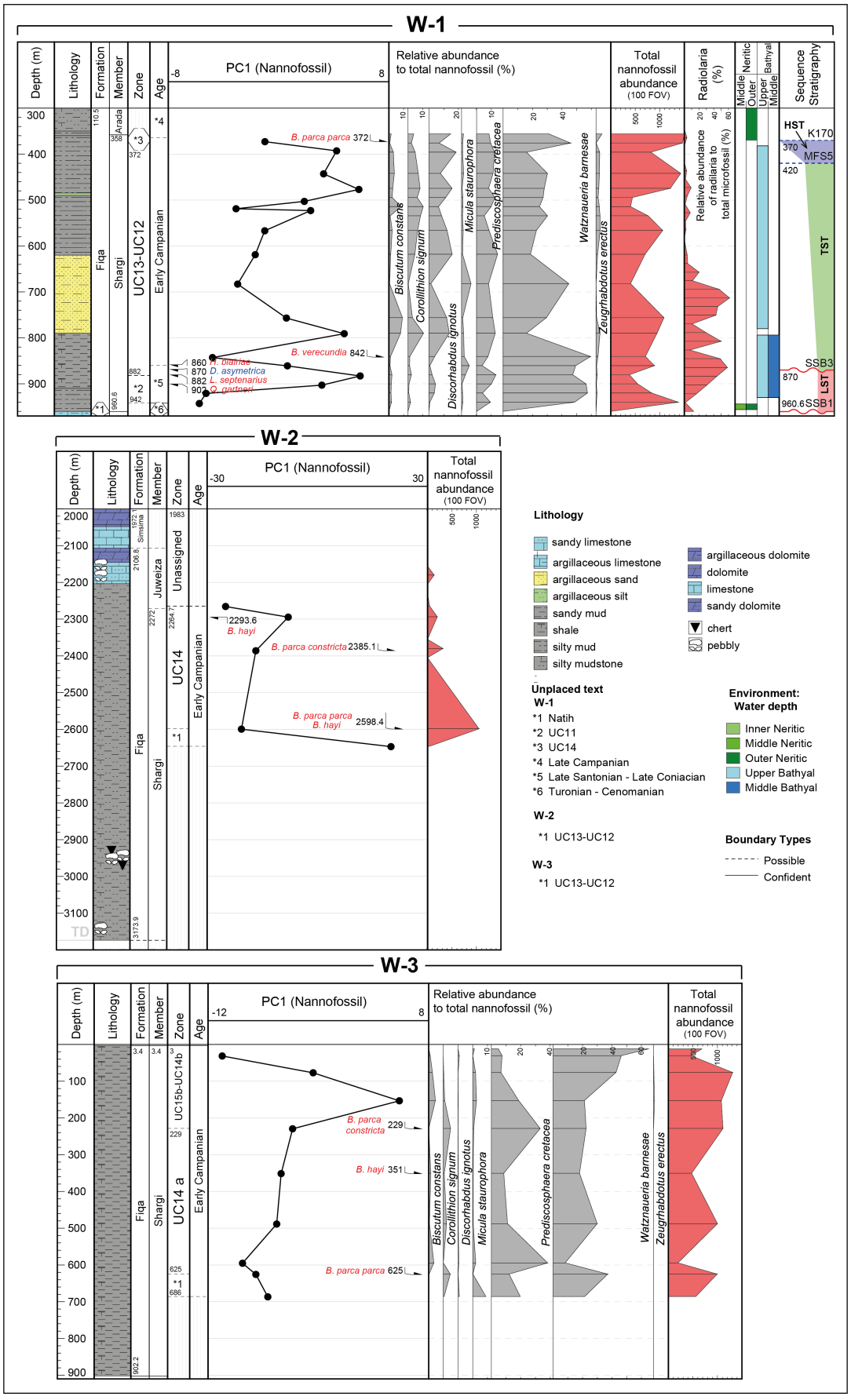

Figure 13. Nannofossil assemblage changes and associated changes in $PC1_N$ curve.

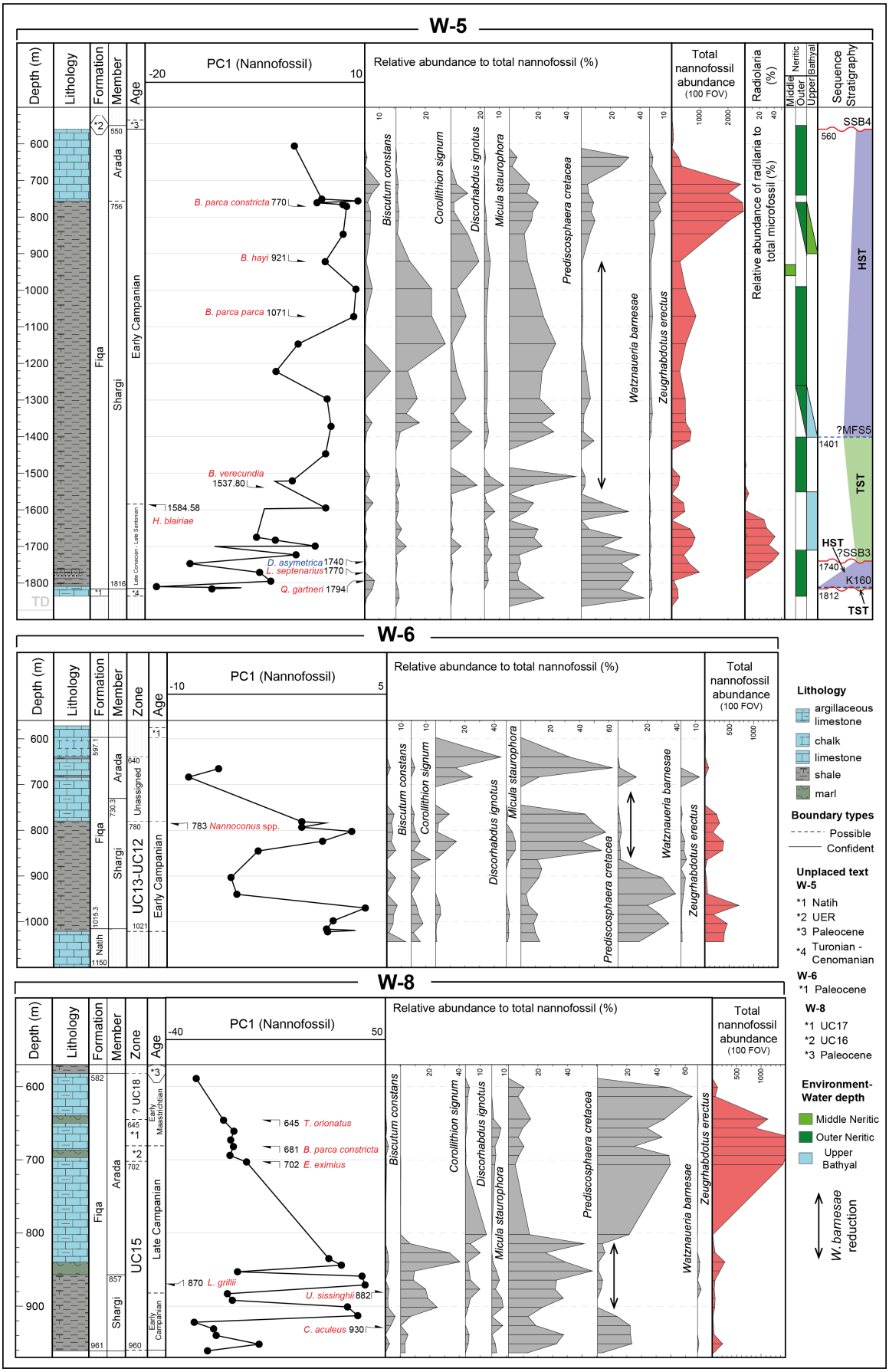

Figure 14. Nannofossil assemblage changes and associated changes in $PC1_N$ curve.

number of samples and these with low nannofossil recovery. The greater range in W-2 $PC1_N$ values might thus reflect lithological controls on nannofossil recovery rather than a primary environmental signal. The nannofossil assemblages in W-4, W-5, W-6, W-7 and W-8 are highly variable with the *Watznaueria barnesiae* reduction interval recorded in all wells (Figs. 12, 14). These wells recover intervals with greater facies variations and more significant variability in nannofossil assemblages. Lithologies from the southern wells - W-9, W-10 and W-11 - are clearly more carbonate-rich, with higher positive values of $PC1_X$, which peaks around carbonate horizons (Fig. 7), reflecting the dominance of shallower marine environments. The samples analysed from these wells are very scarce in or barren of nannofossils (Al Rawahi and Dunkley Jones, 2019b in review; see Chapter 3).

5.2.3 Tectonic Drivers of Palaeoenvironmental Change

The Aruma basin was highly dynamic, affected by several tectonic events throughout the Late Cretaceous which in turn affected sedimentation rate in response to uplift and erosion (e.g. Glennie et al., 1974; Lippard et al., 1986; Boote et al., 1990; Forbes et al., 2010; Filbrandt et al., 2004). The basin was also located at a tropical palaeolatitude (van Hinsbergen et al., 2015; Al Rawahi and Dunkley Jones, 2019a) (see Chapter 2) which might have contributed to the severity of weathering and runoff into the basin. The relatively higher amount of terrestrial input in the lowermost Coniacian-Santonian intervals of the Fiqa Formation (Interval 1; Fig. 12), in W-4 and W-7 might be reflecting the rapid subsidence and deposition at the earliest stages of the basin formation, previously suggested from seismic data (e.g. Boote et al., 1990). Microfossil associations data (Packer, 2002) along with seismic evidences (Filbrandnt et al., 2004) indicated a dominance of inner to middle neritic depositional environment during the Coniacian-lower Santonian within the early stages of the foreland basin development (see Fig. 7 in Al Rawahi and Dunkley Jones, 2019b in review; Chapter 3). By the end of the Santonian, the basin deepened rapidly (palaeobathymetric analysis, Frost et al., 1980 in Boote et al., 1990) and an outer neritic to upper bathyal depositional

settings developed with rapid rates of sediment deposition (thick sequences of Interval 2; Fig. 12) during most of the Santonian and continued to middle Campanian (Packer, 2002). The developed deeper marine settings during this time interval were, however, interrupted by several regression episodes (Filbrandnt et al., 2004). The major influx of sediments into the basin began in the early Campanian as a result of local tectonics and subsequent closure of pathways to the Tethys ocean (Sect. 5.1). This is reflected in the major $\delta^{13}C$ negative excursion event recorded in W-4 and W-7 and associated reduction of nannofossil assemblages, influx of radiolaria, as well as the negative shift in $PC1_X$ curve (Fig. 12), suggesting some degree of basin restriction. This is followed by a gradual shift to the *Watznaueria barnesiae* reduction interval within elevated productivity conditions in the early Campanian in W-4, W-5, W-6, W-7, and within early-late Campanian further to the south in W-8 (Figs. 12, 13, 14). Nannofossil assemblages in these wells (W-4, W-5, W-6, W-7, W-8) show significant response to the changing sea level and nutrient status through time compared to the wells in the deepest part of the basin (W-1, W-3) that seem to be less affected by basin dynamics as reflected in the limited range of $PC1_N$ values and less variable nannofossil assemblage composition (Sect. 5.2.2).

The amount of clastic input into the basin remains high throughout the Shargi Member of all wells. The concentration of terrestrial elements (e.g. Ti, Fe, Al, Si and K) is, however, much higher in the northern wells compared to the shallower wells to the south (Figs. 5, 6, 7), most likely reflecting sediment sources from Huqf area (predominantly Precambrian and Carboniferous sands and orthoquartzites detritus) to the east and the rising ophiolite to the north (igneous and metamorphic detritus) (Higgins and Howarth, 1997b) (see Fig. 2). Although the shallower marine settings in the south of the basin were far from these sediment sources, the variations in weathering indicators in W-9 and W-10 (e.g. Si/Fe; Fig. 7) also indicate a terrestrial influence, most likely from the southern margin of the basin. The highly fluctuating elemental profiles, characteristic of carbonates versus

clastic-dominated deposits and weathering ratios in W-11 (Fig. 7) might indicate a transitional environment at the southwestern margin of the basin (Fig. 2). Weathering ratios, for instance Si/Fe, show a prominent increase in all analysed wells toward the Arada Member, which might indicate a greater influence of sediments sourced from the rising ophiolite in the latest stages of the Fiqa Formation deposition (Figs. 5, 6, 7) in agreement with the findings of Higgins and Howarth (1997b).

The Arada Member, marks the transition into shallow marine environment developing over most of Oman (Packer, 2002) with lower nutrient status and general reduction of nannofossils (Interval 3; Fig. 12) toward the end of ophiolite obduction and Fiqa Formation deposition.

7 Conclusions

The integration of geochemical data with the existing nannofossil biostratigraphic and assemblage data from samples across proximal and distal parts of the Late Cretaceous Aruma basin of Oman provided new constrains on the stratigraphy and palaeoenvironmemt of the Fiqa Formation. A detailed late Coniacian to late Campanian $\delta^{13}C$ curve is established that is tied to the biostratigraphic zones and correlated to regional and global curves providing valuable insights into the depositional settings of the basin. The late Coniacian to early Santonian $\delta^{13}C$ curve is characterised by stable positive values that are gradually shifted toward lighter values similar to Tethyan and global curves. Unlike the positive excursion event in global curves, the $\delta^{13}C$ values at the Campanian-Santonian transition in the Fiqa Formation remain similar to the underlying sections. The recognised $\delta^{13}C$ events are consistent with the sequence stratigraphy and sea level variations within the basin. A pronounced major negative $\delta^{13}C$ excursion within upper part of late Santonian / lower part of the early Campanian is observed and linked to local basinal shifts associated with local environmental factors particularly a sea level fall and the consequent

development of a sequence stratigraphic boundary. This event is linked to increased sediment and nutrient influx into the basin based on evidences from changes in terrestrial elemental composition (increased Ti, Al, Fe) and plankton communities (radiolaria influx) and has been associated with local tectonics and the beginning of basin restriction. This negative excursion event is followed by a general long term increase in $\delta^{13}C$ values throughout the early Campanian and late Campanian except for a negative shift event at the base of late Campanian, a trend that is very consistent with local and global curves. This new, biostratigraphically-constrained $\delta^{13}C$ curve can work as a reference point for Oman and nearby areas. Throughout the Fiqa Formation, nannofossil assemblages show distinctive variations through time and a cross the basin based on analysis from several, spatially distributed locations. The dominant assemblage change through the Fiqa Formation is an interval of low *Watznaueria barnesiae* relative abundance coupled with an increase in *Corollithion signum* with or without an increase in *Biscutum constans*, *Discorhabdus ignotus* and *Zeugrhabdotus erectus* recorded within neretic settings in five, proximal and distal wells during early (distal wells) to late (proximal well) Campanian. This change is not recorded in deeper parts of the basin that seem to be less affected by the changing sea level and nutrient dynamics and, through integration with existing sequence stratigraphic data and other environmental proxy data, is interpreted to represent a regressive phase with increased nutrient and sediment influx to the basin.

CHAPTER 5

CONCLUSIONS

5.1 Conclusions

This study provided the first detailed overview of calcareous nannofossil taxonomy and biostratigraphy as well as inorganic geochemistry, throughout the Coniacian-Maastrichtian Fiqa Formation, deposited in the Aruma foreland basin of Oman. A total of 657 nanno-palaeontological and geochemical analyses were undertaken on 341 subsurface samples from 11 hydrocarbon exploration wells, integrated with existing analyses of microfossil data from 180 samples. The study wells are distributed across Oman, and span both more proximal (southerly) and more distal (northerly) environmental settings of the basin and recovered both the carbonates of the Arada Member and the shales of the Shargi Member of the Fiqa Formation. Analyses included the detailed examination of smear-slide samples for nannofossil taxonomy, biostratigraphy and assemblage characterisation as well as the analysis of bulk sediment carbonate isotopic and elemental compositions which are integrated with microfossil biostratigraphy, palaeoenvironmental and sequence stratigraphic interpretations.

The studied material yielded moderately to well-preserved and diverse nannofossil assemblages for the northern wells (distal settings) but scarce of nannofossil in the southern wells (proximal settings). The quality of preservation allowed the identification of two new species; *Staurolithites ormae* sp. nov. and *Chiastozygus fahudensis* sp. nov., as well as a close investigation of some poorly described groups such as *Staurolithites, Chiastozygus* and *Eiffellithus*, in which their problematic taxonomy and potential stratigraphic application is

discussed. Nannofossil assemblages from the tropical Fiqa Formation provided new constraints on the palaeobiogeography of Late Cretaceous nannofossil taxa, when abundance data was integrated with patterns of the global abundance distributions from other locations. Assemblages within the Fiqa Formation are dominated by taxa which are consistent with tropical Late Cretaceous Tethyan assemblages recorded elsewhere and are characterised by either absence or rare occurrences of higher-latitude species. Some taxa, however, showed different patterns than expected providing new insights into their palaeogeographic distribution. The common occurrence of *Discorhabdus ignotus* in the Fiqa Formation, for instance, is opposite to its previously suggested preference for higher-latitude regions, whilst *Lucianorhabdus* spp. and *Calculites obscurus*, which were previously considered as tropical taxa, are relatively rare in the Fiqa Formation. The occurrence of the rare Santonian *Helicolithus blairiae* species in the Fiqa Formation provides new information about its palaeogeographic range that was previously claimed to be limited to the Western Interior Seaway of North America. Intervals of slight cooling have been suggested in the Fiqa Formation by abundance peaks of *Ahmuellerella octoradiata* and *Lithastrinus grillii*. New insights into the palaeo-productivity of the basin are revealed by investigation of the changing abundance patterns of fertility-index species including *Discorhabdus ignotus*, *Biscutum constans* and *Zeugrhabdotus erectus* in relation to *Watznaueria barnesiae* and *Micula staurophora* throughout the Formation.

The detailed nannofossil taxonomy allowed the establishment of a new, high-resolution biostratigraphic zonation scheme that is correlated to global UC biozonation scheme of Burnett et al. (1998) for the Tethyan Province with 7 biohorizons based on 15 bioevents and 5

additional local, supplementary bioevents. The new biostratigraphic framework is used to refine the global UC biozonation scheme for the study area where possible especially the early Campanian-Santonian UC13-12 zones with the consistently recognised local bioevents across the basin. This new biostratigraphic scheme has also been integrated to existing local microfossil zonation schemes and used to generate a basin wide, well-to-well stratigraphic correlation. This subdivision allowed detailed biostratigraphic correlation across the study area which revealed the diachronous nature of the top and base of the Fiqa Formaation, as well as the transition from the carbonates of the Arada Member to the underlying shales of the Shargi Member, which had been suspected but not proven by the local foraminiferal zonation schemes. Nannofossil biostratigraphy showed that the onset of deposition of the Formation started in the north ~7 Ma than in the south, and that there is a general younging trend from northern part of the basin toward the south with upper Coniacian sediments only preserved in the north, whilst at the top of the Formation lower Maastrichtian sediments are only recorded in the south. The transition from the carbonates of the Arada Member to the shales of the Shargi Member also youngs southward from the lower to upper Campanian. Compared to the previously established local foraminiferal biozonation scheme, the nannofossil biozonation scheme provides finer resolution dating and enabled the recognition of Coniacian-Santonian and Santonian-Campanian stage boundaries. It has also allowed better time correlation across different palaeo-bathymetric facies recovered in wells across the basin, as nannofossil bioevents are more independent of changing water depth compared to the facies-dependent microfossil bioevents and zonation schemes. The new biostratigraphy has been tied with the tectonic evolution of the basin as well as the major sequence stratigraphic events of the Arabian Plate which are clearly reflected in the nannofossil assemblage changes and help to

refine the complex tectonic controls on the paleoenvironments of the basin. Nannofossil abundances are higher in the transgressive and highstand sequence tracts of the formation, with maximum abundance and diversity recorded around the maximum flooding surfaces. Abundances of nannofossil are reduced following sequence stratigraphic boundaries associated with local tectonics.

New bulk rock carbon isotope and elemental data are presented for five wells distributed across north and south Oman, throughout the Fiqa Formation. This is integrated with nannofossil assemblage data from eight exploration wells, as well as micropalaeontological data where available. This allowed the establishment of detailed late Coniacian to late Campanian $\delta^{13}C$ curve that is tied to the nannofossil biostratigraphic zones and correlated to regional and global carbon isotope events providing valuable insights into the stratigraphy, depositional settings and palaeoenvironment of the Fiqa Formation across the basin. The $\delta^{13}C$ record of the Fiqa Formation is generally consistent with global $\delta^{13}C$ curves but diverge in a regional negative excursion event recorded in the early Campanian. Integration of the $\delta^{13}C$ curve with elemental data, sequence stratigraphy, microfossil and nannofossil assemblage data as well as statistical analysis of elemental data and nannofossil assemblages associated this major negative excursion event with local tectonics that resulted in basin restriction with increased sediment and nutrient influx following a sequence stratigraphic boundary. Through the rest of the early Campanian, sea-level and basin-ocean connections increased as deposition shifted to transgressive and highstand sequence tracts, and $\delta^{13}C$ curve shifted to positive values consistent with the global ocean records. At the base of the early Campanian, a globally recognised negative excursion event (LCE) is recorded that is considered a useful

event for stratigraphic correlation of global $\delta^{13}C$ curves, especially in the southern Tethys area. A long term increase in $\delta^{13}C$ values is followed throughout the late Campanian within a highstand sequence tract. Statistical analysis of nannofossil assemblages and elemental data shows a clear interrelationship between changing terrestrial input and changes in fertility-related nannofossil taxa. A gradual reduction in *Watznaueria barnesiae* abundances with an increase in *Corollithion signum*, *Biscutum constans*, *Discorhabdus ignotus* and *Zeugrhabdotus erectus* is recorded following the early Campanian negative $\delta^{13}C$ excursion event. These changes in nannofossil assemblages are recorded in several wells across the basin within lower Campanian intervals in the more distal wells but in a lower to upper Campanian intervals in a proximal well. In the deepest part of the basin, the nannofossil assemblages remain high throughout the studied intervals of the Fiqa Formation and show less significant changes in assemblages through time. Nannofossil assemblage changes are linked to intervals of elevated surface ocean nutrient conditions in the highly dynamic basin as reflected in the high terrestrial input inferred from existing sequence stratigraphic data, sediment composition and $\delta^{13}C$ records. Following this, nannofossil abundances remain high up to the development of shallow marine environment toward the Arada Member where nannofossil abundances decrease.

The quality of preservation and continuity of these tropical nannofossil assemblages is important for future assessments of Late Cretaceous provincialism as the assemblages fill a gap between the austral and western Tethys provinces with the potential to constrain patterns of tropical diversity. The data presented within this thesis improves our understanding of the assemblage changes in this part of the Cretaceous oceans and the applicability of global

zonation schemes to this location and time interval. At the regional scale, the new combined nannofossil and geochemical analyses provide a new understanding of the palaeogeographic setting, relative sea level change and basin dynamics through the Late Cretaceous. This research is a reference point for future biostratigraphic or palaeoenvironmental analyses in the Middle East and southern Tethyan areas, especially when there has been limited work published on the geochemistry, nannofossil taxonomy and biostratigraphy of Late Cretaceous sequences in the region. The new zonation scheme developed for the Fiqa Formation will also be useful for future biostratigraphic studies on Upper Cretaceous subsurface and outcrop sections of Oman.

5.2 Future Work Recommendations

This study provides a wide spatial and temporal investigation of the Late Cretaceous foreland Aruma Basin with integrated taxonomic, biostratigraphic, petrophysical, lithological and geochemical interpretations. However, many questions for the southern part of the basin remain unanswered compared to the well-established history of the northern part of the basin. This study recommends using new biostratigraphic approaches, for instance palynostratigraphy (rock subdivision based on palynomorphs), or high resolution elemental stratigraphy (rock subdivision based on chemical characteristics) in order to refine the age dating and regional correlation of the southern wells which lack good nannofossil preservation. The more hydrocarbon wells added from other parts of the basin, especially wells from outside PDO concessions - e.g offshore wells and wells from the easternmost and southeastern parts of the basin - along with outcrop data from north and east Oman, the better constrained the basin evolution model and spatial distribution of palaeoenvironments will be.

Although some information from seismic data has been integrated into this study, comparisons with more detailed seismic sections will definitely add valuable sub-surface spatial information to the basin evolution model. Furthermore, the lower Maastrichtian sediments were only encountered in one study well based on nannofossil age dating, refinement within this interval would be improved if more wells with Maastrichtian sediments became available for study, including a higher resolution definition of the Campanian-Maastrichtian stage boundary in Oman. The Aruma Group remains a significant area, with good microfossil carbonate preservation, for potential Late Cretaceous palaeoenvironmental and palaeoclimate research and, as good successions become available, should be a target for future work.

References

Al Rawahi, Z. and Dunkley Jones, T. (2019a) Calcareous nannofossil assemblages of the Late Cretaceous Fiqa Formation, north Oman. **Journal of Micropalaeontology**, 38: 25-54

Al Rawahi, Z. and Dunkley Jones, T. (2019b in review) Nannofossil biostratigraphic correlation of the Late Cretaceous Fiqa Formation across North Oman

Ali, M.Y. and Watts, A.B. (2009) Subsidence history, gravity anomalies and flexure of the United Arab Emirates (UAE) foreland basin. **GeoArabia**, 14 (2):17-44

Ali, M.Y., Watts, A.B. and Searle, M.P. (2013) "Seismic stratigraphy and subsidence history of the United Arab Emirates (UAE) rifted margin and overlying foreland basin." In Al Hosani, K., Roure, F., Ellison, R. and Lokier, S. (eds.) **Lithosphere Dynamics and Sedimentary Basins: The Arabian Plate and Analogues; Frontiers in Earth Sciences, Part 1**. Berlin: Springer. pp. 127-143

Alsharhan, A.S. and Nairn, A.E.M. (1990) A review of the Cretaceous Formations in the Arabian Peninsula and Gulf: part III. Upper Cretaceous (Aruma Group) stratigraphy and palaeogeography. **Journal of Petroleum Geology**, 13 (3): 247-266

Al-Wosabi, A. and Alaug, S. (2013) Calcareous nannofossil biostratigraphy of the Late Early Maastrichtian Age, Block 16, Jiza'-Qamar Basin, Eastern Yemen. **Arabian Journal of Geoscience**, 6: 3581-3594

Bechennec, F., Le Metour, J., Rabu, D., Bourdillon-de-Grissac, C., de Wever, P., Beurrier, M., and Villey, M. (1990) "The Hawasina Nappes: stratigraphy, palaeogeography and structural

evolution of a fragment of the south-Tethyan passive continental margin." In Robertson, A.H.F., Searle, M.P. and Ries, A.C. (eds.) **The Geology and Tectonics of the Oman Region.** London: Geological Society Publishing House. pp. 213-223

Boote, D.R.D., Mou, D. and Waite, R.I. (1990) "Structural evolution of the Suneinah Foreland, Central Oman Mountains." In Robertson, A.H.F., Searle, M.P. and Ries, A.C. (eds.) **The Geology and Tectonics of the Oman Region.** London: Geological Society Publishing House. pp. 397-418

Booth, G.A. (2015) Biostratigraphy of Oman. Internal PDO book.

Bown, P.R., Lees, J.A. and Young, J.R. (2004) "Calcareous nannoplankton evolution and diversity through time." In Thierstein, H.R. and Young, J.R. (eds.) **Coccolithophores From Molecular Processes to Global Impact**. Berlin: Springer-Verlag. pp. 481–508

Bown, P.R. and Young, J.R. (1997) Mesozoic calcareous nannoplankton classification. **Journal of Nannoplankton Research**, 19: 21–36

Bown, P.R. and Young, J.R. (1998a) "Introduction." In Bown, P. R. (ed.) **Calcareous Nannofossil Biostratigraphy**. London: Chapman & Hall/ Kluwer Academic Publishers. pp. 1- 15

Bown, P.R. and Young, J.R. (1998b) "Techniques." In Bown, P. R. (ed.) **Calcareous Nannofossil Biostratigraphy**. London: Chapman & Hall/ Kluwer Academic Publishers. pp. 16- 28

Bukry, D. (1973) Coccolith and silicoflagellate stratigraphy, Tasman Sea and southwestern Pacific Ocean, Deep Sea Drilling Project Leg 21. **Initial Reports of the Deep Sea Drilling Project**, 21: 885–893

Burnett, J.A. (1997) New species and new combinations of Cretaceous nannofossil and a note on the origin of Petrarhabdus (Deflandre) Wind and Wise. **Journal of Nannoplankton Research**, 19: 133–146

Burnett, J.A. (1998) "Upper Cretaceous." In Bown, P. R. (ed.) **Calcareous Nannofossil Biostratigraphy**. London: Chapman & Hall/ Kluwer Academic Publishers. pp. 132- 199

Carr, I. and Jones, P. (1998) Micropalaeontological and palynological analysis of Ibtihaj-1 well. Internal Robertson report for PDO.

Clarke, R.F.A. and Hoogkamer, P.J.C. (1967) A time stratigraphic subdivision of the Aruma Shale Formation (Upper Cretaceous) in Oman based on Palynology and Palaeontology. Internal PDO report.

Cooper, D.J.W., Ali, M.Y. and Searle, M.P. (2014) "Structure of the northern Oman Mountains from the Semail Ophiolite to the Foreland Basin." In Rollinson, H.R., Searle, M.P., Abbasi, I.A., Al-Lazki, A.I., and Al Kindi, M.H. (eds.) **Geological Society Special Publications Volume 392: Tectonic Evolution of the Oman Mountains.** London: Geological Society of London. pp. 129-153

van Buchem, F.S., Razin, P., Homewood, P.W., Oterdoom, W.H. and Philip, J. (2002) Stratigraphic organization of carbonate ramps and organic-rich intrashelf basins: Natih Formation (middle Cretaceous) of northern Oman. **AAPG Bulletin**, 86: 21–53

Calvert, S.E. and T.F. Pedersen (2007) "Elemental Proxies for Palaeoclimatic and Palaeoceanographic Variability in Marine Sediments: Interpretation and Application." In Hillaire-Marcel, C. and De Vernal, A. (eds.) **Proxies in Late Cenozoic Paleoceanography**. Amsterdam: Elsevier. pp. 567-644

Cramer, B.S., Miller, K.G., Barrett, P.J., and Wright J.D. (2011) Late Cretaceous–Neogene trends in deep ocean temperature and continental ice volume: Reconciling records of benthic foraminiferal geochemistry ($\delta^{18}O$ and Mg/Ca) with sea level history. **Journal of Geophysical Research**, 116 (C12): 1-23

Crux, J.A. (1991) Albian calcareous nannofossil from the Gault Clay of Munday's Hill (Bedfordshire, England). **Journal o f Micropalaeontology**, 10: 203-221

Droste, H. (2001) Oman Subsurface Stratigraphy. Internal PDO chart.

Droste, H. and van Steenwinkel, M. (2004) "Stratal geometries and patterns of platform carbonates: The Cretaceous of Oman." In Eberli, G.P., Masaferro, J.L. and Sarg, J.F. (eds.) **Seismic imaging of carbonate reservoirs and systems: AAPG Memoir 81**. USA: American Association of Petroleum Geologists. pp. 185-206

Droste, H. J. (2012) Petroleum Geology of the Sultanate of Oman. Shell internal report.

Eleson, J.W. and Bralower, T.J. (2005) Evidence of changes in surface water temperature and productivity at the Cenomanian/ Turonian Boundary. **Micropaleontology**, 51(4): 319-332

Erba, E. (1992) Middle Cretaceous calcareous nannofossil from the western Pacific (Leg 129): evidence for paleoequatorial crossings. **Proceedings of the ODP Scientific Results**, 129: 189-201

Erba, E., Castradori, D., Guasti, G. and Ripepe, M. (1992) Calcareous nannofossil and Milankovitch cycles: the example of the Albian Gault Clay Formation (southern England). **Palaeogeography, Palaeoclimatology, Palaeoecology**, 93: 47–69

Erba, E. (2004) Calcareous nannofossil and oceanic anoxic events. **Marine Micropaleontology,** 52: 85-106

Faris, M. and Abu Shama, A.M. (2006) Calcareous nannofossils of the Campanian-Maastrichtian Sudr Formation in Abu Zenima area, West Central Sinai, Egypt. **Egyptian Journal of Paleontology**, 6: 251–274

Farouk, S. and Faris, M. (2012) Late Cretaceous calcareous nannofossil and planktonic foraminiferal bioevents of the shallow-marine carbonate platform in the Mitla Pass, west central Sinai, Egypt. **Cretaceous Research**, 33 (1): 50-65

Farouk, S., Thibault, N., Jaff, R.B., Faris, M., Ahmad, F., and Khashaba, A. (2018a) An integrated study of Upper Campanian- Lower Maastrichtian carbon isotopes and calcareous plankton biostratigraphy of the Kurdistan Region, northeastern Iraq. **Cretaceous Research**, 82: 64–80.

Farouk, S., Faris, M., Elamri, Z., Ahmad, F. and Wagreich, M. (2018b) Tethyan plankton bioevents calibrated to stable isotopes across the upper Santonian–lower Campanian transition in north-western Tunisia. **Cretaceous Research**, 85: 128–141

Filbrandt, J., Al Mazrui, S., Osterloff, P., Packer, S., Al Harthy, A. and Mohiudeen, U. (2004) Proposed subdivision and sequence stratigraphy of the Fiqa Formation, North Oman. Internal PDO report.

Fisher, C.G. and Hay, W.W. (1999) "Calcareous nannofossil as indicators of Mid-Cretaceous paleofertility along an ocean front, U.S. Western Interior." In Barrera, E. and Johnson, C.C. (eds.) **Evolution of the Cretaceous Ocean-Climate System, The Geological Society of America Special Paper 332**. USA: Geological Society of America. pp. 161-180

Forbes, G. A., Jansen H. S. M. and Schreurs, J. (2010) **Lexicon of Oman subsurface stratigraphy: Reference guide to the stratigraphy of Oman's hydrocarbon basins**. Bahrain: Gulf PetroLink.

Foroughi, F., Gadin, S., Lotfali Kani, A. and Vahidinia, M. (2017) Calcareous Nannofossil biostratigraphy of Campanian strata (Abtalkh Formation) from East of Koppeh-Dagh Basin, NE Iran. **Cretaceous Research**, 70: 55-70

Frakes, L. A., Francis, J. E. and Syktus, J. I. (1992) **Climate Modes of the Phanerozoic: The History of the Earth's Climate over the Past 600 Million Years**. Cambridge: Cambridge University Press.

Friedrich, O., Norris, R.D. and Erbacher J. (2012) Evolution of middle to Late Cretaceous oceans - a 55 my record of Earth's temperature and carbon cycle. **Geology**, 40: 107-110

Gaina, C., van Hinsbergen, D. and Spakman, W. (2015) Tectonic interactions between India and Arabia since the Jurassic reconstructed from marine geophysics, ophiolite geology, and seismic tomography: India-Arabia Tectonic interactions. **Tectonics**, 34 (5): 875-906

Gardin, S., Del Panta, F., Monechi S. and Pozzi, M. (2001a) "A Tethyan reference record for the Campanian and Maastrichtian stages: the Bottaccione section (Central Italy); review of data and new calcareous nannofossil results." In Odin, G.S. (ed.) **The Campanian-Maastrichtian stage boundary: characterisation at Tercis les Bains (France) and correlation with Europe and other continents: Developments in Palaeontology and Stratigraphy 19**. Elsevier. pp. 745-757

Gardin, S., Odin, G.S., Melinte, M., Monechi S., and von Salis, K. (2001b) "Results of the cooperative study on the calcareous nannofossils across the Campanian-Maastrichtian boundary at Tercis les Bains (Landes, France)." In Odin, G.S. (ed.) **The Campanian-Maastrichtian stage boundary: characterisation at Tercis les Bains (France) and correlation with Europe and other continents: Developments in Palaeontology and Stratigraphy 19**. Elsevier. pp. 293-309

Gartner, S. (1968) Coccoliths and Related Calcareous Nannofossils from Upper Cretaceous Deposits of Texas and Arkansas. **University of Kansas Paleontological Contributions: Protista**, 1: 1-56

Gartner, S. (1977) Nannofossils and Biostratigraphy: An Overview. **Earth Science Reviews,** 13: 227-250

Giner, J.A., Klein H. B. and Boynton, C. H. (1992). A Catalogue of Stratigraphic Trap Plays in the PDO Concession. PDO internal report.

Glennie, K.W., Boeuf, M.G., Hughes-Clarke M.W.H., Moody-Stuart, M., Pilaar, W.F. and Reinhardt, B.M. (1973) Late Cretaceous Nappes in Oman Mountains and Their Geologic Evolution: Reply. **AAPG Bulletin**, 57: 5-27

Glennie K.W., Boeuf M.G., Hughes-Clarke M.H.W., Moody-Stuart M., Pilaar W.F. and Reinhardt, B.M. (1974) **Geology of the Oman Mountains**. Amsterdam: Verhandelingen Koninklijk Nederlands geologisch mijnbouwkundidg Genootschap.

Gombos, A.M., Strohmenger, C.J. and Huang T.C. (2008) High resolution age dating of the Shuaiba Formation by means of calcareous nannofossils. **EAGE First Break**, 26: 69-74

Gradstein, F. M., Ogg, J. G, Schmitz, M. and Ogg, G. (2012) **The Geologic Time Scale**. Amsterdam: Elsevier.

Hammer, Ø. and Harper, D. (2006) **Paleontological Data Analysis**. Oxford: Blackwell Publishing.

Haq, B.U., Hardenbol, J. and Vail, P.R. (1987) Chronology of fluctuating sea levels since the Triassic. **Science**, 235: 1156 -1167

Haq, B.U. (1998) "Calcareous nannoplankton." In Haq, B.U. and Boersma, A. (eds.) Introduction to marine micropaleontology. Singapore: Elsevier. pp. 79-107

Haq, B.U. (2014) Cretaceous eustasy revisited. **Global and Planetary Change**, 113: 44–58

Hardenbol, J., Thierry, J., Farley, M.B., Jacquin, T., De Graciansky, P.C. and Vail, P.R. (1998) "Mesozoic and Cenozoic sequence chronostratigraphic framework of European basins" In Graciansky, P.C., Hardenbol, J., Jacquin, T. and Vail, P.R. (eds.) **Mesozoic and Cenozoic Sequence Stratigraphy of European Basins: SEPM Special Publication 60**. USA: SEPM Society For Sedimentary Geology. pp. 3-13

Hardas, P. and Mutterlose, J. (2007) Calcareous nannofossil assemblages of Oceanic Anoxic Event 2 in the equatorial Atlantic: Evidence of an eutrophication event. **Marine Micropaleontology**, 66 (1): 52-69

Herrle, J.O. (2002) Paleoceanographic and paleoclimatic implications on mid-Cretaceous black shale formation in the Vocontian Basin and the Atlantic: evidence from calcareous nannofossil and stable isotopes. **Tubinger Mikropalaontologische Mitteilungen Nr**, 27: 1-115

Herrle, J.O., Pross, J., Friedrich, O. and Hemleben, C. (2003) Short-term environmental changes in the Cretaceous Tethyan Ocean: micropaleontological evidence from the Early Albian Oceanic Anoxic Event lb. **Terra Nova**, 15 (1): 14-19

Hersi O.S., Abbasi, I.A., Al-Harthy, A, Cherchi, A. and Schroeder, R. (2014) Stratigraphic Evolution and Depositional System of Lower Cretaceous Qishn Formation, Dhofar, Oman. **Geological Society of London Special Publication**, 392: 303-323

Higgins, A.C. and Howarth, R.J. (1997a) Chemostratigraphy of the interval 550 metres to 1960 metres in the Santonian-?Campanian sediments of Ibtihaj-1, Oman Mountains Foreland Basin, Oman. Internal StrataData report for PDO.

Higgins, A.C. and Howarth, R.J. (1997b) Final report on the pilot project on the provenance of the Late Cretaceous sediments of the Oman Mountains Foreland Basin, based on 415 samples from eight wells. Internal StrataData report for PDO.

van Hinsbergen, D.J.J., de Groot, L.V., van Schaik, S.J., Spakman, W., Bijl, P.K., Sluijs, A., Langereis, C.G. and Brinkhuis, H. (2015) A paleolatitude calculator for paleoclimate studies (model version 2.1). **PLoS ONE** [online], 10: 1–21. Available from: doi: 10.1371/ journal.pone.0126946.

Hoffmann, G., Meschede, M., Zacke, A. and Al Kindi, M. (2016) **Field Guide to the Geology of Northeastern Oman**. Johannesstr: Borntraeger Science Publishers.

Horsfield, W.T. (1983) Fiqa Sands, a New Play in Northern Afar. PDO internal report.

Howe, R.W., Sikora, P.J., Gale, A.S., Bergen, J.A. (2007) Calcareous nannofossil and planktonic foraminiferal biostratigraphy of proposed stratotypes for the Coniacian/ Santonian boundary: Olazagutía, northern Spain; Seaford Head, southern England; and Ten Mile Creek, Texas, USA. **Cretaceous Research**, 28: 61-92

Hughes-Clarke, M.W. (1988) Stratigraphy and Rock Unit Nomenclature in the Oil Producing Area of Interior Oman. **Journal of Petroleum Geology**, 11 (1): 5-60

Immenhauser, A., Schreurs, G., Peters, T., Matter, A., Hauser, M. and Dumitrica, P. (1998) Stratigraphy, sedimentology and depositional environments of the Permian to uppermost Cretaceous Batain Group, East Oman. **Eclogae Geologicae Helvetiae**, 91: 217-35

Jacovides, J. and Varol O. (2000) The biostratigraphy and palaeoenvironmental interpretation of the Natih Formation of North Oman within wells: Al Ghubar-15, Fahud-16, Fahud-175, Fahud-180, Fahud-316, and Shurooq-2. Internal Millennia report for PDO.

Jarvis, I., Gale, A.S., Jenkyns, H.C. and Pearce, M.A. (2006) Secular variation in Late Cretaceous carbon isotopes: a new δ13C carbonate reference curve for the Cenomanian–Campanian (99.6–70.6 Ma). **Geological Magazine**,143 (5): 561-608

Joo, Y.J. and Sageman, B.B. (2014) Cenomanian To Campanian Carbon Isotope Chemostratigraphy from the Western Interior Basin, U.S.A. **Journal of Sedimentary Research**, 84: 529-542

Keller, G. (2008) Cretaceous climate, volcanism, impacts, and biotic effects. **Cretaceous Research,** 29: 754-771

Kita, Z., Watkins, D. and Bergen, J. (2016) A new calcareous nannofossil species of the genus *Helicolithus* from the Santonian and its biostratigraphic significance in the Cretaceous Western Interior Seaway. **Journal of Nannoplankton Research**, 36 (1): 77-82

Kita, Z.A., Watkins, D.K., and Sageman, B.B. (2017) High-resolution calcareous nannofossil biostratigraphy of the Santonian/Campanian stage boundary, Western Interior Basin, USA. **Cretaceous Research**, 69: 49-55

Lauer, G. (1973) Manual of Upper Cretaceous nannoplankton (Arkhangelskiellaceae) based on the Fiqa Formation of Central Oman (Santonian-Campanian). Internal PDO report.

Lees, J.A. (2002) Calcareous nannofossil biogeography illustrates palaeoclimate change in the Late Cretaceous Indian Ocean. **Cretaceous Research**, 23: 537–634

Lees, J.A. and Bown, P.R. (2005) "Upper Cretaceous calcareous nannofossil biostratigraphy, ODP Leg 198 (Shatsky Rise, northwest Pacific Ocean)" In: T.J. Bralower, I. Premoli Silva and M.J. Malone (eds.) **Proceedings of the Ocean Drilling Program, Scientific Results Volume 198**. USA: Ocean Drilling Program. pp. 1-60

Lees, J.A. (2007) New and rarely reported calcareous nannofossil from the Late Cretaceous of coastal Tanzania: outcrop samples and Tanzania Drilling Project Sites 5, 9 and 15. **Journal of Nannoplankton Research**, 29 (1): 39-65

Linnert, C., Mutterlose, J. (2009a) Biometry of the Late Cretaceous Arkhangelskiella group: ecophenotypes controlled by nutrient flux. **Cretaceous Research**, 30: 1193-1204

Linnert, C. and Mutterlose, J. (2009b) Evidence of increasing surface water oligotrophy during the Campanian–Maastrichtian boundary interval: Calcareous nannofossils from DSDP Hole 390A (Blake Nose). **Marine Micropaleontology**, 73: 26-36

Linnert, C., Mutterlose, J., and Herrle, J.O. (2011) Late Cretaceous (Cenomanian–Maastrichtian) calcareous nannofossils from Goban Spur (DSDP Sites 549, 551): Implications for the palaeoceanography of the proto North Atlantic. **Palaeogeography, Palaeoclimatology, Palaeoecolog**, 299: 507-528

Linnert, C., Mutterlose, J. and Bown, P. (2014a) Biometry of Upper Cretaceous (Cenomanian-Maastrichtian) coccoliths - a record of long-term stability and interspecies size shifts. **Revue de Micropaleontologie** , 57 (4): 125-140

Linnert, C., Robinson, S.A., Lees, J.A., Bown, P., Pérez Rodríguez, I., Petrizzo, M. R., Falzoni, F., Littler, K., Arz, J.A. and Russell, E.E. (2014b) Evidence for global cooling in the Late Cretaceous. **Nature Communications**, 5: 4194

Linnert, C., Engelke, J., Wilmsen, M., and Mutterlose, J. (2016) The impact of the Maastrichtian cooling on the marine nutrient regime-Evidence from mid-latitudinal calcareous nannofossils. **Paleoceanography**, 31: 694-714

Lippard, S.J., Shelton, A.W. and Gass, I.G. (1986) **The ophiolite of Northern Oman**. London: Blackwell Scientific Publications.

Mandur, M. (2016) Late Cretaceous Calcareous Nannofossil Biostratigraphy and Paleoecology in the Northwestern Desert, Egypt. **Arabian Journal for Science and Engineering**, 41 (6): 2271-2284

Melinte, M.C., Lamolda, M.A. (2002) "Calcareous nannofossils around the Coniacian/ Santonian boundary in the Olazagutía section (N. Spain)." In: Wagreich, M. (ed.) **Aspects of Cretaceous Stratigraphy and Palaeobiogeography**. Vienna: Publishing House of the Austrian Academy of Sciences. 351-364

Melinte, M.C. and Lamolda, M.A. (2007) Calcareous nannofossil biostratigraphy of theConiacian/Santonian boundary interval in Romania and comparison with otherEuropean regions. **Cretaceous Research**, 28: 119-127

Miller, K.G., Kominz, M.A., Browning, J.V., Wright, J.D., Mountain, G.S., Katz, M.E., Sugarman, P.J., Cramer, B.S., Christie-Blick, N. and Pekar, S.F. (2005) The Phanerozoic record of global sea-level change. **Science**, 310 (5752): 1293-1298

Mohiuddin, U. (2002) **Late Cretaceous palynology and seismic-sequence stratigraphy of the subsurface formations of the interior of North Oman.** PhD thesis, University of Sheffield

Muller, C., Higazi, F., Hamdan, W. and Mroueh, M. (2010) "Revised stratigraphy of the Upper Cretaceous and Cenozoic series of Lebanon based on nannofossil." In Homberg, C. and Bachmann, M. (eds.) **Evolution of the Levant Margin and Western Arabia Platform since the Mesozoic**. London: The Geological Society of London Publishing House. pp. 287-303

Mutterlose, J., Bornemann, A. and Herrle, J. (2005) Mesozoic calcareous nannofossils – state of the art, **Paläontologische Zeitschrift**, 79 (1): 113-133

New Play Development, The Fiqa Play. Internal PDO XEM repot. 2015

Nolan, S.C., Skelton, P.W., Clissold, B.P. and Smewing, J.D. (1990) "Maastrichtian to Tertiary palaeogeography of the Central and Northern Oman Mountains." In Roburtson, A.H.F.,

Searle, M.P. and Ries, A.C. (eds.) **The Geology and Tectonics of the Oman Region**: **Geological Society Special Publication 49**. London: Elsevier. pp. 495-519

Nour El Din, M. (1992) The Fiqa Formation In Oman (Santonian-Campanian) Stratigraphy, Deposition Environments and Reservoir Potential of Turbiditic Sandstones. PDO internal report.

O'Brien, C.L., Robinson, S.A., Pancost, R.D., Sinninghe Damsté, J.S., Schoulten, S., Lunt, D.J., Alsenz, H., Bornemann, A., Bottini, C., Brassell, S.C., Farnsworth, A., Forster, A., Huber, B.T., Inglis, G.N., Jenkyns, H.C., Linnert, C., Littler, K., Markwick, P., McAnena, A., Mutterlose, J., Naafs, B.D.A., Püttmann, W., Sluijs, A., van Helmond, N.A.G. M., Vellekoop, J., Wagner, T. and Wrobel, N.E. (2017) Cretaceous sea-surface temperature evolution: constraints from TEX86 and planktonic foraminiferal oxygen isotopes. **Earth-Science Reviews**, 172: 224-247

Odin, G.S. (2001) T**he Campanian-Maastrichtian stage boundary: characterisation at Tercis les Bains (France) and correlation with Europe and other continents**; Developments in Palaeontology and Stratigraphy 19. Amsterdam: Elsevier.

Odin, G.S. and Lamaurelle, M.A. (2001) The global Campanian-Maastrichtian stage boundary. **Episode**, 24 (4): 229-238

Ogg, J.G. and Hinnov, L.A. (2012) "Cretaceous." In Gradstein, F. M., Ogg, J. G, Schmitz, M. and Ogg, G. (eds.) **The Geologic Time Scale 2012**. Amsterdam: Elsevier. pp. 793-853.

Osterloff, P., Al Harthy, A., Nasser Al Rahmah, M., and Al Zadjali, F. (2001) Basal Fiqa Formation, North Oman: a stratigraphic review. Internal PDO report.

Owen, R.M.S. and Nasr, S.N. (1958) "Stratigraphy of the Kuwait-Basra Area." In Weeks, L.G. (ed.) **Habitat of Oil**; Special Publication of the American Association of Petroleum Geologists. USA: American Association of Petroleum Geologists. pp. 1252-1278

Packer, S.R., Al-Zadjali, F. and Zucchi, D. (2000) Biostratigraphic analysis of selected intervals from PDO wells Habiba-1, Baqlah-1, Abeer-1, Ayoun-1, Jebel Madar-1, Saih Rawl-135 and selected field samples from the Salakh Arch area, North Oman. Internal Millennia report for PDO.

Packer, S.R. (2001a) Fiqa Formation study 2: Biostratigraphic analysis of selected intervals from PDO wells Saih Rawl-83, Musallim Deep-1, Kauther-1 and Khazzan-1, North Oman. Internal Millennia report for PDO.

Packer, S.R. (2001b) Fiqa Formation study 3: Biostratigraphic analysis of selected intervals from PDO wells Sufrid-1, Ibtihaj-1, Fahud South-9 and Humaimah-1, North Oman. Internal Millennia report for PDO.

Packer, S.R. (2001c) Biostratigraphic analysis of selected intervals from PDO wells Tawf Dahm-1, Umm as Samim-1, and Rakha-1, North Oman. Internal Millennia report for PDO.

Packer, S.R. (2002) Fiqa Formation study 4: Biostratigraphic analysis of selected intervals from PDO wells Qahlah-2, Burhaan-5, Hanya-1, Wadi Umaryi-2 and Jahiz-1, North Oman. Internal Millennia report for PDO.

Packer, S.R. (2004) Biostratigraphic analysis of selected samples from the Nahr Umr Formation, Oman. Internal Millennia report for PDO.

Packer, S.R., Booth G.A. and Taylor C.M. (2004) Biostratigraphic analysis Well; Jaleel-1. Internal Millennia report for PDO.

Packer, S.R. and Starkie, S. (2005) Biostratigraphic analysis of the well Salama-1 (interval: 870' – 5300') Oman. Internal Millennia report for Oolithica Geoscience.

Packer, S.R and S. Starkie (2008) Biostratigraphic analysis of selected samples from The Nimr area, Oman. Internal Millennia report for PDO.

Packer, S.R. (2010) Biostratigraphic analysis of PDO wells Fahud South West-305H1, Khulud- 1H1, and Khulud West-1H1, North Oman. Internal Millennia report for PDO.

Perch-Nielsen, K. (1979) Calcareous nannofossils from the Cretaceous between the North Sea and the Mediterranean. In Wiedmann, J. (ed.) Aspekte der Kreide Europas. IUGS Series A 6. E. Stuttgart: Schweizerbart'sche Verlagbuchhandlung (Nägelle u. Obermiller). pp. 223-272

Perch-Nielsen, K. (1989) "Mesozoic calcareous nannofossil." In Bolli, H.M., Saunders, J.B. and Perch-Nielsen, K. (eds.) **Plankton Stratigraphy**. Cambridge: Cambridge University Press. pp. 329-426

Philip, J.M. and Platel, J.P. (1995) "Stratigraphy and rudist biozonation of the Campanian and the Maastrichtian of eastern Oman." In Alencaster G. and Buitron-Sanchez, B.E. (eds.) **The Third International Conference on Rudistae**. Revista Mexicana de Ciencias Geologicas 12. pp. 257-266

Platel, J. P., Philip, J., Bourdillon de Grissac, C., Babinot, J.F., Roger, J. and Mercadier, C. (1995) "Geodynamic setting, stratigraphy and paleoenvironments of the Aruma Group in eastern Oman: the Campanian platform around Haushi-Huqf." In Al-Husseini, M.I. (ed.) **Middle East Geosciences Conference GEO 94**. Bahrain: Gulf PetroLink. pp. 771-783

Pollastro, R. M. (1999) Ghaba Salt Basin province and Fahud Salt Basin province – Oman: geological overview and total petroleum systems. **United States Geological Survey Bulletin,** 2167: 1-41

Prins, B. and Roersma, H.J. (1983) **Late Santonian to Late Campanian calcareous nannoplankton from the Fiqa Formation, Central Oman.** Internal SIPM report for PDO.

Raffi, I., Backman, J., Fornaciari, E., Pälike, H., Rio, D., Lourens, L., and Hilgen, F. (2006) A review of calcareous nannofossil astrobiochronology encompassing the past 25 million years. **Quaternary Science Reviews**, 25 (23-24): 3113-3137

Ratcliffe, K.T., Morton, A.C., Ritcey, D.H. and Evenchick, C.A. (2007) Whole-rock geochemistry and heavy mineral analysis as petroleum exploration tools in the Bowser and Sustut basins, British Columbia, Canada. **Bulletin of Canadian Petroleum Geology**, 55 (4): 320-336

Razmjooei, M., Thibault, N., Kani, A., Mahanipour, A., Boussah, M. and Korte, C. (2014) Coniacian–Maastrichtian calcareous nannofossil biostratigraphy and carbon-isotope stratigraphy in the Zagros Basin (Iran): consequences for the correlation of Late Cretaceous Stage Boundaries between the Tethyan and Boreal realms. **Newsletters on Stratigraphy**, 47 (2): 183–209

Razmjooei, M.J., Thibault, N., Kani, A., Dinarès-Turell, J., Pucéat, E., Shahriari, S., Radmacher, W., Jamali, A.M., Ullmann, C.V., Voigt, S. and Cocquerez, T. (2018) Integrated bio- and carbon-isotope stratigraphy of the Upper Cretaceous Gurpi Formation (Iran): A new reference for the eastern Tethys and its implications for large-scale correlation of stage boundaries. **Cretaceous Research**, 91: 312–340

Rioux, M., Bowring, S., Kelemen, P., Gordon, S., Dudas, F. and Miller, R. (2012) Rapid crustal accretion and magma assimilation in the Oman-UAE ophiolite: High precision U-Pb zircon geochronology of the gabbroic crust. **Journal of Geophysical Research**, 117 (B7): 1-12

Robertson, A. (1987) Upper Cretaceous Muti formation: transition of a Mesozoic carbonate platform to a foreland basin in the Oman Mountains. **Sedimentology**, 34 (6): 1123 -1142

Rollinson, H. (1993) **Using Geochemical Data: Evaluation, Presentation, Interpretation**. London: Taylor and Francis

Romine, K. and Stuart-Smith, P. (2003) Regional Seismic Interpretation: Western Deformation Front, South Oman Salt Basin. Internal PDO report.

Roth, P.H. (1973) “Calcareous nannofossils - Leg 17, Deep Sea Drilling Project.” In Winterer, E.L., Ewing, J.I., et al., (eds.) **Initial Reports of the Deep Sea Drilling Project 17 (2)**. Washington: U.S. Government Printing Office. pp. 695-795

Roth, P.H. (1981) Mid-Cretaceous calcareous nannoplankton from the central Pacific: Implications for paleoceanography. **Initial Reports of the DSDP**, 62: 471-489

Roth, P.H. and Bowdler, J.L. (1981) Middle Cretaceous calcareous nannoplankton biogeography and oceanography of the Atlantic ocean. **Society of Economic Paleontologists and Mineralogists, Special Publication**, 32: 517–546

Roth, P.H. (1984) "Preservation of calcareous nannofossil and fine-grained carbonate particles in mid-Cretaceous sediments from the southern Angola Basin, Site 530." In Hay, W.W., Sibuet, J.C., et al. (eds.) **Initial Reports of the Deep Sea Drilling Project**. Washington: U.S. Government Printing Office. pp. 651-655

Rothwell R. and Croudace, I. (2015) "Twenty Years of XRF Core Scanning Marine Sediments: What Do Geochemical Proxies Tell Us?." In Croudace, I. and Rothwell, R. (eds.) **Micro-XRF Studies of Sediment Cores**. Dordrecht: Springer. pp. 25-102

Shafik, S. (1990) Late Cretaceous nannofossil biostratigraphy and biogeography of the Australian western margin. **BMR bulletin**, 295: 1-164

Shamrock, J. L. and Watkins D.K. (2009) Evolution of the Cretaceous calcareous nannofossil genus *Eiffellithus* and its biostratigraphic significance**. Cretaceous Research**, 30: 1083-1102

Schumann, D. (1995) Upper Cretaceous rudist and stromatoporid associations of central Oman (Arabian Peninsula). **Facies**, 32: 198-202

Searle, M.P. (1988) Thrust tectonics of the Dibba zone and the structural evolution of the Arabian continental margin along the Musandam Mountains (Oman and United Arab Emirates). **Journal of the Geological Society**, 145 (1): 43-53

Searle, M.P and Cox, J. (1999) Tectonic setting, origin, and obduction of the Oman ophiolite. **GSA Bulletin**, 111 (1): 104-122

Searle, M.P. (2007) Structural geometry, style and timing of deformation in the Hawasina Window, Al Jabal al Akhdar and Saih Hatat culminations, Oman Mountains. **GeoArabia**, 12: 99-130

Searle, M.P. and Ali, M.Y. (2009) Structural and tectonic evolution of the Jabal Sumeini, Al Ain-Buraimi region, northern Oman and eastern United Arab Emirates. **GeoArabia**, 14: 115-142

Shackleton, R.M., Ries, A.C., Bird, P.R., Filbrandt, J., Lee, C.W. and Cunningham, G.L. (1990) "The Batain melange of NE Oman." In Robertson, A.H.F., Searle, M.P. and Ries, A.C. (eds.) **The Geology and Tectonics of the Oman Region.** London: Geological Society Publishing House. pp. 673-696

Sharland, P.R., Archer, R., Casey, D.M., Davies, R.B., Hall, S.H., Heward, A.P., Horbury, A.D. and Simmons M.D. (2001) **Arabian Plate Sequence Stratigraphy; GeoArabia Special Publication 2**, Bahrain: Gulf PetroLink.

Sikkema, W. (1991) Micropalaeontological zonation and range charts of the Cretaceous in Oman. Internal Millennia report for PDO.

Sissingh, W. (1974) A preliminary calcareous nannoplankton zonation of the Cretaceous-Early Paleocene interval. Internal SIPM report.

Sissingh, W., 1977. Biostratigraphy of Cretaceous calcareous nannoplankton. **Geologie en Mijnbouw**, 56 (1): 37-65

Skelton, P. W., Nolan, S. C. & Scoti', R. W. (1990) "The Maastrichtian transgression onto the North- western flank of the Proto-Oman Mountains: sequences of rudist-bearing beach to open shelf facies." In Robertson, A.H.F., Searle, M.P. and Ries, A.C. (eds.) **The Geology and Tectonics of the Oman Region.** London: Geological Society Publishing House. pp. 521-547

Street, C. and Bown, P.R. (2000) Palaeobiogeography of Early Cretaceous (Berriasian-Barremian) calcareous nannoplankton. **Marine Micropaleontology***,* 39: 265-291

Styzen M. (1997) Cascading counts of nannofossil abundance. **Journal of Nannoplankton Research**, 19 (1): 49

Sugden, W. and Standring, A.J. (1975) **Qatar Peninsula**. Lexique Stratigraphque International 3, Paris: Centre National De La Recherche.

Takahashi, G. (2015) Sample preparation for X-ray fluorescence analysis III. Pressed and loose powder methods. **Rigaku Journal**, 31: 26-30

Terken, J.M. (1999) The Natih petroleum system of North Oman. **GeoArabia**, 4: 157-180

Thibault, N. (2010) Biometric analysis of the Arkhangelskiella group in the upper Campanian–Maastrichtian of the Stevns-1 borehole, Denmark: taxonomic implications and evolutionary trends. **Geobios**, 43: 639-652

Thibault, N., Harlou, R., Schovsbo, N., Schioler, P., Minoletti, F., Galbrun, B., Lauridsen, B. W., Sheldon, E., Stemmerik, L. and Surlyk, F. (2012) Upper Campanian-Maastrichtian

nannofossil biostratigraphy and high-resolution carbon-isotope stratigraphy of the Danish Basin: Towards a standard $d^{13}C$ curve for the Boreal Realm. **Cretaceous Research**, 33: 72-90

Thibault, N., Jarvis, I., Voigt, S., Gale, A.S., Attree, K. and Jenkyns, H.C. (2016) Astronomical calibration and global correlation of the Santonian (Cretaceous) based on the marine carbon isotope record. **Paleoceanography**, 31: 847-865

Thierstein, H. R. (1976) Mesozoic calcareous nannoplankton biostratigraphy of marine sediments. **Marine Micropaleontology,** 1: 325-362

Thierstein, H.R. (1981) "Late Cretaceous nannoplankton and the change at the Cretaceous-Tertiary boundary." In Warme, J.E., Douglas, R.G. and Winterer, E.L. (eds.) **The Deep Sea Drilling Project: a decade of progress**. Tulsa: Society of Economic Paleontologists and Mineralogists. pp. 355-394

Thierstein, H.P. (1980) Selective dissolution of Late Cretaceous and earliest Tertiary calcareous nannofossil: experimental evidence. **Cretaceous Research**, 2: 2-12

Thöle, H., Bornemann, A, Heimhofer, U., Luppold, F.W., Blumenberg, M., Dohrmann, R. and Erbacher, J. (2019) Using high−resolution XRF analyses as a sequence stratigraphic tool in a mudstone−dominated succession (Early Cretaceous, Lower Saxony Basin, Northern Germany). **The Depositional Research**, 1-23

Torsvik, H. T. and Cocks, L. R. (2016) **Earth History and Palaeogeography**. Cambridge: Cambridge University Press. pp. 219-239

Vahrenkamp, V.C. (2010) Chemostratigraphy of the Lower Cretaceous Shu'aiba Formation: a $d^{13}C$ reference profile for the Aptian Stage from the southern Neo-TethysOcean. **GeoArabia Special Publication**, 4: 107-137

Varol, O., (1989) Quantitative analysis of the Arkhangelskiella cymbiformis group and biostratigraphic usefulness in the North Sea Area. **Journal of Micropalaeontology**, 8: 131-134

Varol, O. (1992) Revision of the Polycyclolithaceae and its contribution to Cretaceous biostratigraphy. **Newsletters on Stratigraphy**, 27 (3): 93-127

Varol, O. (1996) Nannofossil biostratigraphy of Petroleum Development Oman wells Al Husain-1, Musallim-2 and Yibal-5. Internal Varol Research report for PDO.

Varol, O. (1997) Nannofossil biostratigraphy of Petroleum Development Oman wells Mabrouk-2 & Al Ghubar-15. Internal Varol Research report for PDO.

Voigt, S., Aurag, A., Leis, F. and Kaplan, U. (2007) Late Cenomanian to Middle Turonian high-resolution carbon isotope stratigraphy: new data from the Munsterland Cretaceous Basin, Germany. **Earth and Planetary Science Letters**, 235: 196-210

Voigt, S., Friedrich, O., Norris, R.D. and Schonfeld, J. (2010) Campanian-Maastrichtian carbon isotope stratigraphy: shelf-ocean correlation between the European shelf sea and the tropical Pacific Ocean. **Newsletters on Stratigraphy**, 44: 57-72

Voigt, S., Gale, A.S., Jung, C. and Jenkyns, H.C. (2012) Global correlation of Upper Campanian-Maastrichtian successions using carbon-isotope stratigraphy: development of a new Maastrichtian timescale. **Newsletters on Stratigraphy**, 45 (1): 25-53

Wagreich, M. (1992) "A review of low-latitude Tethyan calcareous nannoplankton assemblages of the Cretaceous". In Kollmann, H.A. and Zapfe, H. (eds.) **New Aspects on Tethyan Cretaceous Fossil Assemblages**. Vienna: Springer-Verlag GmbH. pp. 45-55

Warburton, J., Burnhill, T.J., Graham R. and Isaac K.P. (1990) The evolution of the Oman Mountain Foreland Basin. In: Roburtson, A.H.F., Searle, M. P. and Ries, A. C. (eds.) **The Geology and Tectonics of the Oman Region.** London: Geological Society Publishing House. pp. 419-427

Warren, C.J., Parrish, R.R., Waters, D.J. and Searle, M.P. (2005) Dating the geologic history of Oman's Semail ophiolite: insights from U–Pb geochronology. **Contributions to Mineralogy and Petrology**, 150: 403-422

Watkins, D.K., Wise, S.W., Pospichal, J.J. and Crux, J. (1996) "Upper Cretaceous calcareous nannofossil biostratigraphy and paleoceanography of the Southern Ocean." In Moguilevsky, A. and Whatley, R. (eds.) **Microfossil and Oceanic Environments**. University of Wales: Aberystwyth Press. pp. 355-381

Weltje G.J and Tjallingii, R. (2008) Calibration of XRF core scanners for quantitative geochemical logging of sediment cores: Theory and application. **Earth and Planetary Science Letters**, 274: 423-438

Wendler, I. (2013) A critical evaluation of carbon isotope stratigraphy and biostratigraphic implications for Late Cretaceous global correlation. **Earth Science Reviews**, 126: 116-146

Williams, J. R. and Bralower, J. (1995) Nannofossil assemblages, fine fraction stable isotopes, and the paleoceanography of the Valanginian−Barremian (Early Cretaceous) North Sea Basin. **Paleoceanography**, 10 (4): 815-839

Wind, F. H. (1979) "Maestrichtian–Campanian nannofloral prov inces of the southern Atlantic and Indian Oceans" In Talwani, M., Hay, W. W. and Ryan, W. B. F. (eds.) **Deep drilling results in the Atlantic Ocean: continental margins and paleoenvironment.** Washington DC: American Geophysical Union. pp.123–137

Wise, S.W. (1983) Mesozoic and Cenozoic calcareous nannofossil recovered by Deep Sea Drilling project Leg 71 in the Falkland Plateau Region, Southwest Atlantic Ocean. I**nitial Reports of the Deep Sea Drilling Project**, 71: 481-550

Wise, S.W. (1988) Mesozoic-Cenozoic history of calcareous nannofossil in the region of the Southern Ocean. **Palaeogeography, Palaeoclimatology, Palaeoecology**, 67: 157-179

Wohlwend, S., Hart, M. and Weissert, H. (2016) Chemostratigraphy of the Upper Albian to mid-Turonian Natih Formation (Oman) - how authigenic carbonate changes a global pattern. **The Depositional Record**, 2 (1): 97-117

Wolfgring, E., Wagreich, M., Dinarès-Turell, J., Yilmaz, I.O. and Bohm, K. (2017) Plankton biostratigraphy and magnetostratigraphy of the Santonian-Campanian boundary interval in the Mudurnu-Goynük Basin, northwestern Turkey. **Cretaceous Research**, 87: 296-311

Wolfgring, E., Wagreich, M., Dinarès-Turell, J., Gier, S., Böhm, K., Sames, B., Spötl, C. and Popp, F. (2018) The Santonian-Campanian boundary and the end of the Long Cretaceous Normal Polarity-Chron: Isotope and plankton stratigraphy of a pelagic reference section in the NW Tethys (Austria). **Newsletters on Stratigraphy**, 51 (4): 1-32

Woollam, R., Packer S.R. and Varol O. (1999) Biostratigraphic analysis of selected intervals from Lekhwair wells L-319, L-70 and LE-2, Oman. Internal Millennia for PDO.

Wyton, J. and Bown, P. (2007) Palaeoecological trends in Turonian- Coniacian (Late Cretaceous) calcareous nannofossils from Chalk Group sections, SE England. **Journal of Nannoplankton Research**, 29: 31-37

Young, J.R., Bergen, J.A., Bown, P.R., Burnett, J.A., Fiorentino, A., Jordan, R.W., Kleijne, A., van Niel, B.E., Ton Romein, A.J. and von Salis, K. (1997) Guidelines for coccolith and calcareous nannofossil terminology. **Paleontology***,* 40: 875–912

Ziegler, M. A. (2001) Late Permian to Holocene Paleofacies Evolution of the Arabian Plate and its Hydrocarbon Occurrences. **GeoArabia,** 6 (3): 445- 504

Appendices

Appendix A. List of total number of samples analysed and/or interpreted in this study.

Samples	Study Wells													Total Samples
	W-1	**W-2**	**W-3**	**W-4**	**W-5**	**W-6**	**W-7**	**W-8**	**W-9**	**W-10**	**W-11**	**W-12**	**W-13**	
Number of Samples														
Nannofossil smear-slides	20	17	10	50	44	22	30	24	13	11	8	11	13	273
Stable isotopes				91			72		22	11	8			204
XRF				91			72		22	11	8			204
Samples of microfossil data*	44			52	25		59							180
Total Samples	20	17	10	232	44	22	174	24	57	33	24	11	13	681
Total Samples (including microfossil samples)	64	17	10	284	69	22	233	24	57	33	24	11	13	861

* Samples analysed by PDO micropalaeontologists, data is integrated and interpreted in this study.

** Samples have been found to cover Palaeocene sediments and are excluded from the interpretations of the study.

Appendix B. Samples analysed for nannofossil (smear-slides) for other Formations, information used in introduction section only.

Well	Number of samples	Formation
F-1	4	Natih Formation
F-175	7	Natih Formation
MM-824	4	Natih Formation
MM-730	12	Natih Formation
AG-25	6	Natih Formation
MM-730	3	Natih Formation
L-27	3	Rayda Formation
L-6	3	Rayda Formation
AH-47	5	Salil Formation
CH- 1	4	Salil Formation
F-1	3	Salil Formation
HBB-3	2	Salil Formation
Shurooq-2	3	Nahr Umr Formation
Total Samples	**56**	

Appendix C. Results of nannofossil analysis from core and cutting samples from Natih to Salil Formations, information used in introduction section only.

Well Name	Sample Depth (m)	Sample Type	Sample Lithology	Foramtion	Nannofossil Recovery	Comments
F-1H1	768.62	CO	Gray shale	Natih G	Barren	
F-1H1	770.45	CO	Green shale	Natih G	Very low	*Micrantholithus* spp. recorded
F-1H1	771.25	CO	Green shale	Natih G	Barren	-
F-1H1	771.70	CO	Green shale	Natih G	Barren	-
F-175H1	573.38	CO	Hard carbonate with HC content	Natih A	Barren	-
F-175H1	599.34	CO	Hard carbonate with HC content	Natih B	Barren	-
F-175H1	613.60	CO	Hard carbonate with HC content	Natih B	Low to moderate	Dominated by *Watznaueria barnesiae*
F-175H1	646.11	CO	Carbonate	Natih B	Barren	-
F-175H1	692.56	CO	Carbonate	Natih C	Barren	-
F-175H1	733.70	CO	Carbonate	Natih D	Barren	-
MM-824 H1	860.74	CO	Green shale	Natih F/G	Barren	-
MM-824 H1	863.31	CO	Green shale	Nahr Umr	Barren	-
MM-824 H1	864.40	CO	Brown, very soft shale	Nahr Umr	Barren	-
MM-824 H1	866.18	CO	Green shale	Nahr Umr	Very low	Dominated by *Quadrum* spp.
MM-730 H1	906.38	CO	Brown, very soft shale	Natih C	Barren	-
MM-730 H1	909.93	CO	Shale	Natih C/D	Barren	-
MM-730 H1	913.45	CO	Green, very soft shale	Natih D	Barren	-
MM-730 H1	920.44	CO	Green shale	Natih E Shale	Barren	-
MM-730 H1	924.24	CO	Green, very soft shale	Natih E Shale	Barren	-
MM-730 H1	929.05	CO	Green shale	Natih E Shale	Barren	-
MM-730 H1	930.28	CO	Green shale	Natih E Shale	Barren	-
MM-730 H1	972.00	CO	Gray shale	Natih E Carbonate	Barren	-
MM-730 H1	978.23	CO	Gray, hard shale	Natih E Carbonate	Barren	-
MM-730 H1	920	CU	Mixture of purple and green shale	Natih E Shale	Low	Only green shale sampled
MM-730 H1	933	CU	Mixture of purple and green shale	Natih E Shale	Barren	Only purple shale sampled

Well Name	Sample Depth (m)	Sample Type	Sample Lithology	Foramtion	Nannofossil Recovery	Comments
MM-730 H1	952	CU	Mixture of different colours of shale	Natih E Carbonate	Low	Only finest fraction sampled
AG-25H1	485	CU	Mixture of green and brown shale	Natih C	moderate	Only brown shale sampled
AG-25H1	495	CU	Very sandy shale	Natih C	Very low	-
AG-25H1	620	CU	White chalk	Natih E	Barren	-
AG-25H1	630	CU	Green, soft shale	Natih E	Moderate	-
AG-25H1	660	CU	silty chalky slightly green shale	Natih F	Barren	-
AG-25H1	670	CU	Shale	Natih G	Low	-
Shurooq-2	704-736	CO	Green, flaky, shale	Nahr Umr	Low	*Marthasterites* spp. recorded
Shurooq-2	704-736	CO	Green, flaky, shale	Nahr Umr	Low	Eiffellithales spp. recorded
Shurooq-2	704-736	CO	Green, flaky, shale, shell fossil fragments and *orbitolina*	Nahr Umr	Low	Eiffellithales spp. recorded
L-27H1	2113.483	SWS	white, powder (chalk?)	Rayda	Barren	-
L-27H1	2131.162	SWS	green, flaky, silty, shale	Rayda	Barren	-
L-27H1	2219.249	SWS	green, silt	Rayda	Barren	-
L-6	2140	CU	mixture of green and brown cuttings. Pale brown fraction sampled, hard	Rayda	Barren	-
L-6	2150	CU	mixture of green and brown cuttings. green fraction sampled, very soft	Rayda	Barren	-
L-6	2200	CU	mainly pale brown cuttings. Pale brown fraction sampled, soft, chalky	Rayda	Barren	-
AH-47H1	2151.80	CO	Shale	Salil	Barren	-
AH-47H1	2142.90	CO	Shale	Salil	Barren	-
AH-47H1	2154.80	CO	Shale	Salil	Barren	-
AH-47H1	2138	CO	Shale	Salil	Barren	-
AH-47H1	2248.1	CO	Shale	Salil	Barren	-

Well Name	Sample Depth (m)	Sample Type	Sample Lithology	Foramtion	Nannofossil Recovery	Comments
CH- 1 (W.MIAI DIN)	33-42	CO	Shale	Salil	Barren	-
CH- 1 (W.MIAI DIN)	155-163	CO	Shale	Salil	Low - Moderate	-
CH- 1 (W.MIAI DIN)	190-194	CO	Shale	Salil	Low - Moderate	-
CH- 1 (W.MIAI DIN)	190-194	CO	Shale	Salil	Barren	-
F-1H1	1452.63	CO	Shale	Salil	Barren	-
F-1H2	1461.09	CO	Shale	Salil	Barren	-
F-1H3	1530.80	CO	Shale	Salil	Barren	-
HBB-3H 1	2210.28	CO	Shale	Salil	Low - Moderate	-
HBB-3H 2	2218.12	CO	Shale	Salil	Barren	-

Appendix D. Bulk rock carbon and oxygen isotope analysis.

Sample depth	Lithostratigraphy	$\delta^{13}C$	$\delta^{18}O$
W-4			
21.031	Arada	0.94	-3.89
27.127	Arada	1.55	-3.85
35.966	Arada	1.91	-3.81
42.06	Arada	1.80	-3.91
48.158	Arada	2.04	-3.84
56.998	Arada	1.41	-4.70
60.046	Arada	1.71	-4.08
63.094	Arada	1.62	-3.91
66.142	Arada	1.71	-3.87
71.933	Arada	1.53	-4.33
78.029	Arada	1.28	-3.82
81.077	Arada	0.69	-4.76
86.868	Arada	1.72	-3.92
89.916	Arada	1.82	-3.85
92.964	Arada	1.34	-3.67
105.156	Shargi	0.66	-4.27
117.04	Shargi	0.64	-4.44
123.14	Shargi	1.02	-5.94
131.98	Shargi	1.28	-6.68
167.945	Shargi	2.32	-6.46
180.137	Shargi	2.65	-6.85
213.1	Shargi	0.41	-8.89
227.99	Shargi	2.88	-7.72
237.134	Shargi	-0.22	-6.90
248.412	Shargi	1.86	-5.33
262.128	Shargi	1.52	-5.07
274.32	Shargi	1.64	-4.55
291.084	Shargi	1.68	-5.06
307.848	Shargi	1.67	-5.03
329.184	Shargi	1.68	-4.65
344.424	Shargi	1.89	-5.94

Sample depth	Lithostratigraphy	$\delta^{13}C$	$\delta^{18}O$
359.664	Shargi	0.28	-5.55
377.952	Shargi	0.39	-5.47
391.973	Shargi	0.53	-5.24
408.432	Shargi	0.75	-4.71
445.008	Shargi	1.41	-4.90
463.906	Shargi	-0.72	-5.52
480.06	Shargi	1.29	-5.30
495.3	Shargi	0.70	-5.45
515.112	Shargi	1.66	-5.47
524.256	Shargi	-0.10	-4.39
541.02	Shargi	0.83	-4.93
571.5	Shargi	0.84	-4.98
586.74	Shargi	1.56	-5.36
609.6	Shargi	2.24	-4.68
624.84	Shargi	2.05	-5.30
646.176	Shargi	1.72	-5.13
656.844	Shargi	0.63	-5.63
673.608	Shargi	1.92	-5.10
688.848	Shargi	1.33	-5.22
704.088	Shargi	-0.97	-5.48
719.328	Shargi	-12.29	-3.80
734.568	Shargi	1.95	-4.95
749.808	Shargi	0.54	-5.30
772.668	Shargi	0.72	-5.27
789.432	Shargi	0.48	-5.69
804.672	Shargi	0.84	-5.72
819.912	Shargi	0.54	-5.62
835.152	Shargi	-0.01	-5.14
850.392	Shargi	0.24	-5.75
865.632	Shargi	-0.71	-6.14
880.872	Shargi	0.53	-5.93
896.112	Shargi	-1.37	-5.95
911.352	Shargi	-0.12	-5.73
944.88	Shargi	0.80	-5.82

Sample depth	Lithostratigraphy	$\delta^{13}C$	$\delta^{18}O$
963.168	Shargi	-1.36	-5.65
978.408	Shargi	-4.65	-5.36
996.696	Shargi	-1.02	-6.36
1011.936	Shargi	-1.03	-5.87
1033.272	Shargi	-1.62	-6.39
1043.94	Shargi	-2.30	-6.43
1059.18	Shargi	-0.81	-6.15
1074.42	Shargi	-0.61	-5.33
1089.66	Shargi	-1.74	-6.17
1104.9	Shargi	-0.91	-5.42
1120.14	Shargi	0.10	-5.31
1135.38	Shargi	-3.21	-5.60
1191.9	Shargi	0.06	-5.35
1203.96	Shargi	0.54	-4.88
1234.44	Shargi	0.79	-5.29
1254.252	Shargi	0.50	-4.89
1264.92	Shargi	0.59	-5.31
1280.16	Shargi	0.64	-5.40
1295.4	Shargi	0.58	-5.28
1325.88	Shargi	0.88	-5.57
1341.12	Shargi	-0.09	-7.66
1348.74	Natih	0.89	-7.17
1362.15	Natih	2.47	-5.76
1401.166	Natih	1.74	-5.35
W-7			
400	Shammar	1.78	-2.86
410	Shammar	1.60	-2.93
420	Arada	1.62	-2.81
430	Arada	1.49	-2.96
440	Arada	0.77	-3.42
450	Arada	0.90	-3.25
460	Arada	1.95	-3.56
520	Shargi	2.65	-3.11
530	Shargi	2.51	-3.06

Sample depth	Lithostratigraphy	$\delta^{13}C$	$\delta^{18}O$
540	Shargi	2.49	-3.18
550	Shargi	2.48	-3.16
560	Shargi	2.20	-2.87
570	Shargi	1.92	-3.01
580	Shargi	1.77	-2.91
610	Shargi	1.56	-2.94
620	Shargi	0.74	-3.53
630	Shargi	1.00	-3.39
640	Shargi	0.92	-3.84
650	Shargi	-0.53	-4.64
660	Shargi	1.68	-4.03
670	Shargi	1.18	-3.89
680	Shargi	1.83	-4.74
690	Shargi	0.81	-4.38
700	Shargi	1.01	-4.29
710	Shargi	0.65	-4.17
720	Shargi	0.54	-3.99
730	Shargi	0.02	-4.70
740	Shargi	-0.55	-4.74
750	Shargi	-0.95	-4.85
760	Shargi	0.82	-4.03
770	Shargi	-0.43	-4.55
780	Shargi	-0.67	-4.57
790	Shargi	0.13	-4.21
800	Shargi	-0.47	-4.86
810	Shargi	-0.98	-4.66
820	Shargi	0.70	-4.79
830	Shargi	-0.68	-5.76
840	Shargi	-0.04	-4.29
850	Shargi	-0.35	-4.24
860	Shargi	-2.30	-5.86
870	Shargi	-1.65	-4.94
880	Shargi	-3.21	-4.54
890	Shargi	-1.43	-4.94

Sample depth	Lithostratigraphy	$\delta^{13}C$	$\delta^{18}O$
900	Shargi	-1.86	-5.01
910	Shargi	-0.84	-5.72
920	Shargi	-2.14	-5.67
930	Shargi	-1.56	-3.58
935	Shargi	-2.59	-3.79
940	Shargi	-0.76	-4.39
950	Shargi	-1.77	-4.61
960	Shargi	0.25	-4.35
970	Shargi	-0.42	-4.98
975	Shargi	0.05	-4.79
980	Shargi	0.35	-4.62
985	Shargi	0.56	-4.86
990	Shargi	0.10	-5.14
995	Shargi	1.00	-4.23
1000	Shargi	0.71	-4.79
1005	Shargi	1.10	-4.38
1010	Shargi	1.09	-4.63
1015	Shargi	1.23	-4.47
1020	Shargi	0.87	-6.04
1025	Shargi	1.16	-6.00
1030	Shargi	0.98	-5.76
1035	Shargi	0.98	-5.85
1040	Shargi	0.84	-6.11
1045	Shargi	0.92	-4.94
1050	Shargi	0.74	-5.62
1055	Shargi	1.23	-4.89
1060	Natih	1.53	-4.92
1065	Natih	2.54	-5.56
1070	Natih	3.34	-5.01
W-9			
432	Shammar	-10.49	-11.37
435	Shammar	0.87	-3.56
438	Arada	2.51	-3.45
482	Arada	2.72	-3.48

Sample depth	Lithostratigraphy	$\delta^{13}C$	$\delta^{18}O$
487	Arada	2.33	-3.29
493	Arada	2.23	-3.69
497	Arada	2.19	-3.49
500	Arada	2.30	-3.31
506	Arada	2.16	-3.34
510	Arada	1.80	-3.63
514	Arada	1.96	-3.28
520.5	Arada	1.86	-3.21
523	Arada	1.93	-3.25
529	Arada	1.31	-3.30
532	Arada	1.44	-3.44
536	Arada	1.57	-3.82
538	Shargi	1.36	-3.58
541	Shargi	1.49	-3.23
545	Shargi	1.40	-3.86
549.5	Shargi	1.66	-3.52
554.5	Shargi	3.40	-3.78
559.5	Shargi	-14.50	-3.52
W-10			
610*	Arada	-	-
615	Arada	-5.28	-6.72
630	Shargi	2.19	-3.87
635	Shargi	0.17	-6.96
640	Shargi	0.94	-5.13
645	Shargi	2.02	-5.37
650	Natih	1.98	-5.86
655	Natih	4.74	-4.09
W-11			
685.7	Fiqa	3.32	-4.32
708.1	Fiqa	2.21	-3.65
729.1	Fiqa	3.70	-3.64
761.5	Fiqa	1.89	-4.98
787.9*	Fiqa	-	-
807.3	Fiqa	2.74	-4.15

Sample depth	Lithostratigraphy	$\delta^{13}C$	$\delta^{18}O$
825.8	Fiqa	-35.55	12.28
839.2	Fiqa	-43.01	11.11
841	Fiqa	-0.13	-4.93
859.5	Fiqa	-0.89	-5.34
877*	Fiqa	-	-
* erroneous result even with repeated runs of samples.			

Appendix E. Elements concentration (from XRF analysis).

W-4 XRF data (%)

Depth (m)	Ca	Si	Al	Fe	Mg	K	Sr	Na	Cl	P	S	La	Ce
21.03	47.73	9.19	0.84	0.75	0.37	0.17	0.15	0.15	0.08	0.06	0	0	0
27.13	46.81	9.24	0.99	0.94	0.51	0.23	0.19	0.31	0.1	0	0.14	0.12	0
35.96	47.15	7.4	1.18	1.13	0.51	0.18	0.17	0.41	0.24	0	0.4	0	0.11
42.06	48.24	6.83	1	1.71	0.46	0	0.23	0.44	0.35	0.06	0.28	0	0
48.16	46.17	7.68	1.06	1.21	0.59	0.21	0.18	0.42	0.34	0.04	0.42	0	0
56.99	51.59	5.32	0.69	0.75	0.44	0.15	0.19	0.16	0.07	0	0.16	0	0
60.05	47.84	8.51	0.95	0.75	0.44	0.2	0.18	0.35	0.3	0	0.29	0	0
63.09	45.29	8.95	1.21	1.07	0.47	0.19	0.16	0.36	0.37	0	0.36	0	0
66.14	44.98	9.53	0.86	1	0.57	0	0.16	0.31	0.26	0	0.3	0	0
71.93	45.5	9.45	0.91	0.83	0.37	0.17	0.17	0.23	0.18	0.06	0.04	0	0
78.03	43.73	9.49	1.01	0.96	0.64	0.24	0.16	0.33	0.3	0	0.27	0	0
81.07	46.03	8.66	1.1	0.94	0.58	0.16	0.18	0.22	0.16	0	0.34	0	0
86.87	46.92	9.11	0.69	0.55	0.39	0.15	0.16	0.26	0.14	0.04	0.2	0	0.15
89.92	48.98	6.87	0.82	0.87	0.47	0.23	0.17	0	0.08	0	0.27	0	0
92.96	49.85	4.96	0.75	0.84	0.47	0.26	0.15	0.3	0	0	0.17	0	0.18
105.16	22.96	4.36	1.19	25.9	0.25	0.2	0.06	0	0.11	0.16	11.01	0	0
117.04	25.5	3.47	0.83	21.44	0.34	0.16	0.08	0	0	0.22	10.6	0	0
123.14	39.19	7.04	2.13	7.29	0.44	0.29	0.12	0	0	0.15	2.35	0	0
131.98	28.8	10.79	4.1	7.41	0.39	0.64	0.11	0.2	0	0.19	1.73	0	0
167.95	38.54	6.18	2.76	9.99	0.44	0.42	0.12	0	0	0	3.76	0	0
180.14	34.44	8.18	3.67	7.15	0.44	0.41	0.13	0	0.09	0	1.67	0	0
213.1	42.68	5.22	1.26	6.84	0.39	0.24	0.12	0	0	0	1.64	0	0
228	38.11	7.97	3.51	6.5	0.44	0.37	0.15	0.26	0	0.12	1.19	0	0
237.13	20.29	13.93	5.8	8.36	0.6	0.89	0.11	0.15	0	0	0.68	0	0
248.4	8.59	15.9	7.67	8.71	0.56	1.02	0.11	0.52	0.36	0	0.52	0	0.2
262.13	17.12	14.68	7.1	7.8	0.6	1	0.14	0.53	0.3	0	0.37	0	0
274.32	7.55	16.32	6.98	7.17	0.62	0.99	0.25	0.67	0.33	0	0.99	0	0
291.08	3.6	17.45	7.76	7.84	0.57	0.98	0.22	0.6	0.35	0	0.41	0	0.11
307.85	3.6	17.45	7.76	7.84	0.57	0.98	0.22	0.6	0.35	0	0.41	0	0.11
329.18	3.22	16.48	7.37	9.03	0.59	0.74	0.24	0.53	0.23	0	0.48	0	0
344.42	10.28	14.86	6.58	7.62	0.5	0.75	0.3	0.5	0.31	0	0.43	0	0

W-4 XRF data (%)

Depth (m)	Ca	Si	Al	Fe	Mg	K	Sr	Na	Cl	P	S	La	Ce
359.66	4.39	17.27	7.48	8.92	0.48	1.03	0.21	0.47	0.34	0.09	0.48	0	0
377.95	6.66	17.37	7.19	7.48	0.52	1.02	0.22	0.64	0.26	0.05	0.45	0	0
391.97	5.41	17	7.02	8.72	0.59	1.09	0.2	0.52	0.32	0.09	0.46	0	0
403.86	11.29	14.33	7.25	8.81	0.53	0.96	0.14	0.61	0.28	0	0.95	0	0
408.43	2.17	18.67	8.26	8.2	0.57	1.09	0.2	0.45	0.37	0	0.62	0	0
445.01	5.43	16.52	7.76	8.46	0.49	0.9	0.24	0.52	0.32	0	0.38	0	0
463.906	2.9	17.16	7.03	8.35	0.54	1.02	0.2	0.49	0.42	0	0.4	0	0
480.06	11.08	15.17	6.83	7.42	0.51	0.72	0.38	0.45	0.41	0	0.52	0	0
495.3	6.24	17.56	7.73	9.51	0.66	0.76	0.18	0.63	0.56	0	0.32	0	0
515.11	26.85	11.01	4.78	5	0.56	0.71	0.12	0.43	0.37	0.08	0.34	0	0
524.26	5.58	15.39	7.78	17.04	0.81	0.93	0.11	0.67	0.4	0	0.34	0	0
541.02	9.51	15.23	6.68	8.36	0.66	1.01	0.3	0.51	0.47	0	0.78	0	0
571.5	9.26	16.44	7.56	7.82	0.54	1.19	0.23	0.56	0.44	0	0.37	0	0
586.74	24.04	11.87	5.2	5.25	0.65	0.77	0.13	0.48	0.25	0.12	0.39	0	0.11
609.6	8.53	15.89	7.69	7.74	0.51	0.82	0.22	0.52	0.2	0	0.49	0	0
624.84	16.81	13.69	5.3	6.02	0.62	0.74	0.12	0.58	0.37	0.08	0.45	0	0.09
646.18	4.88	16.56	7.67	8.77	0.62	0.86	0.22	0.44	0.3	0.07	0.43	0	0.09
656.84	17.83	14.06	6.44	7.54	0.63	0.79	0.1	0.42	0.2	0.07	0.47	0	0
673.61	5.2	17.24	7.99	8.07	0.52	0.98	0.21	0.68	0.35	0.07	0.36	0	0
688.85	4.84	18.08	6.94	8.06	0.54	1.04	0.22	0.5	0.36	0	0.6	0	0
704.08	3.26	17.82	8	8.29	0.54	1.02	0.14	0.54	0.29	0.06	1.6	0	0
719.33	8.26	16.23	7.14	7.79	0.64	0.84	0.17	0.52	0.23	0.06	1.13	0	0
734.57	5.24	18.07	7.43	7.52	0.61	0.96	0.21	0.51	0.22	0	0.35	0	0.03
749.81	2.32	17.73	7.95	6.47	0.44	0.92	0.15	0.41	0.42	0	0.5	0	0
772.67	8.76	16.73	7.14	7.79	0.55	0.89	0.18	0.37	0.26	0	0.37	0	0
789.43	5.98	16.1	7.91	8.94	0.42	0.96	0.2	0.55	0.24	0.05	0.29	0	0
804.67	12.01	16.16	6.37	6.84	0.5	0.97	0.23	0.4	0.29	0	0.27	0	0.1
819.91	2.37	16.97	7.4	6.93	0.46	1.17	0.16	0.39	0	0.05	0.38	0	0
835.15	2.98	17.01	7.94	9.16	0.58	1.05	0.16	0.39	0.31	0	0.19	0	0
850.39	6.74	16.88	7.67	7.27	0.55	0.94	0.2	0.43	0	0.06	0.52	0	0
865.63	7.17	16.63	7.85	9.69	0.58	1.17	0.08	0.48	0.31	0.05	0.38	0.11	0
880.87	5.99	16.42	7.68	7.4	0.47	0.93	0.2	0.38	0	0	0.35	0	0
896.11	2.76	18.39	8.63	8.17	0.52	0.91	0.11	0.44	0.36	0	0.34	0.13	0.13

W-4 XRF data (%)

Depth (m)	Ca	Si	Al	Fe	Mg	K	Sr	Na	Cl	P	S	La	Ce
911.35	3.21	16.77	7.28	7.52	0.44	1	0.14	0.41	0.24	0	0.79	0	0.14
944.88	9.17	15.94	7.4	8.41	0.54	1.02	0.09	0.43	0.31	0	0.53	0.19	0
963.17	8.08	14.13	6.43	7.56	0.49	0.97	0.2	0.41	0.26	0.06	0.96	0	0
978.41	3.62	16.46	7.58	8.37	0.53	1.12	0.11	0.38	0.18	0.07	1.4	0	0.13
996.69	3.53	17.08	8.18	7.71	0.49	1.16	0.12	0.4	0	0	0.61	0	0
1011.94	3.11	17.53	8.35	8.83	0.47	1.15	0.12	0.49	0.28	0	0.4	0	0.04
1033.27	3.89	18.5	8.05	8.14	0.58	1.33	0.11	0.44	0.21	0	0.51	0	0
1043.94	4.08	17.7	8.3	8.53	0.55	1.2	0.12	0.36	0.21	0	1.21	0	0
1059.18	2.18	18.19	8.78	6.96	0.49	1.16	0.1	0.48	0.25	0	0.2	0	0
1074.42	2.24	16.64	8.13	8.37	0.48	1.32	0.1	0.45	0.32	0	0.47	0	0
1089.66	3.65	18.52	8.59	8.29	0.59	1.15	0.09	0.46	0.34	0	0.42	0	0
1104.9	2.97	17.61	8.44	8.01	0.5	1.21	0.1	0.4	0.41	0	0.48	0	0
1120.14	2.8	17.94	8.97	7.55	0.51	1.24	0.12	0.36	0.34	0.07	0.35	0	0
1135.38	2.51	16.62	7.83	22.87	0.96	0.75	0.03	0.51	0.25	0	0.18	0	0
1191.9	4.84	18.31	7.8	9.42	0.53	1.3	0.1	0.42	0	0.25	0.37	0	0
1203.96	10.26	18.15	5.31	6.42	0.51	1.5	0.14	0.42	0.2	0	0.8	0.09	0
1234.44	10.63	18.6	5.48	6.01	0.59	1.94	0.14	0.43	0.24	0	0.49	0	0.13
1254.25	10.02	19.81	4.41	5.46	0.57	1.92	0.13	0.34	0	0	0.36	0.09	0
1264.92	11.33	19.11	4.71	5.86	0.59	1.91	0.13	0.32	0.23	0	0.34	0	0
1280.16	11.37	18.15	4.61	6.16	0.63	1.66	0.13	0.32	0.25	0.3	0.18	0	0
1295.4	9.81	16.85	4.47	5.46	0.47	2.13	0.13	0.34	0.34	0.08	0.37	0	0
1310.64	17.65	14.55	5.2	6.03	0.49	1.65	0.07	0.34	0.32	0.09	0.4	0	0.12
1325.88	12.35	15.49	8.74	7.33	0.37	1.19	0.06	0.32	0	0.1	0.36	0.14	0
1341.12	3.28	9.36	7.33	10.98	0.9	0.85	0.71	0	0.08	0.8	4.93	0	0
1348.79	1.43	15.34	8.22	7.16	0.28	1.69	0.05	0.36	0	0	2.74	0	0
1362.15	35.74	9.06	3.95	6.57	0.48	0.88	0.08	0	0	0	0.8	0	0
1401.17	16.49	15.52	5.77	5.97	0.57	1.51	0.04	0.3	0.15	0	0.31	0	0

W-4 XRF data (%) continued

Depth (m)	Ti	Sc	Zn	Zr	V	Ba	Mn	Co	Cu	Cr	Mo	Rb	Ni
21.03	0	0	0	0	0	0.16	0	0	0	0	0	0	0
27.13	0	0	0	0	0	0	0	0	0	0	0	0	0

W-4 XRF data (%) continued

Depth (m)	Ti	Sc	Zn	Zr	V	Ba	Mn	Co	Cu	Cr	Mo	Rb	Ni
35.96	0.14	0	0	0	0	0	0	0	0	0	0	0	0
42.06	0	0.06	0.04	0	0	0	0	0	0	0	0	0	0
48.16	0.16	0	0	2 PPM	0	0	0	0	0	0	0	0	0
56.99	0	0	0	0	0.04	0	0	0	0	0	0	0	0
60.05	0	0.06	0	0	0	0	0	0	0	0	0	0	0
63.09	0	0	0	5 PPM	0	0	0	0	0	0	0	0	0
66.14	0	0.04	0.07	0	0	0	0	0	0	0	0	0	0
71.93	0.09	0	0	7 PPM	0	0	0	0	0	0	0	0	0
78.03	0	0	0	56 PPM	0	0	0	0	0	0	0	0	0
81.07	0	0.06	0.02	6 PPM	0.03	0.14	0	0	0	0	0	0	0
86.87	0.08	0	0	0	0	0	0	0	0	0	0	0	0
89.92	0	0	0	0	0	0	0	0	0	0	0	0	0
92.96	0.11	0	0	12 PPM	0	0	0	0	0	0	0	0	0
105.16	0	0	0.07	0	0	0.08	0	0	0	0	0	0	0
117.04	0.07	0	0.06	0	0	0	0	0	0.02	0	0	0	0
123.14	0.17	0	0.19	1 PPM	0.05	0.11	0.09	0	0	0	0	0	0
131.98	0.44	0.04	0.16	61 PPM	0	0.13	0.06	46 PPM	0	0	0	0	0
167.95	0	0	0.05	40 PPM	0	0	0	0	0	0	0	0	0
180.14	0.34	0	0.14	63 PPM	0	0	0.05	0	0	0	0	0	0
213.1	0.12	0	0.15	0	0	0	0.11	0	0.07	0	0	0	0
228	0.35	0	0.05	3 PPM	0	0	0.09	0	0	0	0	0	0
237.13	0.61	0.03	0.06	0.01	0.07	0	0.05	0	0.03	0	0	0	0
248.4	0.9	0	0	0.04	0	0	0.05	0	0	0.05	0	0	0
262.13	0.8	0	0	95 PPM	0	0.14	0.06	0	0	0	0	0	0
274.32	0.95	0	0.02	0	0	0	0.07	0	0	0	0	0	0
291.08	1.03	0	0.01	0	0	0.08	0.06	0	0	0	0	0	0

W-4 XRF data (%) continued

Depth (m)	Ti	Sc	Zn	Zr	V	Ba	Mn	Co	Cu	Cr	Mo	Rb	Ni
307.85	1.03	0	0.01	0	0	0.08	0.06	0	0	0	0	0	0
329.18	1.03	0	0.02	0	0	0	0.2	0	0	0	0	0	0
344.42	1.03	0	0.02	0	0.07	0	0.08	0	0	0.02	0	0	0
359.66	1.04	0.02	0.02	31 PPM	0.07	0	0.04	0	0	0	0	0	0
377.95	1.14	0	0	0	0.08	0.14	0	0	0	0	0	0	0
391.97	1.03	0.02	0.05	0	0	0	0.05	0	0	0	0.04	0	0
403.86	0.88	0	0	0.03	0.05	0	0.09	0	0	0	0	0	0
408.43	1.07	0	0.02	0	0.05	0	0.05	0	0	0	0	0	0
445.01	1	0	0.02	0	0.05	0	0.05	0	0	0	0	0.02	0
463.906	1.04	0.03	0.02	0	0	0	0.07	0	0	0.02	0.03	0	0
480.06	0.92	0	0.02	0	0.09	0	0.14	0	0	0.02	0	0	0
495.3	0.94	0	0.02	0.05	0.04	0	0.14	9 PPM	0	0	0	0	0
515.11	0.66	0	0	0.01	0	0	0.06	0	0	0	0	0	0
524.26	1.02	0.05	0.04	98 PPM	0.07	0	0.33	0	0	0	0	0	0
541.02	0.95	0.03	0.03	0.04	0.07	0	0.07	0	0	0.03	0	80	0
571.5	0.92	0	0	0	0.03	0	0.03	0	0	0	0	0	0
586.74	0.75	0	0.02	73 PPM	0	0	0.07	0	0	0	0	0	0
609.6	1.05	0	0.03	0	0.06	0	0.15	0	0	0.04	0	0	0
624.84	0.9	0	0	0.04	0.07	0	0.05	0	0	0	0	0	0
646.18	1.09	0.02	0	0	0.08	0	0.14	0	0	0	0	0	0
656.84	0.9	0	0.02	0.03	0.04	0	0.17	0	0	0	0	0	0
673.61	1.03	0	0.02	0	0	0	0.13	0	0	0	0	0	0
688.85	0.99	0	0	0	0.04	0.1	0.1	0	0	0.02	0	0	0
704.08	1.29	0	0.02	0.01	0	0	0.12	0	0	0.03	0	0	0.02
719.33	1.1	0	0.02	0	0	0	0.09	0	0	0	0	0	0
734.57	1.1	0	0	0	0	0.12	0	0	0	0.04	0.03	0	0
749.81	1.22	0	0.02	0	0.05	0	0	0	0	0.03	0	0	0
772.67	0.99	0.04	0.02	28 PPM	0	0	0.07	0	0	0	0	0	0
789.43	1.11	0.03	0	0	0.04	0.14	0.09	0	0	0	0	0	0
804.67	0.92	0	0	0.06	0	0.12	0.03	0	0	0.05	0	0	0

W-4 XRF data (%) continued

Depth (m)	Ti	Sc	Zn	Zr	V	Ba	Mn	Co	Cu	Cr	Mo	Rb	Ni
819.91	1.32	0	0.02	30 PPM	0.05	0	0.06	0	0	0	0	0	0
835.15	1.03	0	0.02	0	0	0	0.06	0	0	0	0	0	0
850.39	0.93	0	0.03	0	0	0	0.04	0	0	0.04	0	0.02	0
865.63	0.87	0	0.04	0.04	0	0	0.08	0	0	0	0	0	0
880.87	1.09	0	0.02	0	0.04	0	0	0	0	0	0	0	0
896.11	1.02	0	0.02	0.03	0	0	0.03	0	0	0.03	0	0	0
911.35	1.08	0	0	92 PPM	0	0.09	0	0	0	0	0	0	0
944.88	0.93	0	0.02	0.05	0	0	0	0	0	0	0	0	0
963.17	0.93	0	0.03	0	0	0	0.05	0	0	0	0	0	0
978.41	0.97	0	0.02	0.03	0.07	0	0	0	0	0	0	0	0
996.69	0.93	0	0.03	0.02	0	0	0	0	0	0	0	0.02	0
1011.94	1.11	0	0	0.01	0	0.09	0.05	1 PPM	0	0	0	0	0
1033.27	0.97	0	0	0.03	0	0	0.04	0	0	0.03	0	0.02	0
1043.94	0.95	0.02	0.03	0.02	0	0	0.04	0	0	0.03	0	0	0
1059.18	1.11	0.02	0.02	0.03	0	0.04	0.05	0	0	0	0	0.02	0
1074.42	0.95	0	0.02	0.01	0	0	0	0	0	0.04	0	0	0
1089.66	0.94	0	0.02	0.02	0	0	0	0	0	0	0	0	0
1104.9	0.9	0	0.02	0.01	0.04	0.12	0	0	0	0.02	0	0	0
1120.14	1.09	0	0	0	0	0	0	0	0	0	0	0	0
1135.38	0.76	0	0	0.02	0	0	0.29	0	0	0.03	0	0	0
1191.9	0.88	0.02	0.03	0.01	0	0	0.09	0	0	0	0	0	0
1203.96	0.54	0	0.03	0	0	0	0.12	0	0	0	0	0	0
1234.44	0.54	0	0	0	0.05	0	0.07	0	0	0	0	0	0
1254.25	0.47	0	0.02	0	0	0	0.04	0	0	0	0	0	0
1264.92	0.55	0	0.03	0	0	0	0.05	0	0	0	0.02	97	0
1280.16	0.57	0	0.02	0	0.04	0	0.07	0	0	0	0	0	0.02
1295.4	0.55	0	0.02	0	0	0	0.05	0	0	0	0	0.03	0
1310.64	0.64	0	0	0.03	0	0	0	0	0	0	0	91	0
1325.88	0.83	0	0.03	0.05	0	0	0	0	0	0.03	0	0	0
1341.12	0.4	0	0	0	0	35.81	0.18	0	0	0	0	0	0
1348.79	1.14	0	0	0.07	0	0	0.03	0	0	0	0	0.02	0

W-4 XRF data (%) continued

Depth (m)	Ti	Sc	Zn	Zr	V	Ba	Mn	Co	Cu	Cr	Mo	Rb	Ni
1362.15	0.47	0	0	0	0.04	3.26	0.09	0	0	0	0	0	0
1401.17	0.58	0	0	0.04	0	0.11	0.09	0	0	0	0	0	0

W-7 XRF data (%)

Depth (m)	Ca	Si	Al	K	Fe	Sr	Mg	Ba	Cl	S	Na	Ti	Ce
400	23.92	0.8	0.49	0.32	0.26	0.25	0.2	0.15	0.15	0.1	0.08	0	0
410	26.9	0.96	0.31	0.2	0.39	0.33	0.31	0	0.19	0.15	0.08	0	0
420	27.85	0.95	0.27	0.13	0.48	0.47	0.32	0	0.15	0.14	0	0.04	0
430	30.08	0.98	0.28	0.2	0.69	0.61	0.39	0	0.17	0.28	0	0.04	0.16
440	26.37	0.92	0.31	0	0.79	0.19	0.27	0	0.22	0.23	0	0	0.12
450	28.46	1.26	0.45	0.08	0.94	0.22	0.34	0.1	0.25	0.28	0	0.07	0
460	25	2.4	0.1	0.06	0.3	0.18	0.16	0	0.22	0.12	0.1	0	0
510	25.12	4.01	0.51	0.25	0.99	0.55	0.16	0	0.36	0.11	0	0	0
520	25.26	2.36	0	0.06	0.13	0.34	0.12	0	0.16	0.08	0	0	0
530	29.65	2.25	0.14	0	0.1	0.37	0.14	0	0.2	0.1	0.13	0	0
540	28.11	3.13	0	0.05	0.23	0.54	0.18	0	0.2	0.1	0	0	0
550	30.18	3.5	0.12	0	0.25	0.52	0.18	0.12	0.22	0	0	0.03	0
560	23.74	4.14	0.38	0.21	0.88	0.56	0.15	0	0.23	0	0	0	0
580	26.15	3.48	0.4	0.1	0.47	0.41	0.2	0	0.35	0.14	0.12	0.05	0
610	25.37	3.81	0.34	0.13	0.81	0.37	0.16	0	0.2	0.12	0	0.09	0
620	5.67	7.37	3.47	0.51	7.63	0.16	0.27	0	0.15	0.23	0	0.43	0
630	8.65	6.15	2.7	0.42	5.75	0.19	0.23	0.09	0	0.33	0.18	0.36	0
640	10.05	7.2	3.09	0.49	5.51	0.22	0.26	0	0.3	0.22	0.21	0.33	0
650	9.81	5.92	2.57	0.35	4.48	0.3	0.24	0	0.29	0.27	0	0.28	0
660	14.79	5.11	1.7	0.33	3.55	0.33	0.26	0	0	0.34	0	0.29	0
670	9.63	6.07	2.39	0.37	4.55	0.34	0.21	0	0.14	0.27	0	0.3	0
680	9.58	6.63	2.85	0.38	4.76	0.32	0.29	0	0.14	0.34	0.16	0.36	0

W-7 XRF data (%)

Depth (m)	Ca	Si	Al	K	Fe	Sr	Mg	Ba	Cl	S	Na	Ti	Ce
690	7.65	7.03	2.99	0.44	5.66	0.28	0.28	0.1	0.08	0.18	0	0.43	0
700	4.73	8.79	4.05	0.46	9.49	0.23	0.33	0	0	0.25	0	0.42	0
710	2.86	9.51	4.58	0.47	10.17	0.2	0.37	0	0.18	0.26	0	0.37	0
720	2.61	8.99	4.17	0.47	10.41	0.2	0.31	0	0.13	0.36	0.26	0.5	0
730	2.21	9.12	4.55	0.43	10.89	0.17	0.24	0	0.07	0.25	0.19	0.51	0.14
740	1.97	9.99	4.77	0.48	11.09	0.17	0.3	0	0.12	0.26	0	0.54	0
750	1.88	9.83	4.66	0.53	11.58	0.14	0.28	0	0.18	0.23	0.25	0.48	0
760	3.76	8.04	4.04	0.47	10.81	0.19	0.3	0	0.18	0.25	0	0.44	0
770	1.92	11.97	5.09	0.5	10.82	0.12	0.3	0	0.21	0.24	0.41	0.51	0.13
780	1.99	10.47	4.79	0.41	11.52	0.1	0.37	0	0.26	0.23	0.28	0.47	0
790	3.96	8.94	4.34	0.46	10.54	0.14	0.29	0.08	0.2	0.29	0.3	0.46	0
800	6.12	7.83	3.42	0.4	9.06	0.13	0.23	0	0.15	0.23	0.18	0.5	0
810	5.01	9	4.25	0.48	6.25	0.16	0.26	0	0	0.21	0	0.53	0
820	3.5	9.26	4.51	0.33	9.97	0.15	0.24	0	0.25	0.28	0.29	0.47	0
830	5.07	8.52	3.78	0.42	9.3	0.15	0.25	0	0.21	0.33	0.23	0.49	0
840	3.39	9.13	4.29	0.45	10.11	0.17	0.31	0	0.08	0.25	0.29	0.5	0
850	1.62	8.99	4.36	0.43	6.86	0.1	0.23	0	0	0.22	0.17	0.53	0
860	4.42	9.16	4.24	0.38	6.55	0.16	0.23	0.07	0.22	0.24	0.18	0.58	0
870	1.73	10.48	4.29	0.48	10.26	0.12	0.26	0	0.27	0.2	0.34	0.52	0
880	0.87	10.63	5.11	0.47	10.69	0.09	0.3	0	0.2	0.17	0.28	0.76	0
890	0.8	11.29	5.08	0.46	10.44	0.07	0.3	0	0.1	0.24	0.19	0.55	0
900	0.68	9.31	4.25	0.44	10.5	0.08	0.24	0	0.21	0.21	0.22	0.68	0.06
910	0.68	10.61	5.07	0.44	11.17	0.07	0.32	0	0.27	0.23	0.28	0.68	0.1
920	0.58	10.87	5.2	0.5	11.52	0.08	0.23	0	0.17	0.25	0.23	0.76	0
930	1.52	9.93	4.98	0.41	11.83	0.13	0.25	0.1	0.08	0.21	0	0.53	0
935	1.8	10.24	4.74	0.43	12.68	0.12	0.27	0.04	0.09	0.26	0.21	0.58	0
940	0.84	10.33	4.97	0.45	10.63	0.07	0.25	0	0.29	0.27	0.21	0.51	0

W-7 XRF data (%)

Depth (m)	Ca	Si	Al	K	Fe	Sr	Mg	Ba	Cl	S	Na	Ti	Ce
950	1.54	9.74	5.09	0.41	11.61	0.08	0.33	0	0	0.24	0	0.52	0
960	2.01	9.07	4.29	0.43	11.15	0.1	0.19	0	0.18	0.19	0	0.4	0
970	4.86	8.96	4.08	0.49	9.16	0.21	0.22	0	0.17	0.22	0.17	0.34	0
975	4.38	9.18	4.42	0.46	8.99	0.12	0.31	0	0.15	0.24	0.18	0.44	0
980	3.67	7.64	3.34	0.55	8.77	0.13	0.21	0	0.22	0.27	0.08	0.39	0
985	4.34	8.37	4.22	0.62	8.94	0.16	0.26	0	0.13	0.23	0.16	0.37	0
990	5	8.79	3.55	0.64	8.2	0.15	0.32	0	0.31	0.32	0.26	0.36	0
995	4.42	9.11	3.78	0.81	8.12	0.16	0.29	0.11	1.15	0.44	0.57	0.29	0
1000	4.19	9.24	4.12	0.8	8.49	0.15	0.31	0.21	0.87	0.27	0.36	0.39	0
1005	4.27	8.96	3.51	1.01	4.93	0.15	0.32	0.15	1.53	0.33	1.02	0.36	0
1010	4.6	7.93	3.37	0.87	5.06	0.14	0.22	0	0.8	0.35	0.36	0.32	0
1015	4.86	9.43	3.68	0.78	7.34	0.16	0.29	0	1.23	0.27	0.66	0.32	0
1020	8.41	7.69	3.09	0.79	4.68	0.2	0.25	0	0.9	0.43	0.44	0.3	0
1025	7.25	8.14	3	0.8	4.68	0.16	0.21	0	1.18	0.49	0.51	0.27	0
1030	7.58	7.22	2.61	0.72	6.5	0.19	0.23	0	0.35	0.33	0.22	0.32	0
1035	7.53	8.43	2.79	0.82	4.25	0.16	0.25	0	1.01	0.34	0.43	0.35	0
1040	9.18	7.37	2.33	0.77	4.46	0.18	0.19	0	0.77	0.33	0.4	0.3	0
1045	3.05	11	4.1	0.76	9.13	0.1	0.21	0.04	0.42	0.28	0.22	0.54	0
1050	1.56	10.1	2.68	0.32	7.88	0.07	0.16	0	0.24	0.21	0	0.57	0
1055	9.79	7.61	2.18	0.33	3.81	0.14	0.15	0	0.41	0.29	0.23	0.34	0
1060	21.29	2.45	0.74	0.22	2.16	0.2	0.15	0.12	0.23	0.24	0.08	0.13	0
1065	23.14	2.25	0.94	0.25	2.3	0.11	0.17	0	0.49	0.16	0.19	0.08	0
1070	28.82	1.22	0.6	0.15	1.09	0.11	0.17	0	0.27	0.1	0.14	0.09	0

W-7 XRF data (%) continued

Depth (m)	La	Mn	P	Sc	V	Cr	Zn	I	Zr	Mo	Ni	Rb
400	0	0	0	0	0	0	0	0	0	0	0	0

W-7 XRF data (%) continued

Depth (m)	La	Mn	P	Sc	V	Cr	Zn	I	Zr	Mo	Ni	Rb
410	0	0	0	0	0	0	0	0	0	0	0	0
420	0	0	0	0	0	0	0	0	0	0	0	0
430	0	0	0	0	0	0	0	0	0	0	0	0
440	0.15	0.05	0	0	0	0	0	0	0	0	0	0
450	0	0	0	0	0	0	0	0	0	0	0	0
460	0	0	0.04	0	0	0	0	0	0	0	0	0
510	0	0	0	0.05	0.02	0	0	0	0	0	0	0
520	0	0	0	0	0	0	0	0	0	0	0	0
530	0	0	0	0.04	0	0	0	0	0	0	0	0
540	0	0	0	0.05	0.02	0	0	0	0	0	0	0
550	0	0	0	0	0	0.04	0	0	0	0	0	0
560	0	0	0.03	0	0	0	0	0	0	0	0	0
580	0	0	0	0	0	0	0	0	0	0	0	0
610	0	0	0.06	0	0	0	0	0	0	0	0	0
620	0	0.08	0.07	0	0.03	0	0	0	0	0	0	0
630	0	0.07	0	0.51	0	0	0.02	0	0	0	0	0
640	0.12	0.05	0.06	0	0	0	0	0	0	0	0	0
650	0	0.03	0	0	0	0	0	0	0	0	0	0
660	0	0.04	0	0	0	0.03	0	0	0	0	0	0
670	0	0.03	0.04	0	0	0	0.03	0	0	0	0	0
680	0	0.04	0.06	0	0	0	0	0	0	0	0	0
690	0	0.05	0	0	0	0	0	0	0	0	0	0
700	0	0.05	0	0.02	0	0	0	0	0	0	0	0
710	0	0.1	0	0.02	0	0	0.02	0.42	0	0	0	0
720	0	0.09	0	0	0	0	0	0	0	0	0	0
730	0	0.07	0	0	0	0	0	0	0	0	0	0
740	0	0.08	0.05	0	0	0	0.03	0	0	0	0	0

W-7 XRF data (%) continued

Depth (m)	La	Mn	P	Sc	V	Cr	Zn	I	Zr	Mo	Ni	Rb
750	0.12	0.08	0	0	0.04	0	0.04	0	0	0	0	0
760	0	0.08	0	0	0	0	0.03	0	0	0	0	0
770	0	0.05	0.08	0	0	0	0.02	0	0	0	0	0
780	0	0.09	0.06	0	0.06	0	0.02	0	83 PPM	0	0	0
790	0	0.06	0.05	0	0	0	0	0	0	0	0	0
800	0	0.06	0	0	0	0	0.02	0	0	0	0	0
810	0	0.07	0	0	0	0	0.01	0	0	0	0	0
820	0.14	0.06	0	0	0	0.03	0	0	0	0.03	0	0
830	0	0.07	0	0	0	0.03	0	0	0	0	0	0
840	0	0.1	0	0	0	0	0.03	0	0	0	0	0
850	0.11	0.1	0	0.02	0.01	0	0	0	0.05	0.02	0	0
860	0.09	0.11	0	0	0.02	0	0.02	0	0	0	0	0
870	0	0.11	0	0	0	0	0.02	0	23 PPM	0	0	0
880	0.08	0.13	0.07	0	0	0.03	0	0	0.05	0	0	0
890	0	0.05	0	0.02	0	0	0.02	0	0.09	0	0	0
900	0	0.04	0.06	0	0	0	0.02	0	0.08	0	0.02	0
910	0	0.07	0	0	0	0.05	0.03	0	0.05	0	0	0
920	0.1	0.07	0	0	0	0	0.03	0	0.03	0	0	0
930	0	0.06	0.11	0	0.04	0	0.04	0	0	0	0	0
935	0	0.1	0	0	0	0	0.03	0	0	0	0	0
940	0	0	0	0	0	0	0.02	0	0.06	0	0	0
950	0.14	0.06	0.08	0	0.02	0.04	0	0	0.04	0	0	0
960	0	0.04	0.06	0	0	0	0.03	0	0.02	0	0	0
970	0	0.03	0	0	0.04	0	0	0	0	0.03	0	0
975	0	0.04	0.05	0	0.02	0	0.04	0	0	0	0	0
980	0	0	0	0	0.03	0	0.03	0	33 PPM	0	0	0

W-7 XRF data (%) continued

Depth (m)	La	Mn	P	Sc	V	Cr	Zn	I	Zr	Mo	Ni	Rb
985	0	0.06	0	0	0	0	0.04	0	0	0	0	0
990	0	0	0.1	0	0	0	0.04	0	0	0	0	0.02
995	0	0	0	0	91 PPM	0	0.03	0	0	0	0	0.03
1000	0	0.03	0	0	0	0.03	0.04	0	0	0	0	0.02
1005	0.12	0.03	0	0	0.02	0	0.07	0	0	0	0	0
1010	0.16	0.02	0	0	0	0.02	0.03	0	0	0	0.02	0.02
1015	0	0.03	0	0	0	0	0.03	0	0	0	0	0.02
1020	0	0	0.07	0	0	0	0.02	0	0	0	0	0
1025	0	0	0	0.03	0	0	0.02	0	0	0.02	0	0.02
1030	0	0	0	0	0	0	0	0	0	0	0	0
1035	0	0	0	0	0	0	0.03	0	0	0	0	0
1040	0	0.04	0	0	0.01	0	0	0	0	0	0	0
1045	0	0.08	0.1	0	84 PPM	0	0.02	0	0.04	0	0	0
1050	0	0.31	0	0	0	0	0	0	0.12	0	0	0
1055	0	0.12	0.07	0	0	0	0	0	0	0	0	0
1060	0	0.05	0.06	0	0	0	0	0	0	0.02	0	0
1065	0	0.05	0	0	0	0	0	0	0	0	0	0
1070	0.12	0.05	0	0.03	0	0	0	0	0	0	0	0

W-9 XRF data (%)

Depth (m)	Al	Ba	Ca	Cl	Fe	K	La	Mg	Mn
432	0.89	0	11.21	0.22	3.56	0.42	0	0.16	0.07
435	0.61	0	20.4	0	1.22	0.21	0	0.56	0
438	0.65	0	20.98	0.07	1.16	0.18	0	0.29	0
482	0.53	0	21.95	0.1	0.83	0	0	0.4	0
487	0.14	0	22.94	0	0.26	0.05	0	0.49	0

W-9 XRF data (%)

Depth (m)	Al	Ba	Ca	Cl	Fe	K	La	Mg	Mn
493	0.89	0	22.16	0	1.47	0.17	0	0.43	0
497	0.68	0	22.15	0.06	1.07	0.22	0.14	0.32	0
500	0.22	0	31.34	0	0.48	0	0	0.18	0
506	0.24	0	31.63	0	0.9	0	0	0.19	0.03
510	0	0	29.09	0	0.88	0	0.13	0.16	0.04
514	0.24	0.11	24.71	0	0.62	0.08	0	0.13	0.04
520	0.39	0	26.23	0.06	1.26	0.1	0	0.21	0
523	0.29	0	24.69	0.06	0.74	0.07	0	0.18	0
529	0.3	0	25.67	0	1.18	0.08	0.12	0.18	0.08
532	0.46	0	25.08	0.08	1.46	0.11	0	0.19	0.05
536	1.57	0.06	16.46	0	3.61	0.27	0	0.26	0.05
538	1.95	0	12.38	0.07	4.38	0.21	0	0.21	0.06
541	1.66	0	15.47	0	5.51	0.25	0	0.21	0.13
545	1.91	0.13	13.48	0	4.17	0.29	0	0.29	0.06
549.5	2.28	0	9.73	0	4.78	0.27	0	0.2	0.07
554.5	0.87	0	19.24	0	2.42	0.19	0	0.16	0
559.5	0	0.42	25.33	0	1.7	0	0	0.09	0

W-9 XRF data (%) continued

Depth (m)	Na	Ni	P	S	Sc	Si	Sr	Ti	V
432	0.18	0	0	0.5	0	4.03	0.26	0	0
435	0	0	0	0.31	0	2.96	0.19	0.09	0.04
438	0	0	0	0.15	0	2.68	0.25	0	0
482	0.12	0	0	0.19	0	2.3	0.21	0.04	0
487	0.09	0.02	0	0.08	0.04	1.5	0.32	0	0.02
493	0.09	0	0	0.25	0	2.97	0.21	0.07	0.02
497	0	0	0.06	0.28	0	2.4	0.22	0	0

W-9 XRF data (%) continued

Depth (m)	Na	Ni	P	S	Sc	Si	Sr	Ti	V
500	0	0	0	0.1	0	0.73	0.2	0.04	0
506	0	0	0	0.23	0	0.87	0.19	0	0.03
510	0	0	0.03	0.18	0	0.85	0.17	0	0
514	0	0	0	0.15	0	0.77	0.19	0.04	0.02
520	0	0	0.04	0.31	0	1.01	0.2	0	0
523	0	0	0	0.21	0	0.97	0.21	0	0
529	0	0	0	0.18	0	0.76	0.22	0	0
532	0.1	0	0.07	0.27	0	1.08	0.94	0.06	0
536	0.13	0	0.05	0.19	0.04	4.33	0.15	0.21	0
538	0.18	0	0	0.27	0	4.51	0.16	0.21	0
541	0.23	0	0.08	0.44	0	4.34	0.18	0.26	0
545	0.12	0	0	0.23	0	4.37	0.14	0.22	0
549.5	0.16	0	0.08	0.28	0	5.29	0.14	0.32	0.01
554.5	0.13	0	0	0.43	0	2.3	0.13	0.14	0
559.5	0	0	0	0.6	0	0.39	0.1	0	0.03

W-10 XRF data (%)

Depth (m)	Al	Ba	Ca	Ce	Cl	Fe	K	La	Mg	Na
610	1.09	0	16.77	0	0.08	1.96	0.25	0	0.22	0
615	0.95	1.25	18.77	0	0.16	2.1	0	0	0.27	0.11
630	0	0	24.59	0	0.06	1.28	0	0	0.19	0
635	1.74	0	5.51	0	0.1	3.44	0.18	0.12	0.13	0.11
640	1.99	0.17	5.46	0	0.05	4.33	0.1	0	0.08	0
645	0.75	0.67	7.37	0	0.08	1.55	0.16	0	0.08	0
650	0.92	0	5.54	0.05	0.09	1.66	0	0.16	0.08	0
655	0.07	0	20.94	0.03	0	0.27	0	0	0.11	0

W-10 XRF data (%) continued

Depth (m)	Nb	Ni	P	S	Sc	Si	Sr	Ti	Zn
610	0	0.01	0	0.36	0	4.05	0.34	0	0.05
615	0	0	0.08	0.44	0	3.45	0.38	0	0.03
630	0	0	0	0.26	0	0.98	0.21	0.04	0
635	0	0	0	2.35	0.04	5.23	0.17	0.32	0.02
640	0	0	0	2.5	0	4.25	0.19	0.46	0.02
645	0	0	0	0.73	0	5.58	0.08	0.25	0
650	0.03	0	0	0.99	0	6.1	0.09	0.22	0
655	0	0	0	0.09	0	0.96	0.12	0	0

W-11 XRF data (%)

Depth (m)	Al	Ba	Ca	Ce	Cl	Cr	Fe	K	Mg	Mn	Mo	Na
685.7	0.1	0	27.49	0	1.02	0	0.25	0	0.4	0	0	0.22
708.1	0.42	0	22.16	0	0.76	0	0.85	0.33	0.23	0	0	0.21
729.1	0.31	0	28.71	0	0.4	0	0.47	0	0.2	0	0	0.17
761.5	3.71	0.12	1.48	0	0.84	0	10.21	0.5	0.39	0	0	0.47
787.9	1.56	0.05	0.2	0	2.14	0	4.7	0.12	0	0	0	0.81
807.3	0	0	27.7	0	0.44	0	0.21	0	0.13	0	0	0.19
825.8	0	0	28.42	0	0.54	0	0.24	0	0.16	0	0	0
839.2	0.66	0	24.77	0	0.79	0	1.14	0.17	0.15	0.13	0	0
841	4.97	0	0.45	0.15	1.07	0.51	11.52	0.71	0.31	0.12	0.03	0.64
859.5	0.07	0	27.88	0	0.65	0	0.25	0	0.16	0	0	0
877	3.28	0	1.36	0	0.74	0.13	8.59	0.55	0.25	0	0.02	0.46

W-11 XRF data (%) continued

Depth (m)	Ni	P	Rb	S	Sc	Si	Sr	Ti	V	Zn	Zr
685.7	0	0	0	0	0	0.51	0.2	0	0	0	0

W-11 XRF data (%) continued

Depth (m)	Ni	P	Rb	S	Sc	Si	Sr	Ti	V	Zn	Zr
708.1	0	0	0	0.27	0	1.64	0.22	0	0	0	0
729.1	0	0.04	0	0.21	0	1.06	0.43	0	0	0	0
761.5	0	0	0.02	0.38	0	8.65	0.21	0.44	0.02	0.01	0
787.9	0	0	0	1.14	0	15.32	0	0.39	0	0.03	0.24
807.3	0	0	0	0.04	0	0.08	0.1	0	0	0	0
825.8	0	0	0	0.08	0	0	0.12	0	0	0	0
839.2	0	0	0	0.15	0	1.41	0.16	0	0	0	0
841	0.09	0	0	0.28	0	8.95	0.09	0.51	0	0.04	0
859.5	0	0.05	0	0.07	0.03	0.1	0.11	0	0	0	0
877	0.05	0	0.02	0.17	0	7.78	0.09	0.29	0	0	0.03

Appendix F. PCA loadings and scores for nannofossil assemblages and XRF data.

Nannofossil assemblages PCA loadings																					
Variables	**PC 1**	**PC 2**	**PC 3**	**PC 4**	**PC 5**	**PC 6**	**PC 7**	**PC 8**	**PC 9**	**PC 10**	**PC 11**	**PC 12**	**PC 13**	**PC 14**	**PC 15**	**PC 16**	**PC 17**	**PC 18**	**PC 19**	**PC 20**	**PC 21**
1. *Ahmuellerella regularis*, 2. *Biscutum constans*, 3. *Broinsonia*, 4. *Calculites obscurus*, 5. *Chiastozygus*, 6. *Corollithion signum*, 7. *Discorhabdus ignotus*, 8. *Eiffellithus*, 9. *Eiffellithus eximius*, 10. Holococcoliths, 11. *Lithraphidites carniolensis*, 12. *Micula staurophora*, 13. *Prediscosphaera cretacea*, 14. *Prediscosphaera*, 15. *Retacapsa*, 16. *Staurolithites*, 17. *Tranolithus minimus*, 18. *Tranolithus orionatus*, 19. *Watznaueria barnesae*, 20. *Zeugrhabdotus erectus*, 21. *Zeugrhabdotus*.																				
1	0.23	-0.40	0.11	-0.25	0.23	-0.12	0.14	-0.05	0.48	-0.26	0.43	-0.18	0.17	0.07	0.02	-0.11	-0.17	-0.12	-0.13	0.00	0.02
2	0.23	-0.06	-0.26	-0.18	0.05	-0.01	-0.13	-0.20	0.14	-0.05	-0.04	0.44	-0.06	0.44	-0.32	0.07	0.06	0.42	0.21	0.12	0.17
3	0.21	0.21	0.52	-0.09	-0.15	-0.06	-0.55	-0.25	0.18	-0.24	-0.26	0.01	-0.02	-0.14	0.03	-0.24	-0.02	0.02	0.03	-0.02	-0.01
4	0.24	0.15	-0.08	0.80	-0.22	0.08	0.10	-0.24	0.17	-0.12	0.20	-0.09	0.05	0.18	0.09	-0.07	-0.03	0.00	0.05	0.08	0.04
5	0.20	0.18	0.10	-0.23	-0.29	-0.07	0.15	0.11	-0.22	0.27	0.18	0.01	0.27	0.32	0.12	-0.51	0.29	0.06	-0.21	0.05	-0.04
6	0.32	0.29	-0.44	-0.18	0.09	0.09	0.19	0.09	0.34	0.05	-0.27	-0.06	-0.09	-0.33	0.33	-0.23	0.01	-0.01	0.19	0.15	0.06
7	0.30	0.05	-0.02	-0.18	-0.31	0.20	0.29	-0.03	-0.37	-0.37	0.09	-0.03	-0.18	-0.16	-0.16	-0.01	-0.43	0.21	-0.02	-0.14	-0.20
8	0.17	0.12	0.05	-0.03	0.07	0.09	0.11	-0.11	0.20	0.14	0.04	0.24	-0.02	0.08	0.01	0.17	0.23	-0.20	0.14	-0.58	-0.56
9	0.18	0.30	0.01	-0.11	0.22	0.22	-0.04	-0.01	-0.02	0.04	-0.21	-0.64	0.22	0.30	-0.30	0.27	0.00	0.00	-0.05	0.02	-0.03
10	0.24	0.04	-0.16	0.13	0.21	-0.29	-0.19	0.38	-0.26	-0.44	-0.12	0.19	0.43	0.04	0.23	0.15	0.02	-0.02	-0.05	-0.06	-0.09
11	0.26	-0.33	0.09	0.09	-0.38	-0.41	0.11	0.39	0.16	0.09	-0.34	-0.20	-0.27	0.12	-0.17	0.10	0.08	-0.06	0.09	-0.02	-0.04
12	0.25	0.24	-0.09	0.04	0.23	-0.38	-0.31	0.08	-0.18	0.23	0.51	-0.16	-0.38	-0.15	-0.10	0.01	-0.01	0.07	0.09	-0.07	0.02
13	0.18	0.12	0.09	0.00	-0.09	0.01	0.14	-0.03	0.14	0.02	0.02	0.10	0.00	-0.27	0.02	0.36	0.27	0.25	-0.58	-0.24	0.40
14	0.16	-0.12	0.28	0.27	0.46	0.30	0.16	0.30	-0.07	-0.05	-0.09	0.12	-0.11	-0.17	-0.36	-0.37	0.22	0.09	0.01	0.02	0.02
15	0.12	0.11	0.27	-0.08	-0.11	0.05	0.17	0.09	-0.10	0.06	0.13	0.10	0.25	-0.06	-0.04	0.16	-0.06	-0.28	0.57	-0.15	0.53
16	0.24	-0.26	0.09	0.05	0.26	-0.33	0.26	-0.59	-0.33	0.21	-0.26	-0.06	0.12	-0.13	0.12	0.01	0.01	0.05	0.05	0.05	-0.02
17	0.22	-0.34	-0.04	-0.11	-0.07	0.39	-0.21	-0.06	-0.24	-0.18	0.12	-0.15	-0.26	0.06	0.34	0.17	0.48	-0.14	0.10	0.13	0.04
18	0.19	0.22	0.09	-0.05	0.07	-0.02	0.11	-0.05	-0.05	0.00	-0.03	0.33	-0.23	0.12	-0.12	0.15	-0.12	-0.61	-0.30	0.44	-0.03
19	0.08	0.01	0.31	0.00	-0.07	0.07	0.04	0.15	0.12	0.20	0.18	0.08	0.22	-0.22	0.08	0.36	0.01	0.34	0.16	0.52	-0.37
20	0.26	-0.31	-0.30	0.06	-0.20	0.23	-0.38	0.00	-0.03	0.36	0.00	0.08	0.34	-0.28	-0.28	-0.06	-0.16	-0.20	-0.14	-0.05	-0.02
21	0.16	-0.10	0.20	0.07	0.18	0.23	-0.10	0.19	-0.01	0.34	-0.11	0.09	-0.17	0.32	0.45	0.03	-0.49	0.14	-0.11	-0.16	0.11

Nannofossil assemblages PCA scores																					
depth (m)	PC 1	PC 2	PC 3	PC 4	PC 5	PC 6	PC 7	PC 8	PC 9	PC 10	PC 11	PC 12	PC 13	PC 14	PC 15	PC 16	PC 17	PC 18	PC 19	PC 20	PC 21
W-1																					
364	0.12	0.91	-1.97	-0.16	0.84	5.77	-2.38	1.73	2.88	-3.57	6.50	2.09	1.51	-1.73	-0.21	-3.75	-2.26	-0.48	-0.54	0.06	-0.46
372	-0.99	-0.38	4.03	-4.37	3.55	-2.21	3.19	1.23	0.22	-3.46	-0.67	-1.13	-3.04	0.16	2.23	-1.29	0.73	1.57	1.37	0.16	-1.37
392	4.21	-5.12	-0.50	-3.83	1.37	-0.53	-0.14	1.87	-1.18	-0.72	-1.64	0.53	-0.52	-1.87	-0.24	-1.90	-0.07	-0.01	0.00	-0.41	-1.24
442	3.26	-1.04	-0.74	-4.95	-0.66	2.57	-3.13	6.21	2.21	-2.08	1.27	0.63	-0.99	-0.72	-1.80	-1.34	0.09	-1.16	0.03	0.37	-0.49
476	5.82	-5.02	0.10	-4.49	1.22	0.21	0.38	1.62	0.34	-0.52	-1.28	-0.76	-0.07	-1.91	-0.67	-1.55	-0.31	0.16	0.88	0.07	-0.99
502	1.87	0.57	-1.52	1.19	-3.40	2.95	-2.44	4.78	3.00	-3.34	1.40	-1.96	-0.51	1.23	-1.01	-1.67	-0.21	-0.58	0.56	0.44	-0.08
518	-3.08	1.46	-2.61	-6.42	2.17	5.80	-4.20	2.75	1.53	-2.64	3.55	1.00	1.51	-0.59	-0.07	-2.33	-1.79	0.09	-0.47	0.39	0.69
522	2.33	0.94	-1.21	3.99	-2.35	1.16	-0.38	0.44	-2.90	1.85	-4.63	-0.59	-0.99	-1.56	-1.05	-1.86	0.51	0.44	2.14	0.87	-1.23
566	-1.00	-1.06	-0.93	-4.79	-0.85	2.56	-2.79	6.56	2.36	-1.73	0.38	-0.77	-1.05	-0.59	-2.53	-2.42	-0.98	-0.64	-0.07	-0.53	-0.66
618	-1.69	-0.73	0.86	-5.01	-2.31	4.98	-0.31	4.29	3.70	1.84	0.67	-2.34	-4.26	-1.00	-4.30	-2.92	-1.04	0.43	0.44	-0.77	0.34
682	-2.97	0.26	0.05	-3.00	4.39	-0.59	4.21	9.37	0.41	-2.49	4.43	-2.14	-2.83	3.70	-0.48	2.25	0.78	0.76	0.82	0.16	0.12
756	0.57	-3.59	-0.13	-4.65	1.38	-1.27	0.04	0.44	-0.36	-1.72	-0.95	0.14	-0.29	-1.48	-1.12	-1.26	-0.21	0.58	1.29	0.41	-0.20
790	4.76	-3.58	-1.02	-4.48	1.93	-0.32	-0.47	1.52	-0.22	-0.45	-1.62	-0.72	0.20	-1.57	-1.63	-1.53	-0.20	0.52	0.76	-0.39	-0.61
842	-4.80	1.41	0.63	-5.50	1.15	7.33	-3.08	0.47	2.98	1.39	4.61	-1.07	-1.63	-1.98	-2.69	-3.07	-1.86	1.09	-0.31	0.25	-0.05
860	0.64	-2.02	0.42	-3.54	3.93	-1.48	-0.99	2.10	-0.91	0.83	0.13	-1.76	0.71	0.02	-0.51	-0.66	0.27	-1.08	0.20	0.89	-1.38
882	5.92	-2.94	1.27	-4.33	1.77	-1.80	-1.82	1.14	-0.49	0.64	-1.54	-2.00	0.67	-0.44	0.09	-0.02	0.14	0.22	0.34	0.42	-0.70
902	3.14	-2.24	1.90	-3.94	1.56	-0.65	0.05	0.83	-1.04	-0.12	-1.65	-0.95	0.70	-0.23	-0.74	-0.10	-0.44	0.51	0.09	1.05	-0.75
920	-5.26	4.37	-5.16	-2.50	1.82	6.25	-0.19	5.63	-4.76	2.06	2.08	1.34	1.80	0.96	-2.00	1.83	-0.70	0.80	0.09	0.97	-0.50
942	-5.75	2.64	-3.97	-2.50	7.17	-0.27	4.22	1.79	-1.12	3.09	1.56	1.40	5.30	-0.49	-3.21	-0.44	-3.51	1.01	-1.13	0.56	-0.18
W-2																					
2182.37	-27.94	0.85	10.08	5.02	2.38	2.59	-0.87	1.11	4.50	-0.56	-3.30	5.31	-2.43	-4.15	0.62	-0.98	-1.23	-2.50	-1.55	-0.99	0.68
2264.66	-24.98	6.43	7.42	3.85	4.20	-0.76	-2.71	2.14	1.95	-8.09	-5.64	0.46	6.21	-3.58	-4.31	3.54	3.43	-5.68	-0.49	-0.39	-1.24
2293.62	-7.94	7.54	8.76	8.62	-0.59	4.56	-2.31	2.64	-5.44	-4.76	4.20	-3.19	0.55	2.86	3.03	-0.39	0.56	-1.49	-0.36	-0.99	-1.51
2385.06	-16.75	4.67	4.85	11.73	4.94	-2.99	-5.75	1.19	3.24	-3.48	2.30	9.69	-1.92	1.36	-0.53	1.21	-1.08	1.54	2.69	-0.58	2.63
2598.42	-20.68	3.89	8.97	5.55	10.20	-4.39	-2.95	-0.99	-2.64	0.95	-3.64	-1.03	0.98	-3.61	0.45	3.34	-1.56	-1.91	0.00	-2.32	0.80

Nannofossil assemblages PCA scores																					
depth (m)	PC 1	PC 2	PC 3	PC 4	PC 5	PC 6	PC 7	PC 8	PC 9	PC 10	PC 11	PC 12	PC 13	PC 14	PC 15	PC 16	PC 17	PC 18	PC 19	PC 20	PC 21
2645.97	20.01	2.10	10.98	6.90	5.26	-4.89	-9.08	4.35	1.29	-3.25	2.60	-0.14	2.27	-8.04	-0.51	0.30	4.45	7.37	-2.08	3.51	-1.56
W-3																					
3.05	-10.72	5.19	10.26	0.81	5.57	-2.63	-2.15	-4.24	-0.50	6.71	-0.54	0.95	0.27	2.51	-1.83	0.01	1.04	2.11	1.02	-0.21	1.25
30.48	-10.72	-6.58	9.91	-4.24	-0.58	1.77	4.42	-4.57	0.21	-1.54	-2.77	-1.78	-1.66	6.33	-0.21	0.95	0.82	0.85	-0.41	0.09	-0.62
76.2	-2.47	-1.56	3.88	-2.76	2.58	-3.89	2.57	-0.82	4.22	6.42	-0.77	-0.60	-0.70	-0.35	-5.72	-2.87	-2.46	0.81	0.82	-0.06	0.32
152.4	5.35	-4.14	1.52	2.79	2.78	-2.31	-0.57	-1.85	1.38	0.43	-0.01	0.28	0.06	0.04	0.85	-1.49	0.66	0.03	0.97	0.48	0.78
228.6	-4.33	0.55	2.83	-4.10	3.92	-3.35	2.27	2.62	1.96	-2.41	-0.95	-2.28	-1.59	0.81	4.15	-0.26	2.47	-0.73	0.20	-0.07	0.05
350.52	-5.37	2.19	3.43	-3.99	8.24	-0.42	1.73	-1.77	-1.59	-3.48	-0.47	0.89	1.34	1.51	2.81	-2.44	2.21	1.52	0.25	0.26	-0.65
487.68	-5.77	2.11	4.51	-5.23	6.59	3.20	3.45	-4.09	2.40	0.85	1.20	-2.43	-2.26	0.32	1.41	-2.17	1.37	2.06	1.92	-0.31	0.38
594.36	-8.88	-2.16	3.52	-3.99	6.52	1.51	5.59	-4.18	-2.97	2.00	7.34	-0.43	-3.32	6.11	-1.94	2.22	1.18	1.22	-2.55	-1.00	0.38
624.84	-7.66	2.08	4.74	-4.90	5.56	2.40	3.85	-4.15	2.56	1.09	0.37	-0.75	-2.12	-0.78	2.60	-3.81	1.56	1.61	1.44	0.61	0.61
685.8	-6.58	9.98	5.03	-1.25	3.72	2.90	-2.67	5.70	-4.27	-2.82	0.53	-2.52	-2.66	-2.52	4.35	-0.25	1.17	-2.06	-1.98	-0.74	-1.68
W-4																					
27	-3.94	-3.23	5.79	-2.99	3.57	2.00	-4.53	-2.46	-3.95	-0.59	3.48	0.98	4.77	1.90	-1.11	0.37	-0.02	-0.66	-2.17	-0.71	0.29
35.9	-0.97	-6.47	4.18	4.38	-1.62	-0.56	-2.40	-1.87	-2.40	-2.30	2.33	-0.97	1.71	3.41	-1.82	1.62	-0.91	-0.72	-0.66	-1.57	-0.33
48.2	-3.89	-4.29	1.12	1.44	-4.28	3.19	2.09	-2.05	0.94	-4.18	-4.39	-0.06	2.92	1.65	0.83	-1.07	-1.82	-0.86	-0.43	1.24	0.04
60	-4.10	-5.52	3.94	4.01	-2.25	-1.31	-1.92	-2.36	-2.12	-1.39	3.04	-1.67	1.46	4.18	-1.37	1.03	-0.49	-1.73	-0.29	0.09	-1.02
63.1	-4.35	-4.89	1.48	2.62	-2.01	3.62	2.02	-3.19	1.73	-3.27	-4.20	0.42	3.44	2.43	0.96	-1.27	0.27	-0.95	0.18	1.08	0.65
81.1	-7.53	0.52	8.99	-1.43	-0.67	-1.08	-0.13	-2.27	-4.57	1.66	-1.36	-0.32	-6.97	3.04	-3.96	1.74	2.05	3.07	2.29	-0.93	0.68
89.9	1.11	-5.01	1.53	1.18	-4.13	3.00	1.14	-3.52	2.76	1.86	0.34	-0.77	-2.51	0.97	-3.35	-1.19	-0.71	-0.51	0.81	0.50	0.68
92.96	-4.37	-5.71	1.71	-4.35	-2.12	2.75	1.00	0.50	0.84	-2.26	-6.15	1.35	2.88	1.37	-0.71	-0.50	-0.05	-1.69	0.21	-0.09	-0.54
99.06	-15.15	-4.80	11.54	-1.43	4.38	5.78	3.82	-6.35	-0.44	-5.68	-0.95	-4.48	-1.18	-2.67	1.16	3.41	-3.07	-3.53	-0.89	-0.39	-0.81
107.89	1.26	-2.89	-0.30	6.43	-4.73	-1.37	-1.27	-0.80	-3.35	1.60	-2.33	5.83	-2.41	-2.45	2.68	-3.05	1.50	0.23	2.58	0.42	-0.40
110.94	-14.80	-5.63	5.81	-1.42	-3.85	6.11	-0.14	-7.23	-5.99	2.39	-2.08	8.82	-0.11	-0.96	-0.36	-3.41	0.42	-0.42	-0.80	-0.33	-0.81
120.1	19.01	-0.39	13.58	5.62	6.69	6.23	4.05	5.37	1.93	6.27	1.32	7.70	1.16	2.85	1.11	3.33	-2.84	-7.13	6.87	1.69	-3.62
141.12	21.87	5.93	7.31	-1.99	-5.57	-3.80	3.44	2.92	-8.32	2.88	12.05	0.51	1.08	0.22	-1.54	-0.73	-4.20	-3.31	4.25	8.55	-1.80

Nannofossil assemblages PCA scores																					
depth (m)	PC 1	PC 2	PC 3	PC 4	PC 5	PC 6	PC 7	PC 8	PC 9	PC 10	PC 11	PC 12	PC 13	PC 14	PC 15	PC 16	PC 17	PC 18	PC 19	PC 20	PC 21
167.95	7.56	-3.89	-0.76	3.10	-0.61	-1.29	0.34	-1.58	0.75	-1.33	-0.21	-0.70	0.93	0.73	0.37	-2.06	-0.70	-0.29	0.28	0.46	0.16
216.1	0.14	-0.53	0.29	1.91	0.65	5.69	0.43	-8.15	1.48	2.47	4.57	-0.83	0.00	-0.63	-0.30	-3.63	-0.74	0.10	0.09	0.58	0.77
227.99	11.12	-2.09	0.63	1.92	-0.17	1.06	-0.74	-2.81	0.07	-0.13	-1.00	0.07	-0.68	-0.32	0.55	-1.40	0.42	-0.18	0.40	0.69	0.05
248.4	5.28	-3.43	-1.07	2.52	-0.24	-0.23	-0.46	-2.88	0.10	-1.89	-1.37	-1.50	1.57	0.09	0.16	-2.05	-0.39	-0.19	0.14	0.65	-0.52
274.32	12.34	-2.51	-0.87	2.57	-0.18	-1.16	0.74	-1.96	1.09	-2.96	-0.97	0.17	1.47	0.44	0.70	-2.36	-0.30	0.35	1.60	0.34	-0.64
307.84	4.02	-6.26	-7.87	5.55	-0.34	-3.73	3.99	1.19	-0.31	0.70	3.30	5.25	-0.02	0.11	2.73	-2.98	0.05	-0.11	0.92	-0.11	-0.16
344.4	6.44	-2.20	-1.50	1.05	-0.36	-1.45	-0.14	-2.48	0.50	-1.69	-1.22	-1.60	0.52	-0.29	0.55	-2.38	-1.06	-0.10	-0.19	0.65	0.06
377.95	4.51	-2.57	-2.31	-4.54	0.95	-1.65	-1.23	0.40	-1.19	-0.45	-1.92	0.17	-1.66	-1.83	-1.80	-3.46	-1.51	0.18	0.24	-0.90	0.59
408.43	-2.10	8.53	-0.48	-0.73	8.01	-2.35	0.52	-2.93	1.40	-2.32	-6.37	2.96	-2.41	-4.00	0.06	2.35	-2.73	1.46	1.49	0.65	0.26
480.06	7.01	-0.14	-5.26	0.28	-5.63	0.92	-1.26	1.34	4.07	-7.58	2.47	-2.69	0.63	-1.14	-5.16	-1.30	3.03	-3.37	-0.45	-0.42	0.08
524.26	13.38	-1.25	-1.00	1.34	-0.71	0.60	0.45	-1.10	1.21	-1.13	-0.99	-1.26	0.66	1.01	-0.49	-1.56	-0.78	1.06	0.77	0.47	-0.97
586.74	-5.11	10.11	-0.75	-7.75	-2.78	3.57	-2.44	-2.40	-1.12	0.86	2.86	-3.10	-6.07	3.52	2.59	3.60	-1.72	2.76	1.59	-0.42	0.02
646.18	-5.60	8.11	-2.61	7.31	-0.70	-8.50	10.53	3.04	-3.41	-0.28	-0.26	-6.04	0.79	-3.90	-1.69	0.05	3.27	-1.55	1.32	-0.30	-4.00
688.85	1.97	11.76	2.14	5.64	-1.55	-4.46	-1.11	5.61	2.11	-3.19	-2.51	-1.07	-2.06	3.84	-2.17	-1.28	-1.08	3.28	1.52	-0.50	0.23
734.57	-7.01	11.19	3.67	3.88	-1.48	6.40	-0.16	-0.24	0.44	-0.25	3.01	-6.61	-5.86	-2.21	5.00	-2.60	1.24	-0.76	-0.48	0.67	0.44
789.43	-4.05	11.87	1.84	-0.91	6.31	-3.11	-4.64	3.94	4.28	1.63	-1.00	3.48	0.94	0.19	1.76	-0.72	3.03	1.97	1.25	-0.20	-0.17
835.15	2.51	5.51	2.49	1.74	2.43	-8.24	2.84	-0.67	4.03	-4.19	0.62	-1.93	0.74	2.45	-0.57	-0.82	-3.21	2.42	1.07	0.02	-0.82
880.87	-0.90	7.07	-2.36	4.22	-4.55	-0.71	-2.41	3.93	1.14	-1.45	-2.70	1.94	0.12	0.73	-6.25	-0.62	-4.15	1.27	-0.10	-1.12	-1.51
944.88	1.59	3.35	-4.33	3.06	-5.41	3.73	-3.52	4.75	-0.98	-2.11	-1.91	0.49	-1.58	1.83	-1.01	-0.51	1.11	1.01	1.53	-0.27	-0.02
996.69	-2.17	3.18	-1.85	-3.13	-2.55	2.61	-5.77	6.47	-3.03	-0.83	-2.65	-0.38	-2.18	-0.12	-2.17	0.37	-0.55	1.48	1.35	1.03	0.65
1043.9	0.60	-0.52	-2.79	-5.62	3.78	2.19	-2.14	-1.85	-3.03	-0.74	2.65	1.45	1.57	-1.64	1.61	-1.23	-1.21	0.83	0.10	0.04	-0.83
1089.66	5.00	-3.06	-2.31	0.29	-1.06	0.70	-1.31	-0.53	1.07	-2.01	0.64	-0.67	1.21	0.25	-0.16	-1.04	-0.43	0.42	1.21	0.16	-0.45
1120.14	6.95	-1.15	-1.16	-5.32	4.21	3.31	-1.99	-1.13	-1.07	-0.81	1.80	1.62	4.61	-2.06	0.50	-0.85	-1.31	0.68	-0.92	-0.11	0.00
1135.38	3.91	0.66	-2.99	0.31	2.24	2.84	-2.09	-4.68	0.39	-1.17	4.52	0.14	2.40	-0.39	0.90	-2.67	-1.67	0.29	-0.46	1.12	0.14
1165.86	1.70	-1.82	-1.49	-5.05	0.23	-1.56	-2.06	1.34	0.59	-0.05	-1.11	-1.26	0.61	-1.67	0.63	-0.67	-0.17	0.47	1.01	-0.38	-0.27
1203.8	-4.09	2.91	-3.11	-4.06	-3.48	3.64	-5.49	5.12	-2.46	-1.02	-2.68	0.17	-2.65	0.24	-0.82	0.33	0.32	1.14	1.69	-0.81	-1.04

Nannofossil assemblages PCA scores																					
depth (m)	PC 1	PC 2	PC 3	PC 4	PC 5	PC 6	PC 7	PC 8	PC 9	PC 10	PC 11	PC 12	PC 13	PC 14	PC 15	PC 16	PC 17	PC 18	PC 19	PC 20	PC 21
1254.25	7.23	-2.12	-0.07	-5.02	1.01	-1.13	-1.55	1.05	-0.73	0.36	0.17	-1.18	0.90	-0.02	0.05	0.58	-0.72	0.82	0.38	0.53	-1.23
1280.16	5.83	-3.90	-3.44	-4.50	2.65	0.10	3.95	3.32	-1.40	1.97	0.49	-1.38	1.06	2.27	-0.39	2.71	-0.52	0.52	0.32	1.48	0.19
1295.4	-0.82	-1.86	0.32	-6.06	1.40	6.89	0.96	-2.63	0.21	-2.46	-2.52	1.56	5.98	0.78	1.01	-0.28	-1.31	-0.17	-1.29	1.50	-0.58
1310.64	-6.80	4.88	-2.35	-3.91	-0.16	6.51	-4.25	3.15	-3.58	-0.48	-0.02	2.31	0.88	0.98	-0.52	0.04	0.05	1.46	0.36	0.58	-0.29
1325.88	-1.39	-2.12	-0.50	-5.25	-0.94	0.98	-1.50	0.56	-0.90	-1.28	-2.21	-1.94	-0.54	-0.16	-1.38	-0.20	0.42	-0.16	0.43	1.06	-0.80
1348.7	11.99	0.00	-1.95	4.28	3.28	-7.31	-6.10	-0.23	-1.80	1.16	6.58	-5.65	-3.95	0.23	-0.58	-2.85	-0.70	-0.52	1.90	-0.71	0.00
W-5																					
560	-11.41	1.99	-0.82	5.77	1.81	4.98	-4.54	-6.34	0.68	7.73	-0.08	-0.18	-0.04	0.79	0.89	-3.08	4.14	-1.00	1.65	3.15	2.85
605	0.40	-2.55	7.17	6.33	-8.76	9.25	-1.84	1.34	0.73	2.29	-2.66	0.28	-0.62	6.46	-4.07	1.36	1.02	-2.75	0.16	0.78	-0.15
750	4.14	-4.64	-2.37	5.39	-0.63	-1.16	-0.46	-0.74	-0.25	-1.23	-3.17	0.55	0.14	1.16	-0.16	-1.22	-1.33	-0.53	-0.27	0.29	0.08
755	9.08	-3.70	-1.13	4.65	-2.75	-1.35	-0.79	-2.12	-0.42	-0.96	-2.27	-0.80	1.44	1.37	0.12	-0.76	-1.08	-0.75	0.33	-0.42	-0.56
760	3.48	-4.37	-1.05	3.69	-1.59	-1.62	-0.43	-1.16	0.63	-0.64	-2.45	-1.20	0.93	0.78	0.27	-0.78	-0.17	-1.50	-0.22	-0.24	-0.49
765	7.03	-3.49	-1.19	4.40	-1.05	-0.84	-1.31	-0.44	0.03	-0.10	-2.09	-0.76	0.23	0.99	0.11	-1.06	0.26	-0.94	0.23	-0.18	-0.30
770	7.53	-3.17	-0.91	4.51	-0.88	-1.12	-0.40	-1.23	-0.75	-0.72	-0.91	-0.91	0.33	1.28	0.83	-1.05	-0.20	-0.54	0.39	0.13	-0.25
846	7.05	-4.14	-0.83	4.18	-0.92	-1.26	-0.70	-2.17	0.01	-2.09	0.30	-1.49	0.74	1.42	0.91	-1.78	-1.31	-0.84	0.05	-0.05	-0.22
921	4.60	-0.10	-7.39	6.28	0.89	0.38	3.64	1.06	-6.58	1.88	-2.51	-0.68	-2.04	0.76	0.51	0.94	-0.27	-0.57	0.18	-0.21	0.30
996	8.80	2.17	-3.09	5.96	-1.19	-0.47	-2.47	-1.38	-2.99	-0.71	-4.99	0.55	-1.64	-0.31	0.89	-1.64	0.95	0.20	0.86	0.41	0.85
1071	8.50	-1.64	-2.45	3.78	-0.43	-0.60	-0.86	-0.73	0.13	-2.38	-1.71	-1.27	-0.57	-1.07	1.84	-1.86	-1.15	-1.28	-0.22	-0.53	0.72
1146	0.90	4.32	-4.32	4.25	2.61	3.37	-2.02	-3.06	-3.73	0.03	-2.21	0.70	0.42	-2.69	3.43	-1.91	0.53	-0.74	-0.46	-0.69	1.33
1221	-2.12	-0.67	-8.51	-0.05	8.04	4.69	-0.61	-0.14	-5.25	0.02	-2.32	3.78	-2.89	-3.30	0.04	5.54	-1.21	1.38	1.20	-0.66	0.21
1296	4.86	5.00	-2.82	3.94	2.23	4.74	-2.04	-3.80	-4.75	0.71	-1.96	-1.23	1.54	-1.73	1.82	-0.92	-0.88	1.79	0.08	0.14	0.11
1371	5.40	-1.62	-2.17	3.70	0.77	0.08	-0.57	-0.34	0.20	-1.01	-0.65	-2.32	0.95	0.17	1.84	-1.58	0.02	-1.40	-0.84	-1.10	0.46
1446	4.66	0.00	-8.39	6.65	0.48	0.39	2.89	2.15	-4.03	1.76	-3.28	-0.21	-1.86	1.68	-0.12	1.77	0.72	0.60	0.01	-0.50	-0.74
1519.9	0.11	1.94	-9.13	6.05	1.27	3.80	1.50	-3.14	-7.64	0.21	1.85	0.78	0.13	0.58	3.15	1.14	0.13	0.11	-1.51	0.81	0.63
1521	-2.25	-0.33	-3.41	3.70	2.49	-2.05	7.53	1.86	-0.96	-4.75	2.73	-3.35	-3.22	4.33	2.83	2.37	1.16	-0.60	0.31	1.10	-0.71
1593.98	4.68	-1.95	-0.99	3.12	-0.84	-1.50	-1.44	-1.77	1.02	-3.54	0.59	-2.34	-1.15	0.92	0.36	-1.01	-0.22	0.39	-0.45	-1.24	0.19

Nannofossil assemblages PCA scores																					
depth (m)	PC 1	PC 2	PC 3	PC 4	PC 5	PC 6	PC 7	PC 8	PC 9	PC 10	PC 11	PC 12	PC 13	PC 14	PC 15	PC 16	PC 17	PC 18	PC 19	PC 20	PC 21
1596	-3.70	0.79	-5.90	5.15	9.04	1.00	4.92	-2.98	-0.64	-8.00	5.18	-2.50	-3.41	0.99	3.47	5.00	-2.85	0.58	1.57	-0.36	0.61
1674	-4.78	4.53	-3.44	4.54	1.85	3.75	-2.34	-3.99	-4.53	0.17	-0.78	0.67	1.50	0.64	1.49	-0.82	1.03	1.47	1.01	0.39	0.26
1681.93	-2.20	-0.79	-2.04	-3.31	2.24	-2.30	5.69	1.42	2.35	8.87	1.89	-2.04	-0.13	-0.43	-5.53	-0.57	-3.72	0.65	-0.01	-0.28	0.66
1698	3.23	-1.56	-1.30	2.60	-0.15	-1.35	0.16	-1.01	0.58	-0.31	-0.78	-3.05	0.56	1.44	0.74	-1.23	0.14	-1.12	0.28	-0.33	0.45
1698.97	-10.51	5.35	1.48	-1.42	-3.27	-6.09	-2.08	-0.63	2.42	12.75	-3.13	-6.12	1.66	-2.16	2.09	1.76	-1.17	-4.62	-1.37	-0.80	0.32
1722	0.62	2.36	-2.70	4.38	-2.19	0.89	-1.43	-1.27	-3.42	0.84	-3.41	-0.38	-1.29	-0.45	1.00	-0.71	0.56	0.60	0.70	0.55	-0.53
1746	-13.86	2.33	4.13	-2.79	-3.52	0.77	-4.43	-6.25	-7.48	6.98	3.40	-5.53	-0.06	-0.97	3.10	3.63	-1.72	-3.51	-2.69	-1.60	-2.05
1770	-4.35	-0.26	0.05	-5.03	5.05	2.32	-2.36	-2.42	-1.93	0.03	1.34	-0.86	2.73	-1.30	0.92	-1.94	-1.03	-0.29	-0.80	0.10	-0.44
1794	-2.83	-1.68	1.94	-3.01	2.20	-2.01	-1.58	1.67	-1.58	1.44	-1.55	-3.50	0.38	0.37	-0.30	0.46	0.29	-2.37	-0.42	0.95	-0.69
1809	-18.44	-1.36	-5.16	12.93	7.84	-0.06	-2.31	-8.22	1.66	8.07	0.21	0.73	-2.09	2.38	-6.82	2.97	-1.74	3.51	-5.04	1.97	-3.90
1812	-6.85	1.62	-7.24	5.81	-1.33	10.94	1.92	3.64	-1.34	-2.37	-1.18	3.89	5.72	3.26	1.49	1.08	0.76	1.30	-0.14	0.20	0.07
1815	-10.87	6.45	3.38	0.15	-1.04	5.13	5.40	-2.72	10.15	-3.44	0.53	-0.07	2.09	4.00	0.21	-3.73	-3.89	2.30	-1.19	1.45	1.17
W-6																					
640.08	18.85	-0.06	4.43	3.94	1.05	3.81	6.91	0.72	-3.68	-7.05	-0.58	2.68	-4.99	-3.71	-6.74	-1.06	-1.50	-1.60	-10.27	0.64	2.00
664.46	28.04	8.16	5.31	-4.62	-5.17	2.46	2.88	-5.25	6.88	-4.39	-1.83	9.45	-0.92	-3.96	-1.22	5.90	-0.70	0.48	2.30	-0.28	-0.12
682.75	22.55	-7.57	2.94	0.05	-10.14	9.43	-0.99	0.04	-5.13	-1.02	5.99	-1.26	5.34	-8.87	0.20	8.49	0.42	0.79	1.70	0.84	4.10
780.28	7.85	-1.33	-0.42	-5.11	-1.11	2.13	-3.66	5.84	1.49	-3.00	0.16	-0.55	-2.41	1.58	-1.81	-0.80	1.17	-1.42	-1.90	-1.42	0.80
783.3	5.46	-6.08	-0.50	-4.52	2.95	1.29	9.10	2.41	0.01	-4.86	-3.22	-0.17	0.50	5.18	3.57	1.70	4.14	1.37	-1.86	0.65	0.31
792.48	4.35	-3.31	-1.97	2.80	-1.12	-1.45	-0.39	-8.13	6.39	-3.32	0.57	-4.68	-4.97	-5.19	-6.29	2.05	2.63	-1.97	2.67	1.26	0.89
801.62	8.63	-2.66	-2.12	-5.14	1.08	-1.47	-1.99	0.94	-1.11	-0.73	-0.23	-1.12	-0.35	-0.64	0.29	-0.40	-0.61	-0.79	-1.46	-1.67	0.46
822.96	4.68	-3.79	-8.98	4.41	1.92	-2.20	2.45	-1.27	0.49	-5.41	2.47	-1.67	-0.11	-3.90	-5.54	5.86	2.12	-2.01	2.24	-0.36	0.25
844.3	36.47	-9.96	0.75	11.81	3.36	5.03	-1.54	6.86	12.85	7.46	5.96	-4.48	-4.41	-4.90	5.81	0.57	4.09	0.86	-1.65	-2.58	-2.17
872	12.01	-1.58	4.51	3.73	-2.04	-1.05	0.54	0.27	4.19	0.92	2.11	-1.02	4.06	-4.06	2.06	6.41	3.15	6.23	-4.82	3.87	0.14
902.2	-15.16	-8.05	-5.98	-2.72	6.02	11.55	-0.93	0.89	11.25	1.97	0.32	-3.33	3.97	-0.31	0.26	2.53	1.98	2.36	3.60	-2.43	3.26
939	-26.19	1.52	-1.11	10.23	-4.24	5.50	2.69	0.05	2.74	4.42	2.72	-5.60	11.22	-1.07	-6.13	-2.90	5.68	-0.31	-0.06	-3.52	-1.82
969	3.04	-3.65	0.09	-3.69	2.89	-3.25	-1.04	1.50	-0.36	-0.54	-3.25	0.34	1.29	-0.39	-0.20	-1.39	-1.11	0.63	0.83	-0.67	-1.43

Nannofossil assemblages PCA scores																					
depth (m)	PC 1	PC 2	PC 3	PC 4	PC 5	PC 6	PC 7	PC 8	PC 9	PC 10	PC 11	PC 12	PC 13	PC 14	PC 15	PC 16	PC 17	PC 18	PC 19	PC 20	PC 21
997	7.88	-4.01	-3.77	6.04	1.07	-6.32	7.29	2.04	2.07	3.02	2.66	5.70	0.91	-1.16	-0.07	-3.24	-3.89	2.41	-0.36	-0.09	-1.42
1015	3.26	-1.77	-4.99	-4.45	7.45	2.21	2.53	0.77	-2.12	1.08	3.74	0.73	4.07	-0.29	1.29	0.85	0.74	0.53	0.12	0.98	-0.27
1018	6.18	-2.93	1.55	-4.09	3.05	-2.85	-2.02	1.56	0.93	0.67	-1.30	-1.93	2.82	-0.24	-0.43	-0.71	1.18	-0.01	0.55	-0.90	-0.99
1021	9.07	-4.17	0.35	-4.34	2.76	-1.44	-1.95	2.06	1.78	-0.10	-1.80	0.09	0.15	0.08	0.17	0.23	-0.05	0.22	0.82	0.01	0.31
W-7																					
540	-35.39	0.01	1.55	0.57	-5.66	-0.92	3.16	1.49	2.03	5.45	2.66	0.96	4.15	1.68	7.81	-0.37	-0.20	2.34	-0.18	-5.75	0.00
560	-35.04	-5.34	3.83	6.12	-2.14	-2.53	3.94	7.41	2.43	1.55	-4.23	0.53	-4.37	-1.76	0.37	1.77	-3.85	-1.48	-1.85	4.02	5.79
580	-17.54	-5.65	-2.71	-0.39	-5.57	3.98	2.00	5.46	3.61	6.89	-2.62	5.81	-1.90	1.64	2.19	-1.38	5.84	-2.41	0.88	2.65	1.91
610	-22.52	0.93	4.44	-5.25	-10.93	1.81	-1.14	-1.43	-0.13	-2.16	-3.25	-2.08	-2.59	7.15	0.97	3.84	1.06	1.60	-0.70	-0.35	0.49
620	-12.11	-0.55	1.95	-1.53	-4.42	1.85	-7.65	4.27	-4.70	-1.09	-0.77	0.58	-0.25	3.74	-3.12	2.82	1.81	0.78	-1.23	-0.63	0.21
640	0.95	-1.62	-5.68	-1.42	0.08	-1.05	2.10	3.73	-6.25	3.41	-3.32	0.65	-1.15	0.23	-1.22	3.74	1.17	1.01	-0.46	0.38	-0.19
660	7.25	-2.09	-3.17	-0.33	-5.65	-3.41	-2.16	-3.96	2.09	-1.59	1.13	-2.55	1.32	2.57	3.90	2.54	-2.57	-0.47	-1.04	0.70	-0.43
680	46.10	-5.29	2.62	-3.68	1.46	-2.53	0.32	-3.40	-2.40	0.01	-1.43	6.42	-1.43	-0.03	1.01	-2.47	1.78	-3.04	-1.92	-4.05	3.77
700	9.22	1.50	0.33	2.93	-3.70	2.03	-0.45	-6.22	-1.33	3.43	-3.70	-0.77	-5.87	-1.41	-1.63	-1.73	0.29	-0.28	0.15	0.04	1.19
730	13.17	1.30	1.55	1.29	1.73	-3.76	2.93	-2.82	0.91	-4.92	-0.63	-1.24	-4.64	3.66	2.70	-0.74	1.53	0.92	0.00	0.74	0.06
760	7.33	-3.34	-4.65	0.40	-5.59	-8.01	-2.34	-4.74	3.13	-2.29	0.49	3.03	-1.29	-0.58	6.68	-1.73	-2.87	-1.42	-0.68	0.05	0.03
790	8.38	5.48	-3.89	-3.34	-2.39	-6.87	-2.35	-1.70	-0.43	3.52	-6.81	0.55	1.84	-1.55	0.79	1.81	-3.92	-0.50	-1.12	-2.50	0.76
820	7.92	-2.05	-2.71	-4.44	2.19	-2.84	-2.01	0.50	0.46	-0.77	-3.79	-1.38	-1.06	-0.63	-0.15	-1.72	-1.35	-1.34	-2.32	-1.48	-0.20
850	1.48	1.14	-2.31	-2.56	0.29	-1.87	-3.53	0.90	-4.32	0.91	-6.93	0.38	-1.66	-1.32	0.47	-0.71	2.16	0.68	0.68	-1.11	-0.01
880	0.19	9.21	-5.35	2.93	-8.69	-5.01	-5.40	2.99	2.41	1.26	-1.55	0.57	2.23	2.43	0.15	0.40	-5.15	0.34	-0.26	-1.91	0.72
910	-18.07	3.96	3.37	-5.40	-2.54	-9.71	-3.55	-5.38	7.62	-0.85	10.63	5.05	-0.01	1.79	-2.58	-1.00	3.14	-1.21	-1.07	-0.05	2.26
940	-0.40	-4.42	-3.83	-3.72	3.75	-6.49	-8.31	-2.40	7.18	0.99	-2.76	-1.54	1.14	-0.24	3.79	7.99	-0.71	-3.88	2.22	0.77	2.49
970	7.78	0.94	-5.11	-0.79	-6.91	-0.77	-3.89	1.58	6.34	-2.93	1.94	-1.46	1.09	3.71	2.43	2.82	-2.87	-0.29	-0.61	0.34	-0.34
1000	3.46	-3.62	-2.01	-3.92	1.42	-2.71	-1.51	0.83	0.36	1.72	-3.43	-1.36	0.55	-0.76	-0.90	0.16	1.12	0.29	0.51	0.20	-0.24
1015	7.57	-2.98	-0.30	1.78	0.08	-2.50	-0.45	-2.39	1.15	0.24	0.58	-1.42	2.37	3.18	0.37	1.00	0.41	-0.29	-0.19	1.02	-0.03
1035	2.42	-2.85	0.02	-4.57	1.80	-3.32	-1.64	0.33	0.33	1.34	-1.54	-1.62	1.38	1.77	0.28	1.36	1.31	-0.25	-0.13	0.23	-0.22

Nannofossil assemblages PCA scores																					
depth (m)	PC 1	PC 2	PC 3	PC 4	PC 5	PC 6	PC 7	PC 8	PC 9	PC 10	PC 11	PC 12	PC 13	PC 14	PC 15	PC 16	PC 17	PC 18	PC 19	PC 20	PC 21
1045	-5.14	-2.31	-3.32	-1.30	6.58	-7.37	3.01	3.62	4.46	7.51	-1.61	-0.83	4.95	2.88	-2.12	1.18	0.06	-0.93	-0.92	0.63	1.23
1060	4.86	-3.91	0.52	-4.70	1.60	-2.31	-1.08	0.53	0.61	1.28	-0.48	-1.22	1.80	0.32	1.07	0.62	0.19	-1.27	-0.62	0.92	-0.76
W-8																					
582	-28.05	-2.25	3.85	3.67	-1.46	4.87	6.44	3.15	-0.30	-1.47	1.09	1.83	-1.03	-5.33	1.01	1.60	-4.80	5.01	1.66	-7.06	-0.92
588	-27.49	-2.97	0.72	-0.66	-15.31	-6.40	7.17	4.68	-2.06	-1.73	1.01	-4.61	2.11	-2.73	-0.37	-1.22	-0.38	4.54	0.25	0.89	2.36
645	-16.30	-13.18	-0.59	0.91	-0.80	-1.65	1.16	-0.58	-0.23	2.37	4.38	1.68	-6.54	-3.22	-2.88	4.60	-2.32	0.15	1.17	-2.11	0.52
660	-12.05	-10.73	-1.14	-0.10	-0.49	-5.92	1.02	3.46	-5.89	0.52	5.68	3.45	-0.82	0.34	0.14	0.75	0.72	1.41	-0.16	-2.29	-0.27
672	-13.38	-9.76	-1.63	0.22	-1.06	-7.54	0.21	4.45	-5.23	0.47	5.01	3.66	-0.46	0.97	0.79	1.54	0.65	-0.92	-1.49	-0.57	-0.83
681	-12.25	-8.72	2.71	-1.56	-2.26	-6.03	-4.62	0.15	-2.92	-0.95	3.18	4.69	-1.64	0.46	0.35	-1.07	1.18	-0.69	-1.51	-0.64	-0.26
693	-13.68	-6.94	2.84	-1.61	-2.09	-4.87	-2.61	0.29	-3.53	0.00	5.02	3.76	-1.09	0.01	0.80	-1.86	0.22	0.77	-1.01	-1.00	-0.38
702	-6.88	0.77	-0.98	3.45	-3.64	-2.09	-3.05	-0.07	-3.34	2.52	-2.56	-2.02	0.03	1.30	0.51	-0.80	1.50	1.16	1.56	1.01	-0.32
834	26.84	-2.34	16.01	-1.10	-13.08	-7.97	5.34	-3.15	-3.84	0.65	-3.26	-3.10	5.44	-4.67	0.87	0.38	0.91	5.91	1.68	0.94	2.44
843	31.98	3.31	9.86	0.00	-4.19	3.44	13.25	9.97	2.84	6.33	-2.53	5.29	-2.13	-0.76	2.75	-0.16	0.75	-1.92	-1.68	-1.62	-0.79
852	-10.59	7.82	-6.09	-7.41	-3.64	-0.75	12.06	-8.10	-0.37	0.72	-3.98	-0.48	3.60	0.12	-1.05	1.57	0.68	1.60	1.08	1.24	-0.87
858	40.44	4.25	0.55	-5.46	-5.49	4.08	-5.62	0.92	4.02	7.39	-2.31	-0.57	-4.58	2.84	1.43	3.04	1.27	2.06	-4.91	0.71	-3.50
870	41.70	12.66	1.03	2.54	-2.68	2.21	-4.78	-0.44	2.60	3.14	2.30	4.10	5.01	2.07	1.16	3.93	-4.30	0.62	-1.75	-1.25	0.91
882	-14.73	15.37	0.02	-6.08	-5.35	-2.85	1.07	-2.73	1.68	-1.12	1.88	-5.13	-1.93	-6.21	-0.28	-0.59	-0.49	-3.21	-0.21	-1.97	-1.86
891	-12.70	2.70	-12.38	-6.74	-8.91	2.23	0.49	-2.46	-1.87	1.65	6.89	4.39	-3.64	-5.46	-0.09	-0.22	3.19	-1.89	1.04	0.63	0.82
900	34.48	15.52	-4.37	0.91	-2.89	0.29	6.91	-4.11	1.95	1.46	6.15	-0.72	-1.00	5.62	-3.23	0.93	2.60	-1.83	0.11	-3.64	3.88
912	38.69	11.06	-1.73	-2.41	9.34	-3.88	7.93	-0.74	-6.29	-0.20	-1.03	2.51	3.08	1.62	-4.35	-0.18	5.25	-1.32	-0.01	-3.69	2.72
921	-28.33	3.62	-11.28	-1.76	-0.92	-2.39	3.00	-4.74	10.61	-1.32	-3.45	7.53	-4.07	-1.36	0.68	3.12	2.91	0.35	-2.94	4.17	-4.66
930	-20.37	8.75	0.88	-1.88	-3.05	-11.82	-6.94	-0.78	-0.10	-3.04	4.91	9.08	3.41	1.94	0.08	0.80	5.08	-0.86	-0.22	-0.20	-0.25
939	-19.31	7.63	-3.20	-4.59	-8.88	-0.20	10.82	-0.36	1.81	-0.56	1.81	3.30	1.23	-5.43	3.54	-0.71	0.66	-3.63	-1.40	-0.08	-2.51
951	-1.74	2.97	-0.32	-4.38	0.61	4.41	-1.64	-5.85	-3.64	6.05	-0.80	1.32	-2.61	-2.65	-0.16	-1.33	1.00	1.21	-0.13	1.02	0.16
960	-22.87	9.13	-2.48	2.01	7.77	-2.13	1.70	9.95	-2.35	2.35	-0.51	-4.04	0.96	-1.40	2.96	-2.39	-1.55	-2.07	-3.40	4.82	7.34

XRF data PCA loadings										
Variables	PC 1	PC 2	PC 3	PC 4	PC 5	PC 6	PC 7	PC 8	PC 9	PC 10
Ca	0.462	-0.278	0.051	-0.224	-0.062	0.230	-0.358	0.569	0.383	0.023
Cl	0.489	0.349	-0.584	0.541	-0.016	-0.050	-0.038	0.030	0.003	0.029
Fe	0.243	-0.072	0.193	0.072	-0.040	-0.163	0.427	-0.371	0.723	-0.150
K	0.092	0.071	0.269	0.192	0.925	0.104	-0.101	-0.002	0.015	-0.012
Mg	0.348	-0.144	0.108	-0.100	-0.049	0.240	0.004	-0.423	-0.162	0.756
Na	0.211	0.791	0.137	-0.554	-0.008	-0.027	-0.028	-0.029	0.012	-0.045
S	0.313	-0.164	0.240	-0.012	-0.009	-0.846	-0.202	0.017	-0.244	0.016
Si	0.231	-0.039	0.127	-0.013	0.033	0.044	0.780	0.464	-0.317	0.042
Sr	0.403	-0.209	0.067	-0.078	-0.072	0.316	-0.063	-0.360	-0.379	-0.633
Ti	-0.012	0.269	0.662	0.540	-0.359	0.176	-0.154	0.109	-0.032	0.009

XRF data PCA scores										
Depth (m)	PC 1	PC 2	PC 3	PC 4	PC 5	PC 6	PC 7	PC 8	PC 9	PC 10
W-4										
21	0.45	1.02	-6.10	-4.61	2.66	6.58	1.90	0.74	1.68	0.22
27.1	2.97	0.22	-4.30	-5.02	2.76	0.10	0.33	0.54	-0.20	0.36
36	3.14	2.56	0.35	-0.60	-0.35	0.42	-1.24	1.30	-0.45	0.49
42.1	3.21	0.16	-6.97	-6.10	-4.97	-1.48	0.96	0.23	0.00	0.19
48.2	3.73	2.77	0.46	-0.30	-0.24	0.45	-1.21	1.22	-0.48	0.57
57	3.48	-0.24	-3.92	-4.82	2.49	-0.01	-0.09	0.50	-0.17	0.30
60.1	3.73	0.64	-4.80	-4.52	2.64	-0.60	-0.01	0.72	-0.46	0.36
63.1	3.27	0.55	-5.14	-4.49	2.51	-0.90	0.10	0.60	-0.26	0.43
66.1	3.28	-0.07	-6.73	-6.05	-4.87	-1.50	1.09	0.58	-0.44	0.69
71.9	2.73	2.48	-0.16	-0.55	-0.09	2.30	-0.54	1.56	-0.15	0.29
78	3.67	0.54	-4.80	-4.49	2.79	-0.53	0.21	0.51	-0.34	0.68
81.1	3.08	-0.13	-4.65	-4.71	2.38	-0.70	0.11	0.50	-0.41	0.53
86.9	3.80	2.37	0.55	-0.80	-0.06	0.99	-0.96	1.72	-0.80	0.45
89.9	1.64	-6.61	-5.01	-0.33	2.90	-0.26	0.22	0.79	-0.35	0.77
93	-0.20	-0.17	5.36	-4.84	0.38	1.57	-1.07	1.05	-0.27	0.31
105.2	1.67	-6.92	-4.31	0.20	2.57	-4.65	0.78	-0.39	1.54	0.45
117	-0.94	-7.61	5.06	-0.05	0.05	-2.82	-0.20	-0.07	1.11	0.39
123.1	-3.70	-7.91	4.25	-0.02	-0.03	-0.84	-0.43	0.72	0.42	0.48

XRF data PCA scores										
Depth (m)	PC 1	PC 2	PC 3	PC 4	PC 5	PC 6	PC 7	PC 8	PC 9	PC 10
132	-4.01	-1.40	5.39	-4.09	0.13	-0.67	-0.54	0.67	0.39	0.05
168	-4.07	-10.21	-1.12	-4.32	3.07	-2.67	0.64	-0.33	0.83	0.34
180.1	-1.70	-5.43	-0.27	4.28	-0.25	-0.77	-0.77	0.98	0.37	0.63
213.1	-2.45	-7.63	4.48	-0.05	0.10	-0.62	-0.43	0.66	0.62	0.40
228	-3.45	-1.25	5.17	-4.46	-0.29	-0.26	-0.75	0.54	0.45	-0.05
237.1	-5.28	-1.58	5.14	-3.83	0.21	0.23	-0.13	0.39	0.41	0.34
248.4	-1.85	2.77	-0.08	0.68	0.01	-0.17	-0.17	0.24	0.18	0.46
262.1	-1.44	2.55	-0.02	0.35	0.01	0.37	-0.43	0.50	0.37	0.38
274.3	-1.12	2.77	0.33	0.49	-0.06	-0.42	-0.36	-0.08	-0.50	0.05
291.1	-2.07	3.04	-0.05	0.78	-0.07	0.10	0.15	-0.42	-0.47	0.03
307.9	-2.07	3.04	-0.05	0.78	-0.07	0.10	0.15	-0.42	-0.47	0.03
329.2	-2.12	2.78	0.23	0.61	-0.31	-0.06	0.23	-0.62	-0.48	-0.03
344.4	-1.20	2.59	0.18	0.58	-0.34	0.35	-0.32	0.06	-0.15	-0.23
359.7	-1.94	2.81	0.05	0.92	-0.02	-0.05	0.10	-0.26	-0.29	-0.08
378	-1.72	2.89	0.35	0.54	-0.07	0.18	-0.11	-0.02	-0.28	-0.03
392.0	-1.64	2.84	0.21	0.79	0.04	0.07	0.03	-0.22	-0.23	0.11
403.9	-1.42	2.62	0.28	0.38	-0.06	-0.56	-0.46	0.28	0.10	0.26
408.4	-2.38	2.90	-0.06	1.11	0.03	-0.38	0.29	-0.64	-0.72	0.09
445	-2.00	2.78	-0.06	0.71	-0.16	0.22	0.02	-0.21	-0.23	-0.14
463.9	-1.90	3.10	-0.06	1.11	0.02	0.02	0.27	-0.51	-0.45	0.05
480.1	-1.00	2.45	-0.06	0.67	-0.38	0.25	-0.39	0.03	-0.29	-0.35
495.3	-1.65	3.10	-0.43	0.81	-0.31	0.30	0.12	-0.17	-0.01	0.26
515.1	-0.39	2.58	-0.02	0.45	-0.11	0.48	-0.81	0.86	0.40	0.52
524.3	-1.85	3.12	-0.03	0.76	-0.14	0.07	0.30	-0.42	0.55	0.61
541	-0.73	2.62	0.14	0.79	-0.06	-0.13	-0.39	-0.11	-0.31	-0.02
571.5	-1.49	2.82	-0.17	0.72	0.10	0.39	-0.22	0.09	-0.07	-0.02
586.7	-0.68	2.49	0.29	0.23	-0.11	0.44	-0.76	0.73	0.28	0.56
609.6	-1.97	2.48	0.30	0.36	-0.28	0.13	-0.23	0.07	-0.15	-0.04
624.8	-0.61	2.90	0.22	0.52	-0.20	0.19	-0.54	0.61	0.20	0.56
646.2	-1.99	2.65	0.07	0.81	-0.23	0.14	0.06	-0.34	-0.29	0.09
656.8	-1.48	2.31	0.36	0.32	-0.20	0.11	-0.47	0.63	0.43	0.64
673.6	-2.04	3.06	-0.09	0.64	-0.09	0.24	0.04	-0.18	-0.24	-0.02
688.9	-1.53	2.83	0.15	0.87	0.02	-0.17	0.04	-0.22	-0.43	0.01
704.1	-2.07	2.84	0.47	0.91	-0.09	-1.19	-0.06	-0.26	-0.64	0.28
719.3	-1.47	2.48	0.56	0.48	-0.25	-0.61	-0.35	0.08	-0.31	0.31
734.6	-2.09	2.72	0.28	0.58	-0.10	0.36	0.08	-0.19	-0.33	0.12

XRF data PCA scores										
Depth (m)	PC 1	PC 2	PC 3	PC 4	PC 5	PC 6	PC 7	PC 8	PC 9	PC 10
749.8	-2.56	3.05	-0.20	1.30	-0.12	-0.30	0.19	-0.31	-0.66	0.12
772.7	-1.82	2.41	0.11	0.70	-0.14	0.33	-0.11	0.15	-0.02	0.16
789.4	-2.33	2.82	0.10	0.60	-0.13	0.41	0.03	-0.06	0.01	-0.17
804.7	-1.35	2.49	0.10	0.65	-0.03	0.73	-0.23	0.30	0.02	-0.04
819.9	-7.07	-0.24	5.55	-3.75	0.24	0.48	0.58	-0.67	-0.58	-0.18
835.2	-2.70	2.88	-0.23	1.05	0.03	0.60	0.44	-0.50	-0.12	0.21
850.4	-6.35	-0.66	5.31	-4.23	0.06	0.46	0.20	-0.28	-0.32	-0.16
865.6	-2.26	2.80	-0.10	0.72	0.18	-0.03	0.05	0.21	0.37	0.66
880.9	-6.64	-0.61	5.30	-4.06	0.01	0.76	0.29	-0.28	-0.23	-0.29
896.1	-2.89	3.00	-0.37	1.04	-0.09	-0.06	0.37	-0.27	-0.24	0.39
911.4	-2.30	2.72	0.32	0.92	0.01	-0.65	0.07	-0.20	-0.49	0.14
944.9	-1.93	2.63	0.03	0.74	0.03	-0.22	-0.19	0.39	0.25	0.57
963.2	-1.28	2.41	0.43	0.68	-0.02	-0.50	-0.40	0.06	-0.27	0.01
978.4	-2.33	2.41	0.55	0.73	0.14	-1.14	-0.04	-0.18	-0.43	0.42
996.7	-7.04	-0.49	5.29	-4.02	0.31	0.01	0.44	-0.43	-0.36	0.05
1011.9	-2.77	2.98	0.01	0.93	0.09	-0.13	0.26	-0.24	-0.18	0.24
1033.3	-2.61	2.68	0.23	0.73	0.28	-0.24	0.18	-0.13	-0.23	0.47
1043.9	-2.43	2.33	0.34	0.78	0.16	-0.96	-0.02	-0.13	-0.40	0.39
1059.2	-3.46	3.16	-0.23	0.94	0.14	0.37	0.46	-0.31	-0.27	0.40
1074.4	-2.82	3.05	-0.12	1.08	0.32	-0.41	0.31	-0.38	-0.29	0.38
1089.7	-2.71	2.92	-0.24	0.93	0.14	-0.20	0.24	-0.10	-0.12	0.62
1104.9	-2.69	2.92	-0.37	1.15	0.22	-0.37	0.23	-0.19	-0.25	0.44
1120.1	-3.03	2.82	-0.29	1.19	0.16	0.01	0.26	-0.26	-0.32	0.34
1135.4	-3.11	3.19	-0.25	0.75	-0.10	-0.03	1.08	-0.60	1.05	1.49
1191.9	-6.81	-0.38	5.21	-4.01	0.44	0.43	0.58	-0.27	0.07	0.20
1204.0	-0.88	2.36	0.54	0.34	0.68	-0.39	-0.20	0.41	-0.18	0.30
1234.4	-0.95	2.50	0.35	0.44	0.90	0.10	-0.16	0.40	-0.12	0.41
1254.3	-4.84	-0.56	5.51	-4.14	1.18	0.76	0.35	0.20	-0.15	0.21
1264.9	-0.73	2.40	0.45	0.64	0.94	0.42	-0.05	0.49	-0.01	0.48
1280.2	-0.82	2.53	0.27	0.69	0.80	0.95	0.07	0.42	0.19	0.51
1295.4	-0.54	2.69	0.28	0.90	1.07	0.26	-0.16	0.48	-0.06	0.32
1310.6	-0.96	2.55	0.17	0.77	0.73	0.12	-0.45	0.93	0.49	0.73
1325.9	-7.17	-0.74	4.83	-4.07	0.34	0.43	0.03	0.62	0.56	0.31
1341.1	-3.41	-6.20	-0.42	4.82	0.10	-1.48	-0.23	-1.32	-1.29	-0.02
1348.8	-7.61	-0.24	5.71	-3.51	0.72	-1.80	0.33	-0.36	-0.67	0.19
1362.2	-5.84	-7.70	4.19	0.57	0.48	0.25	-0.43	1.02	0.62	0.78

XRF data PCA scores										
Depth (m)	PC 1	PC 2	PC 3	PC 4	PC 5	PC 6	PC 7	PC 8	PC 9	PC 10
1401.2	-1.93	2.25	0.29	0.37	0.70	0.19	-0.27	1.03	0.68	1.18
					W-7					
400	3.37	0.01	-5.02	-4.00	3.64	0.12	-1.55	-0.24	-0.46	-0.36
410	5.30	0.10	-4.35	-3.80	3.25	-0.09	-1.23	-0.50	-0.47	-0.22
420	3.99	-4.31	-0.41	4.27	0.34	1.51	-1.97	0.30	-0.76	-0.03
430	4.53	-4.43	-0.11	4.31	0.67	1.05	-2.03	0.06	-0.77	-0.10
440	2.91	-6.72	-7.72	-0.93	-4.84	-1.49	0.11	-0.27	-0.05	0.38
450	2.95	-4.30	-0.82	4.62	-0.46	0.61	-1.76	0.53	-0.27	0.42
460	8.03	1.14	-3.43	-3.58	2.66	-0.30	-0.10	0.48	-0.59	-0.22
510	3.01	-6.18	-6.07	0.88	3.33	0.27	0.37	0.12	-0.38	-0.78
520	28.68	-0.71	5.76	3.65	5.53	0.74	2.00	0.93	-1.36	-0.08
530	6.39	0.56	-5.90	-5.42	-4.46	-0.50	-0.05	0.77	-1.62	-0.55
540	29.08	-0.85	5.79	3.62	5.18	0.73	2.30	0.59	-1.30	-0.14
550	3.12	-2.88	-3.98	3.03	-6.73	7.70	1.48	1.26	0.36	-0.38
560	0.94	-4.87	-7.52	0.82	3.38	7.21	2.14	0.02	1.51	-0.95
580	5.07	2.40	-0.10	0.12	-0.11	1.14	-1.31	0.94	-0.99	-0.60
610	3.50	-4.00	-0.18	4.89	0.05	1.47	-0.78	1.17	-0.64	-0.42
620	-2.98	-4.84	-0.99	5.60	0.02	0.48	0.16	0.04	0.23	0.09
630	-4.48	-0.96	5.47	-4.16	0.03	0.48	-0.14	-0.22	0.20	-0.73
640	-0.14	2.32	-0.23	0.71	-0.01	0.47	-0.41	0.11	0.24	-0.47
650	-1.53	-4.87	-1.42	5.60	-0.14	0.58	-0.34	0.25	-0.12	-0.28
660	-4.67	-7.97	4.58	0.56	0.05	1.04	-0.30	0.17	-0.22	-0.50
670	-1.67	-5.08	-0.84	5.29	-0.08	0.64	-0.29	0.25	-0.15	-0.48
680	-0.12	1.75	0.37	0.43	-0.26	0.30	-0.56	-0.08	-0.13	-0.60
690	-2.68	-5.16	-0.54	5.18	-0.10	1.01	-0.01	0.06	-0.02	-0.20
700	-7.33	-7.94	3.91	0.83	-0.01	0.91	0.71	-0.54	0.05	-0.28
710	-3.59	-4.85	-1.42	5.56	-0.09	0.28	0.64	-0.56	-0.06	0.13
720	-1.59	2.37	0.38	0.58	-0.23	-0.24	0.31	-0.81	-0.01	-0.42
730	-2.54	2.03	0.45	0.46	-0.30	-0.05	0.50	-0.76	0.14	-0.53
740	-4.18	-4.73	-1.01	5.65	-0.17	0.17	0.80	-0.61	-0.08	0.04
750	-2.16	2.63	-0.08	0.86	-0.09	-0.10	0.61	-0.82	0.17	-0.29
760	-3.25	-4.77	-1.18	5.68	-0.12	0.32	0.45	-0.38	0.20	0.00
770	-2.22	3.04	-0.17	0.65	-0.19	-0.16	0.68	-0.67	0.11	-0.14
780	-2.05	2.82	-0.38	0.91	-0.33	-0.17	0.66	-0.75	0.25	0.14
790	-1.50	2.59	-0.02	0.61	-0.23	-0.13	0.21	-0.43	0.36	-0.24
800	-1.15	2.22	0.29	0.77	-0.31	0.14	0.03	-0.05	0.57	-0.32

XRF data PCA scores										
Depth (m)	PC 1	PC 2	PC 3	PC 4	PC 5	PC 6	PC 7	PC 8	PC 9	PC 10
810	-7.88	-7.86	3.89	0.96	-0.02	1.02	0.54	-0.08	-0.03	-0.16
820	-1.65	2.66	-0.32	0.72	-0.55	-0.19	0.27	-0.39	0.27	-0.41
830	-1.07	2.41	0.11	0.80	-0.30	-0.17	0.04	-0.20	0.34	-0.35
840	-1.95	2.29	0.54	0.19	-0.27	0.10	0.31	-0.61	0.21	-0.33
850	-6.88	-0.56	5.01	-3.68	-0.09	0.29	0.77	-0.80	-0.10	-0.39
860	-1.66	2.32	-0.16	1.00	-0.47	0.15	0.01	-0.09	0.07	-0.39
870	-1.86	3.17	-0.21	0.99	-0.16	-0.06	0.67	-0.70	0.14	-0.23
880	-2.96	3.17	-0.11	1.24	-0.31	-0.07	0.91	-1.02	0.01	0.03
890	-3.39	2.55	0.10	0.94	-0.18	-0.46	1.01	-0.98	-0.04	0.19
900	-2.69	3.16	-0.04	1.48	-0.24	-0.41	0.93	-1.08	-0.02	-0.05
910	-2.89	3.30	-0.31	1.40	-0.31	-0.49	0.98	-1.11	-0.04	0.24
920	-3.31	3.05	0.01	1.40	-0.22	-0.58	1.03	-1.11	-0.11	-0.11
930	-4.86	-4.72	-0.97	5.47	-0.28	0.15	1.00	-0.63	0.05	0.04
935	-2.63	2.30	0.39	0.67	-0.33	-0.23	0.70	-0.79	0.23	-0.24
940	-2.81	2.99	-0.54	1.43	-0.18	-0.67	0.88	-0.90	0.03	0.08
950	-8.84	-7.47	3.63	1.19	-0.13	0.35	1.27	-0.80	0.13	0.34
960	-4.19	-4.44	-1.51	5.84	-0.08	0.07	0.89	-0.28	0.33	0.04
970	-1.47	1.99	-0.20	0.65	-0.06	0.21	0.19	-0.31	0.30	-0.66
975	-1.88	2.10	-0.05	0.68	-0.20	0.07	0.20	-0.27	0.37	-0.05
980	-1.26	1.81	-0.10	1.48	0.12	-0.14	0.16	-0.29	0.34	-0.35
985	-1.80	1.93	0.02	0.65	0.14	0.16	0.14	-0.37	0.32	-0.37
990	-0.59	2.61	-0.12	0.85	0.21	-0.10	0.03	-0.28	0.22	-0.14
995	0.11	3.59	-0.87	1.05	0.46	-0.50	-0.05	-0.32	0.09	-0.26
1000	-0.53	3.26	-0.79	1.30	0.33	-0.03	0.06	-0.33	0.22	-0.17
1005	0.37	4.36	-0.82	1.04	0.63	-0.15	-0.27	-0.17	-0.19	-0.09
1010	-0.19	3.33	-0.69	1.22	0.58	-0.28	-0.29	-0.01	-0.05	-0.31
1015	0.12	3.83	-0.93	1.04	0.40	-0.04	-0.01	-0.21	0.16	-0.25
1020	0.65	3.27	-0.59	0.97	0.47	-0.19	-0.59	0.16	-0.06	-0.41
1025	0.73	3.56	-0.76	1.05	0.56	-0.48	-0.50	0.25	-0.05	-0.40
1030	0.39	2.58	0.07	0.98	0.44	-0.01	-0.31	0.00	0.24	-0.49
1035	0.77	3.52	-0.50	1.21	0.51	-0.04	-0.46	0.28	-0.07	-0.25
1040	1.13	3.39	-0.27	1.05	0.56	-0.02	-0.53	0.36	0.10	-0.54
1045	-1.37	2.91	-0.26	1.49	0.25	-0.26	0.35	-0.12	0.28	-0.21
1050	-3.16	-3.95	-1.04	6.47	-0.26	-0.13	1.01	0.01	0.07	0.23
1055	0.59	2.84	-0.14	0.96	-0.19	-0.02	-0.43	0.67	0.14	-0.51
1060	3.11	1.96	0.45	0.80	0.08	0.34	-1.29	0.58	0.31	-0.62

XRF data PCA scores										
Depth (m)	PC 1	PC 2	PC 3	PC 4	PC 5	PC 6	PC 7	PC 8	PC 9	PC 10
1065	2.72	2.80	-0.58	0.44	0.30	0.39	-1.30	0.66	0.75	-0.20
1070	3.19	2.70	-0.09	0.32	-0.05	0.95	-1.89	0.78	0.58	-0.09
W-9										
432	3.20	0.12	-4.92	-4.18	3.74	-1.87	0.59	-0.82	0.27	-0.93
435	-2.08	-7.70	4.75	0.04	0.41	1.12	-0.74	0.24	-0.56	0.61
438	1.31	-7.04	-5.61	-0.10	3.05	-0.17	0.24	-0.25	-0.08	0.08
482	2.95	1.18	-1.93	-2.29	-7.74	-0.15	-0.51	0.34	-0.57	0.29
487	2.94	-2.50	1.27	-8.77	2.46	0.89	-0.16	-0.70	-0.91	-0.01
493	-1.43	-1.53	5.08	-4.72	0.10	0.96	-0.92	0.03	-0.23	-0.06
497	1.29	-7.16	-5.37	-0.19	3.21	-0.66	-0.05	-0.23	-0.21	0.25
500	-0.96	-7.36	2.33	-1.73	-7.03	0.97	-0.89	0.56	-0.28	-0.08
506	-0.64	-9.46	-2.12	-5.55	-4.52	-1.07	0.41	-0.35	0.16	-0.15
510	23.94	-4.35	9.09	-2.31	-1.49	-0.76	2.89	-0.26	0.27	0.10
514	-0.67	-7.06	4.51	-0.17	0.17	1.26	-1.53	0.50	-0.12	-0.42
520	2.55	-6.77	-4.91	-0.11	2.62	-0.96	-0.52	-0.37	0.32	-0.04
523	3.00	-6.58	-4.91	-0.07	2.45	-0.62	-0.55	-0.19	0.02	-0.10
529	-0.77	-9.23	-0.39	-4.17	2.64	-0.15	-0.27	-0.70	0.45	-0.44
532	4.44	1.42	0.99	-0.47	-0.26	0.70	-1.93	-0.34	-0.29	-1.41
536	-3.15	-1.06	5.35	-4.27	-0.01	0.99	-0.44	0.14	0.44	-0.39
538	0.12	1.81	0.56	-0.24	-0.43	0.13	-0.63	0.22	0.41	-0.42
541	-2.84	-0.73	5.72	-4.44	-0.21	0.21	-0.47	-0.01	0.48	-0.74
545	-3.73	-1.24	5.26	-4.26	-0.02	0.78	-0.39	-0.04	0.42	-0.29
549.5	-4.35	-0.95	5.39	-4.21	-0.25	0.49	-0.21	0.00	0.34	-0.61
554.5	-1.70	-0.90	5.75	-4.38	0.02	0.12	-1.06	0.31	0.35	-0.60
559.5	24.03	-4.42	9.39	-2.18	-1.49	-2.28	2.46	-0.51	0.94	-0.11
W-10										
610	0.38	-7.48	-5.95	-0.08	3.19	-0.99	0.50	-0.36	-0.20	-0.39
615	2.23	-1.28	-7.38	-6.07	-5.36	-2.26	1.01	-0.72	-0.22	-0.56
630	28.17	0.07	9.73	5.75	-4.28	-0.19	1.79	0.43	0.03	0.34
635	0.62	1.66	1.07	0.64	-0.63	-1.88	-0.79	0.21	-0.62	-0.72
640	-2.07	-5.41	0.20	5.15	-1.27	-1.80	-0.64	0.46	-0.50	-0.82
645	0.11	-4.58	0.36	5.54	-0.18	-0.83	-0.38	1.38	-0.56	-0.08
650	-1.22	-5.40	-2.45	3.78	-8.74	-2.11	0.65	1.21	-0.90	-0.06
655	1.33	-8.85	-1.32	-5.29	-4.18	-0.51	0.80	0.25	-0.41	-0.06
W-11										
685.7	5.65	3.02	-8.33	-4.63	-4.44	6.07	0.93	-0.64	1.54	0.34

XRF data PCA scores										
Depth (m)	**PC 1**	**PC 2**	**PC 3**	**PC 4**	**PC 5**	**PC 6**	**PC 7**	**PC 8**	**PC 9**	**PC 10**
708.1	5.53	1.19	-5.05	-3.50	3.66	-1.00	-0.70	-0.36	-0.06	-0.30
729.1	5.17	0.27	-6.88	-5.43	-4.89	-1.36	-0.36	-0.36	-0.57	-0.65
761.5	-0.38	3.63	-0.54	1.34	-0.10	-0.46	0.42	-1.23	-0.28	-0.26
787.9	-5.12	8.42	-1.93	3.56	0.19	-7.06	1.89	5.50	2.89	-1.67
807.3	28.98	6.49	3.73	-1.98	-1.68	-0.32	0.23	-0.58	0.71	0.25
825.8	25.75	-0.27	1.64	3.06	-1.91	-0.94	-5.82	-4.16	2.94	0.35
839.2	1.98	-5.92	-7.15	1.26	2.95	-0.57	-0.41	0.07	0.45	-0.09
841.0	-2.01	4.44	-1.01	1.71	0.21	-0.79	0.88	-1.53	-0.22	0.03
859.5	6.03	-4.95	-7.34	0.24	-4.30	-0.70	-1.51	-0.41	0.43	0.48
877.0	-0.94	3.95	-0.91	1.25	0.28	-0.21	0.60	-0.83	0.20	-0.06

Digital Appendices

See attached CD for the following appendices:

1. All nannofossil and microfossil (where available) samples count data for W-1 to W-11.

2. Nannofossil and microfossil biostratigraphic age range charts for W-1 to W-8.